University of Southampton

Impulse ageing of polymeric materials

By

DAO NGOC LONG

A thesis submitted for the
degree of Doctor of Philosophy

in the
Faculty of Engineering and Applied Science
School of Electronics and Computer Science

July, 2011

UNIVERSITY OF SOUTHAMPTON

ABSTRACT

FACULTY OF ENGINEERING AND APPLIED SCIENCE
SCHOOL OF ELECTRONICS AND COMPUTER SCIENCE

Doctor of Philosophy

IMPULSE AGEING OF POLYMERIC MATERIALS

by DAO NGOC LONG

Impulse over-voltage is a common phenomenon in electric power systems. A switching impulse is created by a switching surge or local fault while a lightning impulse is due to direct lightning strike to high voltage plant such as an overhead line. Both impulse events create travelling waves in the system, damaging insulation components and equipment. This work is concerned with the hypothesis that lightning impulses can lead to accelerated ageing of extruded polymeric cables. The results show that there may well be a reduction in electric field strength of the insulation of a power cable that experiences a lot of impressed lightning impulse over-voltages. Pre-designed shaped polyethylene material sample discs have been manufactured using a mould tool. The samples then have been electrically aged using an impulse generator. A real-time software based monitoring tool has been designed to control the impulse wave-shape and process the measurement data. Sets of identical lightning impulses were applied to samples and this was then followed by ramped AC breakdown tests. The obtained results were analyzed using the Weibull distribution to identify any differences in lifetime between aged and un-aged samples. This thesis also provides insight into the dominant ageing processes through the analysis of dielectric spectroscopy and space charge measurement data. In order to quantify the effects of dielectric ageing due to impressed lighting impulse over voltages, experiments have also been undertaken using samples that have been aged under UV light and thermally. Analysis of obtained results reveals that mechanisms of these two ageing processes are significantly different from the mechanisms due to lightning impulse ageing.

CONTENTS

LIST OF FIGURES

LIST OF TABLES

DECLARATION OF AUTHORSHIP

I, ……..,

declare that the thesis entitled

IMPULSE AGEING OF POLYMERIC MATERIALS

and the work presented in the thesis are both my own, and have been generated by me as the result of my own original research. I confirm that:

- this work was done wholly or mainly while in candidature for a research degree at this University;
- where any part of this thesis has previously been submitted for a degree or any other qualification at this University or any other institution, this has been clearly stated;
- where I have consulted the published work of others, this is always clearly attributed;
- where I have quoted from the work of others, the source is always given. With the exception of such quotations, this thesis is entirely my own work;
- I have acknowledged all main sources of help;
- where the thesis is based on work done by myself jointly with others, I have made clear exactly what was done by others and what I have contributed myself;
- parts of this work have been published as conference papers: [see List of publications]

Signed: ……..

Date:…….

ACKNOWLEDGEMENTS

Firstly, I would like to send my special thanks to Professor Paul Lewin and Professor Steve Swingler, my project supervisors, for all their helpful instructions throughout this project. Without their professional experience, encouragement and patience my project has never been completed.

I would like to express gratitude to all the technicians who work in the Tony Davies High Voltage Laboratory including Neil Palmer, Mike Smith, Brian Rogers and Melvyn Kelly for helping me create a mould for sample making and arrange equipment for my project.

I also appreciate Dr. George Chen and Dr. David Swaffield for giving me valuable ideas about this project; Professor Alun Vaughan and Dr. Ian Hosier for giving me suggestions about material handling and supplied me the materials; my colleagues Dr Chris Green, Dr Martin Reading and my wife, Van Nguyen, for their help and advices on this project.

I would like to acknowledge EPSRC for funding my project.

Finally, I dedicate this work to my family in Vietnam who have supported and encouraged me all the time I study in UK.

SYMBOLS AND ABBREVIATIONS

A_t: fraction of moieties in product state at time t

A_0: fraction of moieties in product state at initial state

A_{eq}: fraction of moieties in product state at equilibrium state

A^*: fraction of moieties in product state at critical state

A_d: admittance

A_i, A_1, A_2: parameters of impulse formula

A_{RD}: Richardson-Dushman constant (=$1.2 \times 10^6 Am^{-2}K^{-2}$)

c: half length of a crack

C: a constant

C_1, C_2: capacitors

C_a: capacitance of the sample replaced by air

C_∞: capacitance of sample at very high frequency

C_v: thermal capacity

C': a constant depending on electrostriction coefficient, Young's modulus, permittivity and geometry of space charge regions

d: sample thickness

d_0: initial thickness

d_{dp}: charge moving distance

D: dielectric displacement

D_m: dielectric displacement amplitude

e: electron charge (=1.602×10^{-19}C)

E: electric field

E_0: threshold electric field

E_B, E_{B1}: breakdown fields of bigger and smaller volumes

E_c: critical field for a crack propagating

E_{max}: maximum field before material becomes unstable

E_m: electric field amplitude

E_e: electron energy

E_f: Fermi energy level

E_c, E_v: energy at bottom of conduction band and top of valence band

f: frequency

f(E): function of electric field

$f_X(y)$: probability density function of random variable X as a function of y

$f_F(t)$: probability density function of an event that is failed at time t

$f_S(t)$: probability density function of an event that survives at time t

F(p): total ageing factor

$F(i,n_d)$: probability distribution of the i^{th} measurement with sample size n_d

$F_X(z)$: probability distribution function of random variable X as a function of z

$F_F(t)$: probability distribution function of an event that is failed at time t

$F_{(Ee,T)}$: probability of an electron occupation at energy state E_e

g(x): function of x

G_1, G_2: reactant and product free energy states

ΔG_0, G_a: energy barrier

h: Planck constant (=6.626×10^{-34}Js)

h(t): hazard function

H_{DK}: parameter defined in terms of the enthalpy of states 1, 2 and a

i: i^{th} measurement

I , i_1, i_2, i_3: currents

j: imaginary unit

J: current density

J_T: total current density

J_0: conduction current density

k: Boltzmann constant (=1.38×10^{-23}JK^{-1})

K: thermal conductivity

K_b, K_r: rates of bond breaking and repairing

K_f, K_{rv}: forward and reverse reaction rate constant

K_D: parameter defined in terms of the activation free energies of states 1 and 2

L: lifetime

n_b: concentration of broken bonds

n_d: sample size

n_v: ratio of two volumes

n_s: density of mobile species

N_b: initial concentration of bonds

$N(E_e)$: density of states

O_1: origin of impulse waveform

p: property relates ageing

p^+, p^-: probability of bond breaking and rebonding

p_L: property relates to end-life

p_0: probability of net transition states

P: polarisation

P_∞: high frequency polarisation

P_o: orientational polarisation

q: charge q

q(t): average charge density

q(x,t): charge density at thickness x

Q_1: rate energy gain by electron from applied field

Q_2: rate of energy transferred to lattice

r_b: proportion of broken bonds

r_c: critical fraction of broken bonds

R_1, R_2: resistance

R_a: ageing rate

s, s_1, s_2: Laplace operator

S: the source term

S_D: activation entropy

t: time

t_0: time at origin of impulse

t_{30}, t_{90}: time at which impulse reaches 30% and 90% of peak value

T: temperature

T_0: threshold temperature

T_E: mechanical tension due to electric field

T_1, T_2, T_i: front time, tail time and time interval of impulse voltage

U_b, U_r: breaking and repairing required energies

v(t): impulse voltage in time domain

v_{30}, v_{90}: 30% and 90% peak voltages

V: applied voltage

V_0: initial suppied voltage

V_p: peak voltage

V_{C1}, V_{C2}: capacitor's voltages

V_1, V_2: capacitor's voltage in frequency domain (s domain)

V^*: initial voltage of output capacitor

V_{th}: threshold voltage

V_c: characteristic voltage

V_N, V_a: sample volumes

W: amount of store energy per unit volume from the application of uni-axial stress

W_e: parameter describing conduction electrons

x_N, x_a: longest free paths in volume V_N and V_a

X, X_g: random variables

Y: Young's modulus

Y_n: maximum of X_g

Z_n: minimum of X_g

α, β, γ: location, shape and scale parameters of Weibull distribution

α_1, α_2: scale and shape parameters of Gumbel's distribution

β(a,b): beta function

β_t: shape parameter of Weibull distribution for lifetime

β_v: shape parameter of Weibull distribution for voltage

γ_b, γ_r: effective volume changes

γ_1: skewness coefficient

τ, τ_0: relaxation time

τ_c: characteristic time constant

τ_{i1}, τ_{i2}: time constants for impulse

ω: angular frequency

ω_p: peak frequency

ω_c: critical frequency

ε, ε_1, ε_2: dielectric permittivity

ε_r: relative permittivity

ε_0: permittivity of free space (=$8.854 \times 10^{-12} m^{-3} kg^{-1} s^4 A^2$)

ε^*: complex permittivity

ε', ε'': real and imaginary permittivity

ε_r', ε_r'': real and imaginary relative permittivity

$\varepsilon_{r\infty}$: relative permittivity due to high frequency components

ε_{rs}: relative permittivity due to static components

σ: electric conductivity

σ_0: DC conductivity

σ_1: uni-axial stress

μ : charge mobility

ρ, ρ_1, ρ_2 : resistivity

ρ_c : charge density

δ : loss angle

υ : ramp rate

λ : wave length

λ_c : max length of sub-microcavity

χ: dielectric susceptibility

χ', χ'': real and imaginary susceptibility

χ_e: electron affinity

χ_p: electron affinity of dielectric

$\Phi(t)$: decay function

ϕ : work function

ϕ_0 : potential energy barrier

ϕ_m : work function of metal

$\Delta\phi$: reduction in barrier height

$\Im$: fracture energy

pdf: Probability density function

PDF: Probability distribution function

VB: Valence band

CB: Conduction band

G: Bandgap

MFI: Melt flow index

HDPE: High density polyethylene

LDPE, LD100: Low density polyethylene

LLDPE: Linear low density polyethylene

LDPE4, LE4421: Silane grafted low density polyethylene

XLPE: Crosslink polyethylene

XL1: Crosslink polyethylene by Trigonox 1%

XL3: Crosslink polyethylene by Trigonox 3%

XL4: Crosslink polyethylene by silane crosslinking

DCP-XLPE: Crosslink polyethylene by Dicumyl peroxide

FEA: Finite element analysis

DE: Double exponential

SDE: Separated double exponential

MWS: Maxwell/Wagner/Sillars polarisation

FTIR: Fourier transform infrared spectroscopy

PEA: Pulsed electro-acoustic

AC: Alternating current

DC: Direct current

UV: Ultra violet radiation

Chapter One

Introduction

Underground power cable systems have replaced overhead line power systems in certain areas and applications. High voltage cables have been used to transfer electrical power through urban areas, crossing motorways and rivers. Underground transmission (using cables) has also been chosen where it is hard to build (crossing forests) or impossible to build (crossing oceans) overhead line systems. Instead of using bare wires in overhead line systems, power cables have to be covered by insulation material. The problems when using power cables are heat dissipation and insulation failure under normal working conditions. Cable insulation was initially made from oil impregnated paper but more recently this technology has been replaced by polymeric materials that are less hazardous to the local environment.

Over a 40-60 year design lifetime, especially under high voltage conditions, insulation will age and may finally breakdown. Ageing and degradation of polymeric insulation materials is a very important topic for research as ageing directly affects

the performance of a power system network. The ageing process of cable insulation can be caused by electrical, thermal, chemical, mechanical processes or by a combination of those processes. Although a lot of research has been undertaken, the understanding of ageing mechanisms is still not well established. Several mechanisms have been proposed but none of them has strong experimental evidence to support their hypothesis.

Under normal working conditions, cable insulation may suffer from a lot of transient over-voltages, that is switching or lightning impulses. Switching impulses are created by switching surges or local faults. Some new types of switchgear can produce hundreds or thousands of impulses for each operation [1, 2]. Lightning impulses occur less frequently but with much higher magnitude and very short durations. Lightning impulses can enter the electric power cable system as an external element, due to lightning strikes to overhead lines or external equipment. These impulse over-voltages may travel through the system as waves to substations, equipment and underground cable systems. Insulation quality of devices and cables will suffer from impulse over-voltages and the life expectancy of power cable insulations that experience a lot of impulse over-voltages may be reduced. Several publications have considered the role of impulse voltages in the ageing processes of polymeric material [3]. In fact, it is very difficult to observe any change in the dielectric properties of a material if the number of repetitive impulses is not high enough or the level of peak voltage is too low [4, 5]. The ageing effects of switching impulses on a cable insulation material are easier to obtain compared to the lightning impulse due to their more frequent occurrence within an electric power system. However, researchers are also interested in the effect of lightning impulses on the ageing processes of insulation cable materials. The behaviour of a material when suffering lightning impulses is different from DC, power frequency or even switching over-voltages due to their high level of over-voltage and extremely short front-times. Space charge injection is considered as a main mechanism for ageing under DC voltages but it may not be significant effect under impulse over-voltages. This has been supported by the work of S. Boev, where homo-charges were injected into LDPE and XLPE under DC voltages but not under impulses with different parameters [6]. The effect of various impulse types on material life expectancy has been observed. The application of repetitive surges or thumper surges reduces the life time of an insulation material [7,

8]. Non-standard lightning impulses are also reported to shorten the life expectancy of cable insulation, but the lightning impulse magnitude does not significantly affect the failure rate [8]. Work of S. Grzybowski shows that the effect of switching impulses has also been obtained for materials such as EPR and XLPE, providing a sufficient number of impulses were applied [9, 10]. In this work, up to 5000 standard switching impulses were applied to insulation material with repetition rate of 1 to 2 impulses per minute. However, the result for XLPE reveals that the AC breakdown strength increases after the impulse ageing process.

1.1. Review of ageing mechanisms in cable insulation systems

After a certain working time, the insulation will be weaker and the chance for failure will increase. Insulation ageing causes a lot of problems as it affects power network performance [11]. However, the ageing of a solid dielectric material is still not well defined. It is generally assumed that when a material is under high stress and working for a long time, it is undergoing an ageing process. Depending on the time base used, L.A.Dissado and J.C.Fothergill have compared and classified breakdown, degradation and ageing processes [12]. There are many sources that can lead to the ageing of insulation material including electrical ageing, mechanical ageing, UV radiation, chemical ageing, thermal ageing, water absorption [13]. Each ageing process may cause different ageing mechanisms. However, all of them directly affect the strength of insulation. Researchers can use many methods to analyze an ageing process such as measurement of partial discharge, space charge accumulation, measuring of electroluminescence, analyzing electrical and water treeing, measurement of dielectric spectroscopy and change in breakdown strength [14-17]. A brief review of research into ageing sources, which are directly related to life time of cable insulation, is included in this section.

Under normal working conditions, a high voltage cable will generate a significant amount of heat. This heat will affect the behaviour of the cable insulation system. Normally, the change in heat generated will lead to the change in temperature and also the temperature gradient between the inner and outer surfaces of the insulation. The increase in temperature may change the mechanical properties, water absorption

and increase the possibility of chemical reactions inside the material. However, to obtain the thermal ageing effects, the materials usually have to experience a high temperature or very long time under elevated temperature. It is necessary to decide the suitable temperature, which is used for ageing that is reasonable given the scale of a PhD project. The work of G.C. Montanari and G. Mazzanti about insulation cable lifetime under a combination effect of thermal and electrical stresses [18, 19] suggests there are threshold temperatures and electric fields. Below these threshold values, it will take a very long time to observe any measureable ageing effects. The threshold temperature depends on the applied electric field and also the material itself. They suggested the threshold temperature for XLPE cable insulation is more or less 100^{o}C. Quite a lot of work has been done and shown that above 100^{o}C there are changes in electrical and also physical properties of materials. However, not all the work said that there is no effect if the temperature is less than 100^{o}C. The situation can be very different in the case of thin samples compared to real cable insulation. In the case of thin samples, the thermal ageing will be more homogeneous, temperature and time for ageing will be also less than for thick samples. This is quite easy to understand as there is a big temperature gradient across the thick samples, and the ageing process here is heterogeneous. Considering previous research about electrical properties of insulation materials and thermal ageing, there is almost no change in DC conductivity for XLPE cable peelings after ageing at 100^{o}C for nearly 300 days [20, 21] but a big increase in both DC conductivity and dielectric loss tan delta when using ageing temperatures of 110 and 130^{o}C. However, other research has reported a change in DC conduction for polypropylene and polystyrene thick film when aged at 80^{o}C for only 3 to 36 days [22]. The work of A. Tzimas, M. Fu, L. A. Dissado shows that there is very little change in space charge formation in XLPE cable after ageing at 90^{o}C for 5000 hours compared with a combination of electrical and thermal ageing or in comparison with service aged samples [23]. However, under identical thermal ageing conditions, the positive charge packet, which is generated for un-aged XLPE under high DC fields, doesn't appear for thermal aged XLPE [24]. It is also reported that the intensity of electroluminescence of polypropylene reduces as the temperature of thermal ageing increases but the spectral distribution of the light remains unchanged [25]. For polyethylene, thermal ageing is thought to increase spherulitic separation, enlarging the amorphous region, and increasing dielectric loss [26]. In fact, results show that 15 kV polyethylene power cable insulation has approximately

a 25% reduction in dielectric strength and the degree of crystallinity decreases from 55% to 45% after ageing at 90^{o}C for 200 hours. The dielectric loss also increases by about one order after ageing for 1200 hours [26]. Work with XLPE cable insulation shows that the cable capacitance increases by about 14-15% after ageing at 110^{o}C and 130^{o}C for 2000 hours but there is no measureable difference if the ageing temperature is less than 90^{o}C. For broadband dielectric spectroscopy, the prolongation of ageing time with temperatures higher than 110^{o}C will shift the loss peak in the medium frequency region to a lower frequency region. For thermal ageing below the crystalline melting temperature, the loss peak is not revealed and tan delta is nearly independent of frequency [27]. When analyzing high frequency dielectric spectroscopy of XLPE, the position of the high frequency loss peak is shown to be generally related to the gel-content of material and the magnitude of loss peak is correlated to the degree of oxidation [28]. The thermal ageing process is responsible for both oxidation and chain scission. The measurement of oxidation using Fourier Transform Infrared Spectroscopy shows that the carbonyl index increases with ageing time and temperature [29]. It has also been observed that the carbonyl index decreases from the surface into the bulk of sample [28]. Changes in mechanical and physical properties of the material such as decreases in tensile strength, elongation at break, changes in gel-content and solvent uptake factor can be obtained under more gentle thermal ageing conditions [30-32].

Weather conditions including ultraviolet (UV) radiation, moisture, salt fog and so on can greatly affect to the lifetime of outdoor insulation [33]. The effect of UV ageing on cable insulation is less common than thermal or electrical ageing as most of cables are buried underground and if not are usually solar shielded. However, there are still cables which were aged by UV radiation and it is necessary to understand this ageing process. UV ageing is more severe compared to other ageing processes and also less homogeneous than thermal ageing. UV ageing can include oxidation, crosslinking and chain scission and a very noticeable effect is that the material becomes extremely fragile. In the laboratory, UV ageing can be simulated using different light sources. Some light sources are representative of the spectrum of sunlight, for example, Xenon lamps which are surrounded by a borosilicate filter. It is also possible to use simple fluorescent UV tubes which generate UV light over a small frequency region, they are usually cheaper and can produce similar results but

under different ageing times [34]. The mechanical properties of common cable insulation materials such as XLPE, LDPE are very sensitive to UV radiation. There is an increase in crystallinity with increased UV ageing times as the result of chain scission. Under a mechanical load there are changes from cold drawing profile to a fragile profile. Also the reductions in elongation and stress at the break point have been reported [35]. The results for increase in solvent uptake factor with UV ageing time suggest the change in mechanical properties of XLPE has a physical nature [32]. Results from FTIR of UV aged ethylene vinyl silane copolymer show changes in the spectral regions of carbonyl, hydroxyl, terminal vinyl, Si-O-Si, Si-O-CH_3. This infers that during UV ageing, oxidation, crosslinking and chain scission can occur [36]. Oxidation is thought to be the main reason for the degraded electrical properties of insulation materials after UV ageing. Increases in space charge formation and dielectric loss have been obtained in UV aged low density polyethylene. The effect on samples UV aged in air is also more significant than in nitrogen or in vacuum [37, 38]. The decrease in electroluminescence intensity and breakdown strength in LDPE as a function of the increase of the carbonyl index have also been reported [25, 39, 40]. However, breakdown measurements are not seen as a good characterisation method for quantifying UV ageing because of fragility of the material and the breakdown may be the cause of brittle fracture rather than an electrically driven process [36].

Understanding about electrical ageing is still very limited, it is accepted that material under continuous electrical stress will gradually lose its insulating properties and when safety margins are exceeded failure will occur. Quite a lot of phenomena can be used as the tools for diagnostic electrical ageing such as the change in partial discharge pattern (although this is more indicative of accelerated degradation), modification of space charge and local field, change in electroluminescence as well as growth of electrical and water trees. There are some mechanisms that can be used to explain electrical ageing. Cavities or voids may exist in cable insulation as part of the manufacturing process. Due to the difference in the permittivity of these cavities and the bulk material, when the electrical field exceeds the inception field partial discharge activity can occur. Continuous partial discharges may lead to material degradation and then ultimate failure. Surface discharge and tracking are also considered as reasons for ageing. If the insulation surface is polluted or wet, partial

arcing can occur along the surface. The discharge can consume a thin layer of surface and destroy the hydrophobicity of insulating material. Surface erosion and the creation of conductive paths will lead to what is called surface tracking. The activity of partial arcing of air surrounding insulation surfaces can produce ozone and nitrogen oxides. These gases combine with water and can attack the insulation surface making the surface brittle. When no gaseous cavities are present in the bulk, space charge formation due to defects and imperfection regions or charge injection from the electrode can be considered as the main ageing mechanism. The existence of space charge in the bulk will vary the electrical field and may lead to failure [41].

Electrical ageing is often accompanied by other ageing process such as thermal, mechanical, chemical and environmental ageing. When different factors influence the ageing process, certain synergies may develop. The consequent result is not necessarily the sum of all single factor effects. The factors can interact with each other directly or indirectly. The insulation material under multi-factor ageing processes will be degraded and consequently breakdown. The possibility of prediction of remaining lifetime of a material under service is of great research interest. However, it is not feasible to wait for material breakdown under natural ageing conditions to then take measurements. Therefore, accelerated methods (high voltage, high frequency, thermal) have to be used to provide data. A model can be built to fit the data and then lifetime determined by extrapolation. A model can be built as a single factor or can be developed as a multi-factor ageing model. An example of a single factor thermal ageing is the application of Arrhenius equation for chemical reactions. According to Dakin [42] the lifetime L of a material can be expressed as:

$$L = A\exp\left(\frac{B}{T}\right) \tag{1.1}$$

Where A and B are two parameters that are produced via experimentation, T is temperature.

Similarly, two empirical models for single electrical ageing which are inverse power and exponential models, have been proposed [41]:

$$L = aE^{-b} \tag{1.2}$$

$$L = Ae^{-BE} \tag{1.3}$$

Where E is the applied electrical field, a, b, A, B are again determined experimentally. However, Equation (1.2) and (1.3) are invalid for electrical fields less than the threshold field.

For multifactor ageing, along with the use of the inverse power law, a number of models have been proposed and some of them show better fits to measured data compared to the traditional law. However, the obtained ageing data are very limited, as the longest time for a monitored ageing test is about 3 years. For this reason, it is hard to judge which model is the most suitable.

An empirical model was proposed by L. Simoni which can be considered as the combination of two single thermal and electrical factor models [43]. The total ageing factor F(p), where property p is related to ageing, is equal to the product of the ageing rate R and time t. When p reaches p_L, t will becomes end life L. With the application of Eyring model [44] ageing rate can be represented as:

$$R = A\exp\left(-\frac{B}{T}\right)\exp\left(\left(a+\frac{b}{T}\right)f(E)\right) \tag{1.4}$$

Where A, B, a, b are constants and f(E) is the function of electrical field. Simoni suggests that if $f(E) = \ln\left(\frac{E}{E_0}\right)$, where E_0 is the reference below which there is no electrical ageing, then the life time can be shown as:

$$L = L_0\left(\frac{E}{E_0}\right)^{-\frac{b}{T}-a}\exp\left[-B\left(\frac{1}{T}-\frac{1}{T_0}\right)\right] \tag{1.5}$$

This is known as Simoni's model 1 which corresponds to the inverse power law of electrical ageing where L_0 is a parameter and T_0 is a threshold temperature. If $f(E) = E - E_0$, then this is Simoni's model 2 which corresponds to an exponential form of electrical ageing, such that:

$$L = \frac{1}{A}\exp\left(\frac{B}{T}\right)\exp\left[-\left(a+\frac{b}{T}\right)(E-E_0)\right] \tag{1.6}$$

Based on this model, an improved threshold model has been proposed by Montanari and Simoni [45].

Recently, interest has been concentrated on three models. All have a good fit to data but have different theoretical explanations. The first one, proposed by Jean Pierre Crine and Parpal is based on thermodynamics to predict the lifetime of a material under AC stress conditions [46-49]. According to the model, the aging process occurs due to Van de Waals bonds between polymer chains being broken. To break that bond, the supplied energy has to pass an energy barrier ΔG_0. After that, the energy of the final state is lower than the energy of initial state by $e\lambda_c E$, where e is the electron charge and λ_c is the maximum length of a submicrocavity. The probabilities of bond breaking and rebonding respectively are:

$$p^+ \approx \frac{kT}{h}\exp\left[-\frac{\Delta G_0 - e\lambda_c E}{kT}\right] \quad \textbf{(1.7)}$$

$$p^- \approx \frac{kT}{h}\exp\left[-\frac{\Delta G_0 + e\lambda_c E}{kT}\right] \quad \textbf{(1.8)}$$

Where k is Boltzmann constant, h is the Planck constant. Thus, the probability of net transition state is:

$$p_0 = p^+ + p^- \approx \frac{2kT}{h}\exp\left[-\frac{\Delta G_0}{kT}\right]\sinh\left[\frac{e\lambda_c E}{kT}\right] \quad \textbf{(1.9)}$$

The time to reach the final state then is the inversion of p_0:

$$t \approx \frac{\frac{h}{2kT}\exp\left[\frac{\Delta G_0}{kT}\right]}{\sinh\left[\frac{e\lambda_c E}{kT}\right]} \quad \textbf{(1.10)}$$

For high fields the equation is reduced to:

$$t \approx \frac{h}{2kT}\exp\left[\frac{\Delta G_0 - e\lambda_c E}{kT}\right] \quad \textbf{(1.11)}$$

This model is a good fit with data represented in AC tests but cannot be applied for lightning impulse ageing due to the short duration time of lightning impulse. In this case the duration is too short for the molecule to respond and gain enough energy to break bonds. The model is based on a concept of sub-micro-cavities which form when a high electric field is applied. Electrons are injected into the cavities, gain enough energy and cause further damage. This model is a kind of physical model and its limitations have been highlighted [41]. This model is not applicable for a zero field condition and therefore not compatible single thermal ageing effects. The relationship between ΔG_0 and λ_c is also unspecified.

The second model is from the Bangor group including Lewis, Llewellyn, Griffiths, Sayers and Betteridge and considers the change of morphology of material during ageing, and the fact that the electro-mechanical force disturbs crystallites [50-52]. In this model, the dielectric is subjected to mechanical tension when an electric field is applied. This tension, T_E, is perpendicular to the applied field and proportional to the field squared such that:

$$T_E = \varepsilon E^2 \tag{1.12}$$

Where ε is dielectric permittivity of the material. This stress if high enough can provide sufficient energy for existing cracks to propagate or create a new crack in dielectric. According to Griffith's criterion the fracture energy, $\Im$, required to create an unit area of new crack surface is given by:

$$\Im = ucW \tag{1.13}$$

Where u is a constant, c is the half length of the crack and W is amount of stored energy per unit volume resulting from the application of a uni-axial stress σ_1 . The critical field, E_c, in propagating a crack is:

$$E_c = \left(\frac{2\Im Y}{u\varepsilon^2 c}\right)^{\frac{1}{4}} \tag{1.14}$$

Where Y is Young's modulus. This critical field is reduced if the temperature increases. Under thermal and electrical fields, the bonds breaking and repairing rates, K_b and K_r, are given by:

$$K_b = w \exp\left[-\frac{U_b - \gamma_b \varepsilon E^2}{kT}\right] \tag{1.15}$$

$$K_r = w \exp\left[-\frac{U_r + \gamma_r \varepsilon E^2}{kT}\right] \tag{1.16}$$

Where $w \propto \frac{kT}{h}$, U_b, U_r are breaking and repairing required energies and γ_b and γ_r are effective volume changes. If n_b is the concentration of broken bonds and N_b is the initial concentration of bonds in the solid dielectric, the proportion of broken bonds $r_b=n_b/N_b$ and the equation to determine the proportion of broken bonds is:

$$\frac{dr_b}{dt} = K_b(1 - r_b) - K_r r_b \tag{1.17}$$

Integration of this equation from 0 to a critical fraction r_c at which the ageing is characterized yields the lifetime of the dielectric. However, J. P. Crine has argued that the critical field proposed by Lewis is not really in agreement with experimental data and there is a problem with the definition of an effective volume change [53].

The third model proposed by Dissado, Montanari and Mazzanti is based on the accumulation of space charge at the centre of the material, enhancing the local electric field [54-57]. This raises the electro-mechanical force and forms a centre of ageing in the form of microcavity-crazing. In this model, ageing is considered as the local reaction which changes the chemical or morphological moieties from their initial free energy state G_1 (reactant state) to a different free energy state G_2 (product state). G_1 and G_2 are separated along a reaction coordinate by the energy barrier G_a. The end of insulation life is considered when the number of moieties in energy state G_2 passes a specific critical number. When considering a single thermal ageing process the life equation is given by:

$$L = \left(K_f + K_{rv}\right)^{-1} \ln\left(\frac{A_{eq} - A_0}{A_{eq} - A^*}\right) \tag{1.18}$$

Where K_f, K_{rv} are forward and reverse reaction rate constants and defined elsewhere [54], A_t is a fraction of moieties in product state at time t, A_0, A_{eq} and A^* are values of A_t at the initial state, the equilibrium state and the critical state respectively. Such that A_{eq} is:

$$A_{eq} = \frac{K_f}{K_f + K_{rv}} \tag{1.19}$$

The presence of electrical stress in the model with space charge injection or field ionization raises the level of free energy G_1. The life equation becomes very complicated:

$$L = \frac{2h}{kT}\exp\left[-\frac{S_D}{k}\right] * \frac{\exp\left[\dfrac{H_{DK} - \left(C' E^{4b^*}\right) \div 2}{T}\right]\left\{\ln\left[\dfrac{A_{eq}(E) - A_0}{A_{eq}(E) - A^*}\right]\right\}}{\cos\left[\dfrac{K_D - C' E^{4b^*}}{2T}\right]} \tag{1.20}$$

The model is characterized by 7 parameters S_D, H_{DK}, K_D, b^*, C', A^*, A_0. These parameters have physical meaning and can be determined from different investigations. There is a threshold temperature and electric field in this model. This

model still has some disadvantages such as it is applicable for DC fields only (even though it can be fitted to AC data), it is valid for homogeneous materials, and it neglects the effect of electrode image charges.

All of the above models fit with experimental data but still have some drawbacks. More research is still needed to provide a more complete ageing model.

1.2. Project aims

The purpose of this project is to identify if impulse over-voltages affect the ageing processes of polymeric cable insulation and analyze possible ageing mechanisms that the insulation materials experience. In order to investigate the effect of lightning impulses on the ageing process of high voltage power cable insulation, various samples have been manufactured using a pre-designed mould tool. The samples are then electrically aged using the impulse generators of the Tony Davies High Voltage Laboratory. A real-time software based monitoring tool has been designed to control the impulse wave-shape and process the measurement data. Sets of identical lightning impulses were applied to samples and the aged samples were then electrically stressed to failure using a ramped AC applied voltage. The obtained results were analyzed using Weibull statistics to identify the difference, if any, in lifetime. Dielectric spectroscopy measurements were taken to investigate whether aged samples are lossier than unaged ones and show the polarisation capability of samples. Space charge measurements show that the charge profile behaviour changes under DC poling after ageing. All of the above results were used to confirm any change in electrical properties after lightning impulse ageing and highlight the mechanisms for this ageing process with respect to each type of material considered. To satisfy the fact that ageing is usually multi-factor additional thermal and UV ageing experiments were conducted. From the results, the mechanisms of each ageing process and their contribution to an overall multi-factor ageing process may be determined.

1.3. Contents of this thesis

Chapter 2 introduces the materials used in this study including polyethylene and crosslinked polyethylene for cable insulation applications. Chapter 3 discusses the theory of lightning impulses and considers impulse generation under laboratory conditions. The lightning impulse ageing process is also outlined in this chapter. Chapter 4 highlights the characterization experiments, namely electrical breakdown measurements, dielectric spectroscopy and space charge measurements used in this research. For breakdown measurements, Weibull statistics were used to determine electric field strength and the consequent impact on lifetime of the insulation. To support the hypothesis that lightning impulses age an insulation system, further analysis has been undertaken to assess the impact of impulses on both the dielectric spectroscopy and distribution of space charge. Chapter 5 gives details of the three ageing processes studied including how the samples were aged and parameters that need to be considered during ageing. Fourier transform infrared spectroscopy (FTIR) has been used to analyze any changes in chemical structure of the material including oxidation and chain scission. The results from FTIR can be used as the tool to test the effect of thermal and UV ageing on material samples. Chapters 6, 7 and 8 detail the results for AC breakdown, dielectric spectroscopy and space charge measurement respectively for all three ageing mechanisms. Finally, chapter 9 presents the discussions, the overall conclusions and outlines future work.

Chapter Two

Materials And Sample Preparation

2.1. Design of the mould tool, Rogowski profile sample

Disc-shape samples were produced by the heat-press method using a four part mould tool (Figure 2.1). The mould tool consists of one cylinder that encloses the piston and the electrode. The piston may attach to the electrode using the screw, but they have to be separable when releasing a manufactured sample. With reference to Figure 2.1 the flat metal plate is the base and mould carrier. A sheet of melinex (100 to 200 μm) was placed between the mould and the metal plate. There are three reasons that the melinex sheet is used. First, the melinex ensures the sample surface is uniformly even. Secondly, it makes the material flow more smoothly and allows effective bubble elimination. Finally, the sample is easier to detach from the melinex sheet as compared to the base plate. Material pellets are put into the manufactured mould and heated to melting temperature to ensure all material has melted. The mould is pressed by two hot plates up to a pressure of between one and two tons. Care is taken during

this pressing process to limit the variation of sample thickness. The basis of this process is that the more pressure applied, the more residual material is pushed out of the mould and the thinner sample becomes. If a very thin sample is needed, the extra melinex layer should be put between the piston and the electrode to prevent excessive pressure application that may result in a non-uniform thickness across the sample surface. This method has an advantage compared to vacuum methods as it ensures the elimination of all bubbles on the sample surface. The mould was quench cooled using cold water and the residual material that had been pushed also blocks water penetration into the sample within the mould. However, to make sure all water is removed, all samples were reheated at 70 to 80^0C in a vacuum oven for 30 minutes and then cleaned using acetone to remove any grease. The produced samples have a shape similar to plastic bottle caps, with a thick rim, flat bottom surface and an inner surface which follows a Rogowski profile (Figure 2.2). This profile was used to reduce the edge effects inherent with applying an electric field to finite dimension samples. The dimensions of the sample are shown in Figure 2.3, the central surface thickness is between 180μm to 200μm, with an outer diameter of 30mm and height of 5mm. Samples were produced in significant numbers to allow a large number of repetitive experiments ensuring results were not significantly affected by factors such as poor sample production.

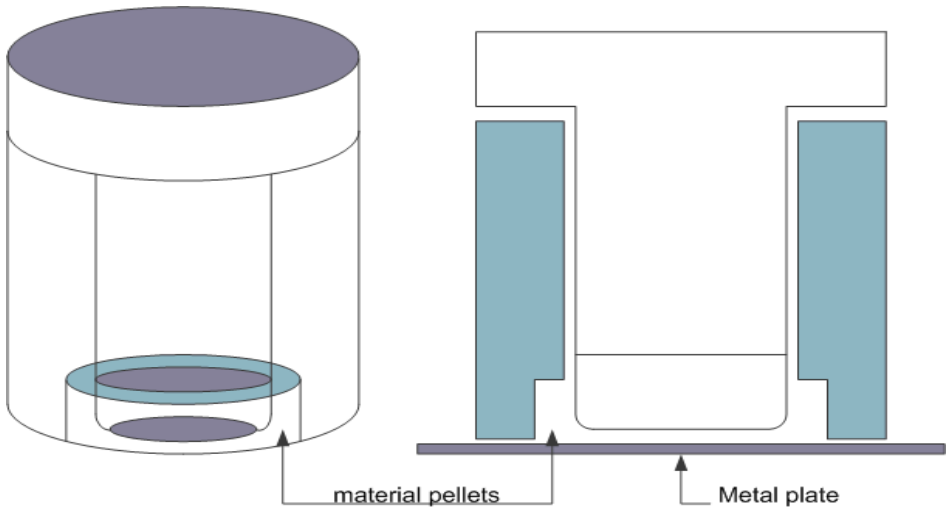

Figure 2.1: Mould tool to manufacture the samples

To ensure good electrical contact, the top and bottom surfaces were sputter coated with gold. This not only creates better contact between the sample and the electrodes but also produces an electrode that follows the profile of sample surface thus

reducing edge effects and the likelihood of triple junctions. Mushroom electrodes were used in the impulse ageing process to reduce electrical and mechanical deformation. The electrode design ensures that the electrical potential will be equally distributed through the sample.

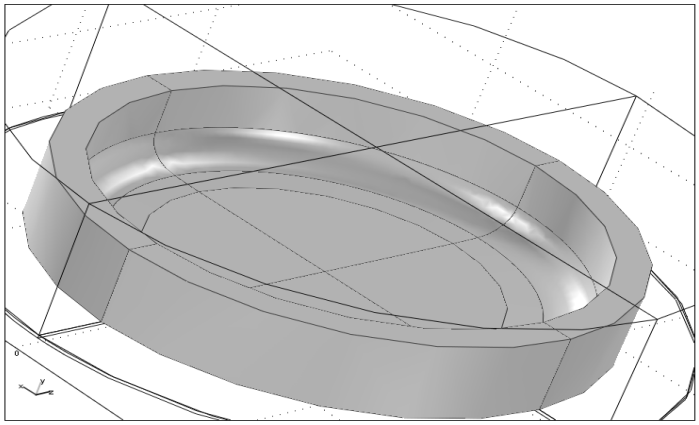

Figure 2.2: Schematic representation for moulded sample

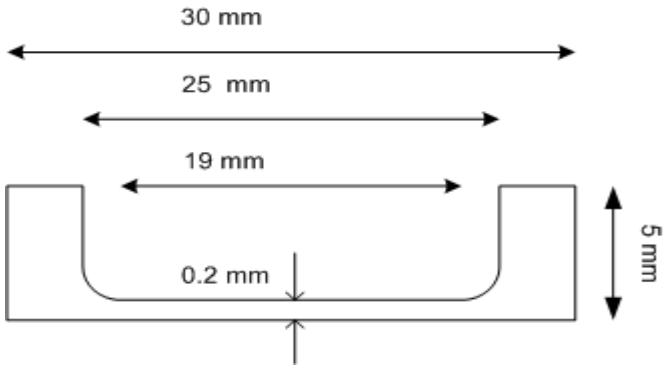

Figure 2.3: Sample dimensions

2.2. FEA analysis of the electrical stress profile

For finite dimension electrodes (small size), the electrical field is usually uniform across the middle region but will be higher at the edges. This leads to a problem when a constant electrical field is required across the sample or the breakdown voltage of sample is to be measured. To overcome the problem, electrode surfaces which follow the equipotential surface should be designed. Such an electrode profile is known as the Rogowski profile. The created samples have an inner surface follows the Rogowski profile and the flat bottom surface. In order to provide better

understanding of the effects of the Rogowski profile of the sample, the electric potential and the electrical field across the sample have been analyzed using a finite-element analysis package. The obtained results are shown in Figures 2.4 to 2.7 (the values shown are per unit values). Figure 2.4 shows the electric potential and electrical field across the sample with the sputter coated Rogowski inner surface or equivalently when the high voltage electrode is in contact with the surface of sample. From the results for the electrical field, there is no obvious electrical stress enhancement at the edge of sample. The electrical field is constant in the middle region of sample surface.

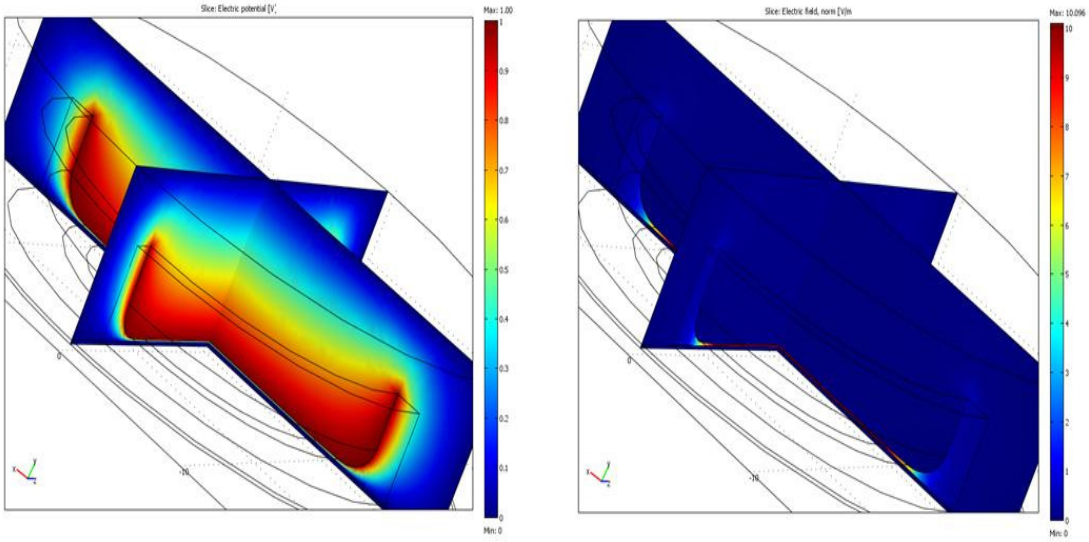

Figure 2.4: Electric potential and electric field distribution for sputter coated sample or HV electrode in contact with sample

From Figures 2.5 to 2.7, the effects of the types of electrode and sample coating are presented. For the un-sputter coated sample using a ball bearing electrode, there is a triple junction and field enhancement at the point where the electrode and sample contact. For sputter coated samples, both ball bearing and mushroom electrodes have no triple point and the electrical field is consistent across the middle region, however, the mushroom electrode provides the smallest mechanical deformation under an electric potential.

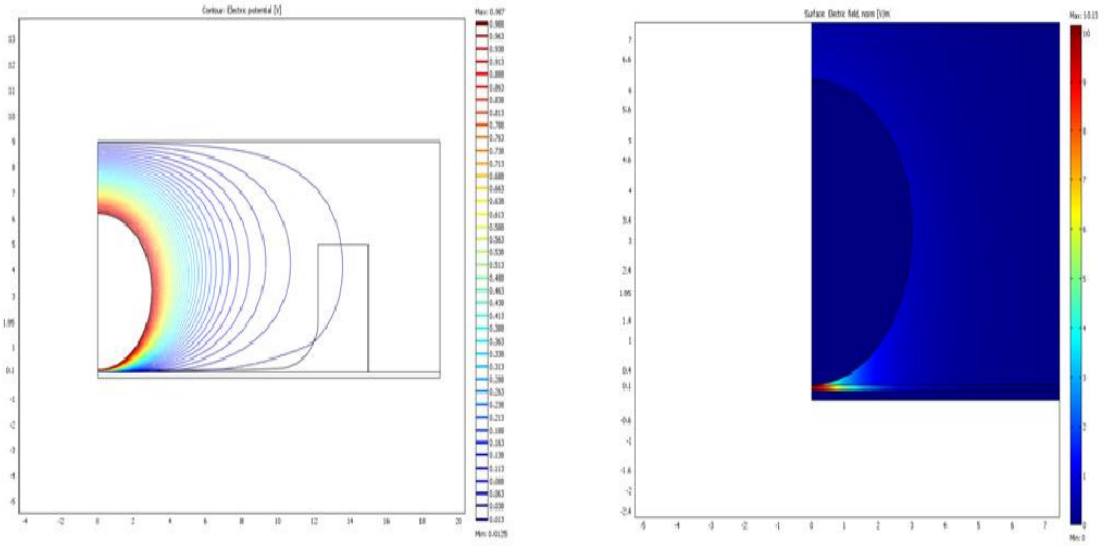

Figure 2.5: Electric potential and electric field distribution for un-sputter coated sample with ball bearing electrode

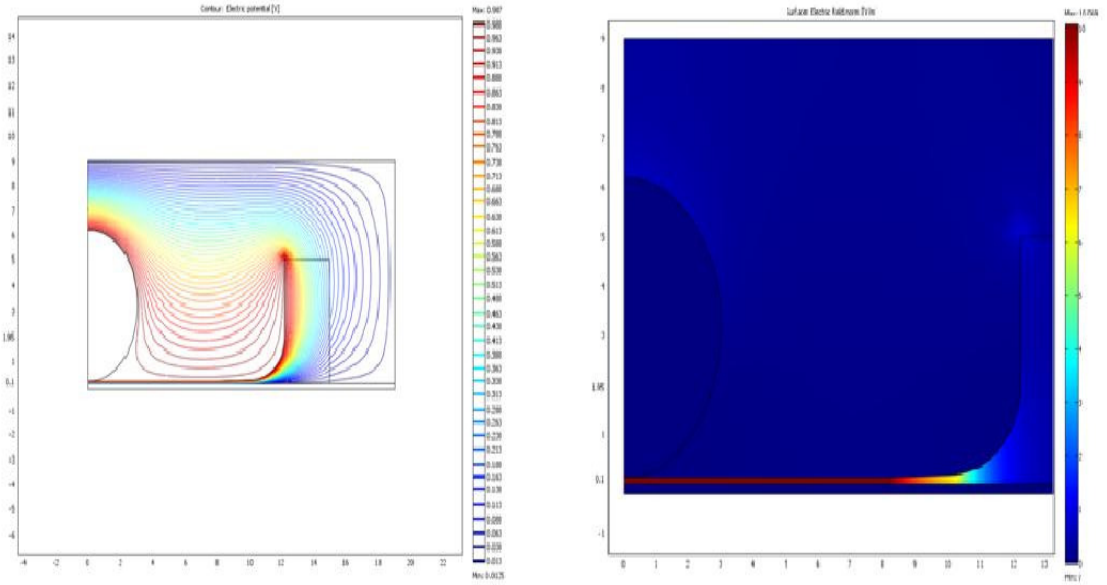

Figure 2.6: Electric potential and electric field distribution for sputter coated sample with ball bearing electrode

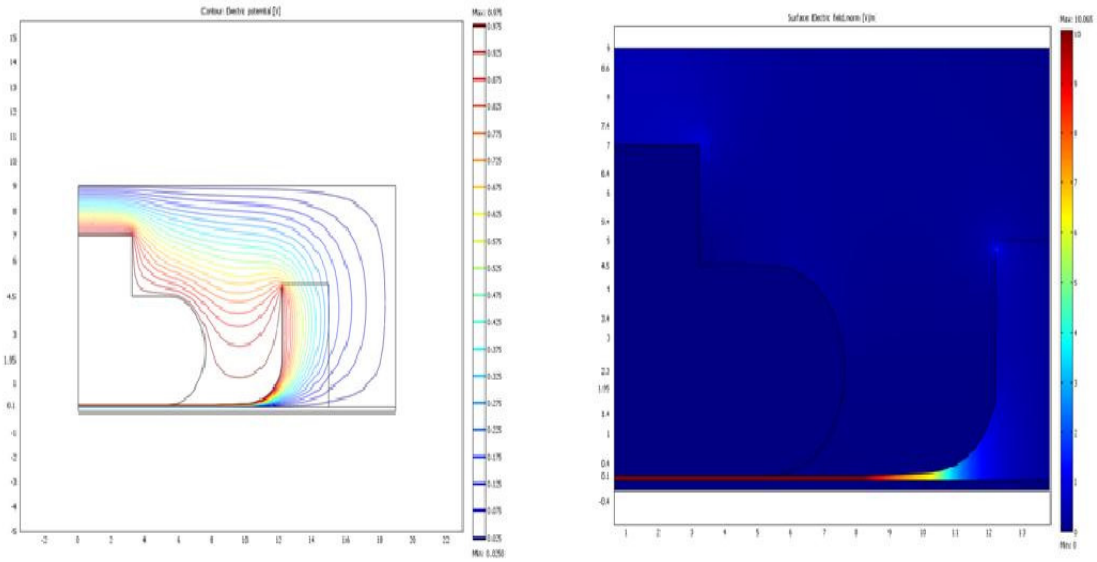

Figure 2.7: Electric potential and electric field distribution for sputter coated sample with mushroom electrode

2.3. Molecular structure and general properties of polyethylene

Polyethylene is the common name for the broad range of polymeric materials that have long carbon based chains of monomer ethylene. The basic chemical structure of pure polyethylene consists of many $–CH_2-$ groups linked together to form a longer backbone (Figure 2.8).

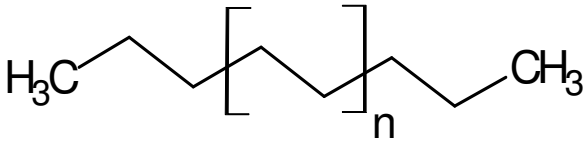

Figure 2.8: Structure of pure polyethylene

The degree of polymerization can vary from 8-100 for low molecular weight polyethylene (where the general properties are not associated with the plastic) to over 250000 for high molecular weight polyethylene. Polyethylene can also be branched at various degrees. Two main types of polyethylene are high density polyethylene (HDPE) and low density polyethylene (LDPE). The HDPE structure is very close to the pure polyethylene. Its branching level is very low and sometimes referred as linear polyethylene. A high degree of crystallinity can be achieved in HDPE and the

typical density is in the range 0.94-0.97 g/cm^3. However, HDPE is not generally used as cable insulation. In contrast, in LDPE the concentration of branches is higher than in HDPE and this hinders the crystallization process, so the density is lower. The density of LDPE is in range of 0.90-0.94 g/cm^3 [58]. The polymerization process of LDPE is from ethylene gas at high pressure, whereas, a low pressure or Ziegler-Natta method is required for polymerisation of HDPE. LDPE is used in many insulation applications to replace oil impregnated paper due to its higher electrical strength, lower dielectric losses, higher thermal conductivity, and greater chemical resistance. However, the use of LDPE is only suitable if its temperature is kept lower than 75^{o}C [28]. The solid state of polyethylene can be either a crystalline morphology or an amorphous morphology. However, real polyethylene is a semicrystalline polymer, which means the two morphologies are mixed together, as shown in Figures 2.9 and 2.10.

In the crystalline state, long polyethylene chains repeatedly fold back on themselves to create what are called “lamellae”. Polyethylene lamellae are usually from 5 to 20 nm thick. The interfaces of lamellae are not smooth since the chains are not equally folded. The surfaces of lamellae can go into other lamellae regions or stay in the amorphous region.

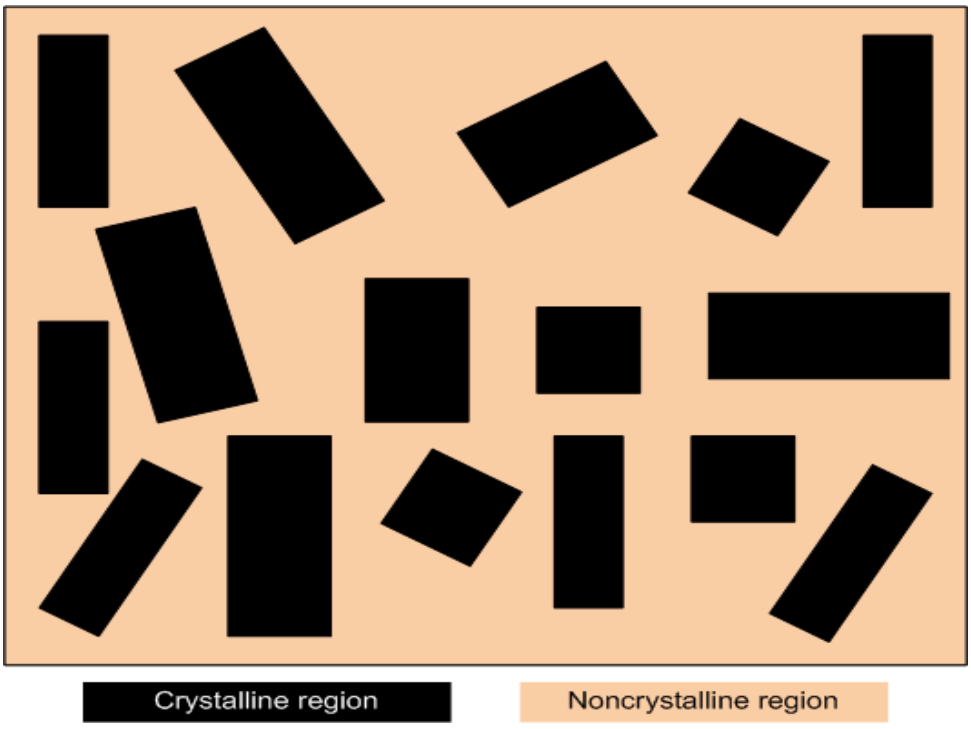

Figure 2.9: Semicrystalline morphology of polyethylene [58]

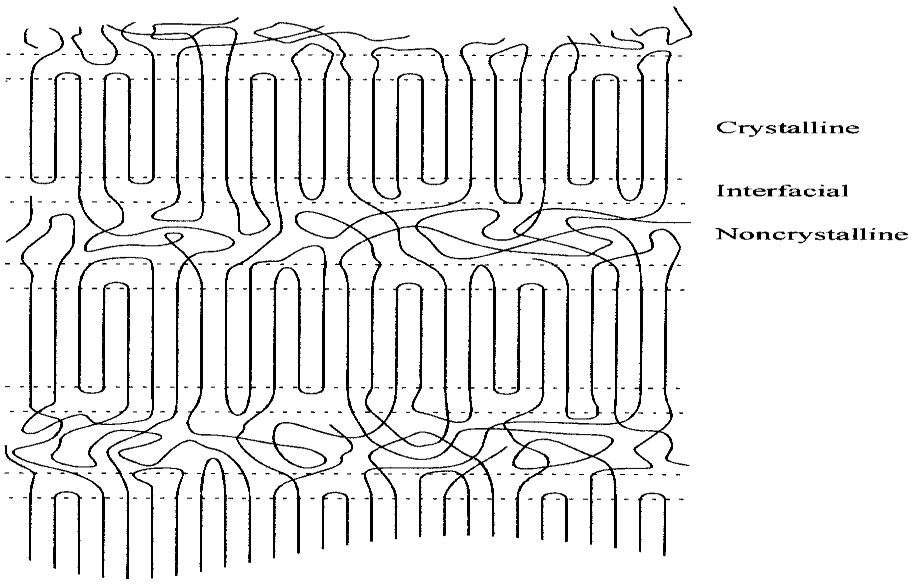

Figure 2.10: Three different regions morphology of polyethylene [58]

A group of lamellae can be brought together to form a "spherulite". In spherulites, lamellae are grown from the nucleus radially outwards. Depending on the concentration of nucleation sites the size of spherulites can vary from nanometres to millimetres. Figure 2.11 is a typical illustration of a spherulite in polyethylene [58].

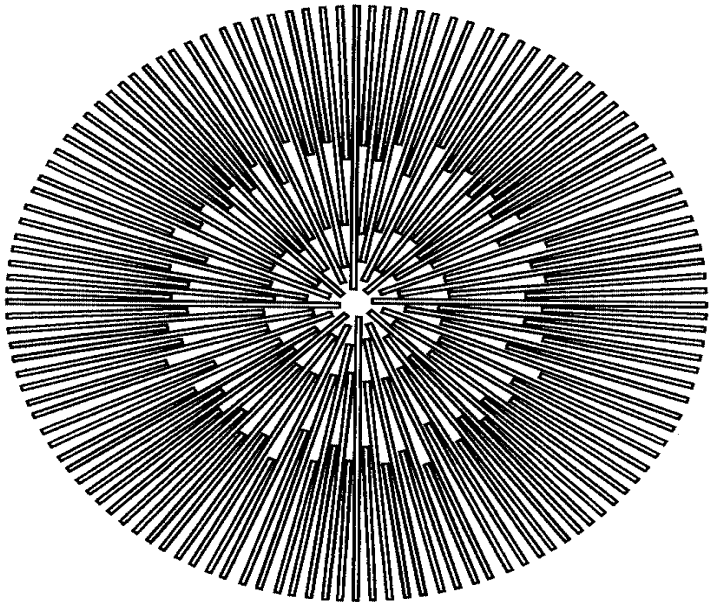

Figure 2.11: Spherulite in polyethylene [58]

The chains of polyethylene are not directly linked together but held together only by weak inter-molecular forces. When heat is applied to the material, the molecular chains move easily with respect to each other. However, at higher temperatures, a weakness of polyethylene is that it becomes soft (deformation) and the resistance to

tensile and creep forces are less than at room temperature. For a high voltage cable operating under normal working conditions, the transmission of electricity will produce a large amount of heat and hence polyethylene that has direct crosslinks between chains has been developed, i.e. crosslinked polyethylene (XLPE) is used for such applications.

2.4. Crosslinked polyethylene (XLPE) and crosslinking processes

XLPE improves heat resistance by holding the chains together by crosslinking and prevents them from moving or deformation under the presence of thermal stress. In XLPE the chains can be linked directly by carbon – carbon bonds or by bridging agent bonds. XLPE is essentially insoluble; this is in contrast to normal polyethylene which is soluble in appropriate solvents at high temperature. XLPE also has a very low degree of crystallization due to lack of chain movement. Therefore, the density of XLPE is usually lower than that of normal polyethylene. After crosslinking, the polymer is changed from a thermoplastic to a thermo-elastic polymer. That means at high temperature instead of melting, the material merely becomes more flexible. Nowadays, XLPE has gradually replaced oil impregnated paper in high voltage cable insulation. It also solves the heat resistance problem of LDPE. In fact, the application of XLPE can be found in very high voltage systems, 500kV power cable for example [59].

XLPE can be produced by chemical crosslinking (Engels/Azo process), or a silane process or an irradiation process. In chemical crosslinking, polyethylene with a high concentration of organic peroxide is held at an elevated temperature (higher than crystallized temperature) and high pressure. The peroxide produces free radicals which react with polyethylene to form carbon-carbon crosslinks (Figure 2.12). This method is also called the “hot” crosslinking process. This provides planar crosslinking (2 dimensions). Although it provides more consistent and uniform crosslinks it takes longer and is more expensive compared with other methods. The silane method is called a “moisture cure” method (Figure 2.13). In this method polyethylene reacts with organosilanes to form an initial product. The initial product, under heat and moisture, can link with a maximum of three more initial products to

form a three dimension crosslinking process. The crosslinks are not carbon-carbon bonds but silane side chains. The final product presents more pressure and heat resistance than the planar one. Both of these methods produce by-products in the form of peroxides, alcohols and organosilanes that need to be eliminated [59]. The final method is irradiation where the polyethylene is passed through an accelerated electron beam (beta or gamma irradiation). Free radicals are created and a planar carbon-carbon bond is formed. This method is not as efficient as the chemical method and the product is less consistent but is the cleanest one of the three.

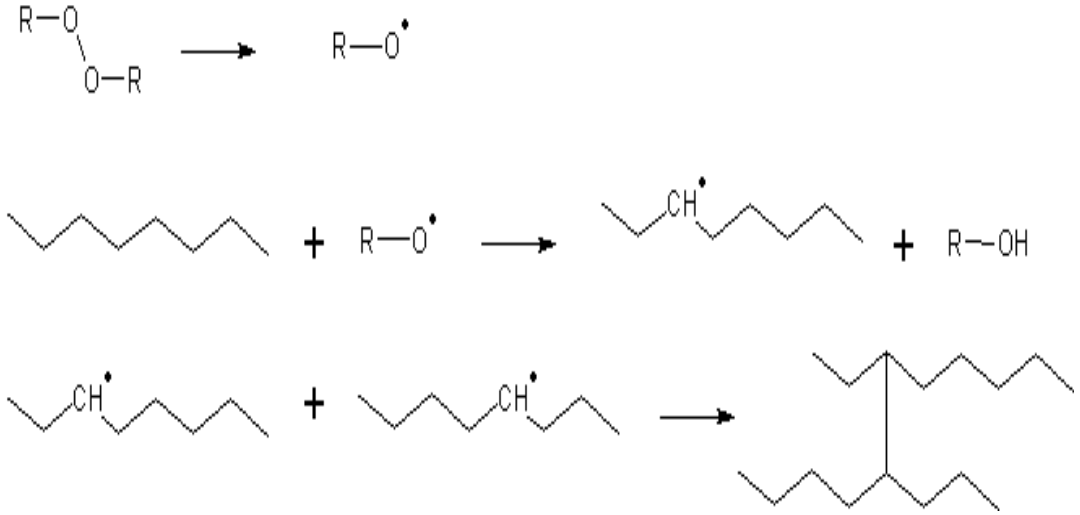

Figure 2.12: Peroxide crosslinking process

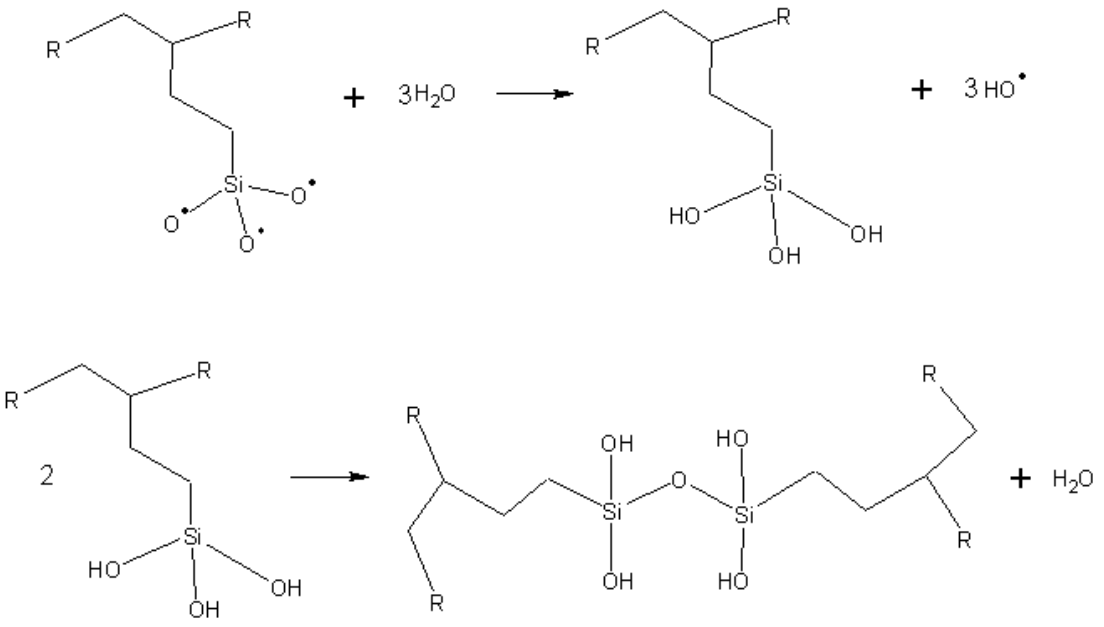

Figure 2.13: Silane crosslinking process

2.5. Materials and sample preparation

This research has considered several types of material including high density polyethylene (HDPE), low density polyethylene LD100 (LDPE), crosslinkable polyethylene using cure-moisture method LE4421 (LDPE4) and crosslinkable polyethylene using hot crosslinking method with different type of catalysts (Dicumyl Peroxide or Trigonox 145-E85).

HDPE from Sigma-Aldrich was used because it has similar thermal properties compared to XLPE. The material has a melt flow index (MFI) of 2.2 g per 10 minutes (190^{o}C/2.16 kg) and a transition temperature of 123^{o}C (MFI is inversely proportional to the molecular weight and the viscosity of the melt).

LDPE from Exxon Mobil Chemical for blown film applications was also used. The material has a MFI of 2 g per 10 minutes (ASTM D 1238) and transition temperature of 103^{o}C. This is a low density (0.923g/mm^{3}) branched polyethylene.

Both HDPE and LDPE were in pellet form. The pellets were put into the mould and heated to 180^{o}C to melt all the material. The temperature between the bottom hot plate and the metal base of the mould was checked using the handheld thermometer RS 206-3722. The results show that the measured temperatures (150^{o}C, 180^{o}C and 200^{o}C) are very close to the temperatures show on the front panel within a variation of ±0.4 K. After that, pressure of one ton was applied to push excessive material out of the mould. The sample was held under pressure for about one minute before the mould was quench cooled using tap water (not placed into a water bath). The water temperature was 15-17^{o}C and the temperature of the sink was 17^{o}C. The water flow was pointed to the central of the top of the mould to make sure the mould was cooled at a relatively constant rate. After 1 minute of cooling, the temperature of the bottom of the mould had reduced from 150^{o}C to 17.3^{o}C and was 16.1^{o}C after 2 minutes of cooling. All samples were cooled for 2 minutes. Received samples were cleaned and degassed in vacuum oven. For HDPE and XLPE melinex was used between the metal plate and the sample but this was not necessary for LDPE.

Low density polyethylene 4421 (LDPE4) is a branched polyethylene with grafted silane groups [60]. The pellets of LDPE4 were heated to 180^{0}C in a pre-shaped mould. When the material melted, a pressure of 1.5 tons was applied to push any

bubbles and residual material out of the mould. The mould was then quenched cooled using tap water. All created samples were then soaked in a water bath for 12 hours at 90^0C. After the crosslinking process, the gel content is about 35% and this is in agreement with the work of Hosier [60]. Details of the chemical reactions are shown in Figure 2.13. This crosslinking method is suitable for laboratory purposes, as the samples just need to be immersed in heated water to crosslink. The crosslinking process does not generate by-products in the form gases as in the method of peroxide crosslinking. The crosslinking process was undertaken after the samples were formed. Therefore, no bubbles were generated in the bulk. However, there are some disadvantages with this process. Firstly, the samples were in water for a long period, and consequently water can penetrate into the sample. Secondly, the crosslink bonds are not the carbon-carbon bond but the oxygen-silicon bond. The appearance of silicons and oxygens in polyethylene molecule may lead to a change in material characteristic. Finally, the cure moisture crosslinking method is not as consistent and uniform as the peroxide crosslinking method. After crosslinking the samples were heated in a vacuum oven at 80^0C for one hour to degas. The produced sample is referred as XL4

Trigonox 145-E85 is the mixture of 85% 2,5-Dimethyl-2,5-di(tert-butylperoxy)hexyne-3 and mineral oil (Figure 2.14) from AkzoNobel . The mixture is liquid at room temperature and was stored in the fridge. It can be used as the initiator for the crosslinking process of polyethylene (Figure 2.12). This peroxide is high-temperature peroxide, it is more stable with increasing temperature than Dicumyl peroxide. The half-life of trigonox145 at 150^oC is about 45 minutes and less than one minute at 200^oC [61]. The LDPE pellets were soaked into the Trigonox 145 to create the crosslinkable polyethylene (trigonox-LDPE). Under room temperature for five hours and following by one hour for drying out in 70^oC oven results in a concentration of 1.1% trigonox 145. Under 70^oC for five hours, the process results in 3.3% trigonox 145 concentration. The material was handled in the fume-cupboard. The trigonox-LDPE was safely heated at 150^oC for ten minutes before the pressure was applied (normally 1.5 tons) for about one minute. After releasing pressure, the mould was moved to another press at 200^oC to crosslink sample for 10 more minutes (this makes sure more than 70% of gel-content would be formed) [61]. As the decomposition products during the crosslinking (Figure 2.14) are gaseous, no

pressure was applied. Otherwise, the bulk would contain bubbles or a bad sample surface would be created. After the crosslinking reaction, the mould was quenched cooled using tap water for 2 minutes and the sample released from the mould. The crosslinked trigonox-LDPE (XL1 for 1% trigonox or XL3 for 3% trigonox) has a more opaque surface compared with the base LDPE.

A material HFDK4202EC for cable insulation from Dow chemical company was also considered. This is compounded thermoplastic polymer which contains less than 5% of Bis(alpha,alpha-dimethylbenzyl) peroxide and a base homo-polymer ethene. The sample preparation and the crosslinking process were similar to that for XL3. The chemical structure of the peroxide and its by-products are shown in Figure 2.15. Unlike XL3, the crosslinked polyethylene from HFDK4202 (DCP-XLPE) has a yellow colour. The more time of the crosslinking process the deeper the yellow colour becomes.

In order to check whether the sample was crosslinked or not, the sample was dissolved using boiling xylene. The gel component can then be extracted as it is not dissolved by the solvent. Crosslinking can also be checked by reheating samples to 180^{o}C or 200^{o}C. If the samples are not crosslinked, they melt and flow. The other way to recognize the peroxide crosslinked samples is observed the colour of samples; the crosslinked samples have a “brown” colour compared to uncrosslinked white samples. A sample was a good sample if it had a smooth surface, no visible bubbles across the testing area and the difference in thickness between the centre point and the thinnest side point of testing area was less than or equal to 5 μm. The success rate for producing uncrosslinked and silane crosslinked samples was 90%, whereas it was less than 70% for peroxide crosslinked samples.

Two surfaces of the sample were then sputter coated with gold using the gold coater EMITECH K550X (Figure 2-16). The sample is covered by a mask so that only the middle region is coated (Figure 2.17). Gold sputter coating is a cold coating method, therefore it does not disrupt the molecular structure of the material. The coating layer has a resistance across the diameter of about ten ohms and a thickness of less than one micrometre. Two coating layers act as the two electrodes providing good contact with the material. However, depending on the purpose of the specific experiments, some samples were not sputter coated. Table 2.1 shows sample condition for different experiments.

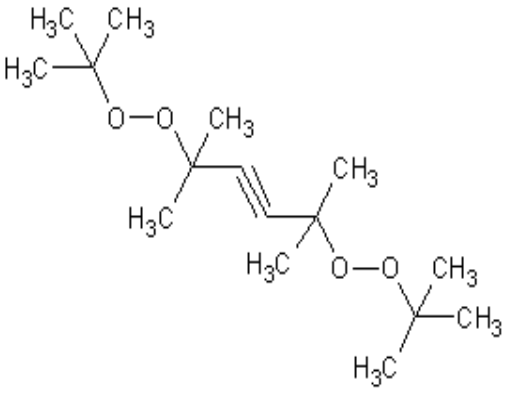

2,5_Dimethyl_2,5_di(tert_butylperoxy)hexyne_3

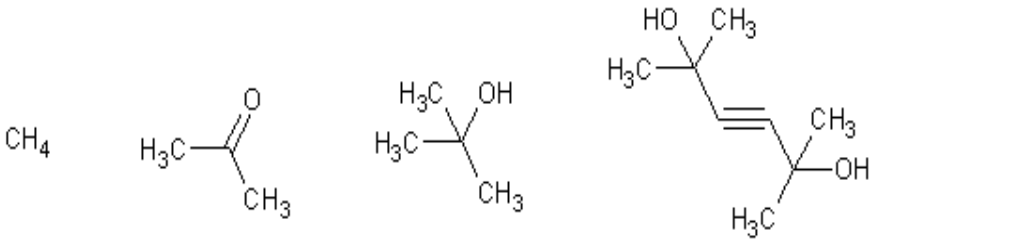

Methane Acetone tert Butanol 2,5_Dimethyl_3_hexyn_2,5_diol

Figure 2.14: Trigonox 145 and its main by-products after XL reaction

.

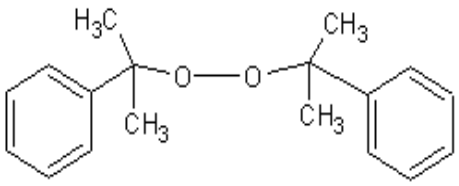

Dicumyl Peroxide

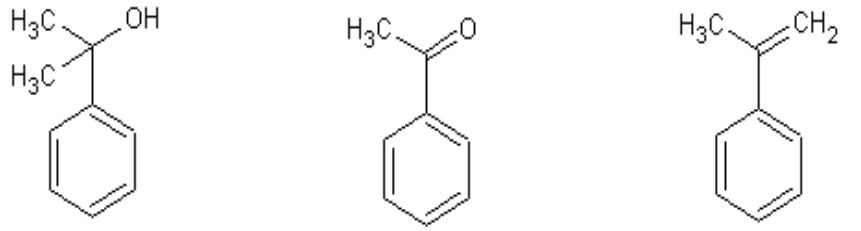

Cumyl Alcohol Acetophenone α Methyl Styrene

Figure 2.15: Dicumyl Peroxide and its main by-products after XL reaction

Experiments	Sample condition	Reason
Impulse, thermal, UV ageing + FTIR	Uncoated (150-170 μm)	Preventing IR wave reflection
Impulse ageing + Breakdown, Dielectric spectroscopy	Coated (180-200 μm)	Evenly electrical stress, good contact with electrode
Thermal, UV ageing + Breakdown	Uncoated (60-70 μm)	Sample may be tore after ageing
Thermal, UV ageing + Dielectric spectroscopy	Uncoated when ageing, coated after ageing (200 μm)	good contact with electrode
Impulse, thermal, UV ageing + Space charge measurement	Uncoated (150-180 μm)	Preventing flash-over during PEA measurement

Table 2.1: Sample conditions for different experiment

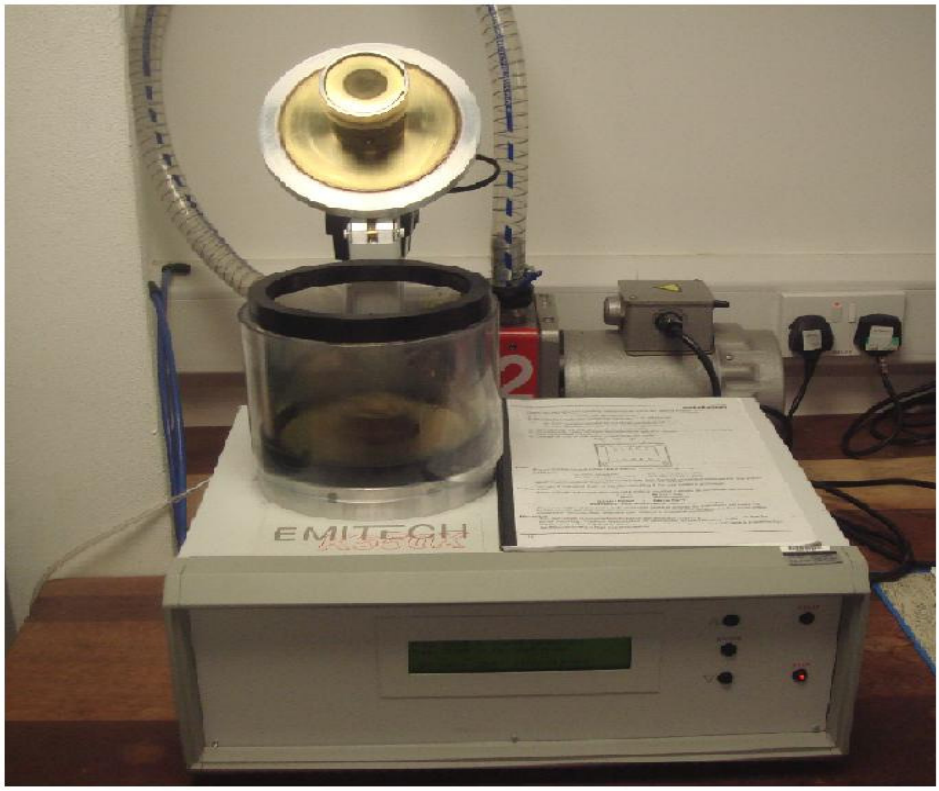

Figure 2.16: Gold coater

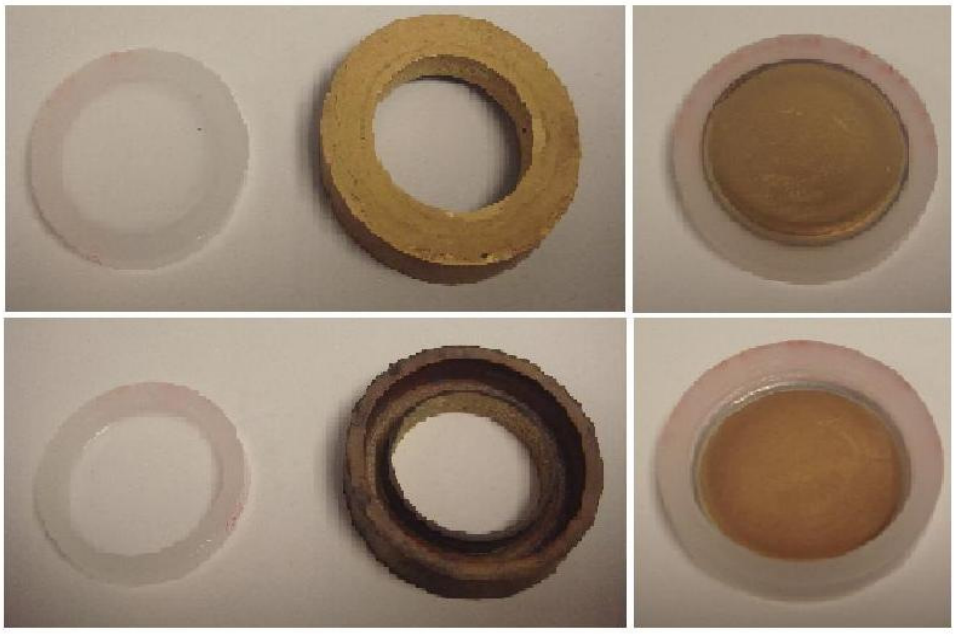

Figure 2.17: Sample coated covered by mask

Chapter Three

Impulse Over-Voltages

3.1. Impulse definition and its parameters

Lightning impulses and switching impulses are high voltage impulses that occur over extremely short times (μs for lightning and ms for switching) with high magnitudes. They frequently happen in electrical industrial systems due to lightning strikes, switching surges that travel along transmission lines as waves and cause damage to transmission systems, substations and elements. According to the IEC 60060-1 the smooth lightning (switching) impulse (Figure 3.1) is defined by a set of parameters [62, 63].

According to the standard the highest voltage, V_p is the peak value of the waveform. Where the waveform has a front time, T_1, that is 1.67 times the interval T_i between the instants when the impulse voltage is 30% and 90% of the peak value. The tail

time, T_2, is defined as the time interval between the virtual origin, O_1, and the instant when the voltage has decayed to half of its peak value.

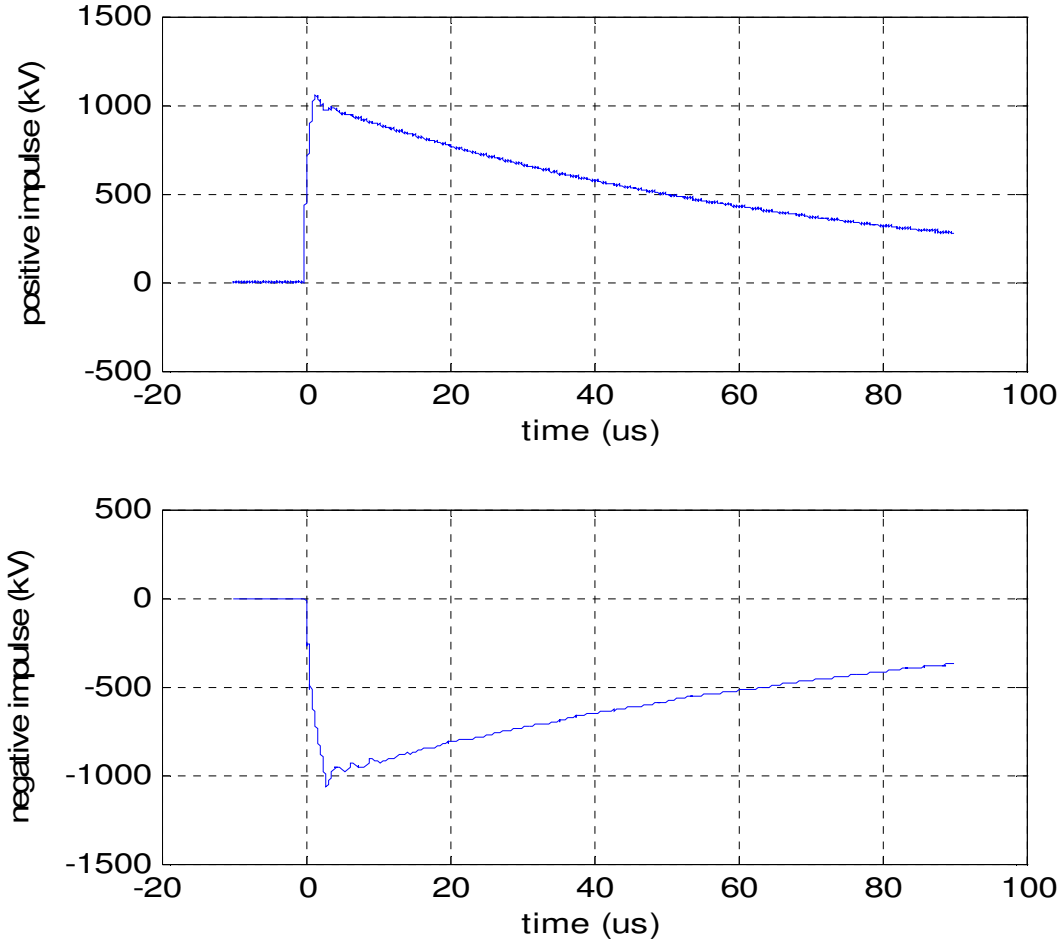

Figure 3.1: Typical lightning impulses

The virtual origin is characterised by the value of t_0 where:

$$t_0 = \frac{t_{90}v_{30} - t_{30}v_{90}}{v_{30} - v_{90}} \qquad \textbf{(3.1)}$$

Typically, the standard lightning impulse has a front time of 1.2 μs ±30%, a tail time of 50 μs ±20% and also the tolerance for variation of the peak value is ±3%. The time parameters for switching impulses are much greater than lightning, they are in order of milliseconds (0.25/2.5 ms). A mathematical formula that represents the smooth impulse usually used is:

$$v_{(t)} = A_i \left(e^{-\frac{t-t_0}{\tau_{i2}}} - e^{-\frac{t-t_0}{\tau_{i1}}} \right) \quad \textbf{(3.2)}$$

3.2. Lightning impulse generation, the mathematical origin of the waveforms

It is necessary to simulate the impulse in the laboratory for experimental purposes. There are several ways to generate the high voltage impulse, using either a single stage or multistage generator [64-66]. However, for simplification, only the single stage (Figure 3.2) will be analyzed here. In fact, in this research the single stage impulse generator was used to create 15 to 20 kV impulses because it is easier to manage a single stage generator at lower voltages compared to a two or multi-stage generator.

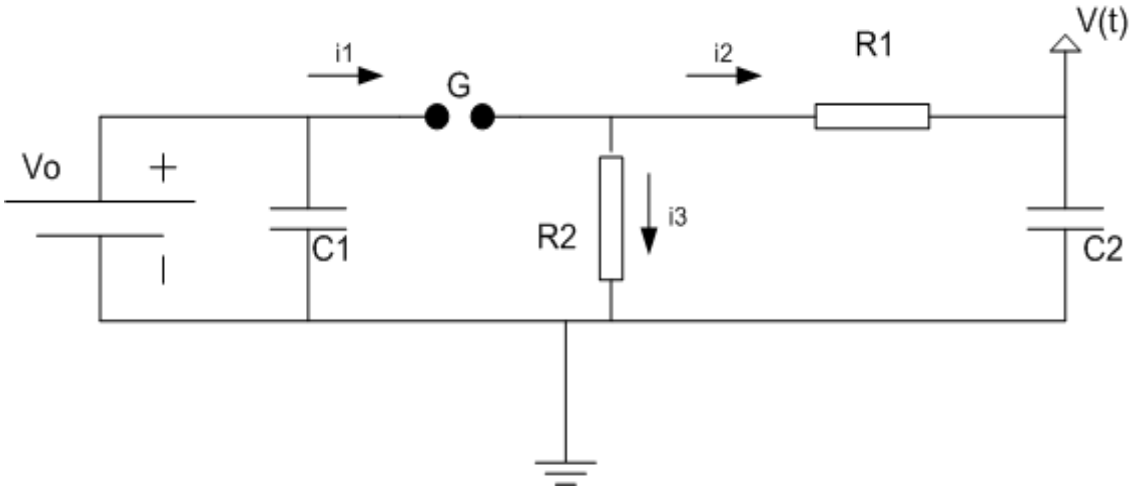

Figure 3.2: The single stage impulse generator circuit

With reference to Figure 3.2, the capacitor C_1 is charged from the DC source until the spark gap G breaks down. A voltage is impressed upon the object under test of capacitance C_2. R_1 and R_2 can be used to control the front and tail of the impulse voltage across C_2. This circuit can be analyzed using the Laplace transformation. Before the discharge (i.e. when t<0) the voltage across C_1 is equal to the DC voltage, V_0. The voltage across the output capacitor C_2 is arbitrary, (i.e. V_{C2}=V*). At the point when the voltage of C_1 exceeds the withstand voltage of the gap G (i.e. when t=0) then a current, i_1, will flow across the gap. Some current will flow through the

resistor, R_2 (i_3) and some will flow through output capacitor C_2 (i_2). Thus, in terms of voltages:

$$-C_1 \frac{dV_{C1}}{dt} = \frac{V_{C1}}{R_2} + \frac{V_{C1} - V_{C2}}{R_1} \quad \textbf{(3.3)}$$

Take the Laplace transformation:

$$-sC_1V_1 + C_1V_0 = \frac{V_1}{R_2} + \frac{V_1 - V_2}{R_1} \quad \textbf{(3.4)}$$

The current flow through output capacitor, C_2, is equal to the current flow across resistor R_1, therefore:

$$\frac{V_{C1} - V_{C2}}{R_1} = C_2 \frac{dV_{C2}}{dt} \quad \textbf{(3.5)}$$

Take the Laplace transformation:

$$\frac{V_1 - V_2}{R_1} = sC_2V_2 - C_2V^* \quad \textbf{(3.6)}$$

Substitute V_1 from Equation (3.6) to (3.4), after several manipulations, the output voltage, V_2, is obtained:

$$V_2 = \frac{sV^* + V^*\left(\frac{1}{R_1C_1} + \frac{1}{R_2C_1}\right) + \frac{V_0}{R_1C_2}}{s^2 + s\left(\frac{1}{R_1C_2} + \frac{1}{R_1C_1} + \frac{1}{R_2C_1}\right) + \frac{1}{R_1R_2C_1C_2}} \quad \textbf{(3.7)}$$

Assuming that at first instant (i.e. t=0) the output capacitor is free of charge, i.e. V*=0, the output voltage V_2 becomes:

$$V_2 = \frac{V_0}{R_1C_2(s + s_1)(s + s_2)} = \frac{V_0}{R_1C_2(s_2 - s_1)}\left(\frac{1}{s + s_1} - \frac{1}{s + s_2}\right) \quad \textbf{(3.8)}$$

Where $s_1 + s_2 = \frac{1}{R_1C_2} + \frac{1}{R_1C_1} + \frac{1}{R_2C_1}$ and $s_1s_2 = \frac{1}{R_1R_2C_1C_2}$

Transfer back to time domain to obtain the output voltage:

$$v_{(t)} = \frac{V_0}{R_1C_2(s_2 - s_1)}\left(e^{s_1t} - e^{s_2t}\right) \quad \textbf{(3.9)}$$

In practice, $R_2C_1 >> R_1C_2$, the output voltage then can be assumed to have the form:

$$v_{(t)} = V_0\left(e^{-\frac{t}{R_2C_1}} - e^{-\frac{t}{R_1C_2}}\right) \quad \textbf{(3.10)}$$

In case of V*≠0, the reverse Laplace transformation returns the separated double exponential (SDE) expression:

$$v_{(t)} = A_2 e^{-\frac{t-t_0}{\tau_{i2}}} - A_1 e^{-\frac{t-t_0}{\tau_{i1}}} \quad \textbf{(3.11)}$$

The impulse generator used in the Tony Davies High Voltage Laboratory is a two stage Marx impulse generator where the output voltage is twice the charging voltage but the general waveform shape is still the same. The circuit can also be modified to provide a single stage generator as shown in Figure 3.3. A HV transformer can supply maximum 100 kV AC voltage. The distance of a sphere gap is controlled by a motor and an integrated electronic trigger circuit. A DC output is measured via a resistive divider whereas AC and Impulse outputs are captured using capacitive dividers. To achieve the 1.2/40 μs lightning impulse, front and tail resistors are 375Ω-60W and 2400Ω-60W respectively. Figure 3.4 shows the 2 stage impulse generator as a reference. The impulse peak voltage can reach up to 200 kV for this circuit.

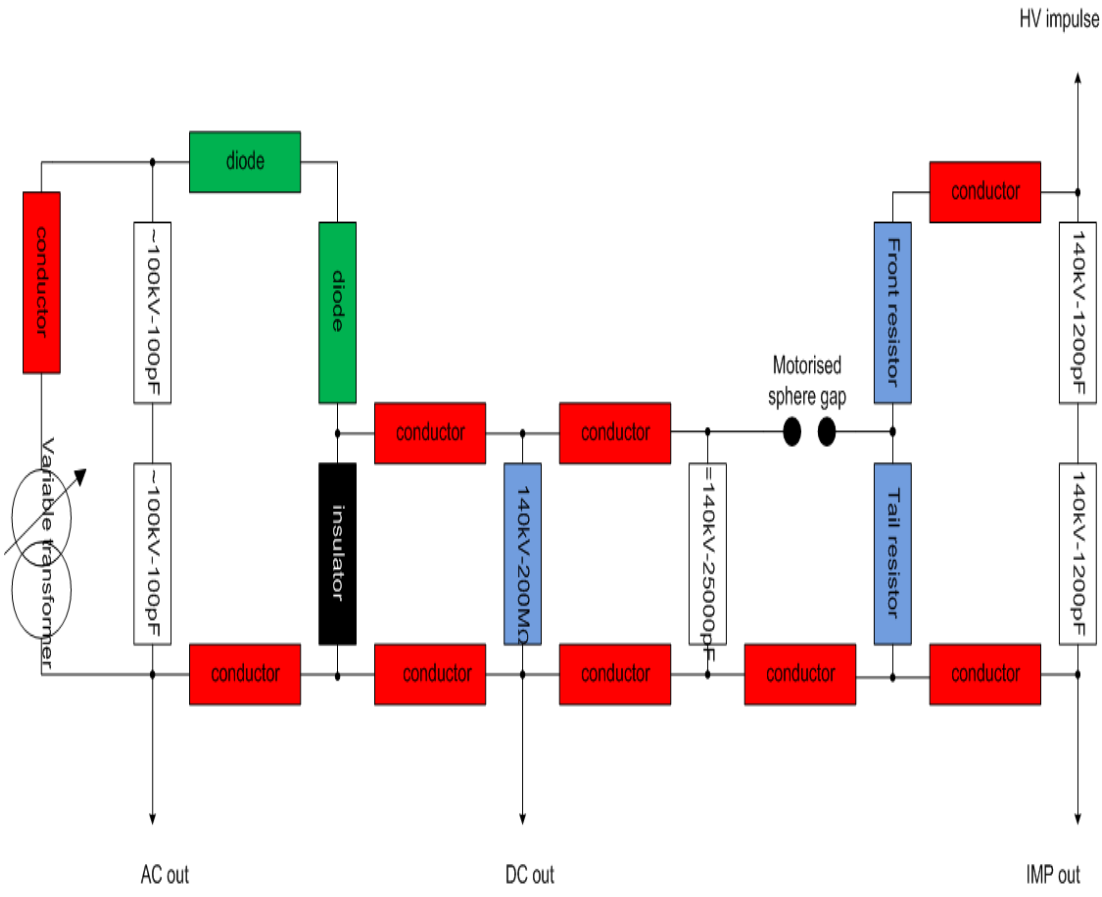

Figure 3.3: Impulse generator in Tony Davies HV Laboratory

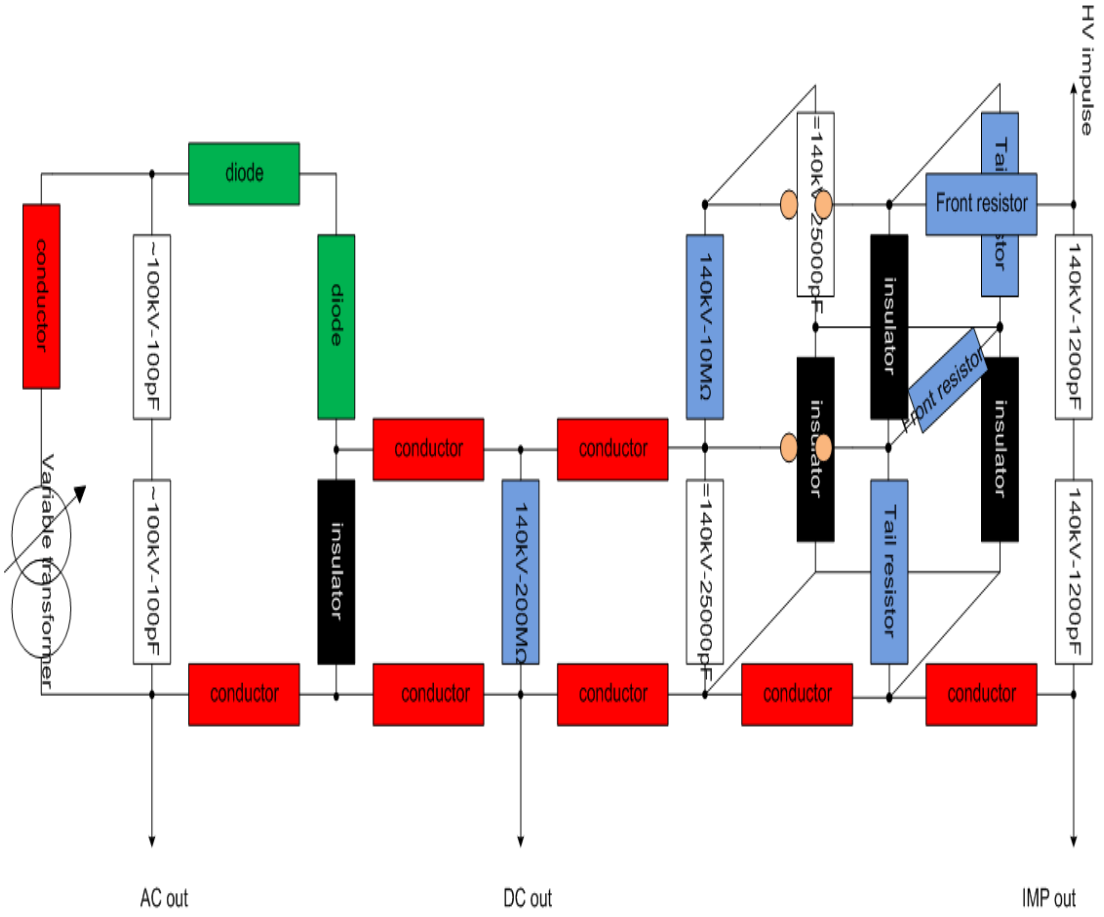

Figure 3.4: 2 stage impulse generator

During the process of impulse generation in the laboratory, the impulse waveforms are always superimposed with overshoots and oscillations due to electromagnetic noise around the working area. The additional noise reduces the accuracy of calculated parameters especially for lightning impulses which have time parameters of very small order. An evaluation for this type of impulse according to IEC 60060-1 (1989) is ambiguous. According to IEC 60060-1, the test voltage that will be determined depends on the frequency of the superimposed oscillation or the duration of overshoot. If the frequency of the superimposed oscillation is less than 500 kHz or the duration of overshoot is longer than 1μs then the test voltage is the peak of the original curve of data, otherwise the mean curve have to be built and this curve will be used for calculation. However, a frequency of 500 kHz is not related to any physical phenomena and there are ambiguities regarding to choice of the mean curve. There is a new approach to IEC 60060-1 where raw measurement data are first taken. Then the best fit curve is found and subtracted from raw data to create a residual. Applying the K-factor to the residual and summing the result with the best fit curve

provides a final curve that can be used for parameter calculation. The recommended K-factor filter has been developed at the University of Southampton [67]. A problem with this approach is how to choose the best fit curve, where the use of a traditional double function raises some issues in the choice of the virtual origin and the goodness of fit to raw data. To overcome those difficulties several ways have been proposed to choose the best curve. One of them is to use a separated double exponential function (SDE) instead of the normal double exponential (DE) [68]. This equation may be the simplest one that provides both flexibility of virtual origin choice, high repeatability and goodness of fit. Compared with other proposals this equation gives a smaller residual with raw data and the virtual origin is automatically selected during the fitting process (this overcomes the difficulty of the DE method where the correct virtual origin has to be chosen to give a good result in fitting that sometimes is not obvious). This equation can be rearranged into a form of DE with an added delay time to the second term:

$$v_{(t)} = A_2 \left(e^{-\frac{t - t_0}{\tau_{i2}}} - e^{-\frac{t - t_0 - \tau_{i1} \ln \frac{A_1}{A_2}}{\tau_{i1}}} \right) \qquad \textbf{(3.12)}$$

To have a form that is a close match to the DE function, some assumptions have to be made, therefore DE also is not a perfect representation for the impulse waveform and neglected terms may be responsible for the equivalent of an added delay time. Furthermore, the proposed SDE method gives a better fit and flexibility of origin choice.

A program, which is shown in Figure 3.5, has been written in Labview (Appendix A) to process the impulse waveform and calculate its parameters [69-71]. The data obtained by the digital oscilloscope is loaded by a GPIB port and processed using the data processing program. The original waveform is displayed on “samp1 origin” window where the filtered waveform is displayed on “samp1 final” window. Data for temperature, atmospheric pressure and relative humidity can be manually supplied by user. The humidity, pressure and temperature factors are included in the calculated lightning impulse parameters. When samples are immersed in silicone oil, the humidity factor can be set to unity and the button which is labelled “completely wet test”, has to be pressed.

This program supplies the outputs of front time, tail time and peak voltage of the lightning impulse. The waveforms are fully filtered by the low pass zero phase filter (based on K factor) and fitted by the separated double exponential equation. During the experiment, the capacitances of 7 parallel samples need to be taken into account as they affect the front time of the lightning impulse.

Figure 3.6 shows the program which manages the risk of breakdown during the impulse ageing process. The data are supplied by the oscilloscope and integrated to provide an area under the curve. Two consecutive areas are compared. If the difference between them is greater than 20%, breakdown occurs and signal will be sent to an external relay. The relay communicates with the software through a serial port. This can be set via "VISA resource name" control. When breakdown occurs, an indicator "1 fail" is activated.

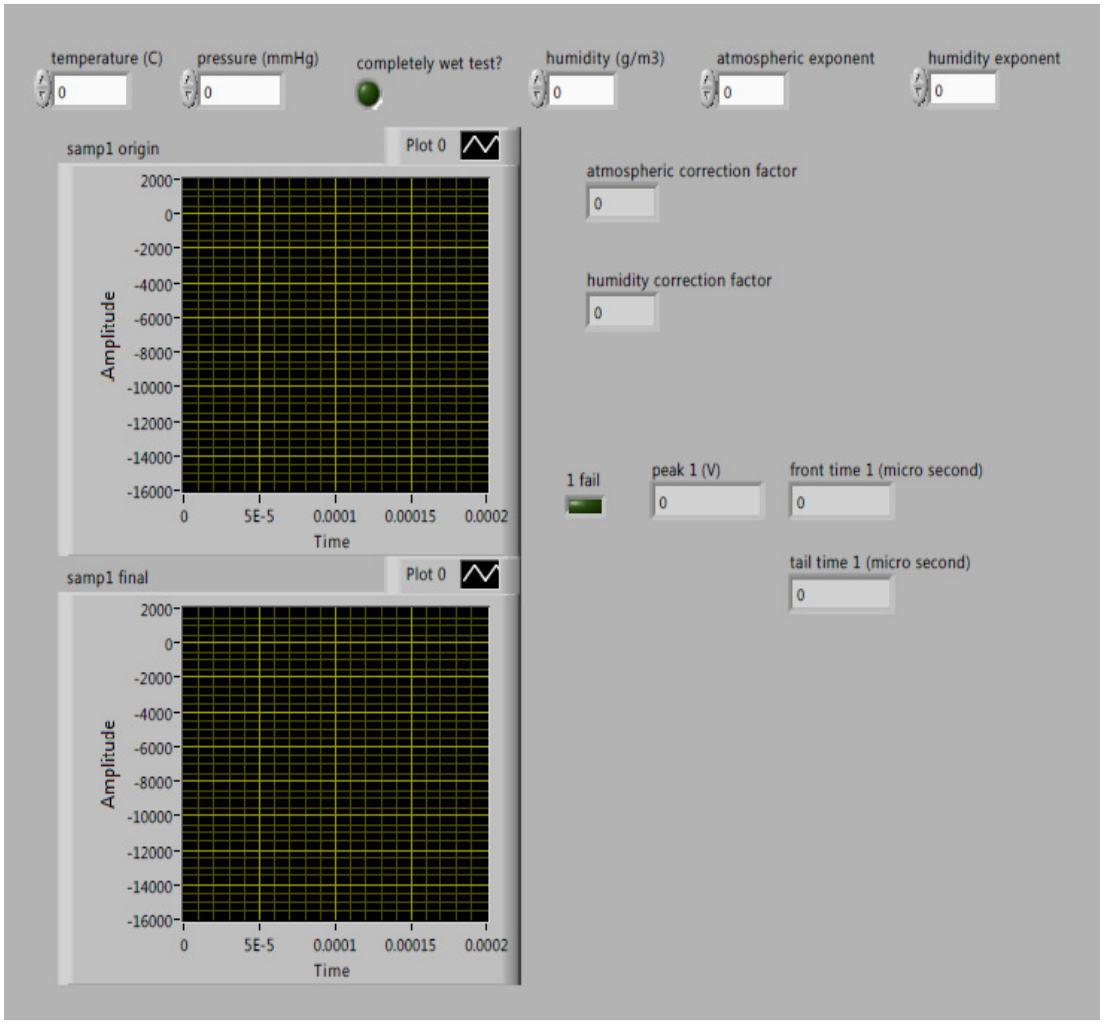

Figure 3.5: Lightning impulse parameters calculating program

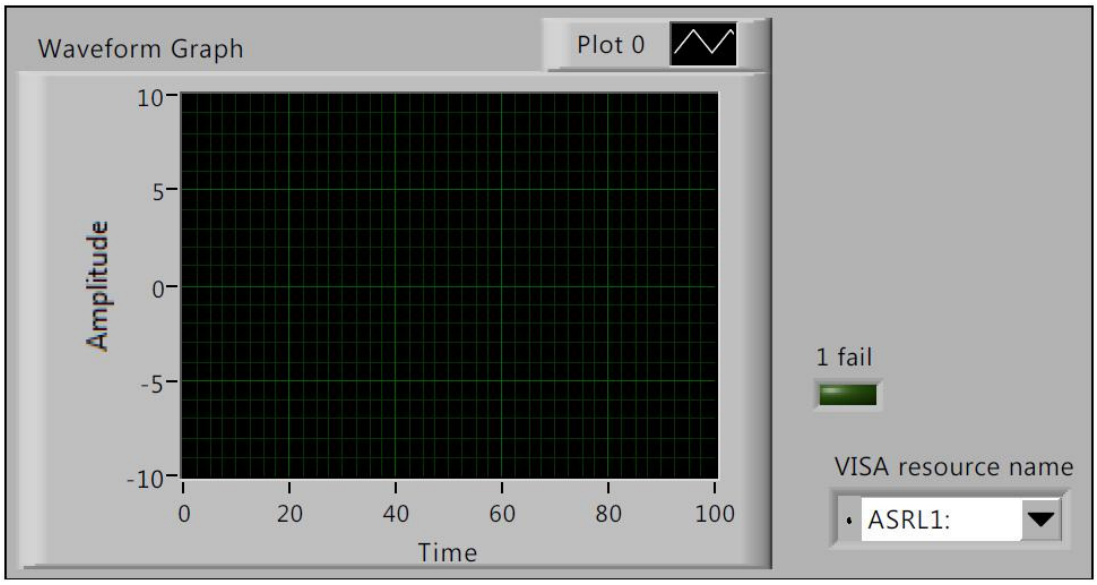

Figure 3.6: Area checking and relay controlling program

Chapter Four

Theory on Characterisation Experiments

4.1. Electrical breakdown characteristics of polymeric insulation

Electrical breakdown is a very common measurement that can be used to characterize insulation materials. Breakdown in gases is understood in more detail than the process of breakdown in insulating liquids or solids. This research is concerned with cable polymeric insulation systems and therefore the mechanisms for breakdown in gases and liquid will not be discussed. Due to the statistical nature of breakdown, the theory of statistic distributions is considered in order to justify the choice of analytical method used for this research.

4.1.1. Breakdown mechanisms in solid insulation

Breakdown in solid dielectrics is not as well understood as breakdown in gases or liquids. However, there is a lot of research involving the measurement of breakdown

strength of polymeric insulation materials. Unlike gases or liquids that can easily change shape with respect to electrodes or containers and can be easily penetrated, solid dielectrics have a fixed shape and most of the time are opaque. It is therefore hard to detect and observe what happens inside the solid. Solid dielectrics are not only used as insulators but can also be used for mechanical support of the conducting parts of the whole system. Practical solid dielectrics are imperfect. They can contain defects, voids, water, or are inherently inhomogeneous. Sometimes, insulation design requires a combination of solid, liquid and/or gas dielectric materials (liquids can be added to fill air gaps between solids; liquids and gases can be used to improve thermal properties). The breakdown process of a solid is influenced by many external factors, for example, temperature, humidity, pressure applied to electrodes, duration of tests [65], as well as the type of applied voltage (AC, DC, impulse, or combination of them [72, 73]). Based on the time taken for breakdown to occur, some breakdown mechanisms for solid insulation have been proposed (Figure 4.1).

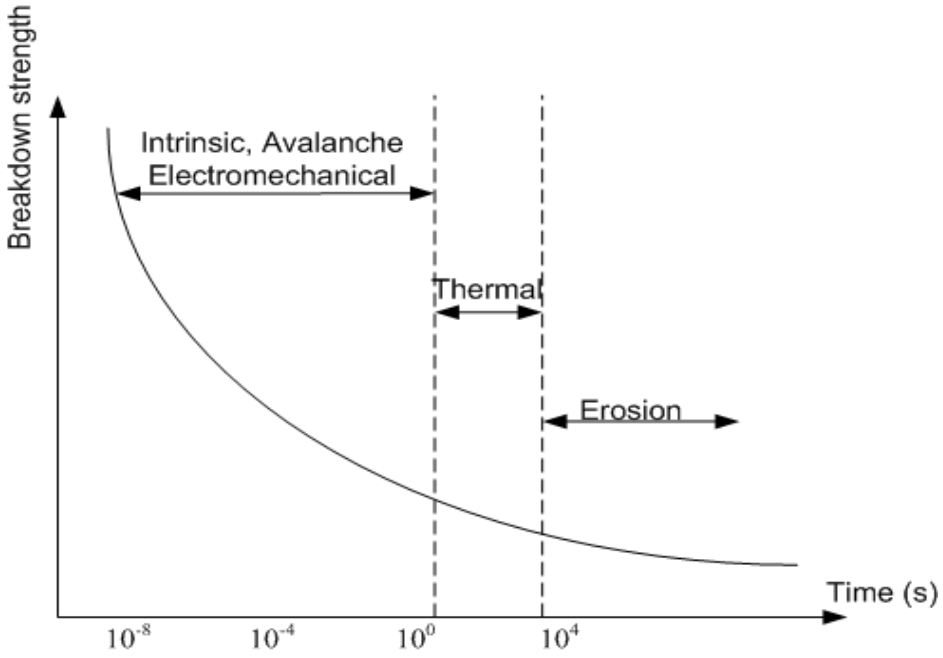

Figure 4.1: Breakdown mechanisms against time of stressing [65]

For a range of less than a second, failure can be due to intrinsic, avalanche or electromechanical breakdown, for longer times (order of minutes to hours) it is due to thermal breakdown and for very long times before breakdown occurs, it can be the result of erosion including partial discharge, water treeing or electrical treeing. The electrical breakdown (intrinsic, avalanche) is due to electronic processes, while thermal breakdown is caused by joule heating, leading to thermal excitation.

Electrical ageing is related to electrochemical processes and ultimately molecular structure modification.

- **Intrinsic breakdown**

Assuming that the material under test is pure and homogeneous, and the sample temperature and environmental conditions are carefully controlled, then when a sample is stressed for a short time with a very high voltage, the electric field will attain an upper limit which is called the intrinsic electric strength. Intrinsic strength is a property of the material and depends on temperature only. Intrinsic breakdown will occur over a time period of the order of 10^{-8}-10^{-7} seconds and is an electronic process in nature [65]. It does not depend on the waveform or duration of the applied voltage. For polyethylene, its value is well in excess of 10^6V/mm [74]. The intrinsic strength is generally assumed to be reached when electrons in the insulator gain sufficient energy from the applied field to cross the energy band gap from the valance to conduction band. The criterion condition is formulated by solving an equation for energy balance between the gain of electron energy from the applied field and its loss to the lattice known as electron-phonon scattering. The rate of energy gained by electrons from the applied field, Q_1, is the function of field strength E and lattice temperature T. The rate at which this energy is transferred to the lattice, Q_2, depends only on T. In addition, both rates depend on parameters describing the conduction electrons. Assuming these parameters can be collectively represented by W_e, then for steady state conditions, the energy equation for conduction electrons may be expressed as:

$$Q_1(E, T, W_e) = Q_2(T, W_e) \qquad \textbf{(4.1)}$$

When Q_1 exceeds Q_2, breakdown will occur.

- **Avalanche breakdown**

This mechanism is an extension of avalanche breakdown in gases and was originally proposed by Seitz [65]. When an electron enters the conduction band, under the influence of an applied field, the electron drifts towards the anode. If the mean free path is long enough and the electron gains energy that exceeds the lattice ionization energy, it can release another electron during collision inside the lattice. The process is repeated, an electron avalanche will be formed leading to breakdown. The main problem with this proposed mechanism is how the electron can gain enough energy

with such a small free path available in a solid dielectric. O'Dwyer postulated that beside the electron created by collision ionization, electrons injected from cathode also have a crucial effect [75]. They can stay near cathode and distort the local field making it much higher than the average field. As a result, the electron avalanche forms and leads to final breakdown. This model can explain the dependence of electric strength with thickness of material but fails to explain many other phenomena.

- **Electromechanical breakdown**

When the electrostatic compression force exceeds the mechanical compression strength of material, the material may collapse. The compression forces arise from the electrostatic attraction between surface charges which appear at the electrode interface when the voltage is applied. The compression force is restrained by the elastic force. Stark and Garton suggested that, when a material is in equilibrium, the following relation is satisfied [76]:

$$\frac{1}{2}DE = \frac{1}{2}\varepsilon_r\varepsilon_0\left(\frac{V}{d}\right)^2 = Y\ln\left(\frac{d_0}{d}\right) \qquad \textbf{(4.2)}$$

Where D is dielectric displacement, d is the thickness of material after stress, d_0 is the initial thickness of material, ε_0 is permittivity of free space, ε_r is the relative permittivity of material and V is the applied voltage. Differentiating Equation (4.2) with respect to d, V is found to be a maximum when:

$$\frac{d}{d_0} = \exp(-0.5) \approx 0.6 \qquad \textbf{(4.3)}$$

If the applied voltage reduces $\frac{d}{d_0}$ to less than 0.6, the material will collapse. The maximum value for electric field that can be applied before the material becomes unstable is:

$$E_{max} = \frac{V}{d_0} = 0.6\left(\frac{Y}{\varepsilon_0\varepsilon_r}\right)^{1/2} \qquad \textbf{(4.4)}$$

A practical solid material is not homogeneous and the surface is not completely smooth, it therefore can suffer from shear stress as well. This means that some regions of the material have to stand a higher local stress than others.

- **Thermal breakdown**

When a material is subjected to an electric field, heat can be generated due to conduction current, dielectric loss and polarisation. If the heat is continuously generated and cannot be extracted fast enough, a condition of instability will be reached where the rate of heating exceeds the rate of cooling, resulting in thermal runaway, and the sample may undergo thermal breakdown (Figure 4.2).

This can be seen as a loop effect where the electrical conductivity of dielectrics increase with increasing temperature. As the conductivity increases, the dielectric conducts more current causing more heat to be produced. Thermal breakdown obeys conservation of energy such that this heat generated equals heat absorbed by material plus heat lost to the surroundings. For a cubical specimen , it is represented as the following equation [65]:

$$\sigma E^2 = C_v \frac{dT}{dt} + \mathrm{div}[K\,\mathrm{grad}(T)] \qquad \textbf{(4.5)}$$

Where C_v is the thermal capacity, K is thermal conductivity and σ is electrical conductivity. In the case of alternating current, heat is mainly generated by dipole relaxation, the conductivity term σ is replaced by $\omega\varepsilon_o\varepsilon_r''$ where ε_r'' is the imaginary part of the complex permittivity and ω is angular frequency.

The equation cannot be solved analytically since C_v, K and σ are the functions of temperature. Two extreme cases are considered. The first one is “impulse thermal breakdown” where the build up of electrical field is so rapid that the heat loss to surroundings can be neglected, all heat is therefore absorbed by the material. If an impulse voltage is applied to the material, the temperature of the material will rise very fast within a short time, when the material reaches a certain temperature it will breakdown. The breakdown strength in this case depends on the duration of the impulse but not the size or shape of material. The second case is “minimum thermal breakdown voltage”. In this case the material has a chance to heat up to its maximum temperature (at the centre point in a thick specimen), after it reaches a maximum temperature all heat is assumed to be transferred to surrounding area, then when the voltage is increased the specimen will reach a critical temperature and breakdown. The thermal breakdown strength is independent of the thickness of the larger specimens but is proportional to the square root of thickness for thin materials [65]. The thermal breakdown strength with an applied AC voltage is always lower than

that for a DC applied voltage due to the large amount of heat generated by dielectric losses as the frequency of the applied voltage increases.

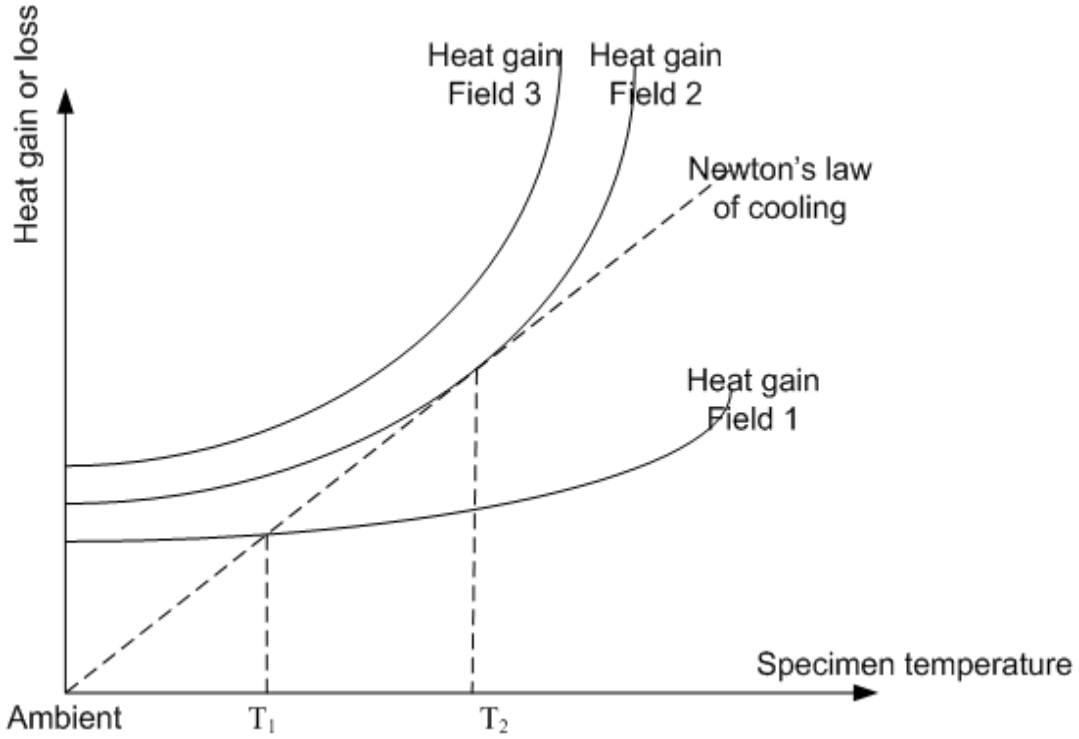

Figure 4.2: Thermal stability or instability under different applied fields

4.1.2. Statistical analysis of breakdown and material lifetime

The Weibull distribution is commonly used to model the time until failure of many physical systems [77, 78]. The parameters in this distribution provide good flexibility to model lifetime especially for electrical insulation materials. It is the third of three extreme value distributions [79, 80]. The first extreme value distribution is known as Gumbel's distribution and can be used to model ramp breakdown initiated by a distribution of field-enhancing defects or partial discharges in voids. However, Gumbel's distribution has some disadvantages compared to the Weibull distribution. Extreme value distributions are concerned with the distributions of maximum or minimum values of a number of random variables. Consider the random variables X_g where g = 1,2,…n which are continuous, independent and identically distributed with a probability distribution function (PDF) of $F_X(x)$,and probability density function (pdf) of $f_X(x)$. If the maximum value of X_g is Y_n and the minimum value is Z_n then the PDF and pdf of Y_n are defined as:

$$F_{Yn}(y) = (F_X(y))^n \quad \textbf{(4.6)}$$

$$f_{Yn}(y) = \frac{dF_{Yn}(y)}{dy} = n\left(F_X(y)\right)^{n-1} f_X(y) \quad \textbf{(4.7)}$$

Similarly, for Z_n:

$$F_{Zn}(z) = 1 - \left(1 - F_X(z)\right)^n \quad \textbf{(4.8)}$$

$$f_{Zn}(z) = \frac{dF_{Zn}(z)}{dz} = n\left(1 - F_X(z)\right)^{n-1} f_X(z) \quad \textbf{(4.9)}$$

As n is increased (tending to infinity) such that Y_n will tend towards Y_∞, the selection of the type of $F_X(x)$ depends on the distribution tails of X_g and results in three types of extreme value distribution.

When $F_X(x)$ has an unbounded right tail, it is of the exponential form:

$$F_X(x) = 1 - e^{-g(x)} \quad \textbf{(4.10)}$$

And this results in Gumbel's distribution

$$F_Y(y) = e^{-\exp\left[-\alpha_1 (y - \alpha_2)\right]}, -\infty < y < \infty \quad \textbf{(4.11)}$$

Where α_1 is greater than zero and along with α_2 are two parameters of the distribution. An interesting characteristic of this distribution is its skewness coefficient, γ_1, (defined as the third statistical moment, that gives a measurement of the symmetry of the distribution) in this case γ_1 is equal to 1.1396 and is independent of both α_1 and α_2 . The probability density function will have a dominant tail on the right. An example of Gumbel's distribution is shown in Figure 4.4.

The expression for $F_Z(z)$ is:

$$F_Z(z) = 1 - e^{-\exp\left[\alpha_1 (z - \alpha_2)\right]}, -\infty < z < \infty \quad \textbf{(4.12)}$$

The limit of using Gumbel's distribution in lifetime prediction is that this distribution has only two parameters, where one is for location (α_2) and the other for scale (α_1), it does not have a shape parameter as in the Weibull distribution. The second problem is that for negative time a probability of failure still exists, this is not realistic.

The second type of asymptotic distribution of extreme values is obtained by choosing $F_X(x)$ of each X_g that has the limit on the left of zero and an unbounded tail that approaches 1 on the right

$$F_X(x) = 1 - ax^{-b}, a > 0, b > 0, x \geq 0 \quad \textbf{(4.13)}$$

This distribution is not as useful as the first and the third distribution as in practice it does not satisfy the required initial distribution.

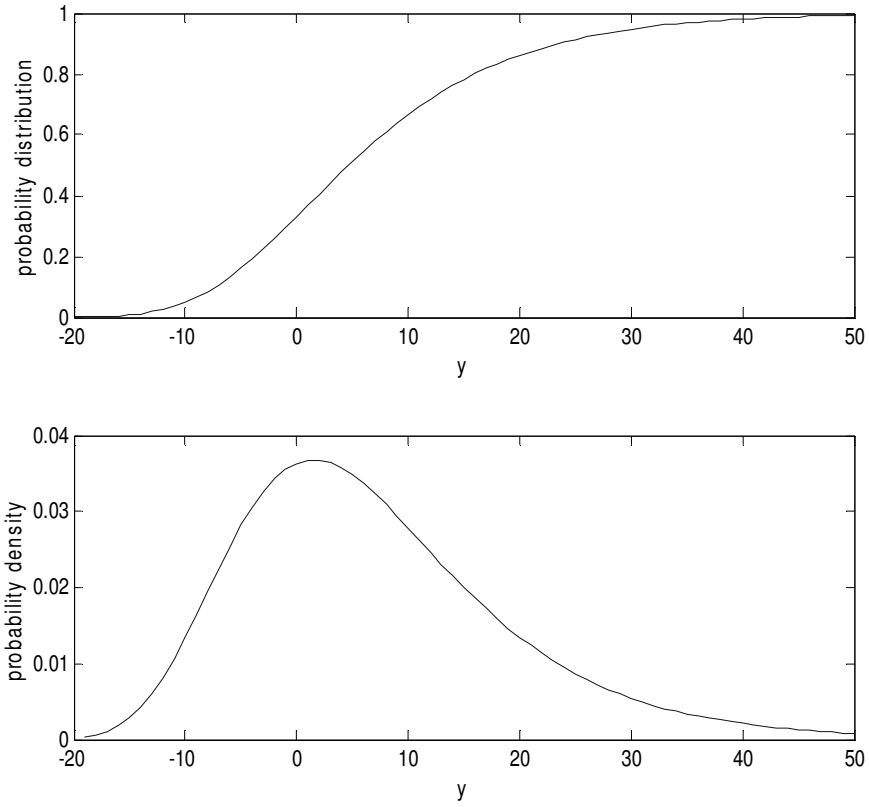

Figure 4.3: Gumbel's cumulative probability distribution and probability density function

Only the type 3 minimum value asymptotic distribution i.e. Weibull distribution (Figure 4.5) is really of practical interest, it is obtained by using the distribution $F_X(x)$ which has a left tail that starts at a value of x equal to α, such that:

$$F_X(x) = c_1(x-\alpha)^{\beta}, c_1 > 0, \beta > 0, x \geq \alpha \qquad \textbf{(4.14)}$$

From this distribution then the Weibull distribution has the form:

$$F_Z(z) = 1 - \exp\left[-\left(\frac{z-\alpha}{\gamma}\right)^{\beta}\right] \qquad \textbf{(4.15)}$$

$$f_Z(z) = \frac{\beta}{\gamma}\left(\frac{z-\alpha}{\gamma}\right)^{\beta-1} \exp\left[-\left(\frac{z-\alpha}{\gamma}\right)^{\beta}\right], \beta > 0, \gamma > \alpha, z \geq \alpha \qquad \textbf{(4.16)}$$

Here α, γ and β are the location, scale and shape parameters, where α is also the threshold value (time or voltage threshold; below this value, there is no breakdown) and γ is known as characteristic time constant in lifetime test (with constant voltage).

In general, for a distribution of time to breakdown with constant voltage the value of β is in the range 0.5 to 3.

In order to estimate the parameters of Weibull distribution, first the data should be ranked from the smallest to the largest, then the cumulative probability distribution $F(i, n_d)$, where i is the i^{th} measurement and n_d is the sample size, of each point estimated exactly by the incomplete beta function or approximated using the Bernard estimator. The incomplete beta function has the form:

$$\beta(a,b) = \frac{\Gamma(a+b)}{\Gamma(a)\Gamma(b)} \int_0^F z^{a-1}(1-z)^{b-1}\,dz, a = i, b = n_d + 1 - i, \Gamma(n+1) = n! \qquad \textbf{(4.17)}$$

The Bernard estimator provides an alternative way to estimate the cumulative probability and is much simpler [81].

$$F(i, n_d) = \frac{i - 0.3}{n_d + 0.4} \qquad \textbf{(4.18)}$$

Taking the logarithm two times from both sides of the Equation (4.15) results in:

$$\ln(-\ln(1 - F_Z(z))) = \beta \ln(z - \alpha) - \beta \ln(\gamma) \qquad \textbf{(4.19)}$$

To reduce the complexity of the equation, α is usually set to 0 and from the above equation, the plot of $\ln(-\ln(1 - F_Z(z)))$ against $\ln(z)$ becomes a straight line with slope β, the intersection of the line with vertical axis will be $-\beta \ln(\gamma)$. The parameters can be obtained from the best fit curve generated by a maximum likelihood algorithm for example.

The Weibull distribution in the lifetime test with constant voltage has the form:

$$F_F(t) = 1 - \exp\left[-\left(\frac{t}{\tau_c}\right)^{\beta_t}\right] \qquad \textbf{(4.20)}$$

Where τ_c is the characteristic time constant and β_t is the shape parameter of Weibull distribution for lifetime. The relationship between τ_c and the applied voltage can be shown to be an inverse power law where τ_c is proportional with $(V\text{-}V_{th})^{-n}$, where V_{th} is the threshold voltage and is usually set to zero. However, n is altered by different breakdown mechanisms, care must be taken when extrapolating from the applied high voltage to the working range voltage in order to obtain a lifetime prediction. The characteristic time constant can be written as ($V_{th} = 0$):

$$\tau_c = C^{\frac{-1}{\beta_t}} V^{\frac{-\beta_v}{\beta_t}} \quad \textbf{(4.21)}$$

Where β_v is the shape parameter of Weibull distribution for voltage and $C^{\frac{-1}{\beta_t}}$ is a constant.

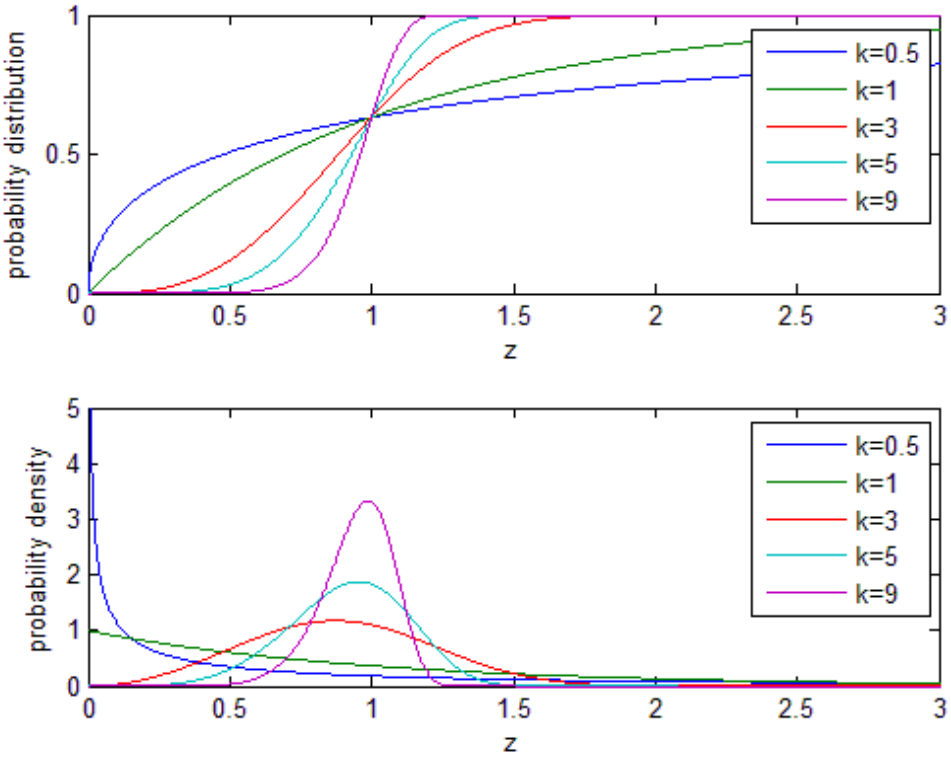

Figure 4.4: Weibull distributions with α=0, γ=1, and β from 0.5 to 9

The hazard function h(t) is defined as the instantaneous rate of failure at time t of a specimen given that it survives to time t.

$$h(t) = \frac{f_F(t)}{F_s(t)} \quad \textbf{(4.22)}$$

$$F_F(t) = 1 - F_S(t) = 1 - \exp\left[-\int_0^t h(t)dt\right] \quad \textbf{(4.23)}$$

The hazard function for the Weibull distribution is:

$$h(t) = \beta_t t^{\beta_t - 1} \tau_c^{-\beta_t} = \beta_t t^{\beta_t - 1} C V^{\beta_v} = \beta_t t^{\beta_t - 1} C V^{\beta_v}(t) \quad \textbf{(4.24)}$$

$$F_F(t) = 1 - \exp\left[-\int_0^t h(t)dt\right] = 1 - \exp\left[-C\int_o^t \beta_t t^{\beta_t - 1} V^{\beta_v}(t)dt\right] \quad \textbf{(4.25)}$$

Parameter β_t can be derived from the best fit curve for the Weibull distribution of the lifetime with constant voltage but β_v cannot be determined from the Weibull distribution of breakdown voltage with a constant time. For several values of constant V, the characteristic time constants τ_c can be obtained using:

$$\log(\tau_c) = \log\left(C^{-\frac{1}{\beta_t}}\right) - \frac{\beta_v}{\beta_t}\log(V) \qquad \textbf{(4.26)}$$

The log-log plot of τ_c against V provides the slope $-\frac{\beta_v}{\beta_t}$. Therefore, β_v can be obtained from this slope.

An alternative way to obtain the parameters is by using the ramp breakdown experiment where the voltage increases with constant rate υ until breakdown, such that V(t) = υt

$$F_F(t) = 1 - \exp\left[-C\int_o^t \beta_t t^{\beta_t - 1}(\upsilon t)^{\beta_v}\, dt\right] = 1 - \exp\left[-C\frac{\beta_t}{\beta_t + \beta_v}\upsilon^{\beta_v} t^{\beta_v + \beta_t}\right] \qquad \textbf{(4.27)}$$

Or:

$$F_F(V) = 1 - \exp\left[-C\int_o^V \beta_t t^{\beta_t - 1} V(t)^{\beta_v}\, \frac{dV}{\upsilon}\right] = 1 - \exp\left[-\left(\frac{V}{V_c}\right)^{\beta_t + \beta_v}\right] \qquad \textbf{(4.28)}$$

With $V_c^{-(\beta_t + \beta_v)} = C\frac{\beta_t}{\beta_t + \beta_v}\upsilon^{-\beta_t}$

Therefore the probability of failure of material due to the application of a ramp voltage also has the form of the Weibull distribution whose shape parameter is $\beta_t + \beta_v$. For each voltage increasing rate υ, one value of characteristic voltage Vc is obtained. The log-log graph of V_C against υ will produce the straight line with slope of $\frac{\beta_t}{\beta_t + \beta_v}$. Therefore, from the two slopes $\beta_t + \beta_v$ and $\frac{\beta_t}{\beta_t + \beta_v}$, the parameters β_t and β_v can be calculated.

An exponential law which is proposed by Dakin [12], is less popular than the inverse power law which describes the relationship between τ_c and the applied voltage:

$$\tau_c = B_1 \frac{\exp\left(\frac{B_2}{V - V_{th}}\right)}{V - V_{th}}, V > V_{th} \quad \textbf{(4.29)}$$

However, this equation is very hard to mathematically handle to determine the parameter B_2 and proportionality constant, B_1.

4.1.3. Breakdown strength of practical insulation materials

The intrinsic breakdown of insulation materials is usually very high, in order of 10^3 $kVmm^{-1}$. However, real insulation can only experience fields of magnitude two to three orders less than the intrinsic value. The fact is that manufactured insulation is not completely homogeneous. It can contain impurities, voids, imperfections and so on. Insulation under stress may experience internal discharges or partial discharges and the insulation strength will be reduced [74]. The idea of free space existing within insulation which can lead to a reduction in breakdown strength can be demonstrated by the application of pressure to insulation [82]. The application of pressure on LDPE delays the time to failure of material, in other words, increases the breakdown strength. The application of pressure has the effect of reducing the size of free space and the chance of submicro-void formations. Some work has also reported the dependence of breakdown strength of insulation on the applied area of the field and sample thickness [83, 84]. The explanation for these observations was given by Artbauer [85] based on the change in free path of electrons and statistical origin of breakdown action. According to Artbauer polymeric insulation material has amorphous regions where free spaces exist with sizes similar to that of the molecular order. Electrons under sufficient field and free path can become conductive by hopping conduction. The larger the free space is, the longer the free path and consequently the lower the breakdown strength of the material. From a statistical point of view, the increase in volume of insulation material will increase the chance of longer free paths existing in the material:

$$x_N = x_a + a_1 \ln\left(\frac{V_N}{V_a}\right) \quad \textbf{(4.30)}$$

Where x_N and x_a are longest free path with respect to volume V_N and V_a, a_1 is a parameter. Previous work also provides an equation to calculate the breakdown field of bigger volume insulation [74]:

$$E_B = \frac{E_{B1}}{n_v^{a_1}} \quad \textbf{(4.31)}$$

Where n_v is the ratio of two volumes, E_B and E_{B1} are breakdown field of bigger and smaller volume, a_1 is the reciprocal of the β parameter from Weibull distribution. This explains the phenomena of higher breakdown strength for the thinner or smaller samples. Artbauer's work also provides the relationship between longest free path and time of field application and vibration frequency of the molecules. From this, the longer the field is applied the lower the resulting breakdown strength. Increases in temperature will increase the vibration frequency of the molecules and lead to increases in the longest free path and therefore lower breakdown strength.

Material morphology, surface condition and the material manufacturing process also play a crucial role in the overall breakdown strength of material. The narrower the amorphous region, the higher breakdown voltages that can be achieved [86-88]. Work from S. G. Swingler shows that poor material preparation and using PET as a backing layer will introduce impurities to a material and subsequently the breakdown strength is reduced significantly [89].

4.2. Dielectric spectroscopy of polymeric insulation

The theory of dielectric spectroscopy has a very long history, originally with the work of Von Schweidler [90], Benedict [91], and more recently the work of Jonscher [92-94], Dissado and Hill [95] but our understanding is still limited. Several books have been written summarizing the theory of dielectric response [96-101]. Dielectric spectroscopy can be used as a tool to analyze the ageing of insulation materials [102-105] or to characterize nanoscale composite dielectrics [106, 107]. This section gives a brief summary about the physical mechanisms, and the formulation of the dielectric response as a function of the frequency of the applied electric field.

4.2.1. Theory of dielectric spectroscopy, polarisation, conduction and losses in dielectric materials

When a constant electric field E is applied to a dielectric, the dielectric material is polarized. The induced surface charge on the electrode includes bound charge and free charge. The bound charge in the dielectric produces polarisation P and free charge is related to the electric flux in free space $\varepsilon_0 E$. When an AC electric field

$E = E_m \cos(\omega t)$ is applied, if the frequency is high enough, the material molecular response may not follow the change in electric field and the dielectric flux D will lag behind by a phase angle of δ, such that:

$$D = D_m \cos(\omega t - \delta) = D_m(\cos(\omega t)\cos(\delta) + \sin(\omega t)\sin(\delta)) = D_1 \cos(\omega t) + D_2 \sin(\omega t) \qquad \textbf{(4.32)}$$

Dielectric flux D contains two components one is in-phase with applied electric field and the other one lags by π/2. However, the dielectric flux, D, is equal to εE, then the concept of complex permittivity ε^* is introduced where:

$$\varepsilon^* = \varepsilon' - j\varepsilon'' = (\varepsilon_r' - j\varepsilon_r'')\varepsilon_0 \qquad \textbf{(4.33)}$$

Consider the total current density, it includes the conduction current density and the displacement current density.

$$J_T = J_0 + \frac{dD}{dt} = J_0 + \varepsilon^* \frac{dE}{dt} \qquad \textbf{(4.34)}$$

When a sinusoidal electric field $E = E_m e^{j\omega t}$ is applied, the total current density will be:

$$J_T = \sigma_0 E + j\omega(\varepsilon' - j\varepsilon'')E = (\sigma_0 + \omega\varepsilon'')E + j\omega\varepsilon' E \qquad \textbf{(4.35)}$$

Therefore the imaginary part of complex permittivity contributes to the total losses of the dielectric material.

There are different mechanisms for polarisation over the frequency spectrum. They are electronic polarisation, atomic or ionic polarisation, orientational polarisation, hopping polarisation and space charge polarisation. Without any external applied field, the electron clouds of either atoms or molecules are distributed so that negative centres are in balance with positive ones. When an electric field is applied, the electron clouds can be deformed, the negative centres displaced and atoms or molecules will be under electronic polarisation. Atomic polarisation is related to the displacement of atomic nuclei in molecules or a lattice under an applied electric field. These two polarisation processes are almost independent of temperature and occur in a very short time after a field is applied and can be considered instantaneous in dielectric spectroscopy.

If the material consists of molecules which possess permanent dipoles, these dipoles can be oriented towards the direction of the field. The material with the aligned arrangement of dipoles will be polarized and this is orientational polarisation. This process is an intermolecular interaction and different to intramolecular interaction of

electronic and atomic polarisation [101]. The energy needed in this process depends on the thermal condition of dipoles and also the interactions of the dipole with its surroundings. Orientational polarisation can take place over a wide range of frequency as it is dependent on the ease of dipole rotations.

Conduction current density is the contribution of the movement of mobile charge carriers inside the bulk of the dielectric. The number of charge carriers in insulation materials is small and the movement of these charge carriers is mainly due to a hopping conduction process [99]. The displacement of a charge q can be considered as the same as superimposing a dipole qd_{dp} in the direction of movement where d_{dp} is the moving distance. Hence, the movement of charge carriers actually contributes to polarisation of the material. In order to hop to another trap, the charge needs to pass over a potential barrier. The carriers need to gain enough energy from the source for long enough to overcome the barrier. Therefore, the period of the applied frequency has to be less than the inverse relaxation time of this process.

In the lower frequency region, there is space charge polarisation (interfacial polarisation) often referred as Maxwell/Wagner/Sillars (MWS) polarisation and electrode polarisation. Both of these processes relate to charge separation and can greatly affect the conduction of material [99]. MWS polarisation occurs due to charge separations and charged blocked at the inner boundary of discontinuity regions in dielectrics while in the case of electrode polarisation, charges are accumulated at the external electrode interfaces which are in contact with sample. These processes lead to strong increases in both the real and imaginary part of the relative permittivity with decreasing frequency, especially for electrode polarisation. This explains why dielectric loss increases at lower frequencies. If only pure conduction occurs, the plot of the imaginary relative permittivity against $\log(\omega)$ will result in a slope of gradient equal to minus one of the imaginary part of the permittivity as the frequency increases (over the low frequency region), while the real part stays constant [101].

Solid polymeric dielectrics and polyethylene in particular can possess various relaxation processes over different temperature ranges. According to Blythe [97], polyethylene as a semi-crystalline polymer that can have three principal relaxation processes namely α (80^{o}C), β (-20^{o}C) and γ (-130^{o}C) relaxation. The β and γ relaxations are concerned with amorphous regions and α relaxation is related to

crystalline regions. For amorphous polymers, the high temperature α relaxation is usually associated with the movement of the whole chains where the β relaxation can involve some mechanisms such as rotation of side groups about the C-C backbone, flips of cyclic conformation or local motion of segments of the main chain (e.g. the effect of a polar group attached directly to main chain or crankshaft rotation of four or more CH_2 units) [97]. The β and γ relaxations are characterized by much broader peaks compared to α relaxation. In crystal polymers, the zigzag conformation of the chain with a polar group attached can experience a 180^o rotation and also translational shifts [108]. The twisting effect can develop with long chains which have more than 60-120 carbon atoms [97]. Pure polyethylene is non-polar and should only present very weak relaxation. However, the introduction of a polar group such as carbonyl during manufacture will enhance the relaxation process. The presence of polar or ionic small impurity molecules may couple with the motion with polymer chains [109]. The branch point motion could also contribute to the process whereas crosslinking restricts molecular motion [110].

4.2.2. Calculation of polarisation and dielectric constant in time and frequency domains

If hopping and space charge polarisation is ignored, the total polarisation P will include the high frequency response polarisation P_∞ (electronic polarisation and ionic polarisation that follows the applied field instantly) and the orientational polarisation P_o, such that:

$$P = P_\infty + P_o = (\varepsilon_{r\infty} - 1)\varepsilon_0 E + (\varepsilon_{rs} - \varepsilon_{r\infty})\varepsilon_0 E \quad \textbf{(4.36)}$$

Where $\varepsilon_{r\infty}$ and ε_{rs} are the relative permittivities with respect to high frequency component and static component. However, when the electric field is applied or removed, only the component due to electronic and ionic response instantly disappears, the orientational component takes some time to change to an equilibrium state. Assume that the rate of change in orientational polarisation is proportional to the change from its equilibrium state:

$$\frac{dP_o(t)}{dt} = \pm \frac{P_o(t)}{\tau_0} \quad \textbf{(4.37)}$$

Where τ_0 is the relaxation time

The equation for decay and polarisation of orientational polarisation will be:

$$P_o(t) = (\varepsilon_{rs} - \varepsilon_{r\infty})\varepsilon_0 E e^{-\frac{t}{\tau_0}} \quad \textbf{(4.38)}$$

$$P_o(t) = (\varepsilon_{rs} - \varepsilon_{r\infty})\varepsilon_0 E(1 - e^{-\frac{t}{\tau_0}}) \quad \textbf{(4.39)}$$

Consider the applied field E(u) over the time interval (u,u+δu), the change in the total polarisation will be:

$$dP(t-u) = dP_\infty(t-u) + (\varepsilon_{rs} - \varepsilon_{r\infty})\varepsilon_0 (1 - e^{-\frac{t-u}{\tau_0}}) dE(u) \quad \textbf{(4.40)}$$

Assuming the superposition is valid, the polarisation P(t) over time from 0 to t will equal to the sum of all small interval polarisations continuously from 0 to t:

$$P(t) = (\varepsilon_{r\infty} - 1)\varepsilon_0 E(t) + (\varepsilon_{rs} - \varepsilon_{r\infty})\varepsilon_0 \int_0^t (1 - e^{-\frac{t-u}{\tau_0}}) dE(u) \quad \textbf{(4.41)}$$

Using the boundary condition that $E_{(0)}=0$ and applying integration by parts it is possible to obtain the general equation for polarisation over time:

$$P(t) = (\varepsilon_{r\infty} - 1)\varepsilon_0 E(t) + (\varepsilon_{rs} - \varepsilon_{r\infty})\varepsilon_0 E(u)(1 - e^{-\frac{t-u}{\tau_0}})\Big|_0^t + (\varepsilon_{rs} - \varepsilon_{r\infty})\varepsilon_0 \int_0^t \frac{E(u)}{\tau_0} e^{-\frac{t-u}{\tau_0}} du \quad \textbf{(4.42)}$$

The second term is equal to zero so:

$$P(t) = (\varepsilon_{r\infty} - 1)\varepsilon_0 E(t) + (\varepsilon_{rs} - \varepsilon_{r\infty})\varepsilon_0 \int_0^t \frac{E(u)}{\tau_0} e^{-\frac{t-u}{\tau_0}} du \quad \textbf{(4.43)}$$

If E(u) is a step function:

$$P(t) = (\varepsilon_{r\infty} - 1)\varepsilon_0 E + (\varepsilon_{rs} - \varepsilon_{r\infty})\varepsilon_0 E(1 - e^{-\frac{t}{\tau_0}}) \quad \textbf{(4.44)}$$

If E(u) is a sinusoidal AC field $E = E_m \cos(\omega u) = \mathrm{Re}\left(E_m e^{j\omega u}\right)$ then:

$$P(t) = (\varepsilon_{r\infty} - 1)\varepsilon_0 E_m \cos(\omega t) + \frac{(\varepsilon_{rs} - \varepsilon_{r\infty})\varepsilon_0 E_m \cos(\omega t)}{1 + \tau_0^2 \omega^2} + \frac{(\varepsilon_{rs} - \varepsilon_{r\infty})\varepsilon_0 E_m \omega \tau_0 \sin(\omega t)}{1 + \tau_0^2 \omega^2} \quad \textbf{(4.45)}$$

From equation (4.43) and the fact that:

$$D = \varepsilon_0 E + P = \mathrm{Re}(\varepsilon_r^* \varepsilon_0 E) \quad \textbf{(4.46)}$$

Gives the Kramers-Kronig relations that provide the relationship between real and imaginary relative permittivity as a function of frequency:

$$\varepsilon_r'(\omega)-\varepsilon_{r\infty}=\frac{2}{\pi}\int_0^{\infty}\varepsilon_r''(u)\frac{u}{u^2-\omega^2}du \quad \textbf{(4.47)}$$

$$\varepsilon_r''(\omega)=\frac{2}{\pi}\int_0^{\infty}[\varepsilon_r'(u)-\varepsilon_{r\infty}]\frac{\omega}{u^2-\omega^2}du \quad \textbf{(4.48)}$$

These equations are used to calculate one parameter from the other if it cannot be measured directly at a certain frequency.

From equation (4.45) and replace $E_m\cos(\omega t)=E_m e^{j\omega t}$ and $E_m\sin(\omega t)=-jE_m e^{j\omega t}$ gives:

$$P(t)=(\varepsilon_{r\infty}-1+\frac{(\varepsilon_{rs}-\varepsilon_{r\infty})}{1+\tau_0^2\omega^2})\varepsilon_0 E_m e^{j\omega t}-j\frac{(\varepsilon_{rs}-\varepsilon_{r\infty})\varepsilon_0 E_m\omega\tau_0}{1+\tau_0^2\omega^2}e^{j\omega t} \quad \textbf{(4.49)}$$

$$P=(\varepsilon_r^*-1)\varepsilon_0 E=(\varepsilon_r'-1-j\varepsilon_r'')\varepsilon_0 E_m e^{j\omega t} \quad \textbf{(4.50)}$$

From this, the Debye equations are obtained:

$$\varepsilon_r'=\varepsilon_{r\infty}+\frac{\varepsilon_{rs}-\varepsilon_{r\infty}}{1+\omega^2\tau_0^2} \quad \textbf{(4.51)}$$

$$\varepsilon_r''=\frac{\varepsilon_{rs}-\varepsilon_{r\infty}}{1+\omega^2\tau_0^2}\omega\tau_0 \quad \textbf{(4.52)}$$

$$\tan\delta=\frac{\varepsilon_r''}{\varepsilon_r'}=\frac{(\varepsilon_{rs}-\varepsilon_{r\infty})\omega\tau_0}{\varepsilon_{rs}+\varepsilon_{r\infty}\omega^2\tau_0^2} \quad \textbf{(4.53)}$$

The maximum value for ε_r'' occurs at $\omega\tau_0=1$ and $\tan\delta$ is a maximum when $\omega\tau_0=\left(\frac{\varepsilon_{rs}}{\varepsilon_{r\infty}}\right)^{\frac{1}{2}}>1$.

Eliminating $\omega\tau_0$ from the equation of real and imaginary permittivity and rearranging the equation the relationship between ε_r' and ε_r'' can be determined:

$$\left(\varepsilon_r'-\frac{\varepsilon_{rs}+\varepsilon_{r\infty}}{2}\right)^2+\varepsilon_r''^2=\left(\frac{\varepsilon_{rs}-\varepsilon_{r\infty}}{2}\right)^2 \quad \textbf{(4.54)}$$

This is the equation of a semi-circle with a centre at $\left(\frac{\varepsilon_{rs}+\varepsilon_{r\infty}}{2},0\right)$ and radius $\left(\frac{\varepsilon_{rs}-\varepsilon_{r\infty}}{2}\right)$. In practice, the graph of ε_r' against ε_r'' is an arc that sits inside the ideal semi-circle and is asymmetrical. To get an improved fit it is necessary to use the Cole-Cole, Davidson-Cole or Havriliak-Negami equations.

For the Debye equation:

$$\varepsilon_r^* = \varepsilon_{rs} + \frac{\varepsilon_{rs} - \varepsilon_{r\infty}}{1 + j\omega\tau_0} \quad \textbf{(4.55)}$$

For the Cole-Cole equation (corresponding to the broadening of peak area of imaginary part):

$$\varepsilon_r^* = \varepsilon_{rs} + \frac{\varepsilon_{rs} - \varepsilon_{r\infty}}{1 + (j\omega\tau_0)^{1-a}} \quad \textbf{(4.56)}$$

For the Davidson-Cole equation: (corresponding to the asymmetric of peak area of imaginary part, with long tail to the right)

$$\varepsilon_r^* = \varepsilon_{rs} + \frac{\varepsilon_{rs} - \varepsilon_{r\infty}}{(1 + j\omega\tau_0)^b} \quad \textbf{(4.57)}$$

And for the Havriliak-Negami equation:

$$\varepsilon_r^* = \varepsilon_{rs} + \frac{\varepsilon_{rs} - \varepsilon_{r\infty}}{(1 + (j\omega\tau_0)^a)^b} \quad \textbf{(4.58)}$$

In the analysis of interfacial polarisation, Maxwell-Wagner used an example of two dielectric layers of different permittivity and resistivity in series [100]. If the condition $\varepsilon_1\rho_1 \neq \varepsilon_2\rho_2$ is satisfied, the charges can migrate from one layer to another under an electric field. If two dielectric layers were considered as a circuit of two parallel capacitors and resistors in series. Then the equivalent admittance, real and imaginary permittivity of the equivalent circuit can be derived as:

$$A_d = j\omega C_0 \varepsilon_r^* \quad \textbf{(4.59)}$$

$$\varepsilon_r' = \varepsilon_{r\infty} + \frac{\varepsilon_{rs} - \varepsilon_{r\infty}}{1 + \omega^2\tau^2} \quad \textbf{(4.60)}$$

$$\varepsilon_r'' = \frac{1}{\omega C_0 (R_1 + R_2)} + \frac{\omega\tau(\varepsilon_{rs} - \varepsilon_{r\infty})}{1 + \omega^2\tau^2} \quad \textbf{(4.61)}$$

(Where $C_0 = \varepsilon_0 \frac{A}{d}$, A is electrode area and d is sample thickness) The expression for the real part is identical as that of the Debye relaxation but the relaxation time τ is much longer than τ_0. The second term in the imaginary part is the same as the Debye loss factor however there is an extra term related to conduction and this term increases with decreasing frequency.

To measure the dielectric spectroscopy of a material from 10^{-2} to 10^6 Hz, a capacitor and resistor bridge can be used. However, for the lower frequency range 10^{-2} to 10^{-5} Hz, it is impractical to use the bridge method as it is time consuming. Instead, the

indirect measurement of dielectric spectroscopy can be done using the measurement of anomalous charging current and Hamon's approximation [111]. According to Gross [112]

$$\varepsilon_r^{'} = \frac{1}{C_a}\left[C_\infty + \int_0^\infty \Phi(t)\cos(\omega t)dt\right] \quad \textbf{(4.62)}$$

$$\varepsilon_r^{''} = \frac{1}{C_a}\left[\frac{\sigma_0}{\omega} + \int_0^\infty \Phi(t)\sin(\omega t)dt\right] \quad \textbf{(4.63)}$$

Where C_a, C_∞ are capacitance of the sample replaced by air and the capacitance of the sample at very high frequency respectively. $\Phi(t)$ is the decay function (which is an exponential function in Equation (4.37)). From observations of polarisation and depolarisation current, $\Phi(t)$ can be determined equal to aC_0t^{-b} (where a and b are constants). Hamon's approximation for loss factor is given by:

$$\varepsilon_r^{''} \approx \frac{I_{(0.1/f)}}{2\Pi f C_a V} \quad \textbf{(4.64)}$$

Where I is the total charging current. The loss factor at frequency f can be calculated using the charging current at time equal to 0.1/f second after the application of a voltage V. To have this approximation, some conditions have to be met, such as, the decay function has to follow the power law where the power, b, is between 0.3 and 1.2 and the magnitude of anomalous current has to be large compared to conduction current. A similar approach was developed for the real permittivity but its application is more limited than the Hamon's approximation [113].

Jonscher has proposed an empirical "universal relaxation law" that can be used to fit dielectric spectroscopy data [92, 94]. In this case, the dielectric susceptibility can be given as:

$$\chi^{''}(\omega) = \frac{1}{\left(\frac{\omega}{\omega_p}\right)^{-m} + \left(\frac{\omega}{\omega_p}\right)^{1-n}}, 0 < n < 1, 0 < m < 1 \quad \textbf{(4.65)}$$

where ω_p is the peak frequency. At low frequency the Quasi-DC or Low frequency dispersion can occur with no loss peak, both real and imaginary susceptibility increases with decreases in frequency [114]. This Quasi-DC situation is characterized by two independent processes, above and below the characteristic frequency ω_c:

For $\omega<\omega_c$:

$$\chi'' \propto \omega^{n_2-1}, 0 < n_2 < 1 \quad \textbf{(4.66)}$$

For $\omega > \omega_c$:

$$\chi'' \propto \omega^{n_1-1}, 0 < n_1 < 1 \quad \textbf{(4.67)}$$

The application of Hamon's approximation and universal relaxation law has been used extensively in the research of Scarpa and Das-Gupta for analyzing ageing processes of polyethylene and XLPE [115-121]. Dissado and Hill used a cluster approach to dielectric spectroscopy [95]. Further details of modelling dielectric relaxation can be found in review papers [122-124].

4.3. Space charge injection into the bulk of the insulation and its measurement

Charge injection and transport in the bulk of a dielectric is a complex phenomenon and is related to the electrical performance of the insulation material. The amount of mobile charge in a dielectric material in general and in polyethylene in particular is very small. However, under a high enough DC electric field, more charge carriers can be induced into the bulk of the insulation. These formed charges are termed space charge. The sources of charge carriers generated in the insulation can be either thermal ionization, impurity ionization or charge injection from electrodes [125].

According to classical band theory for a covalently bonded crystal, there are two electron energy bands separated by a forbidden band gap (Figure 4.6). The highest energy band filled with electrons at absolute zero temperature is called the valence band (VB). The higher energy band, which is empty at absolute zero, is called the conduction band (CB). Electrons can travel freely in the conduction band through the lattice. The promotion of electrons from the valence band to the conduction band will leave vacancies in the valence band which are termed holes. For insulators the band gap is usually greater than 2 eV, between 2 and 0.2 eV for semiconductors while less than 0.2 or a partly filled valence band for conductors [12]. The Fermi level (E_f) is the state which has energy level at which the probability of electron occupation is a half. The Fermi-Dirac distribution function which provides the probability of electron occupation at a certain energy state E_e is given by:

$$F_{(E_e,T)} = \frac{1}{1+\exp\left(\frac{E_e - E_f}{kT}\right)} \quad \textbf{(4.68)}$$

The work function Φ of the material is the energy needed to promote an electron from the Fermi level to a vacuum state where the electron is completely removed from the material. Electron affinity, χ_e , is the energy released when the electron is placed at the bottom of conduction band from the vacuum level. In Figures 4.6 and 4.7, $N(E_e)$ represents the density of localized states.

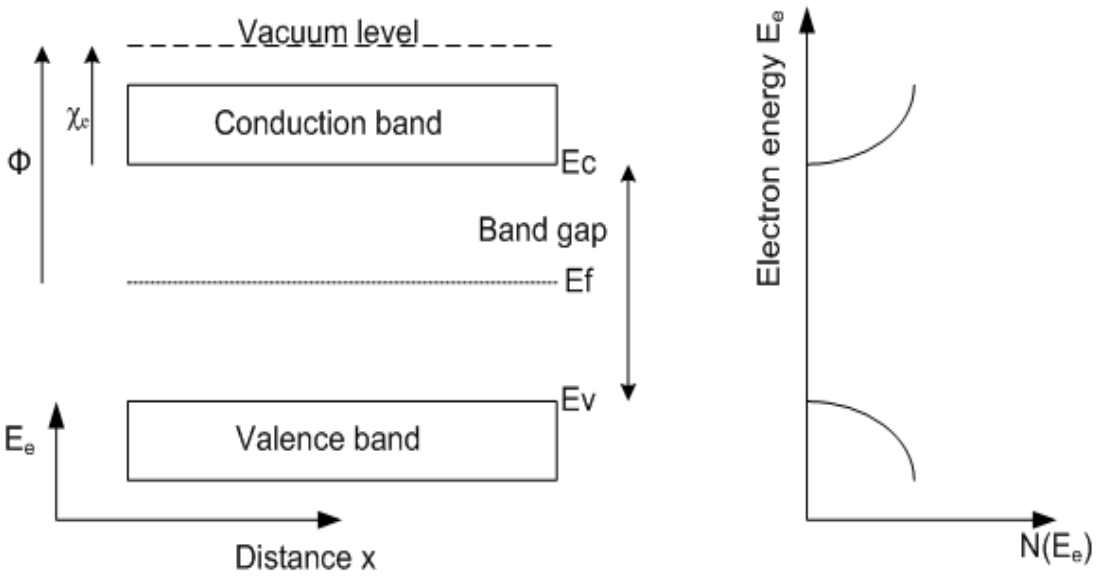

Figure 4.5: An energy band diagram of a covalently-bonded crystal

For polymeric insulation, particularly polyethylene, the structure is semi-crystalline and contains disordered regions. These disorders will distort the band structure of the perfectly crystalline model and introduce localized states into the band gap. Electrons or holes which enter these states are not available for conduction but trapped there. The band structure then can be modelled as shown in Figure 4.7, again $N(E_e)$ represents density of localized states.

There is a potential difference between the dielectric material and the electrode when they are brought in contact. If the charge has enough energy from the external field to overcome this potential, then it will penetrate into the material. The potential barrier that the electron has to overcome to get into the conduction band of the dielectric depends on the work function of the metal and the electron affinity of the dielectrics i.e.

$$\phi_0 = \phi_m - \chi_p \quad \textbf{(4.69)}$$

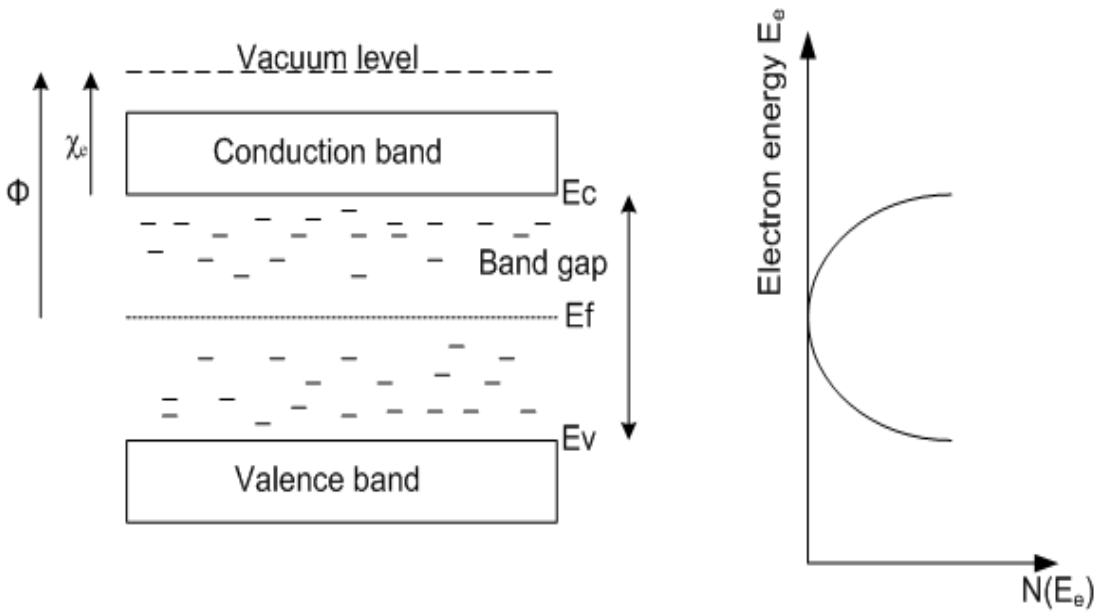

Figure 4.6: An energy band diagram of a non-crystalline material

Where ϕ_0 is the potential energy barrier, ϕ_m is the work function of metal and χ_p is the electron affinity of dielectric (polyethylene has negative electron affinity). Under the effect of Coulombic image force and applied electric field the "triangle" potential barrier is obtained with a reduction in barrier height of [12] :

$$\Delta\phi = -\left(\frac{e^3 E}{4\Pi\varepsilon_0\varepsilon_r}\right)^{\frac{1}{2}} \tag{4.70}$$

The electrons can be thermally activated through the reduced potential barrier and migrate into the dielectric. This is known as Richardson-Schottky injection [12]:

$$J = A_{RD} T^2 \exp\left(-\frac{\phi_0 + \Delta\phi}{kT}\right) \tag{4.71}$$

where A_{RD} is the Richardson-Dushman constant ($1.2\text{x}10^6 \text{Am}^{-2}\text{K}^{-2}$). If the electrical field is increased, the triangle potential may become very thin and electrons can tunnel into the dielectric. This is known as Fowler-Nordheim injection[12]:

$$J = \frac{e^3 E^2}{8\Pi h\phi_0} \exp\left(-\frac{8}{3}\left(\frac{m\Pi\phi_0^3}{he^2E^2}\right)^{\frac{1}{2}}\right) \tag{4.72}$$

The injected charge is usually homo-charge, where their sign is the same as the electrode polarity. On the other hand, it is possible to have hetero-charge, which has the opposite sign compared to that of the electrode forming at or near to the interface. This kind of charge can be the result of ionized species in the bulk of the insulation,

which then travel towards the electrodes or inhomogeneous polarisation at the electrodes. Due to the inhomogenity of insulation, there are defects and impurities in material. These defects and impurities provide localized states within the forbidden gap of the material. These states are known as traps or recombination centres. After charges are formed into the material, they can be trapped with those energy states. Depending on the escape ability of charges from the traps there are shallow and deep traps. It is not very clear whether charge carriers prefer to fill deep traps first [126] or shallow traps [127]. Recent research interest has been concerned with charge packets that can be generated at very high fields and travel through the sample [128].

In order to simulate the space charge phenomena, many models have been proposed. One of them is the Alison and Hill model for bipolar charge transport, trapping and recombination [129]. The model is governed by the following equations:

Transport equation:

$$J(x,t) = \mu n_s(x,t) E(x,t) \tag{4.73}$$

Continuity equation:

$$\frac{\partial n_s}{\partial t} + \frac{\partial J}{\partial x} = S \tag{4.74}$$

Poisson's equation:

$$\frac{\partial E}{\partial x} = \frac{\rho_c(x,t)}{\varepsilon} \tag{4.75}$$

Where μ is the carrier's mobility, n_s is the density of mobile species, ρ_c is net charge density, x is the spatial coordinate and S is the source term. In the model, charge injection is based on Schottky injection. Charges drift through the material under an applied field with constant mobility. Some electrons and holes will be trapped at single deep trap levels and the number of mobile charges reduced. However, the electric field cannot modify the potential barrier to liberate the trapped charges. Trapped charges can only recombine with their opposite species [130].

Measurements of charging and depolarizing current, along with space charge profiles can provide calculated values for carrier mobility and trap depth distribution and consequently give a better understanding about the origin of charge carriers [126, 131]. The injected homo-charge increases the field in the bulk of material while hetero-charge enhances the field in the electrode region. These can lead to a

reduction in the breakdown strength of the material. Previous published papers have mentioned the relationship between space charge formation and the breakdown strength of materials [132-135]. Therefore, space charge measurements can be considered as an alternative tool to monitor ageing of insulation materials because the ageing process may alter the charge profile of material [136-139].

In reference to this research it is necessary to consider some factors that can affect space charge measurement of cable insulation under practical conditions. The measurement of identical materials but in plaque and cable form will provide a quite different charge profiles [140]. This is explained not because of effect of choice of electrodes but the effect of the material itself. A cable sample with a temperature gradient during the crosslinking process will vary from the symmetric profile that is obtained from a plaque sample. Space charge formation in the bulk of the material also depends strongly on the chemical structure and manufacturing condition of the material. XLPE insulation usually contains by-products from the manufacturing process. These by-products may alter the space-charge profile [141-144]. Heat treatment for the sample will improve the space charge profile [145, 146]. The material morphology is also closely related to the space charge profile [147, 148]. An example of this is the space charge profile of LDPE obtained for different cooling rates. With quenched cooled LDPE, significant positive heterocharges are formed near cathode, not the usual bipolar charge injection as would be expected [149, 150]. Additives to polyethylene are also shown to change the morphology and space charge profile [151-153]. The effect of AC stress on space charge formation has been investigated [154, 155]. The AC space charge is far more difficult to measure compared to DC space charge but is still detectable.

4.4. Summary

This chapter has outlined the theory behind dielectric electrical breakdown, measurement of dielectric spectroscopy and space charge. In particular, the application of these techniques for assessing insulation ageing has been highlighted. Breakdown measurements can be used as a diagnostic tool to identify the effect of ageing processes. However, due to the stochastic nature of breakdown, it is very hard to investigate the ageing mechanism using this measurement. Dielectric

spectroscopy, in contrast, is a very good tool to investigate ageing. The information about electrical properties, physical properties, material morphology, and molecular structure can be extracted from this measurement. Space charge measurements can provide additional information about behaviour of material under a high voltage DC condition. The next chapter details ageing experiments undertaken during this research.

Chapter Five

Ageing Experiments

5.1. Impulse ageing experiments

Figure 5.1 shows the flow chart of the impulse ageing process used in this research. The Marx impulse generator was used to generate lightning impulses that were applied to a set of samples. Both samples and generator were placed within a closed screen cage to maintain safety. The multi-sample electrode contains 7 mushroom electrodes (Figure 5.2) to age 7 samples at the same time. Samples and electrodes were immersed in silicone oil to prevent flashover during the ageing process. With low field ageing where the probability of sample breakdown is low, many samples can be aged at the same time to reduce the overall ageing time. During the ageing process, sets of several thousand lightning impulses of positive or negative polarity were produced. Applied voltage signals were obtained using an oscilloscope and sent to the computer for processing. A program based on the best fit curve and K-filter that has been developed at the Tony Davies High Voltage

Laboratory was used to calculate the impulse parameters. The signal from the voltage divider is continuously checked to see whether the samples have broken down or the number of impulses have exceeded the requirement. In this case the oscilloscope has the role of a signal counter. If one of these two aspects is true, a relay is activated to shut the generator down in a safe manner.

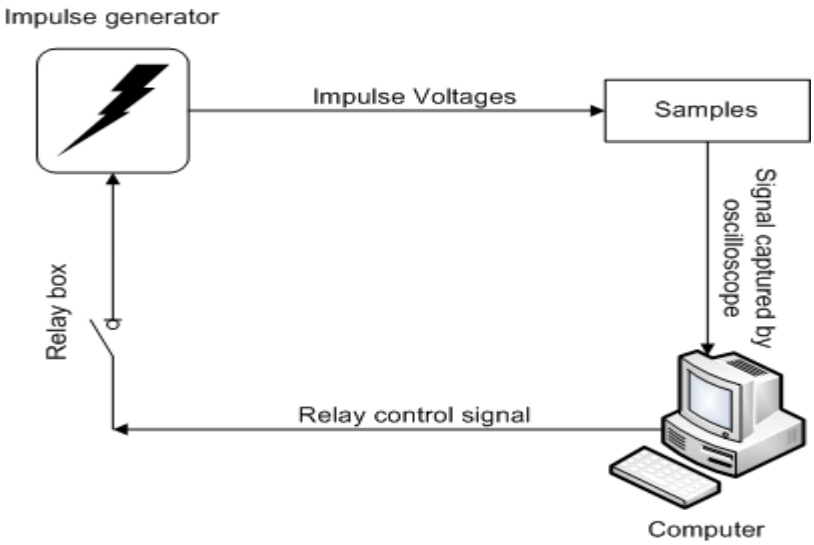

Figure 5.1: Ageing process flow chart

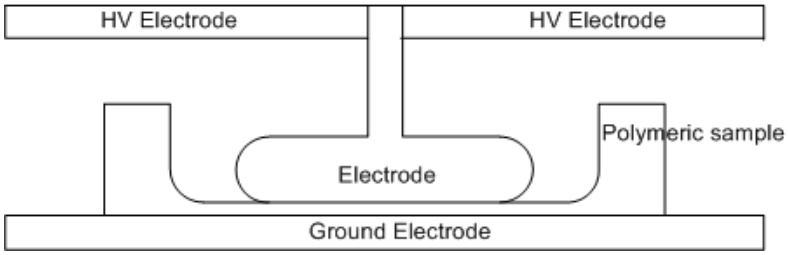

Figure 5.2: Impulse ageing electrode arrangement

Approximately 3000 impulses with front time of 1.2 μs and 40 μs tail time were used to age samples for a duration of 75 minutes. These impulses generated a peak electric field of 84-85 $kVmm^{-1}$ on the samples for both negative and positive polarity impulses. This peak value is equal to 2/3 of the impulse breakdown electrical field of HDPE. The impulse breakdown strength of HDPE was measured using the step increase method with a step of 5 kV and 5 impulses per step. Seven impulse breakdowns were measured for HDPE and the average value was 128 kV/mm. The repetition rate of the lightning impulse can be controlled using the external gap trigger (Appendix B). However, due to the charging time for the capacitor, it is

very hard to achieve a high repetition frequency. If the repetition rate is too high, the effects of space charge and increasing sample temperature may contribute to ageing and if the repetition rate is too low the experiment time would become excessive. Unfortunately, the sample temperature during impulse ageing cannot be easily measured. Since completing this work the laboratory has purchased thermal imaging equipment that may facilitate this measurement in the future.

Mushroom electrodes were used instead of ball bearing electrodes in the ageing process to ensure local field uniformity. The mushroom electrodes also reduce the effect of mechanical deformation. Samples after ageing were used for either ramp breakdown measurements or dielectric loss measurements or space charge measurements.

5.2. Thermal ageing experiments

Rogowski or flat samples can be used in the thermal ageing experiment. Samples were not coated with gold electrodes during the ageing period. Samples were placed on a tray and aged inside a fan oven with air circulating at a temperature of 95^{o}C. This temperature was chosen because if it is too low ageing will take a very long time and if it is too high the samples may melt and the geometry may be changed. For XLPE cables the maximum core conductor operating temperature is specified as 90^{o}C by manufacturers [28], hence this temperature represents worst case operational conditions. HDPE and LDPE were melted at 180-190^{o}C but can be softened at around 110-120^{o}C. XLPE can withstand higher temperatures. Due to the different experiments, samples of different thicknesses were aged, varying from 60 μm to 220 μm. Thin film samples were used to lower the effect of temperature gradient during ageing. It was noticed that some of the test materials became discoloured with increased ageing time. For example, the yellow sample in Figure 5.4 is Dicumyl peroxide crosslinked XLPE.

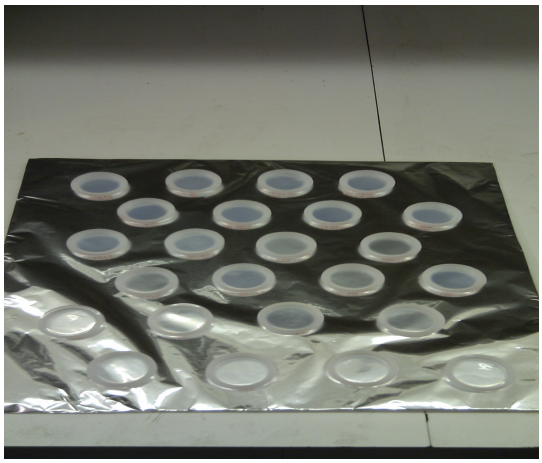

Figure 5.3: Thermal ageing samples

Figure 5.4: Samples after thermal ageing

5.3. Ultra-Violet radiation ageing experiments

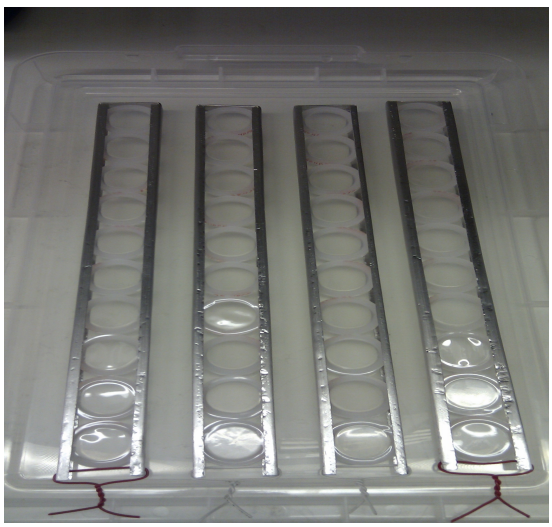

Figure 5.5: UV ageing samples

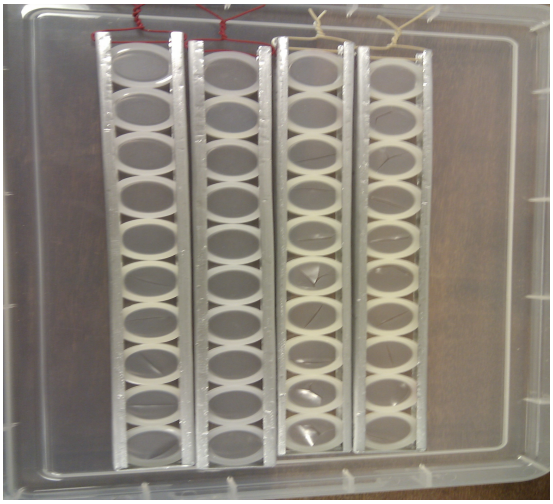

Figure 5.6: Samples after UV ageing

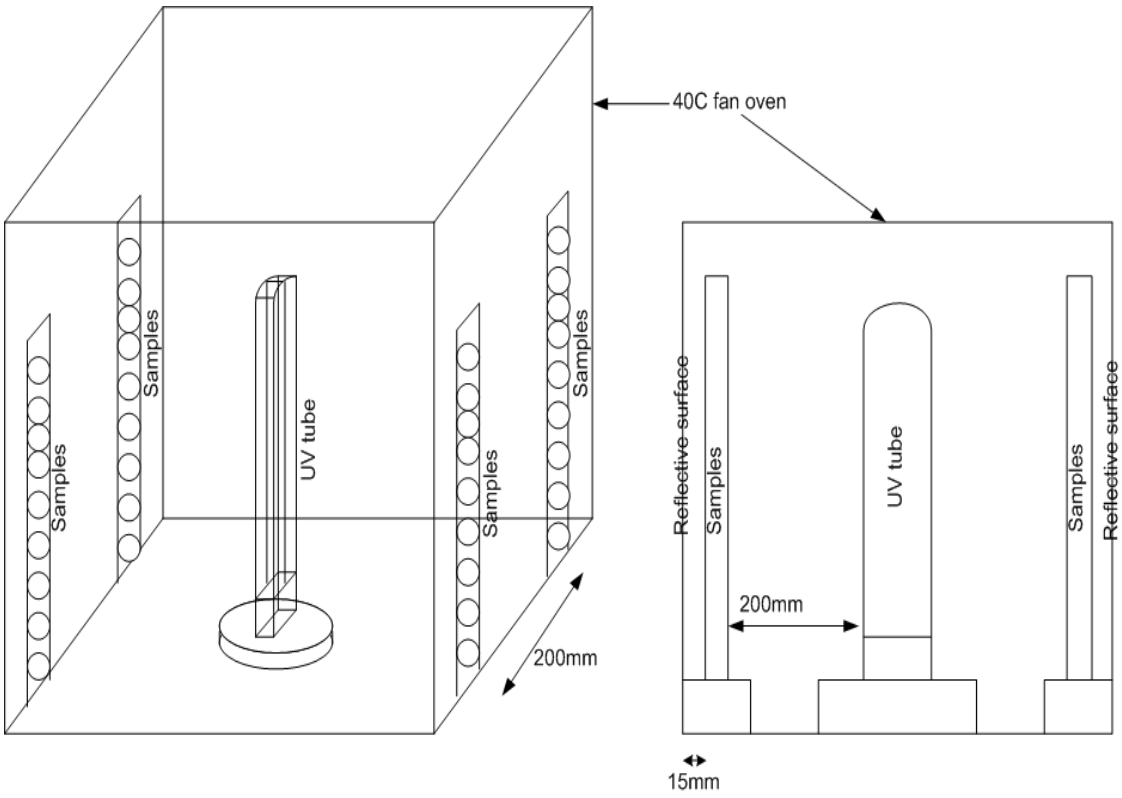

Figure 5.7: UV ageing experiment

Uncoated Rogowski samples were also used for the UV ageing experiment. Samples were mounted in aluminium holders as shown in Figures 5.5 and 5.6. The sample holders were placed around a UV fluorescence tube in a fan oven. The air in the oven was circulated all the time. The temperature was kept at 40^{o}C to stabilize any variation in temperature due to thermal losses of the UV lamp. The distance between samples and UV lamp was around 22 cm. The applied UV wavelength, λ, was 253.4

nm. The mirror surface of the oven was used to reflect the UV light onto the back surface of the sample. However, it was expected that one sample surface will be aged more heavily than the other. It is clear that some samples of the same type of material, same ageing conditions but at different positions with respect to the lamp have different degrees of ageing (it can be observed easily by the change in sample colour). Care has to be taken to ensure the same degree of ageing for all materials. Figure 5.7 shows the experimental arrangement for UV ageing. Sample holders are 7 cm higher than the top of the UV lamp. Samples which were in a higher position compared to the lamp, normally absorbed less UV radiation and were discarded after ageing. Figure 5.9 shows the transmittance of UV light through the four different materials used. Material sample thicknesses used in this case were 150 μm. All materials give very low transmittances at a wavelength of 253 nm, all are less than 10%. XL3 showed a significant drop in light transmittance because the by-products after the crosslinking reaction make the sample less transparent. After 14 days of ageing the deterioration of samples could be observed by eye as many samples were discoloured, brittle, or even cracked (Figure 5.6). The UV lamp can be considered as a line UV source and UV radiation evenly transmitted to the surface area that is contained a cylinder and two hemispheres at the top and bottom (Figure 5.8). If the source height is 20 cm, distance between source and sample holders is 22 cm, and the 36 W UV lamp has 100% efficiency, the power density which is transferred to each sample will be around 4 $mWcm^{-2}$. About 90% of radiation is absorbed by material (Figure 5.9), therefore UV power absorbed by material is about 3.7 $mWcm^{-2}$. In the above calculation, the reflected light from the oven surface was neglected.

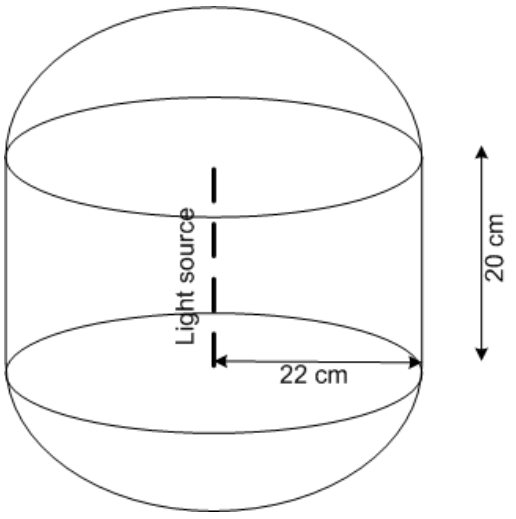

Figure 5.8: UV light source

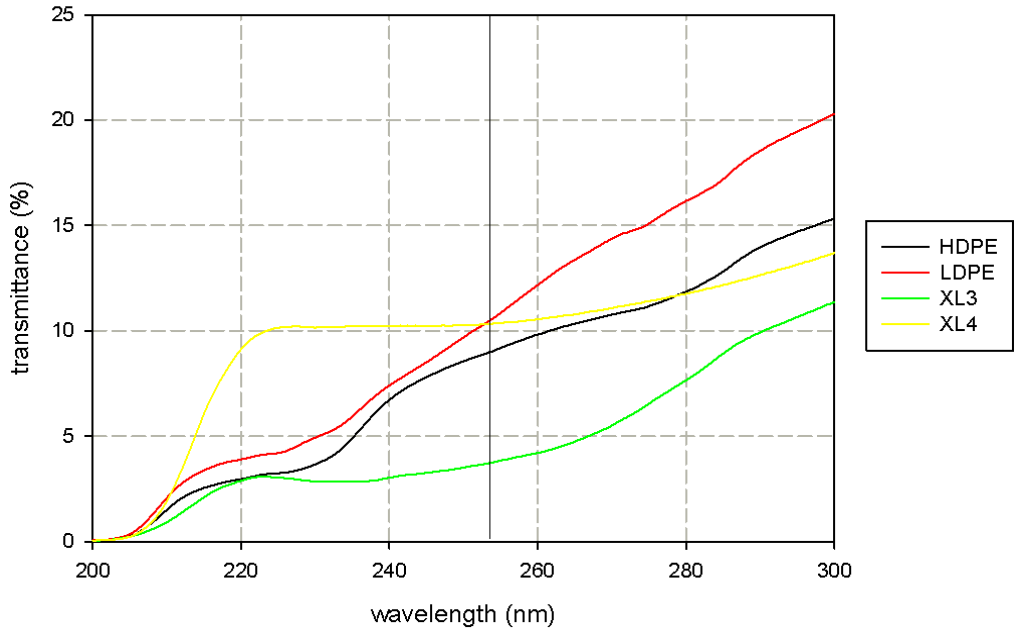

Figure 5.9: Transmittance of UV light through virgin samples

5.4. Material condition characterisation after ageing using Fourier Transformed Infrared Spectroscopy (FTIR)

One way to examine the ageing condition of samples under thermal and UV ageing is to use FTIR to analyze the degree of oxidation. A molecule can absorb selected frequency radiations and be excited to a higher energy state. Absorption in the infrared region usually is related to stretching and bending of molecular bonds. The radiation has the frequency which matches the natural vibration frequency of the molecule and will be absorbed to increase the magnitude of vibrational motion of the bonds. Only bonds which possess dipole moment can absorb infrared radiation, the symmetric bonds do not. In order to measure the infrared spectrum of material, a dispersive infrared spectrometer or a Fourier transform spectrometer can be used. In a dispersive infrared spectrometer, only single wavelength radiations from the radiation beam can pass through the sample. The ratio of inlet and outlet intensity is measured. The spectrum is constructed by collecting all single wavelength measurements. Whereas, in the Fourier transform spectrometer, the interferogram is a complex signal that contains all frequencies over the infrared spectrum and the response is measured with respect to time. The Fourier transform provides the signal information in the frequency domain. The Fourier transform can use the sum of

many accumulated interferograms to improve the signal-to-noise ratio with respect to the dispersive infrared spectrometer. Details can be found in published work on spectroscopy [156, 157]. Table 5.1 shows some common bond absorption peaks.

Bond vibration	Wave number (cm^{-1})	Peak identity
sp^3 C-H stretching	3000-2800	Strong
C-H bending CH_3	1450-1375	Medium
C-H bending CH_2	1465	Medium
CH_2 long chain bending	720	
Out of plane C-H bending	990 and 910	Strong
C=C stretching	1650	Weak, sharp
C=O stretching	1720	Strong, sharp
O-H stretching	3650-3200	Broad
$SiOCH_3$	1261, 1090, 800	
SiOSi	1025	

Table 5.1: Bond absorption peaks

This method is not suitable for characterizing impulse ageing as the samples during impulse ageing were immersed in silicone oil and samples were also sputter coated with gold electrodes. There is very little chance for samples to be oxidized during the impulse ageing experiment. Uncoated samples of LDPE and XL3 for impulse ageing were tested using FTIR (Figures 5.10 and 5.11). After the application of 3000 and 6000 lightning impulses, nearly identical spectra were obtained for these two materials.

Figures 5.12 to 5.15 show the spectrum of samples under thermal ageing. For HDPE and LDPE, after 14 days of ageing, there is almost no difference. However, there are signs of oxidation after 14 days ageing for XL3 and especially XL4. The sharp peak at 1720 cm^{-1} shows an increase in carbonyl content (C=O) and also a rising broad peak from 3200-3500 cm^{-1} indicates an increase in hydroxyl content (-OH). Both the presence of carbonyl and hydroxyl groups are known to aid conduction and indicate that the ageing process may have effect on electrical properties of the samples [38, 121].

Figures 5.16 to 5.19 summarise the results for UV aged samples. All samples were oxidized after 14 days but at different rates and intensities [36, 158, 159]. XL3 showed the heaviest levels of oxidation compared to other materials. This is in agreement with results from UV-Vis spectrometry where XL3 absorbs the most UV light. However, the consequent effects seem more significant with HDPE and LDPE

as these materials become extremely brittle. The result suggests that oxidation may also vary the mechanical properties of HDPE and LDPE. This effect on plastic materials seems more critical than for elastic materials. There is also the noticeable increase in the absorbance over the region from 900 to 1300 cm^{-1}. From the results it can also be assumed that XL3 is more sensitive to UV light ageing than XL4.

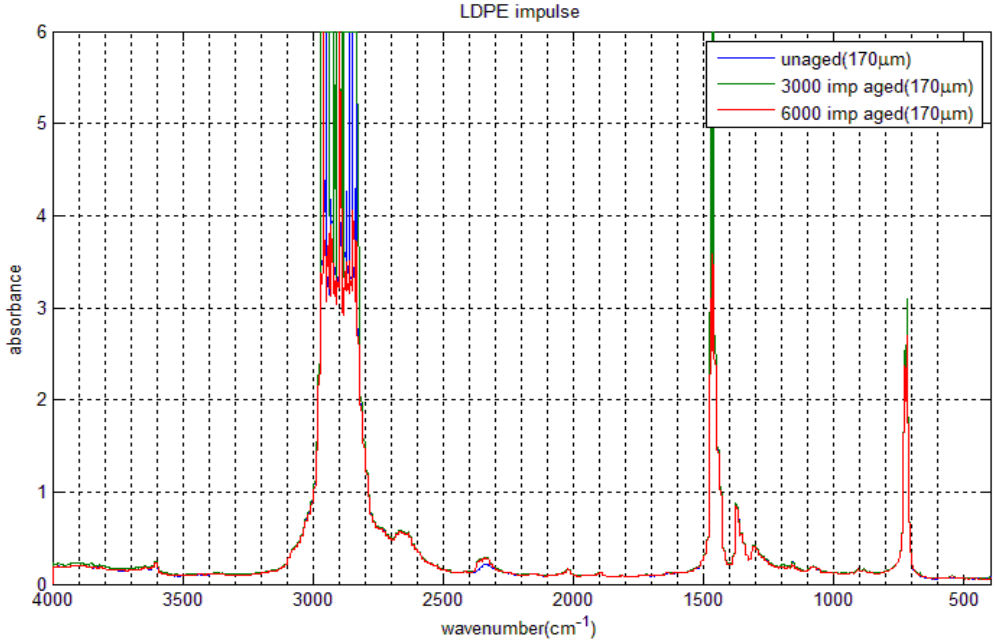

Figure 5.10: FTIR spectrum of impulse aged LDPE

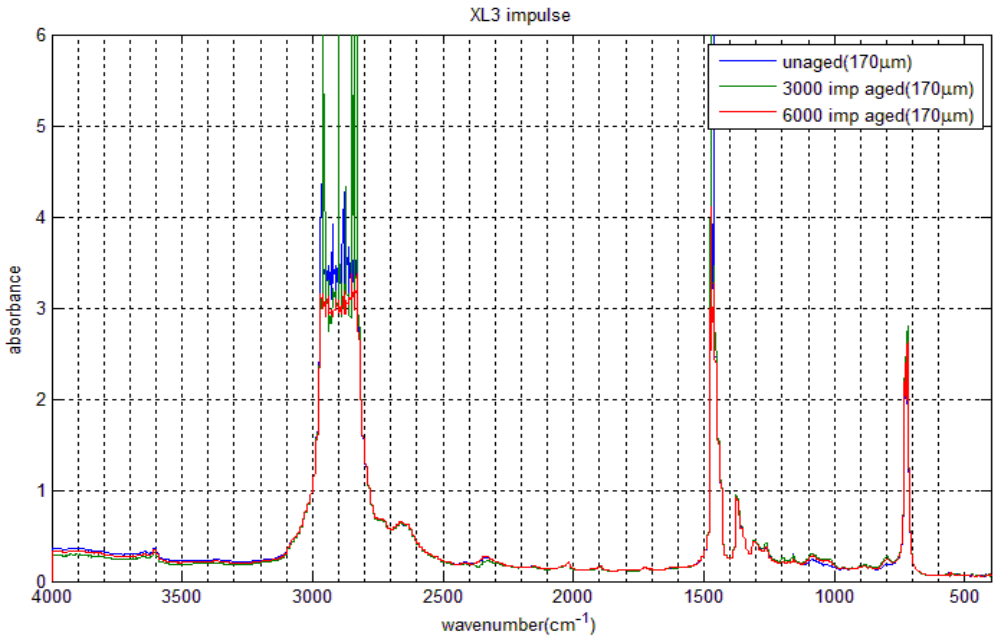

Figure 5.11: FTIR spectrum of impulse aged XL3

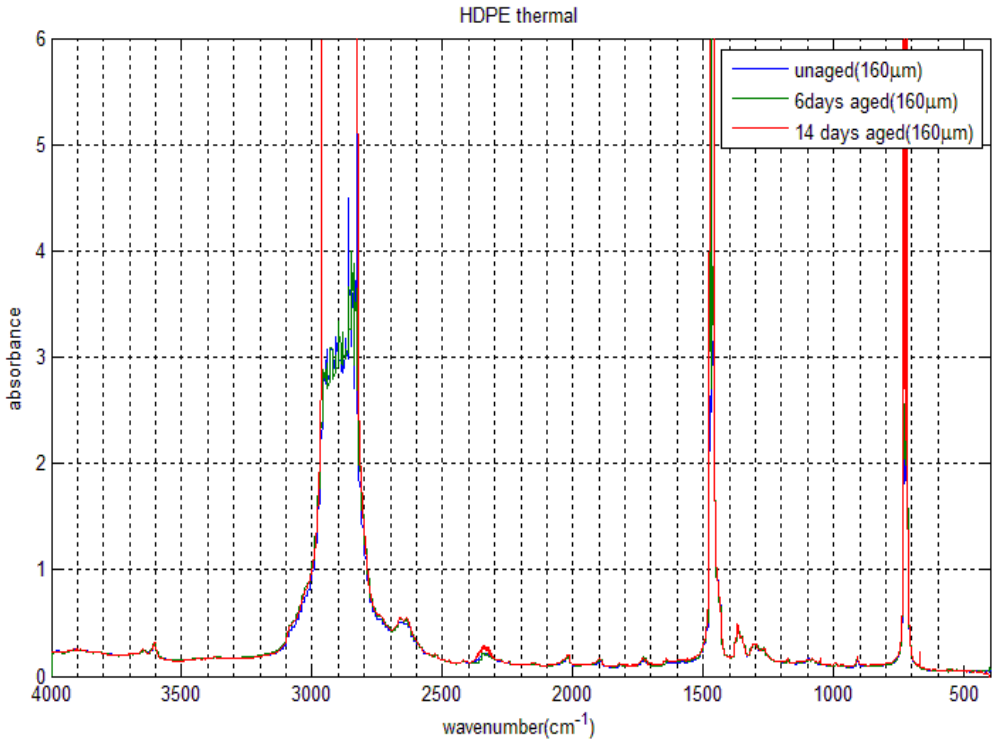

Figure 5.12: FTIR spectrum of thermal aged HDPE

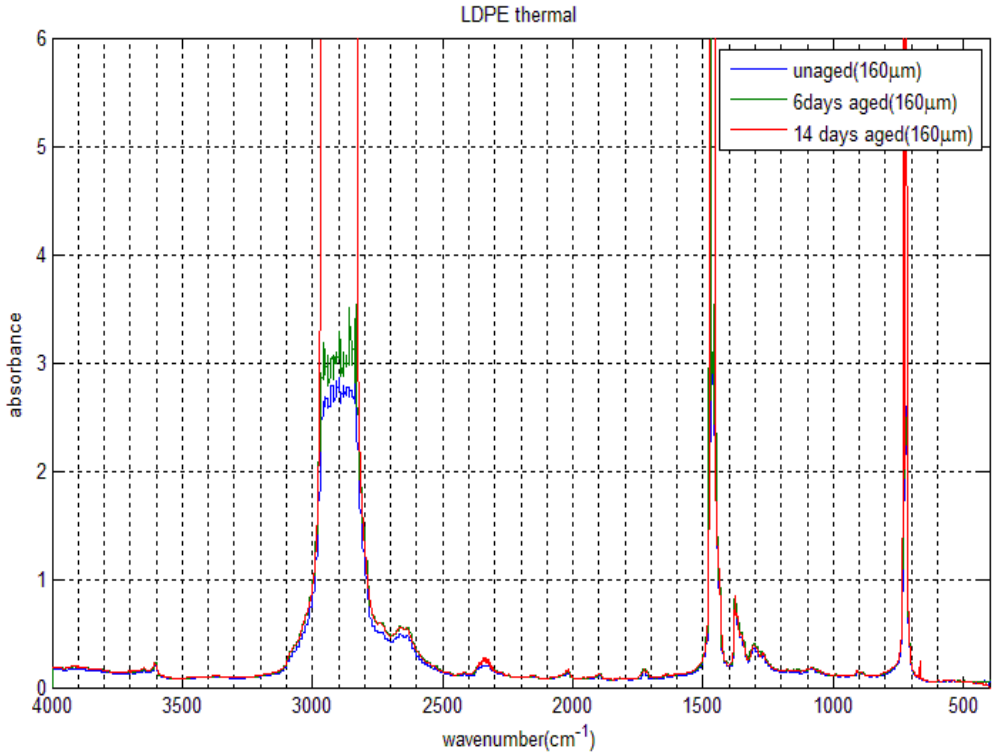

Figure 5.13: FTIR spectrum of thermal aged LDPE

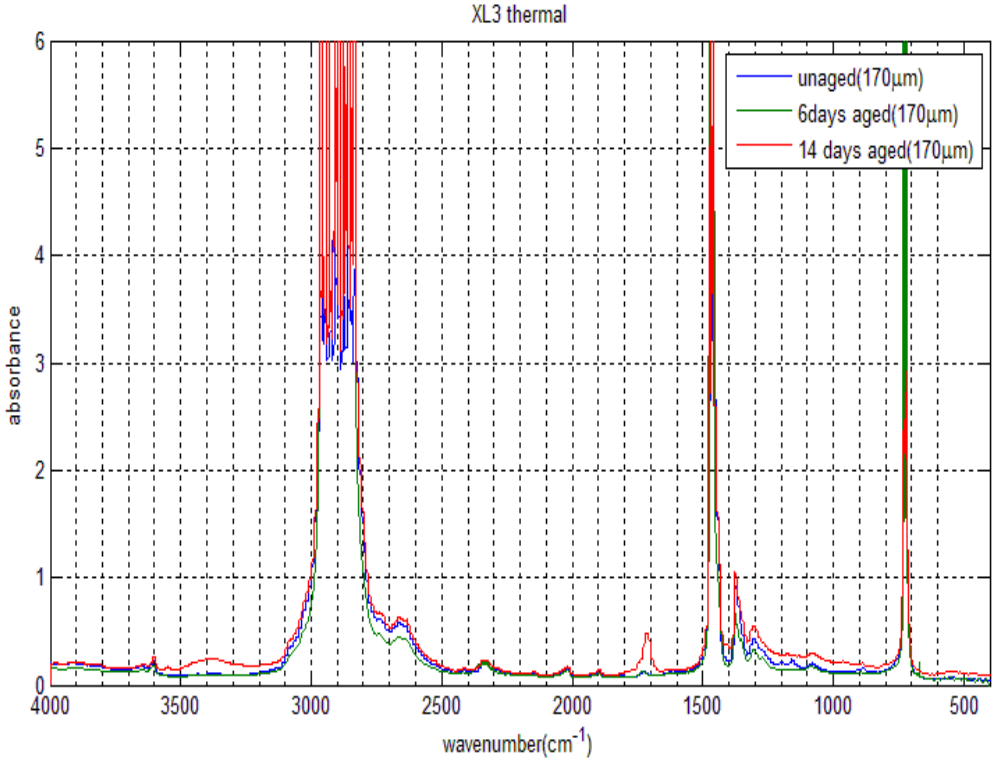

Figure 5.14: FTIR spectrum of thermal aged XL3

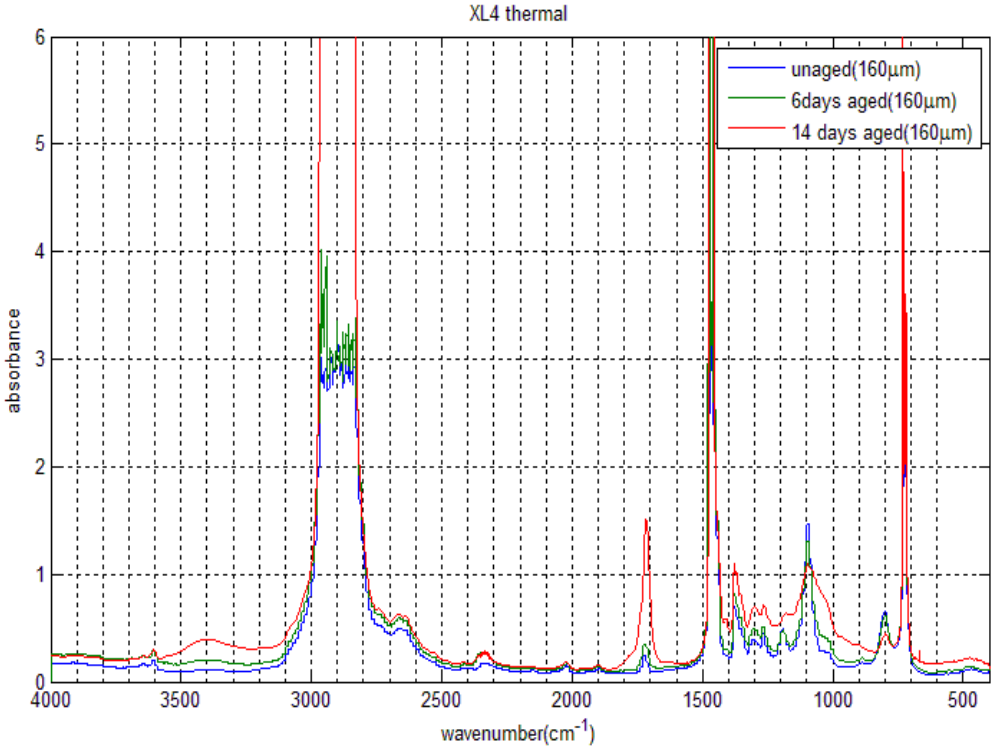

Figure 5.15: FTIR spectrum of thermal aged XL4

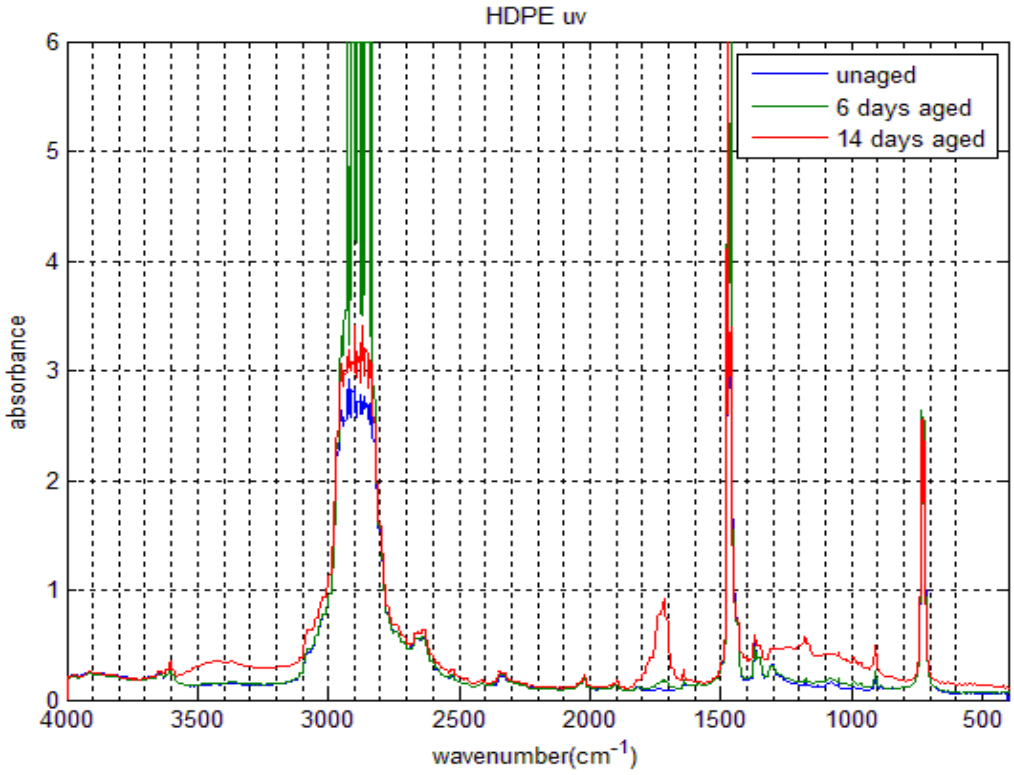

Figure 5.16: FTIR spectrum of UV aged HDPE

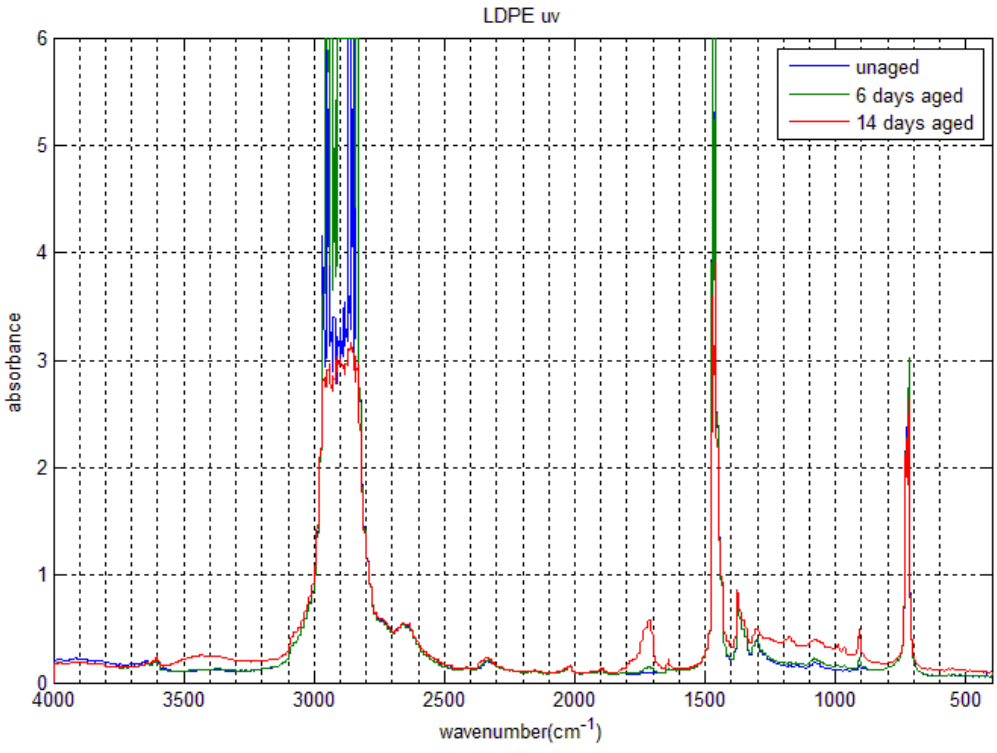

Figure 5.17: FTIR spectrum of UV aged LDPE

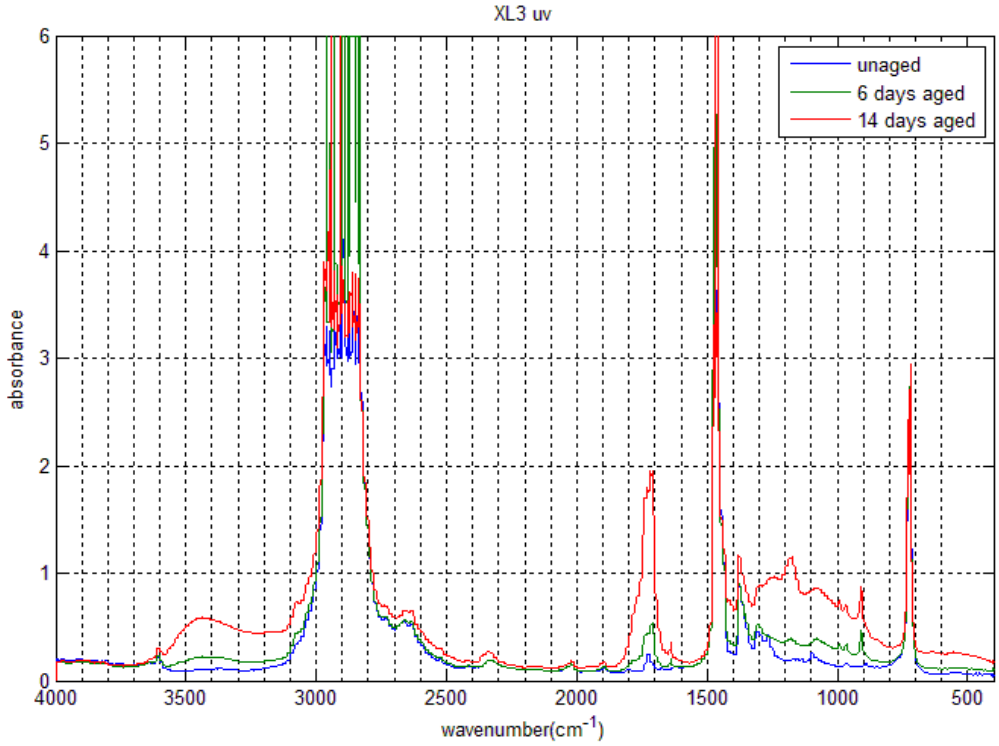

Figure 5.18: FTIR spectrum of UV aged XL3

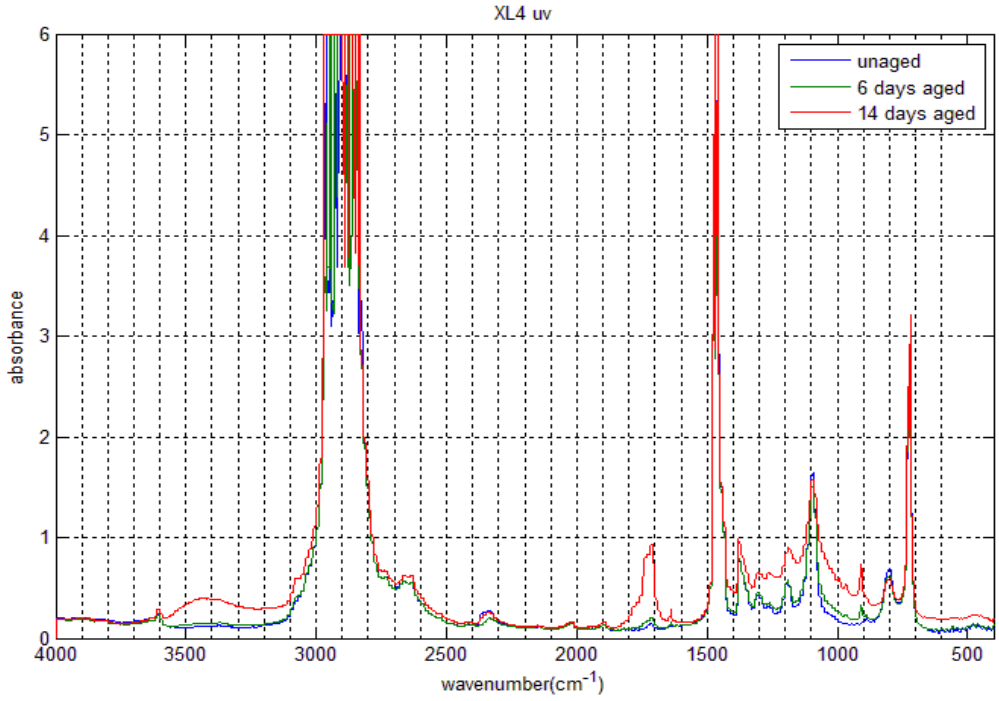

Figure 5.19: FTIR spectrum of UV aged XL4

5.5. Summary

This chapter has summarised the three experiments used to age four different material types prior to analysis of their changes in electrical properties. For impulse ageing, samples were aged using the impulse generator for 3000 lightning impulses with peak electrical field of 85 $kVmm^{-1}$ for 75 minutes. The ageing process was fully controlled using a LabView programme. For thermal ageing, samples were aged with a constant temperature in the fan oven. Samples were also aged by UV radiation. However, care must be taken to make sure samples were evenly aged. Samples after UV ageing were very difficult to handle as they became too brittle. In order to assess whether the ageing experiments have altered the structure and properties of the samples, FTIR spectroscopy has been used to identify any changes in chemical content. The results show that, oxidation does not take part in impulse ageing, whereas it significantly contributes to UV ageing. In thermal ageing, the role of oxidation was become significant when the material was chemically crosslinked. The FTIR method can also be used as the qualitative assessment for crosslinking of silane crosslinked polyethylene by observing the changes in absorption peaks of $SiOCH_3$ and SiOSi [36, 160, 161].

Chapter Six

AC Breakdown Measurements Results

6.1. Breakdown experiment

After impulse ageing, virgin and aged samples were taken immediately to a Faraday cage for breakdown testing. The electrodes were changed to ball bearings (Figure 6.1). All sample and electrodes were immersed in a silicone oil bath to prevent flashover. The transformer is controlled by a motorised variac to create a ramped AC high voltage across the sample with the ramp rate of 100 Vs^{-1}. The disadvantage of this setup is the highest voltage can go up to 100 kV but its motorized variac ramp control is not very stable. In order to ramp up to the applied voltage, the motor speed was first triggered to created 1 kVs^{-1} and then reduced to a slower speed. The ratio between breakdown voltage and the stressing time provides the ramp rate. The obtained ramp rate was 100±10 Vs^{-1}. Breakdown voltage and time to breakdown were recorded using an analogue voltmeter and

stop-clock. The obtained breakdown voltages were then analyzed using a Weibull distribution statistical package (Weibull 7++).

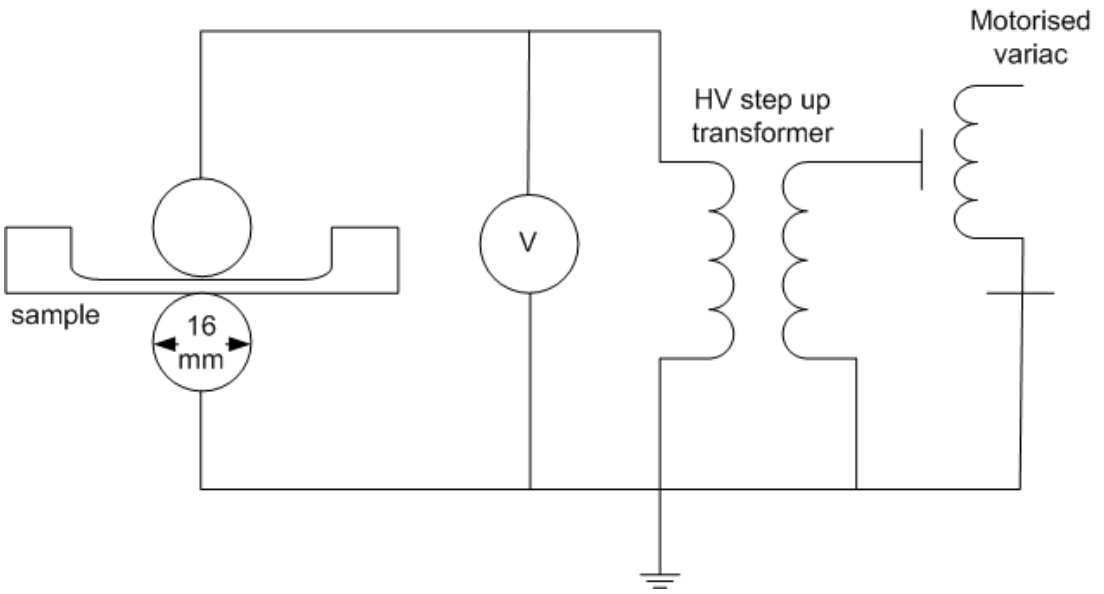

Figure 6.1: AC ramp breakdown arrangement

The samples after thermal and UV ageing were tested using a different experiment. A 50 Hz sine wave signal was generated using signal generator. This signal was amplified by a power amplifier and signal amplitude was increased using an electronic counter. The amplified signal was used to feed a step-up transformer to produce a high voltage. The ramp rate of this equipment is much more stable than the motor-variac used in the other breakdown experiment but the maximum voltage that can be achieved is just over 15 kV. The electrodes used were also ball bearings but with a smaller diameter. Samples that were impulse aged were gold coated; therefore the actual electrode is a Rogowski-plane electrode. While samples that had been UV and thermal aged were uncoated, and the electrode arrangement for breakdown can be considered as a point-point electrode.

6.2. Results obtained for impulse aged samples

The obtained results show that lightning impulses actually reduce the breakdown strength of HDPE (Figure 6.2). The 90% confidence limits for aged and un-aged samples only overlap below 16% in the case of ageing by 3000 negative impulses and do not overlap at all in the case of ageing by 6000 negative lightning impulses.

The mean breakdown strength is reduced quite significantly after the application of impulses (Table 6.1).

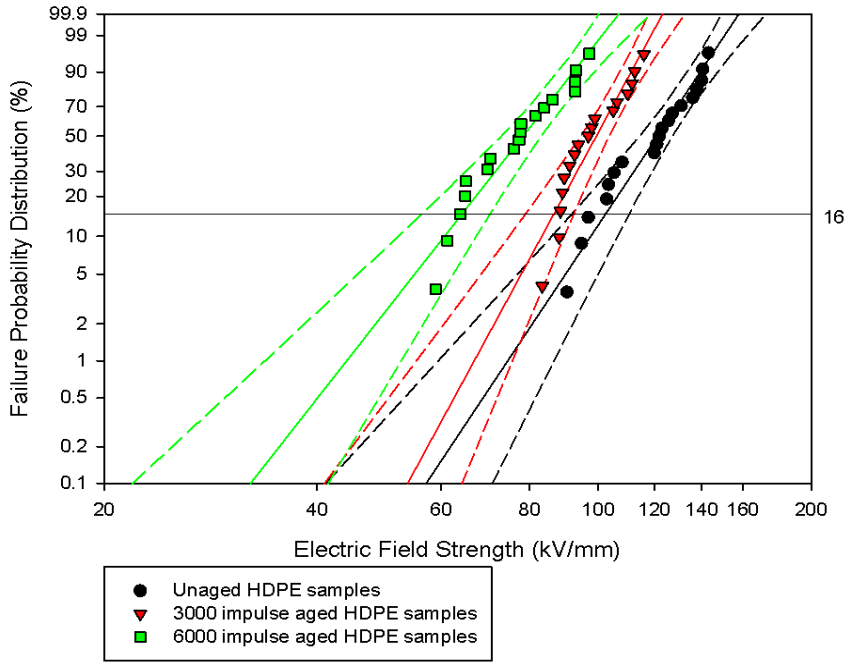

Figure 6.2: Negative Impulse aged and un-aged HDPE

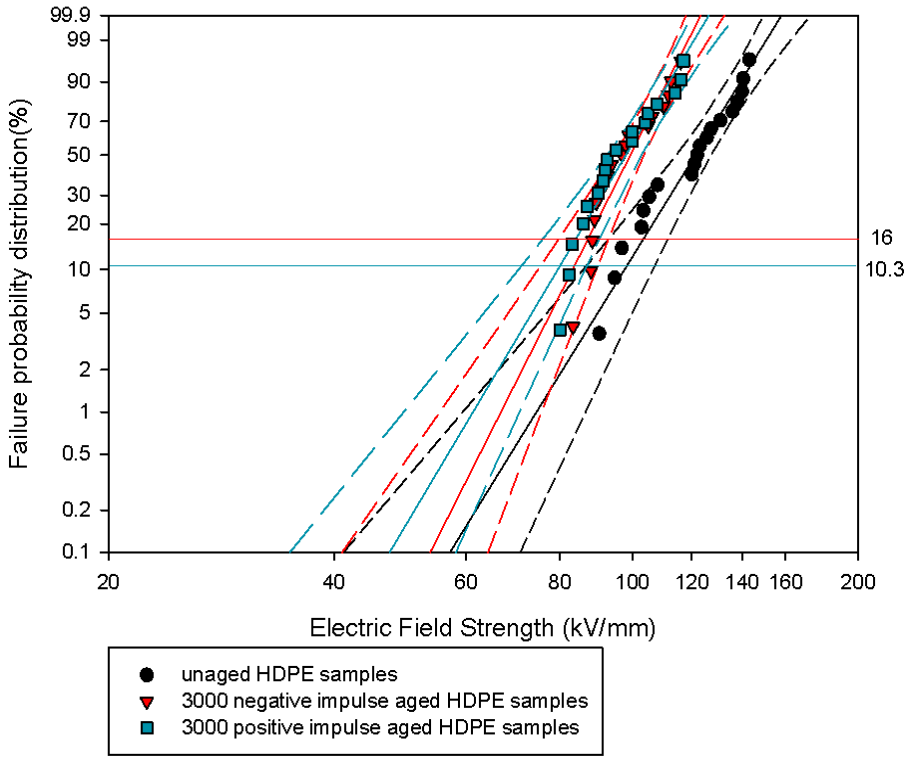

Figure 6.3: Positive and negative impulse ageing HDPE

However, the results presented here show that there is no significant difference between positive and negative impulses on material ageing and subsequent electrical breakdown performance (Figure 6.3). The 90% confidence limits for aged and unaged samples only overlap below 16% in the case of negative impulse ageing and below 10% for positive impulse ageing. The breakdown voltages for positive impulse aged samples are a little bit lower than in the negative case but this difference can be neglected. Table 6.1 shows the Weibull distribution parameters which were obtained from analysis of the different materials used.

With the LDPE the breakdown strength of aged and un-aged samples seems to be no different from a statistical point of view (Figure 6.4). The 90% confidence regions overlap for the whole spectrum. Also, this material has a low dielectric strength compared to HDPE. The mean value for breakdown strength of LDPE is about 98 $kVmm^{-1}$, the same as that for HDPE aged with 3000 lightning impulses. Therefore, it can be assumed that LDPE is not overly sensitive to the effect of repeated lightning impulses.

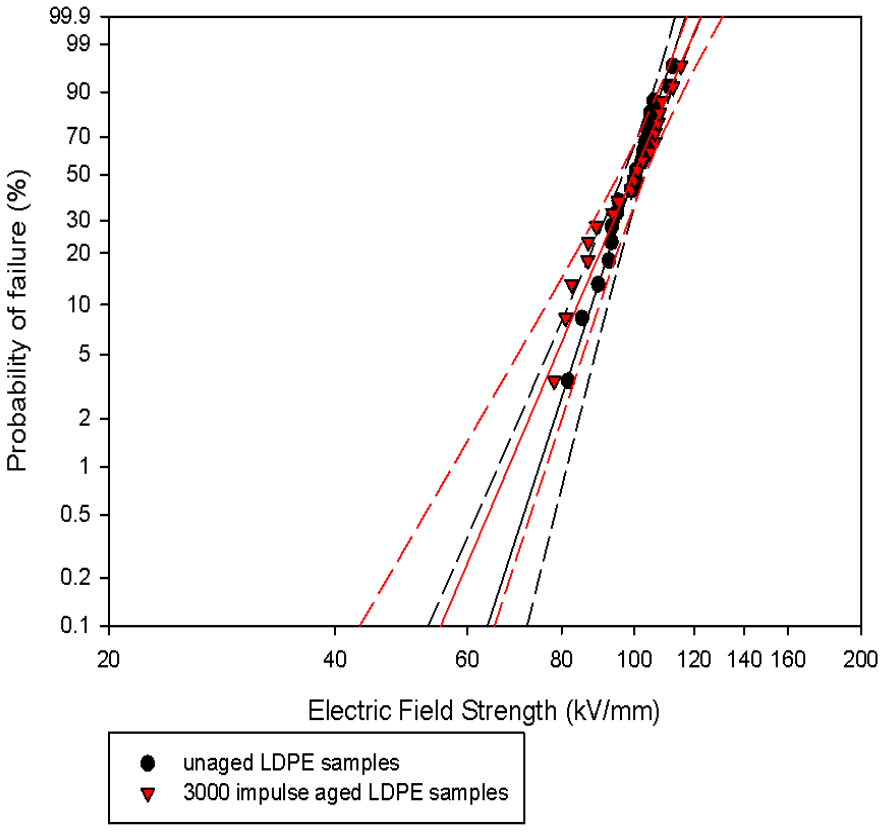

Figure 6.4: Impulse aged and un-aged LDPE

The XL3 uses the LD100 as its base material but provides a much better performance as an insulator (Figure 6.5). It is the best one overall compared to other investigated materials (mean breakdown value of 129 $kVmm^{-1}$).

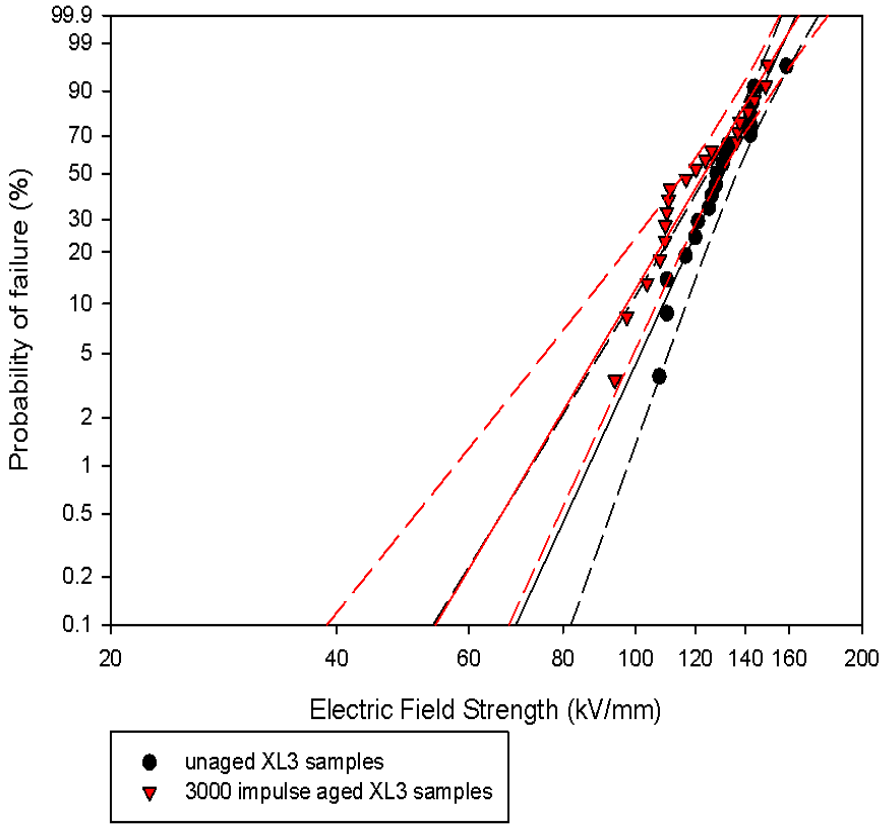

Figure 6.5: BD strength of impulse aged and unaged XL3

The separation in confidence limits for aged and un-aged materials appears again in the case of XL4 (Figure 6.6). Although the separation only exists above 45%, the difference in mean value is quite noticeable. The shape parameter β is much improved for the aged sample, more than 20 indicating that the range of breakdown strength of aged samples is narrowed.

Data from Table 6.1 shows that all investigated materials with an exception of LDPE were aged by repetitive lightning impulses. For HDPE the effect is most noticeable, but the effect reduces for the two crosslinked materials. The β parameters are reasonable as they are around 10 on average and only impulse aged XL4 has a value of β over 20. XL3 is more durable with applied voltage but more sensitive to lightning impulse ageing compared to LDPE.

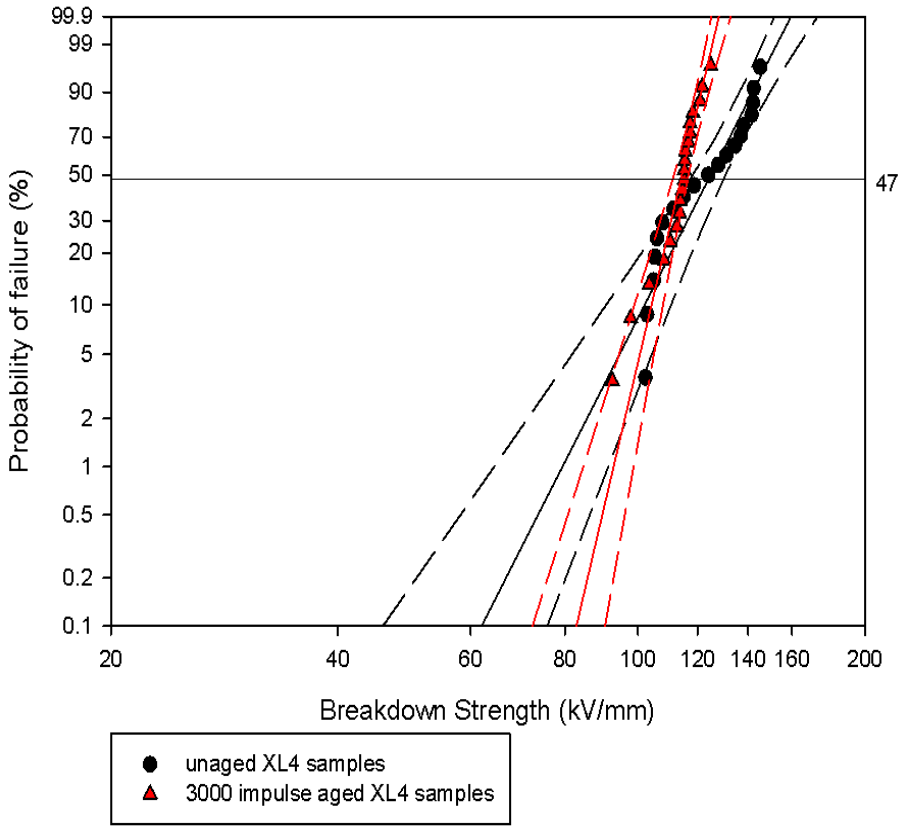

Figure 6.6: BD strength of impulse aged and unaged XL4

Materials	β	γ	Mean
HDPE un-aged	8.68	126.5	119.62
HDPE 3000 -imps	10.60	102.8	98.10
HDPE 3000 +imps	9.00	102.1	96.66
HDPE 6000 - imps	7.37	82.28	77.17
LDPE un-aged	14.60	102.4	98.80
LDPE 3000 -imps	11.10	103.0	98.40
XL3 un-aged	10.30	135.5	129.02
XL3 3000 -imps	7.94	129.0	121.0
XL4 un-aged	9.35	129.8	123.17
XL4 3000 -imps	20.31	116.5	113.41

Table 6.1: Weibull distribution parameters for impulse ageing tests

6.3. Results obtained for thermal aged samples

Figures 6.7 to 6.10 show the breakdown results obtained for thermal ageing. For HDPE the breakdown strength reduces linearly with increases in time (Figure 6.7). The mean breakdown strength reduces quite fast from 194 to 152 $kVmm^{-1}$ after 14 days of ageing. The effect of thermal ageing can be observed after 6 days of thermal ageing.

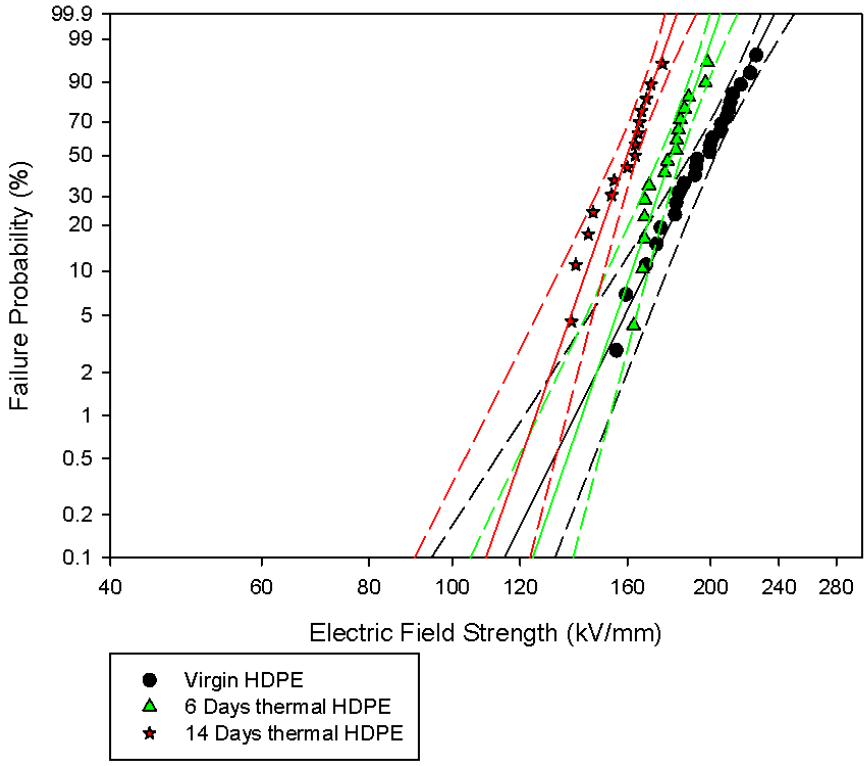

Figure 6.7: BD strength of virgin and thermal aged HDPE

However, the change in breakdown strength of LDPE is negligible after 14 days of thermal ageing (Figure 6.8). The breakdown strength of LDPE stays constant after 6 days of thermal ageing and just slightly reduces after 14 days of ageing. Confidence limits overlap across the whole range of obtained values.

While XL3 behaves differently (Figure 6.9), the breakdown of aged samples did decrease but the samples aged for 14 and 6 days have fairly close breakdown strengths. In other words, the relationship between ageing and time is more nonlinear for XL3 than as seen in the HDPE case.

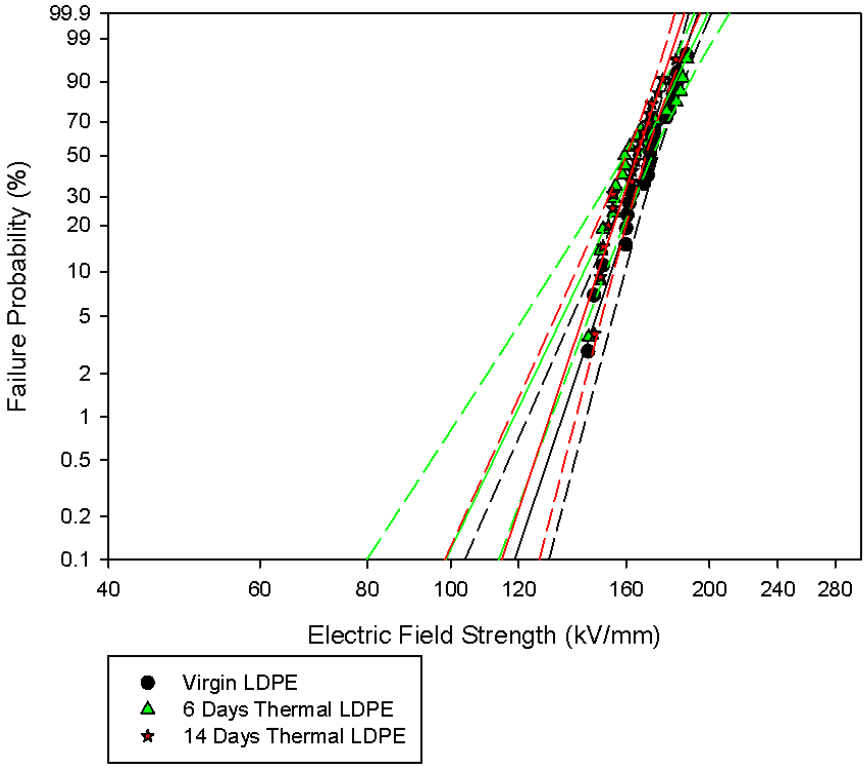

Figure 6.8: BD strength of virgin and thermal aged LDPE

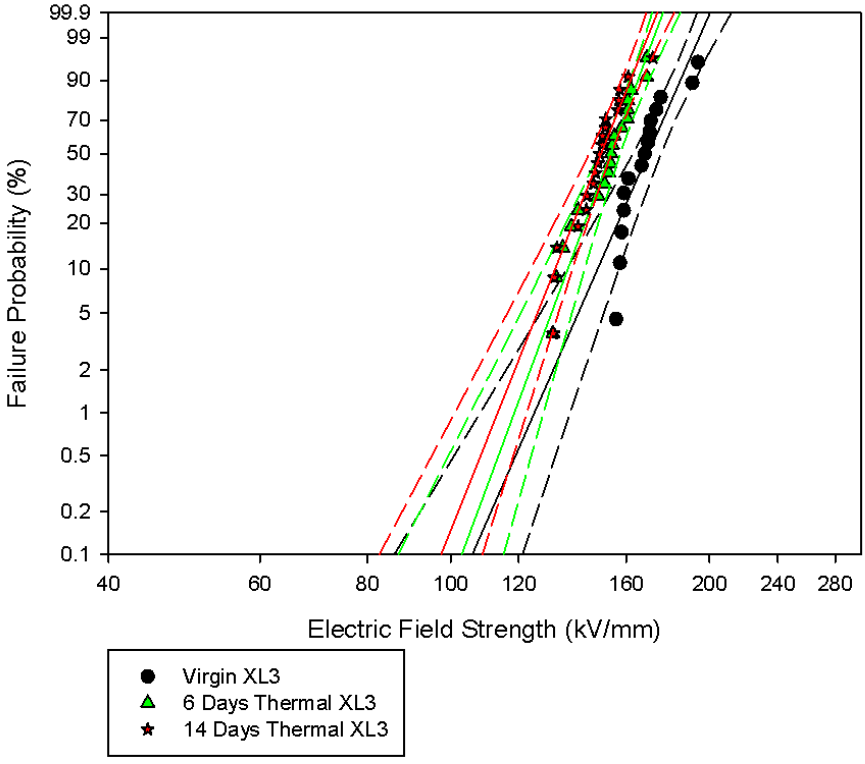

Figure 6.9: BD strength of virgin and thermal aged XL3

Figure 6.10 shows that XL4 seems to behave like HDPE where the breakdown strength continuously decreases with ageing time. However, the decrease rate is slightly lower for XL4 as the data separation is smaller.

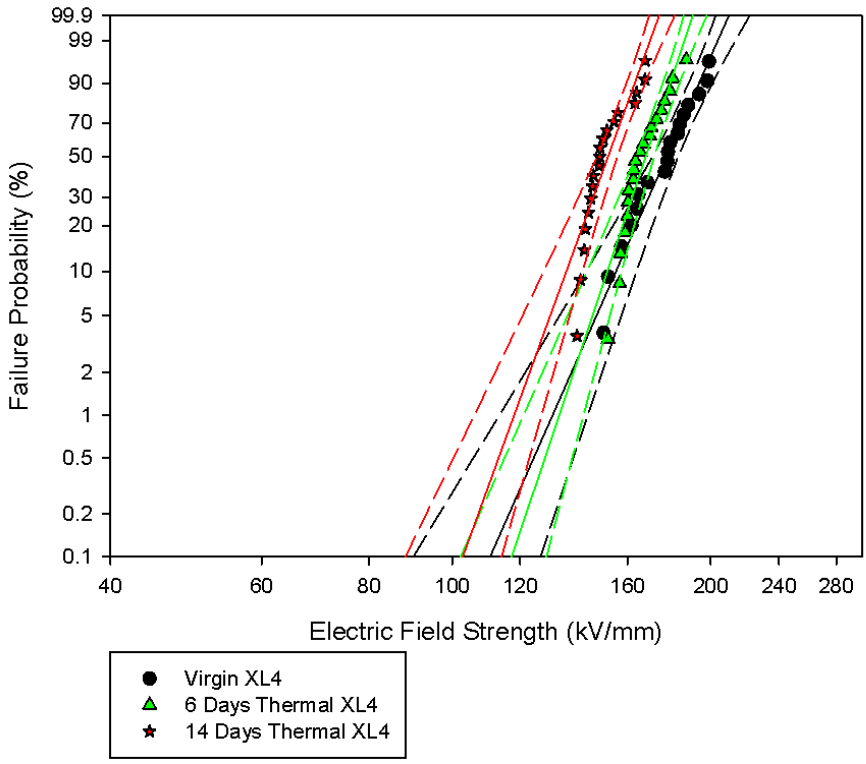

Figure 6.10: BD strength of virgin and thermal aged XL4

Materials	β	γ	Mean
HDPE un-aged	12.2	202.4	194.1
HDPE 6 days 95°C	17.6	183.8	178.3
HDPE 14 days 95°C	17.3	163.2	158.3
LDPE un-aged	18.0	174.1	169.0
LDPE 6 days 95°C	12.6	170.8	163.9
LDPE 14days 95°C	18.1	168.1	163.1
XL3 un-aged	13.9	174.2	167.8
XL3 6 days 95°C	16.4	156.9	151.9
XL3 14 days 95°C	15.2	153.2	148.0
XL4 un-aged	13.8	182	175.7
XL4 6 days 95°C	18.2	171.4	166.4
XL4 14 days 95°C	16.8	155.2	150.4

Table 6.2: Weibull distribution parameters for thermal ageing tests

Table 6.2 shows all the parameters obtained from the Weibull distribution of the breakdown measurement of thermally aged materials. Breakdown strength of all materials monotonically decreases with increasing ageing time. The breakdown strength of HDPE decreases fastest despite its highest virgin breakdown strength.

6.4. Results obtained for UV aged samples

Figures 6.11 to 6.14 and Table 6.3 detail the breakdown results of the UV ageing experiment. Generally, the breakdown strength of sample materials slowly reduces after 6 days and then dramatically drops after 14 days of ageing except for XL3. The significant losses in breakdown strength were observed particularly with samples of HDPE and LDPE. There is a very small reduction of breakdown strength if samples were aged for a short time, the breakdown strengths of LDPE and XL4 were observed to even increase a bit after 6 days of UV ageing. The ageing saturation behaviour was shown in the case of XL3. In this case, the reduction in breakdown strength after 6 days and 14 days are not significantly different.

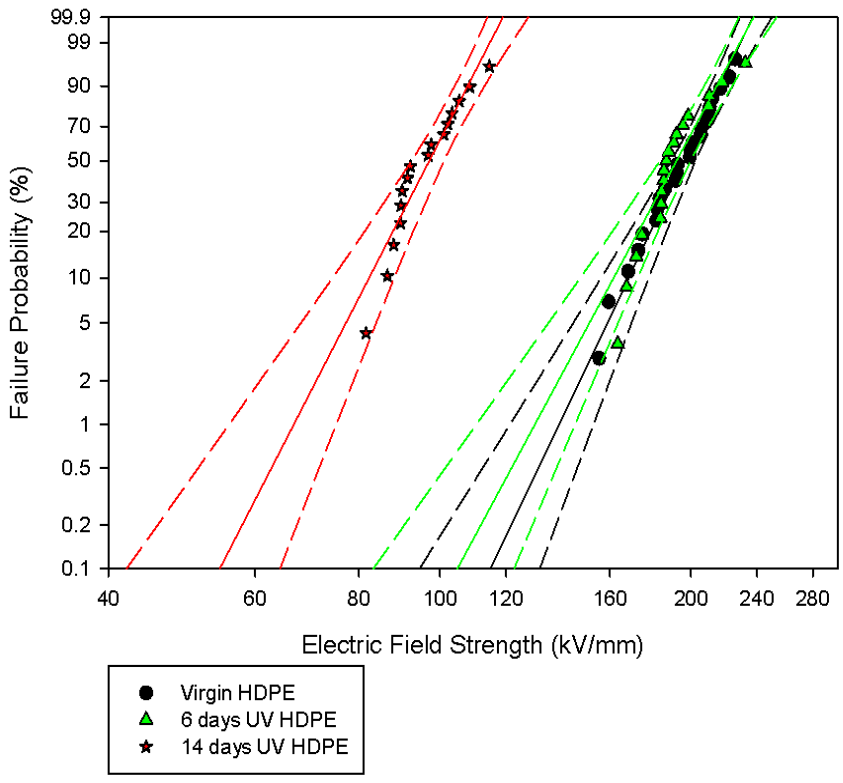

Figure 6.11: BD strength of virgin and UV aged HDPE

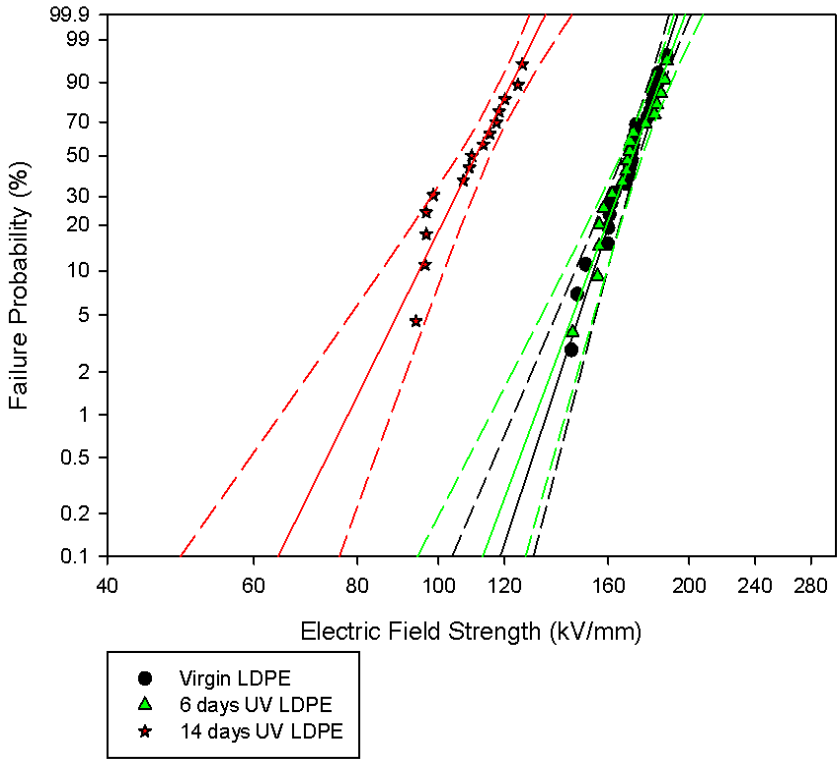

Figure 6.12: BD strength of virgin and UV aged LDPE

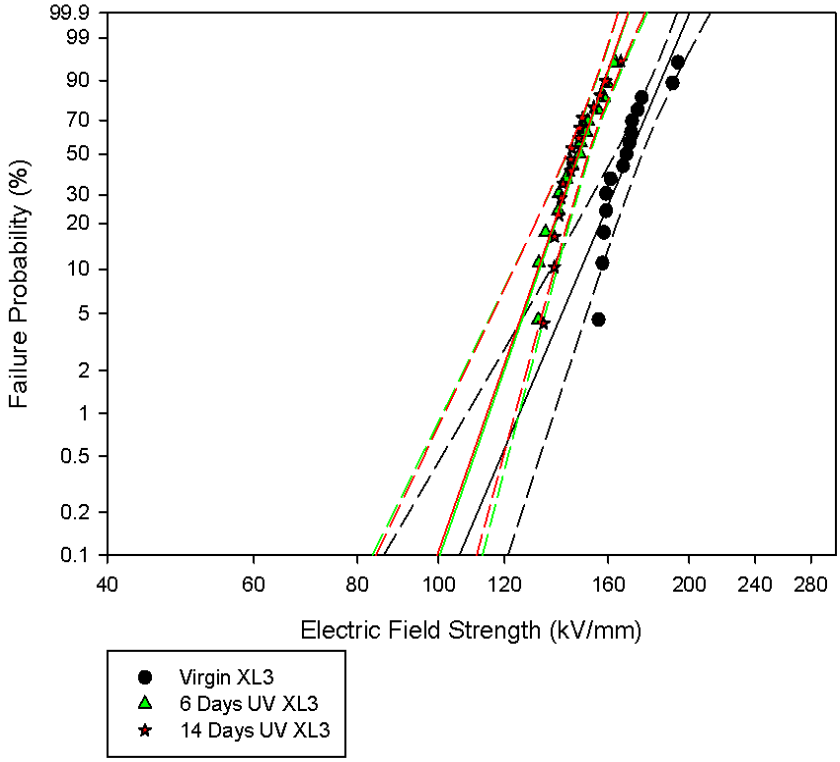

Figure 6.13: BD strength of virgin and UV aged XL3

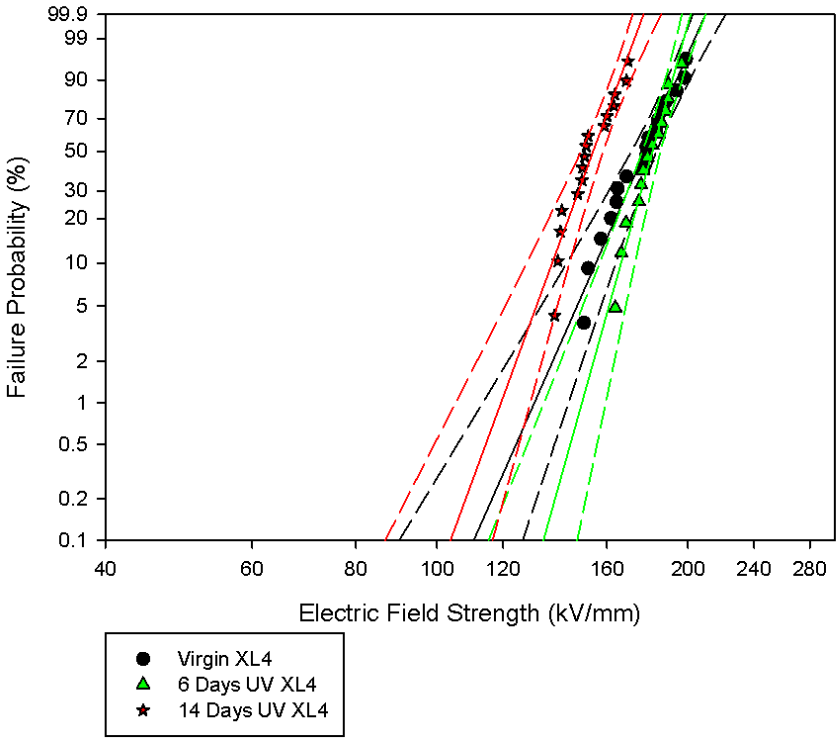

Figure 6.14: BD strength of virgin and UV aged XL4

Data in Table 6.3 shows the breakdown strength of HDPE drops by almost half after 14 days of UV ageing and by a third in the LDPE case. The reduction is less severe in the XLPE cases.

Materials	β	γ	Mean
HDPE un-aged	12.2	202.4	194.1
HDPE 6 days UV	10.8	198.8	189.7
HDPE 14 days UV	11.3	100.3	95.9
LDPE un-aged	18.0	174.2	169.0
LDPE 6 days UV	15.8	175.0	169.2
LDPE 14 days UV	11.9	114.3	109.5
XL3 un-aged	13.9	174.2	167.8
XL3 6 days UV	16/9	151.0	146.3
XL3 14 days UV	16.7	150.5	145.8
XL4 un-aged	13.8	182.0	175.7
XL4 6 days UV	21.7	184.3	179.8
XL4 14 days UV	16.6	157.4	152.4

Table 6.3: Weibull distribution parameters for UV ageing tests

6.5. Discussion and Summary

One interesting observation from the breakdown measurement data, is that most sets of breakdown data can be separated into two different groups, where each group has a different trend slope. The results in Figure 6.6 show this observation clearly. This suggests that there are at least two different breakdown mechanisms occurring within these materials. Due to scale of applied stress, they are believed to be thermal and electromechanical breakdown.

The other point is that breakdown strengths of materials undergoing thermal and UV experimental ageing are much higher than those obtained from impulse aged samples. The reason for this is that the effective volume of samples undergoing impulse ageing experiment is much higher than for the other two cases [85]. The Rogowski electrode is of course bigger than the point-point electrode [83, 84]. The thickness of samples used in impulse ageing was around 200 μm while other samples were only 60 to 80 μm thick in the other ageing processes. To maintain accuracy in the measurement of breakdown for thin samples needs a lot of care. A difference in just a few micrometers in thickness may lead to a big difference in breakdown strength if the thickness of samples is around 50 μm. It is recommended to use a good digital micrometer and a ball attachment anvil in order to determine sample thickness at the breakdown point. Samples are manufactured in the laboratory so the thickness can vary across the sample surface. The β parameters for uncoated samples were also higher than in the coated case. It seems that this parameter is also inversely proportional to the effective volume under stress (it is more likely due to the degree of homogenity of samples throughout volume under test). Therefore, to compare between ageing processes, the percentage of breakdown strength of aged samples compared with the breakdown strength of the virgin samples of the same thickness has been used (Figure 6.15).

The results from FTIR and breakdown measurement show that there is no clear relationship between electric strength and oxidation. The breakdown of impulse aged samples still decreases even when samples were not oxidized. The same effect can be observed in cases of thermally aged HDPE. In most cases, the increase in oxidation index leads to a reduction in breakdown strength except for thermal and UV aged XL3 where the big increases in oxidation content do not lead to a significant change

in breakdown measurement. This is in agreement with work of Montanari when he investigated the effect of thermal ageing with the real XLPE insulation cable. He suggest the threshold temperature is around 100^{o}C [18].

From Figure 6.15, the most sensitive material to ageing processes is HDPE and the most severe ageing occurs due to UV radiation. For impulse aged samples, it is thought that impulses may produce hot electrons with high energy that enter the material bulk. These electrons when colliding with molecules of the sample can damage molecular bonds and disturb the crystalline structure of material. The amorphous region may enlarge and the homogeneity of the material be reduced. This will lead to a reduction in breakdown strength of material. HDPE has higher crystallinity [58, 60] but its chains are not linked together therefore the crystalline structure and therefore will be disturbed easily. The consequent reduction in breakdown strength of HDPE will be the highest of all materials tested. With quenched cooled LDPE, the crystallinity of material is far lower. The contribution of increasing in amorphous region slightly after impulse ageing leads to a small change in breakdown strength. The situation observed for HDPE can be applied for XL3 and XL4 except their chains are linked together.

A similar trend to that observed for impulse aged samples is obtained for thermally aged samples. However, the introduction of oxidation in crosslinked polyethylene makes the electrical strength of these materials reduce further. Here the thermal energy alters the morphology of the sample and increases the chances of chain scission.

The most complicated situation occurs due to UV ageing. Firstly, the significant drop in breakdown strength of HDPE and LDPE after 14 days is believed to be a consequence of mechanical failure. The materials become very brittle with the increase in oxidation content [40, 162]. The sudden change in breakdown strength of HDPE and LDPE after 14 days of UV ageing is believed to be the effect of small amount of antioxidant additives from manufacturer [151-153]. The work from Ho and Bogg shows the consumption of antioxidants in BOPP capacitor by the UV exposure [163]. The breakdown strength of material also increases after short exposure time. After 6 days UV ageing, the antioxidants still exist in materials and the rate of reduction in breakdown strength is small. The XL3 has the highest oxidation content after 14 days but the breakdown strength is the same as 6 days UV.

This material is also less brittle compared to HDPE and LDPE after ageing. The effect of UV ageing after 6 days is not significant for any material except XL3. The UV crosslinking process may contribute to this effect. However, the longer ageing time will lead to the chain scission and the breakdown strength gradually reduces.

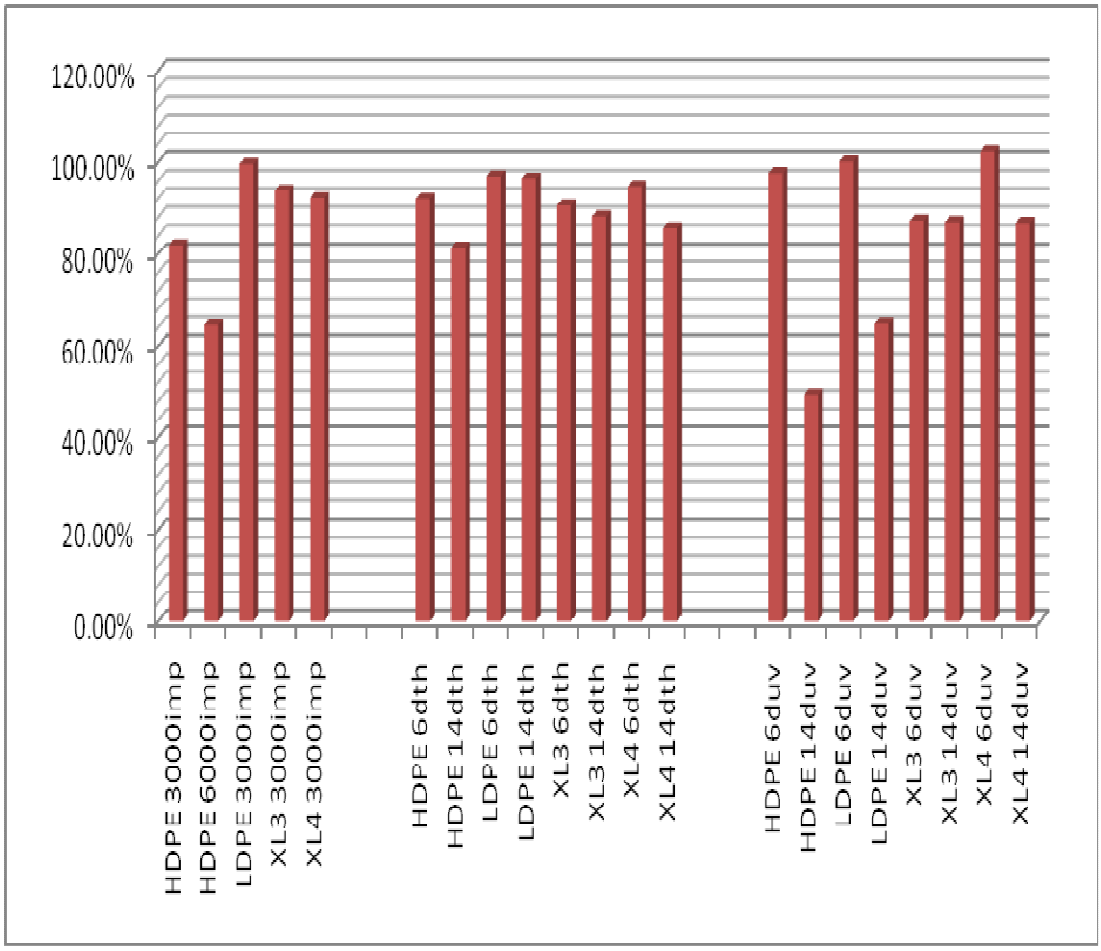

Figure 6.15: Percentage Breakdown Strength after Ageing

In summary, all ageing processes showed an effect on the breakdown strength of materials. Impulse ageing may cause molecular damage by producing hot electrons. Thermal ageing causes changes in morphology, chain scission and oxidation in some materials. UV ageing is the most aggressive as it causes a combination of chain scission, initial crosslinking as well as oxidation.

Chapter Seven

Dielectric Spectroscopy Characterisation

This chapter contains the results obtained from measurements of dielectric loss of materials aged using lightning impulse, thermal ageing and UV ageing. Reasons for the obtained spectra are proposed and take into account results obtained in terms of electrical breakdown and FTIR measurements.

7.1. Experiment for dielectric spectroscopy measurement

In this experiment dielectric response of aged samples was measured and compared with data for un-aged samples to identify any change. After the ageing process, the rims of the samples were cut off in order to produce circular sample discs. These samples were cleaned using water and then acetone. The sample was then put into the measuring cell and the assembly screen using a Faraday cage. There are two types of measuring cell that can be used, one for small samples and

a bigger sample holder (Figure 7.1). Each type has its own advantages. For the small cell (24mm diameter) the sample is isolated from its environment and this cell can also be used to determine the dielectric loss as a function of temperature. However, this cell is very fragile and its two electrodes are spring loaded, meaning that an empty cell measurement is impossible. The larger sample holder has a few electrode diameters for various sample sizes (10, 20, 30, 40mm), the closer the sample matches the electrode size the better the obtained result. An empty cell measurement is possible for this sample holder as it contains a micrometer as well. The sample holder has a guard ring to increase the accuracy of measurement.

The equipment used in this test is a Solartron system including the 1296 dielectric interface, the SI1260 Impedance/gain-phase analyzer and a computer controller. The thermal section is not integrated into the system, the chamber can only be heated using an external heater and the temperature of the chamber is measured using a digital thermometer. The possible frequency spectrum that can be investigated using this system is from 10^{-2} Hz to 10^{6} Hz. The lower frequency range was not considered because of the increased running time required per sample. The results for high frequency measurements (normally $>10^{3}$ Hz) are usually very noisy with low loss materials due to many sources of noise present in a working laboratory. The integration period is the time the system uses to calculate the average dielectric response of a sample and is usually set at 10 or 25 cycles. The greater the integration period the better the result achieved but the experiment time is increased. The Solartron system offers two measurement methods, “normal” and “reference”. The “normal” method measures the dielectric response of the sample and the sample holder directly and then subtracts the calculated result for sample holder to provide a final result. The “reference” method compares the dielectric response of sample with the internal capacitor bridge to provide the closest result with the real sample. The “reference” mode gives better results but normally requires double the measurement time. One disadvantage of this system is the result obtained for relative permittivity depends on the thickness of sample and the quality of fit between the sample and the sample holder. A small correction normally has to be applied to the result if

necessary (especially for the small electrode system), this is detailed in Appendix C.

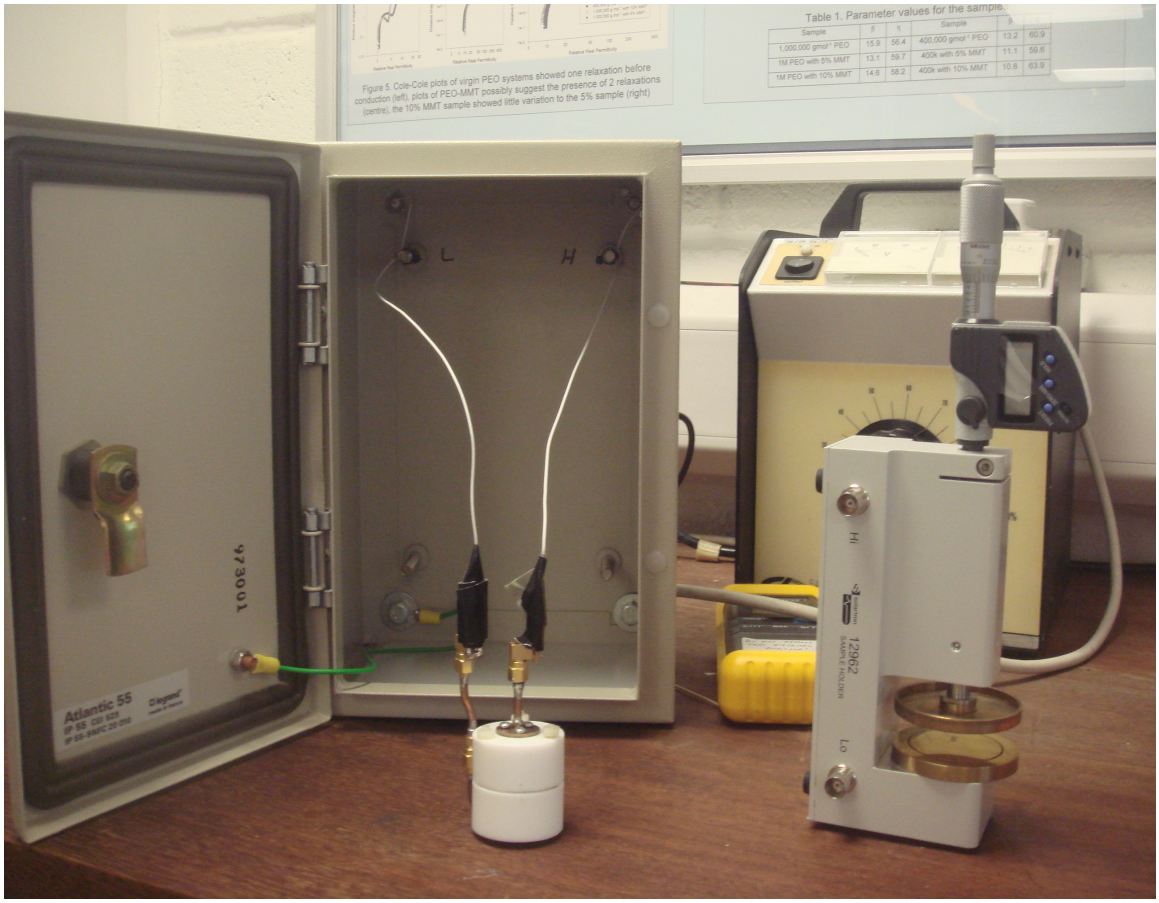

Figure 7.1: Small and large electrodes

7.2. Results obtained for impulse aged samples

Three different types of HDPE samples were tested these were samples that were unaged and did not have gold electrodes sputter coated on them, samples that were unaged and had gold electrodes and samples that were lightning impulse aged and had gold electrodes. The investigated frequency spectrum was from 10^{-1} to 10^{6} Hz. The obtained results are shown in Figure 7.2.

The uncoated sample has a higher loss factor (imaginary relative permittivity) compared to other samples and an increase in the real part of its relative permittivity as the frequency decreases. The reason for this may be the poor contact between the electrodes and the sample. This may lead to increases in interfacial polarisation. To have better contact with electrodes, all samples were then sputter coated prior to the measurement.

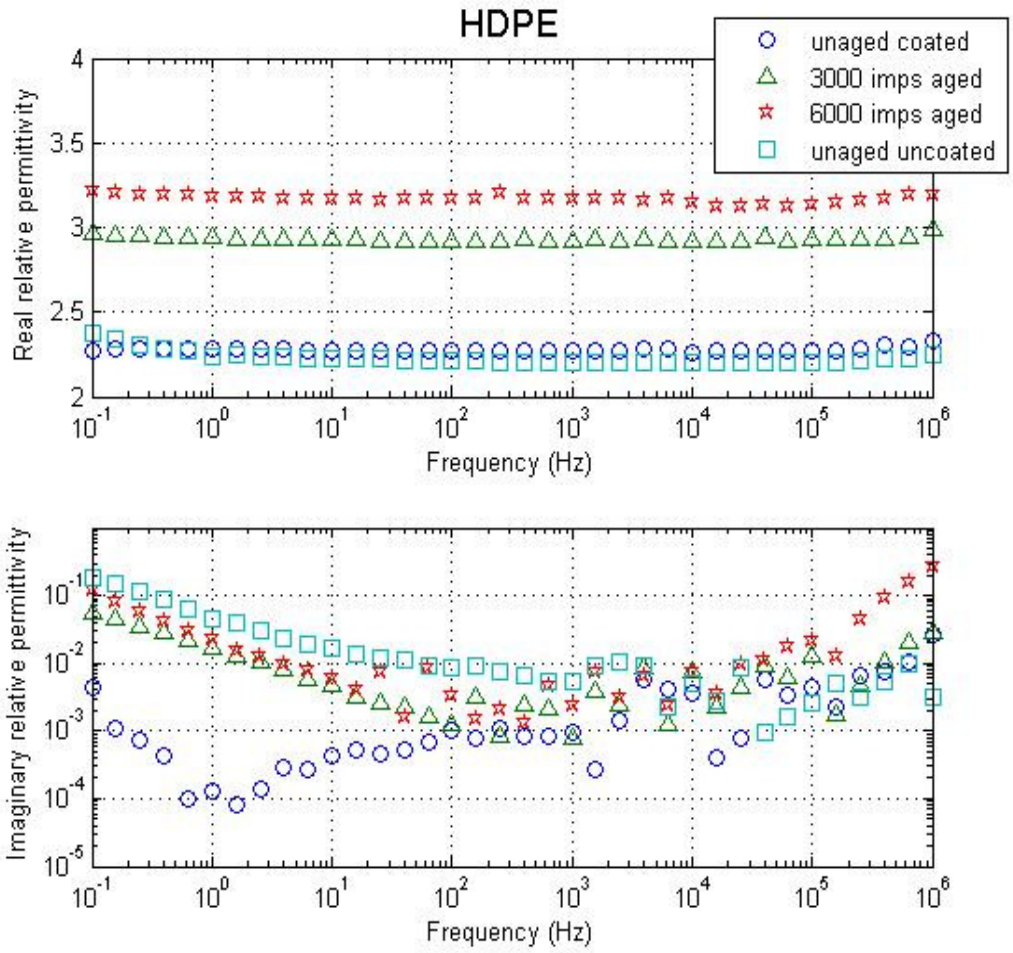

Figure 7.2: Relative permittivity of HDPE

For the unaged coated sample, the dielectric loss factor was much less than the other two sample types. However, with such a small tan delta it is very easy for external noise to affect the measurement. There is an increase in loss factor below 1 Hz and this is believed to be the effect of conduction as the real permittivity stays constant. It is clear that there is a big increase in permittivity of the impulse aged samples. The more impulses experienced by the sample the bigger the permittivity is. In this case the material is easier to polarise after impulse ageing. The loss factor starts to separate from the un-aged sample below 100 Hz. The material becomes more conductive after impulse ageing. This is believed to be the effect of ionic conduction. In fact the interfacial polarisation was obtained for a frequency lower than 0.1 Hz for the 6000 lightning impulse aged sample. The loss factor of 6000 impulse aged sample also has higher values across the high frequency range. It suggests more polar groups were generated or there was more chain scission to create smaller chains after ageing.

For LDPE (Figure 7.3), the loss factor of the aged sample is slightly higher than the un-aged sample over a certain frequency range. However, there is not a clear difference at power frequencies which were used for the breakdown measurements. The real part of the permittivity also stays constant with no difference for both samples. The measured value of the real relative permittivity is about 2.6 and this is a bit high compared to normal LDPE (about 2.3-2.4). This may be the consequence of quenching during sample preparation, the lower molecular weight and more branches on the main chains. All of these may lead to a less dense structure, so that molecules can move more easily. The insensitivity to impulse ageing of this LDPE is believed to be because of the disorder in the amorphous regions after quenching that dominates the properties of material and overshadows any effect of impulse ageing. Only data for dielectric spectroscopy of AC aged LDPE are available [115] where the increase in dielectric loss over the low frequency region was also obtained.

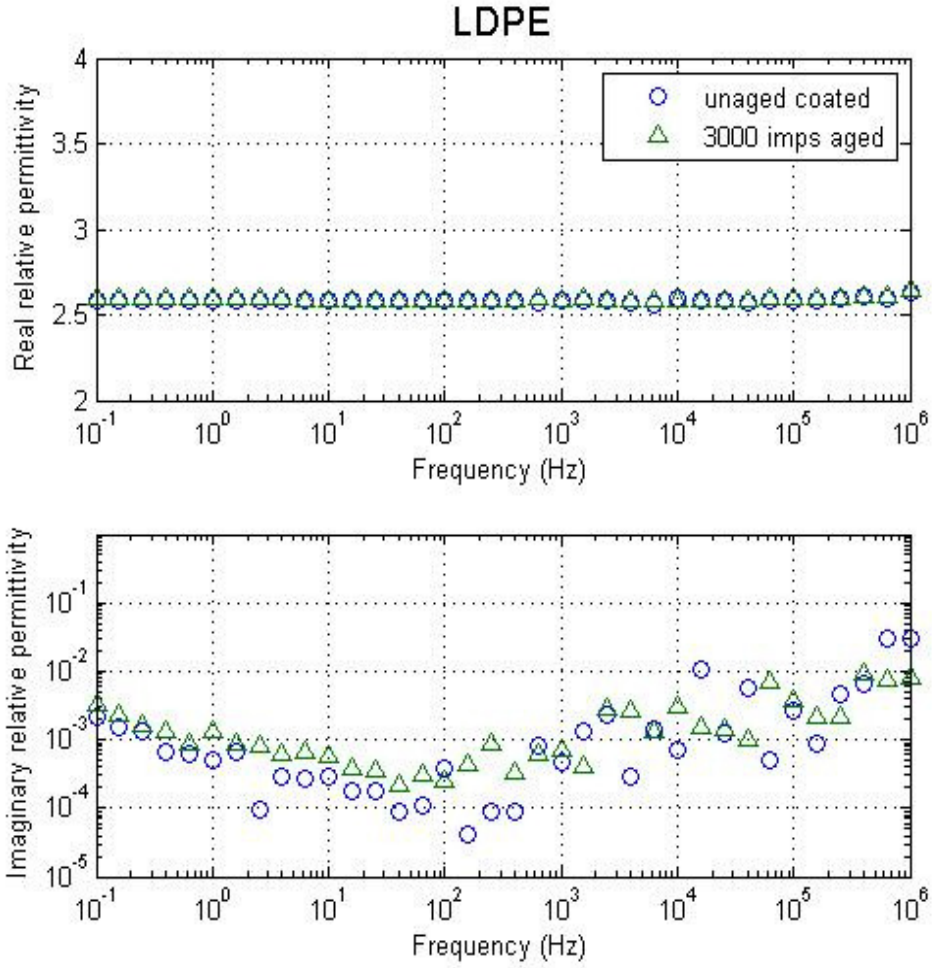

Figure 7.3: Relative permittivity of LDPE

After crosslinking by peroxide, the real part of permittivity is reduced from 2.6 to 2.3 (Figure 7.4). The crosslinking effect limits the movement of chains by linking chains to get a bigger structure. The loss factor of XL3 is not very much different from LDPE but the slope over the low frequency region is a bit steeper as conduction due to by-products may contribute to the losses. The losses for aged XL3 are very much the same as for the virgin sample except for higher values at very low frequencies. Therefore, ionic conduction can occur and increase loss. The real part of the permittivity increases slightly after 3000 lightning impulses. With no appearance of oxidation, this increase may be due to chain scission that allows molecules to move more easily. Again, there are no data for dielectric relaxation of impulse aged XLPE available for comparison. The results for dielectric spectroscopy of AC aged XLPE [116, 119] show that there is change in the dielectric relaxation curve over a very low frequency region (less than 10^{-1}Hz).

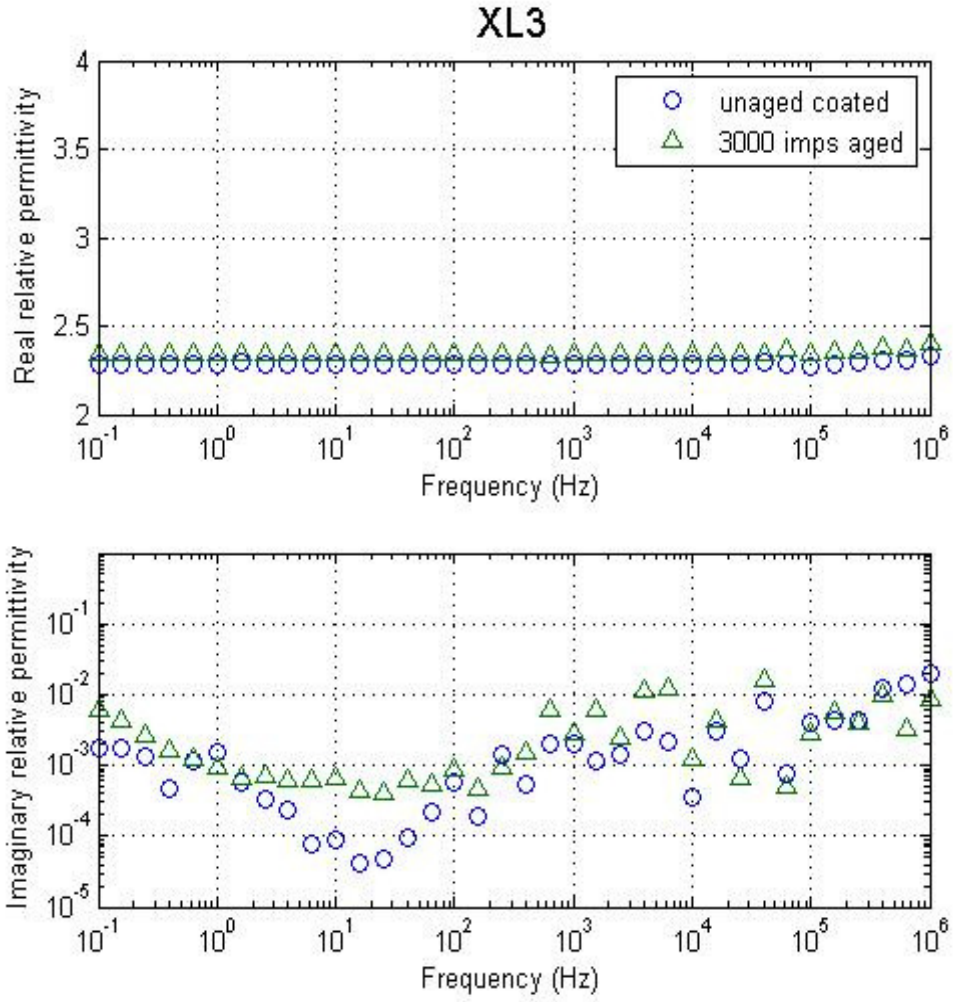

Figure 7.4: Relative permittivity of XL3

Figure 7.5 shows the dielectric spectroscopy of uncrosslinked 4421 (LDPE4), unaged XL4 and 3000 impulse aged XL4. The real part of LDPE4 is higher than XL4 due to the effect of crosslinking. Unlike LDPE, the XL4 behaves similar to the 6000 lightning impulses aged HDPE with an increase in both real permittivity and loss factor over the low frequency region. Again the interfacial polarisation cannot be observed clearly at room temperature as the applied frequency is not low enough. However, a slight increase in real permittivity at low frequencies can be observed.

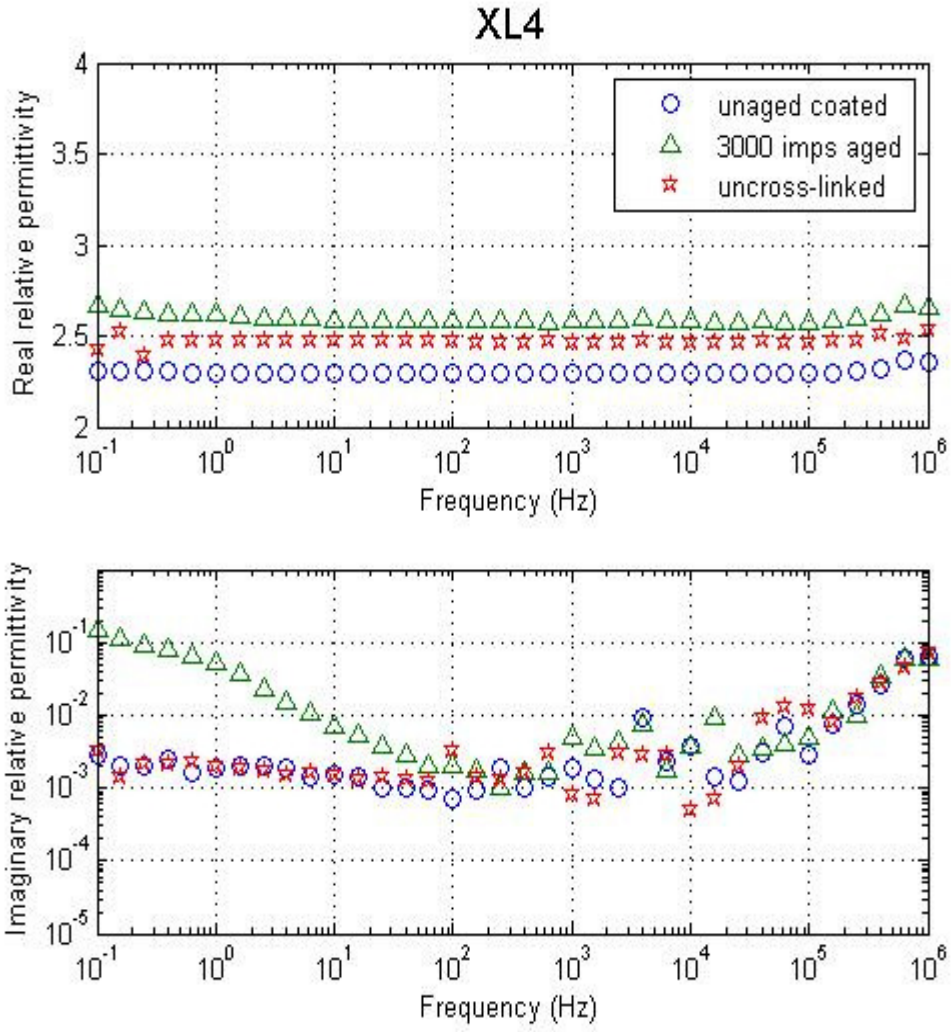

Figure 7.5: Relative permittivity of XL4

7.3. Results obtained for thermally aged samples

Figures 7.6 to 7.9 present the dielectric spectroscopy obtained for thermally aged materials. For HDPE samples the real part of the permittivity increases from 2.3 to

about 2.6 after 6 days of thermal ageing (Figure 7.6). There is a slight drop in permittivity over the high frequency region after 14 days ageing but the loss factor increases for frequencies lower than 1 kHz. Without the significant existence of oxidation from FTIR in Chapter 5, the explanation for thermal ageing affecting the dielectric response could be due to the formation of smaller chains by bond breaking and also the creation of a larger free volume inside the material. The combination of these effects will lead to the increasing the ability of molecules to move. However, a similar result for 14 days of thermal ageing of HDPE was obtained by Ashcraft and Boyd [109]. In this work, they milled HDPE in air at 160-170^{o}C and there was an effect of a small increase in the amount of carbonyl groups in material. Therefore the increase in loss after 14 days of thermal aged HDPE is believed to be due to a small amount of oxidation as well.

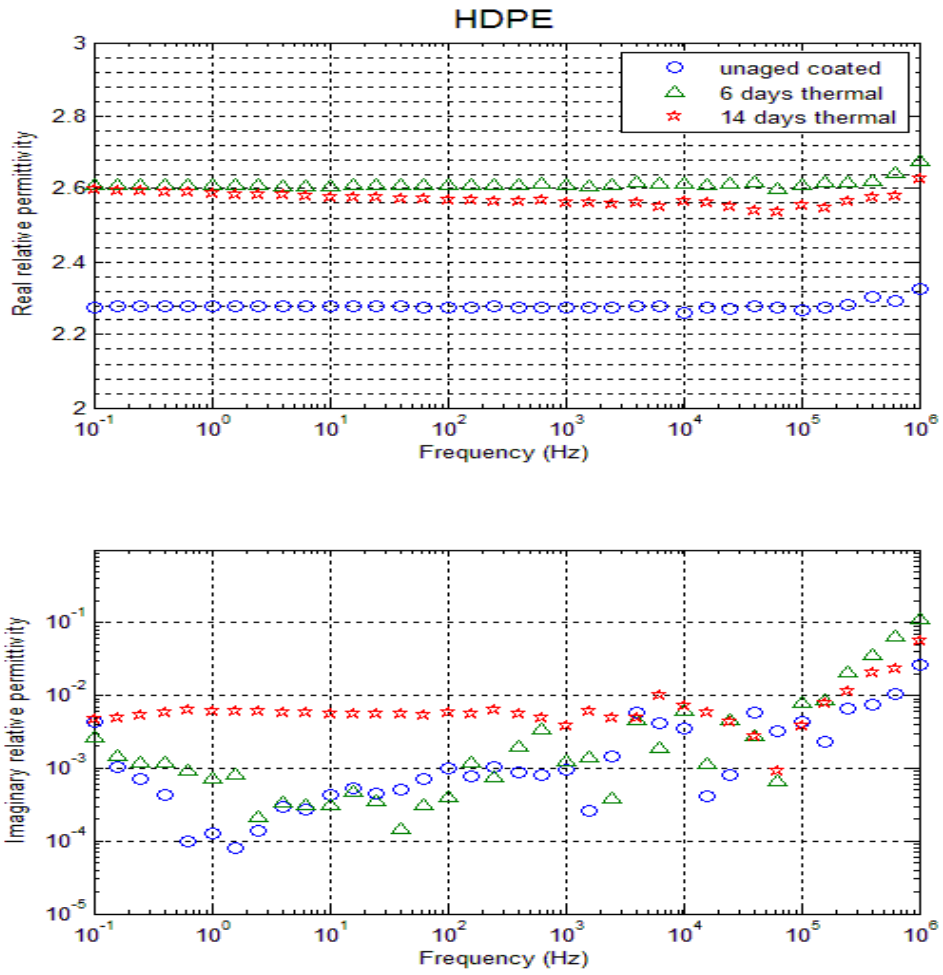

Figure 7.6: Relative permittivity of thermal aged HDPE

For LDPE, after 6 days of thermal ageing, the real permittivity is slightly decreased but then returns to the normal value after 14 days of ageing (Figure 7.7). The dielectric loss factor increases over the range from 1 Hz to 1 kHz after 6 days. This may be the combination effect of chain scission and the crystallization of the material. The former should increase both real and imaginary permittivity while the latter reduces the free volume and consequently the real permittivity. However, a peak is observed near the MegaHertz region. This could be due to the contribution of motions of the smaller molecules that have been created by the ageing process. However, there is a big decrease from 2.6 to 1 in the real relative permittivity after 14 days of thermal ageing of LDPE. This change is too big and may be due to errors during measurement. Similar results which show the dielectric relaxation curve of thermally aged LDPE was referenced by McCrum [96].

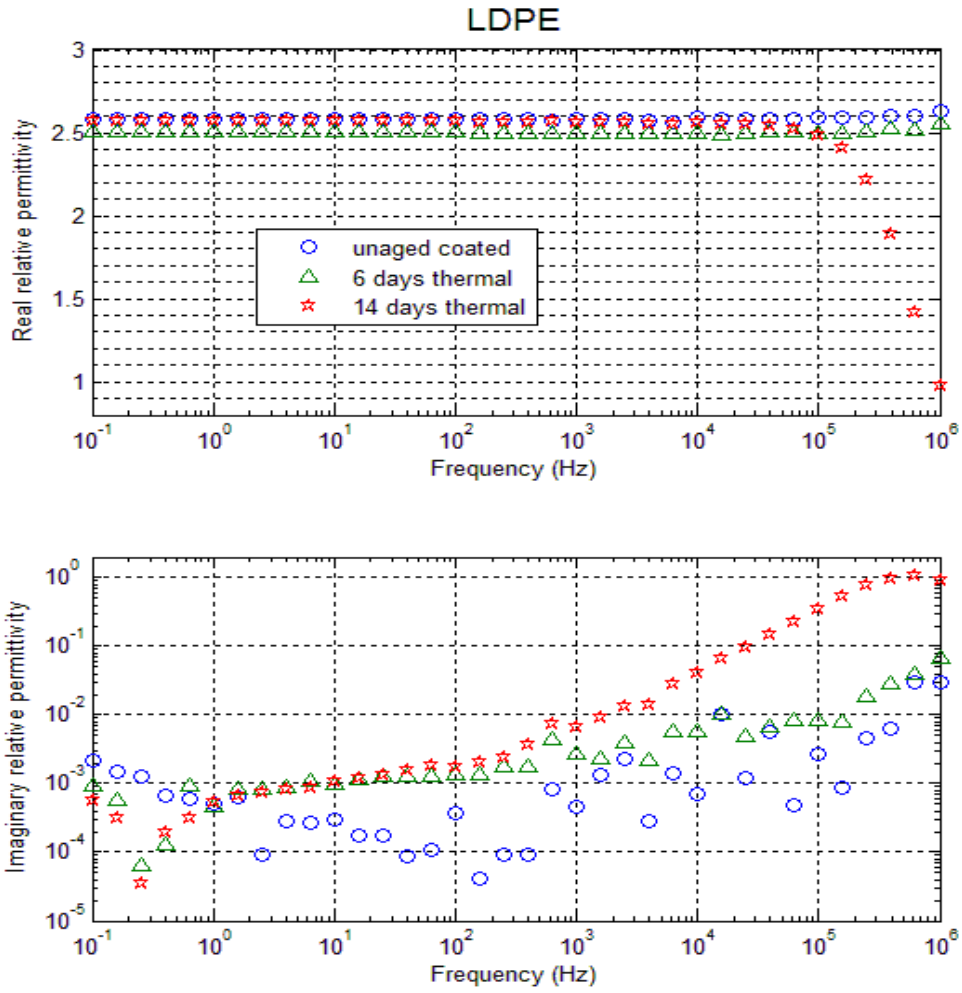

Figure 7.7: Relative permittivity of thermal aged LDPE

The effect of thermal ageing on the dielectric response of XL3 is shown in Figure 7.8. The real permittivity slightly increases after ageing. In this case bond breaking may be less effective because the chains are tightly crosslinked together. Even though, this effect is still noticeable. There is a reduction in conduction over the low frequency region as the consequence of the heat treatment. The amount of by-products in the sample will be reduced significantly after 6 days of ageing. The increase in loss factor over the medium frequency range after 14 days of thermal ageing is the effect of oxidation, where the contents of carbonyl and hydroxyl significantly increase in the sample (Chapter 5, Section 5.4). Motori found that at 100°C after 1000 hours of ageing, XLPE shows only a slightly increase in DC conductivity [20]. However, the dielectric loss increases more significantly when aged at 110°C [21]. The increase in dielectric loss and change in shape of the relaxation peak of XLPE in the very low frequency region was also obtained for temperatures higher than 110°C in the work of Reuter [27].

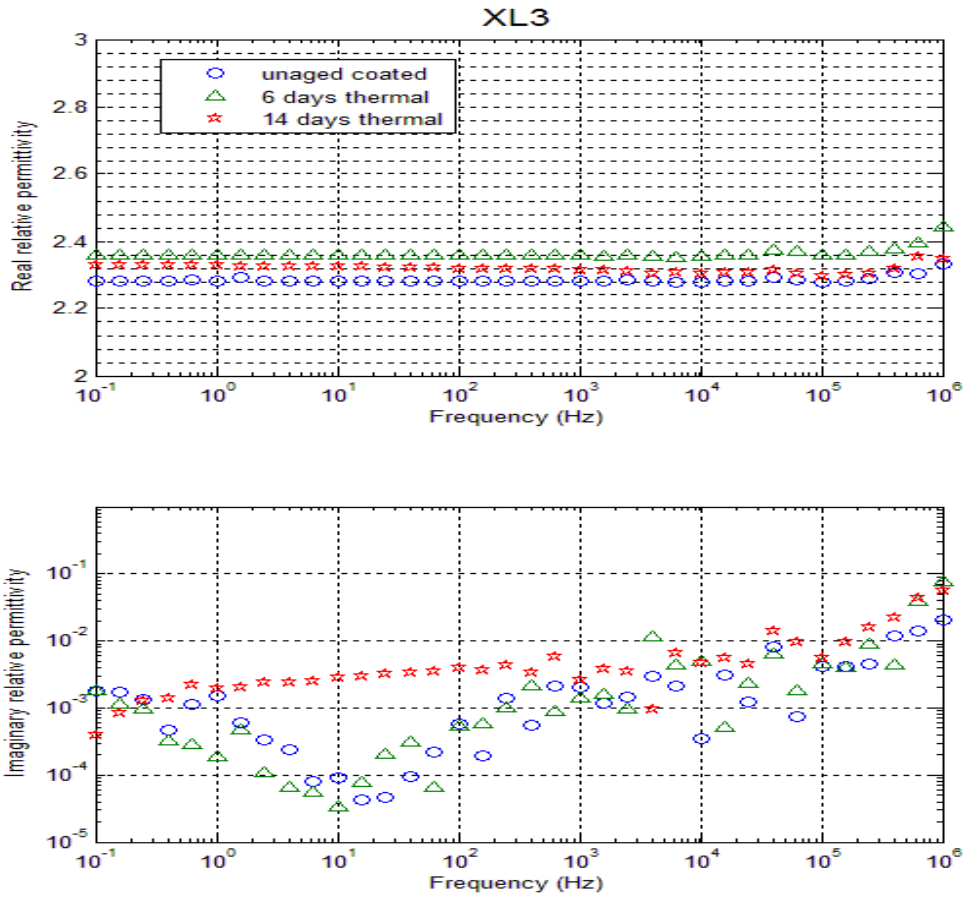

Figure 7.8: Relative permittivity of thermal aged XL3

The results for the change in dielectric response of XL4 show that there is a huge increase in both real and imaginary parts of the relative permittivity after 14 days of ageing (Figure 7.9). This result can be associated with both oxidation and bond breaking which again leads to the smaller size polar molecules. The peak loss should appear beyond the MegaHertz region as the real part gradually reduces at increasing frequency. The low frequency loss factor of the 6 days aged sample is a bit lower than the virgin one and suggests that there may be a reduction of water content in the sample from the moisture crosslinking process.

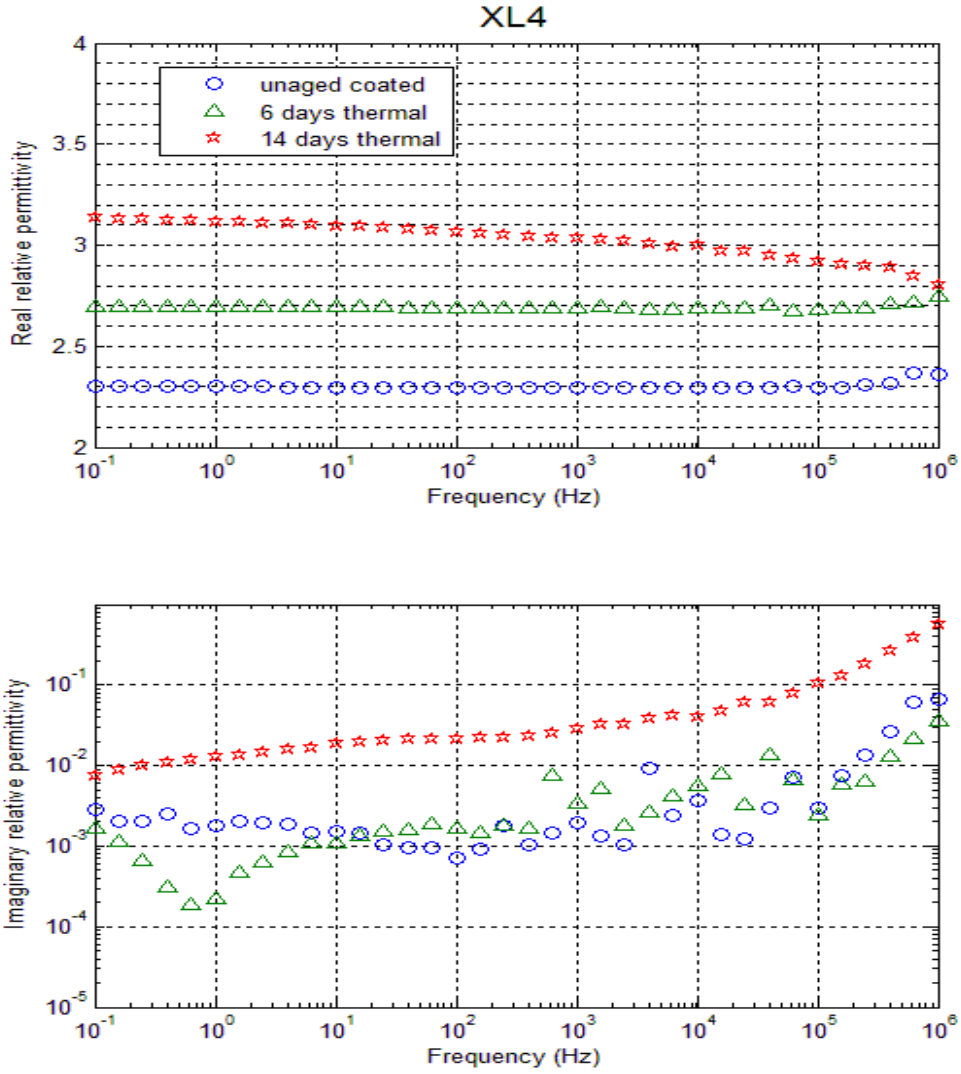

Figure 7.9: Relative permittivity of thermal aged XL4

7.4. Results obtained for UV aged samples

The results for UV ageing of HDPE are shown in Figure 7.10. When the ageing time is increased, both real and imaginary parts of the measured permittivity increase. As expected, UV ageing is a combination of effects including oxidation, bond breaking and crosslinking. However, with HDPE after 6 days of UV ageing, the effect due to additional crosslinking can be considered negligible. The bond breaking enhances both low frequency conduction and the movement ability of molecules in the material. Oxidation increases loss due to dipolar relaxation. This can be by rotation of the whole oxidized chain or the fluctuation of the chain segment which contains an oxidation group. The work of Stamboliev shows that the increase in oxidation in UV aged HDPE can lead to enhancement in α and γ relaxation of polyethylene whereas the β relaxation is limited [164].

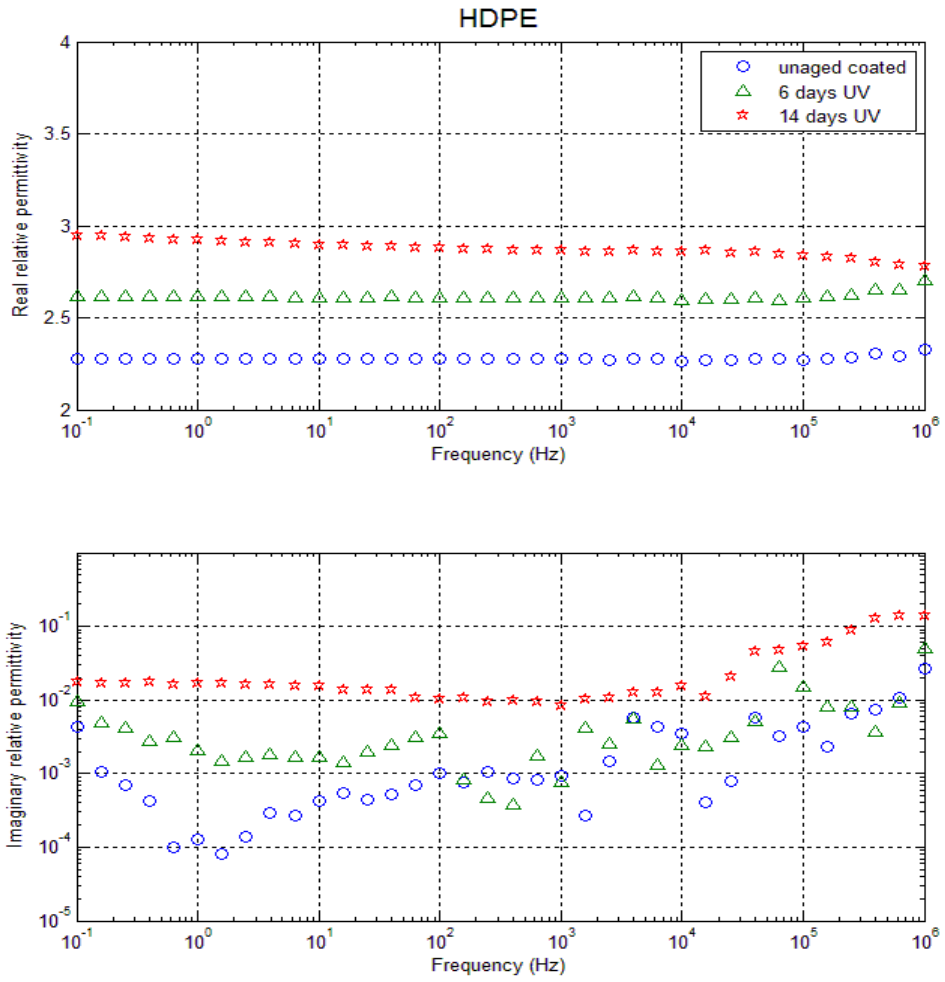

Figure 7.10: Relative permittivity of UV aged HDPE

The behaviour of LDPE is similar to HDPE except for the recovery of the real part of the permittivity after 14 days of ageing. The effect of oxidation is still the same but the effect of bond breaking and crosslinking may be different. The peak loss at high frequency for 14 days UV ageing is not clear (Figure 7.11). The similar effect was obtained in work of Leguenza and Scarpa where a relaxation peak in region of 10-100 Hz is observed for UV aged polyethylene without carbon black [120, 121].

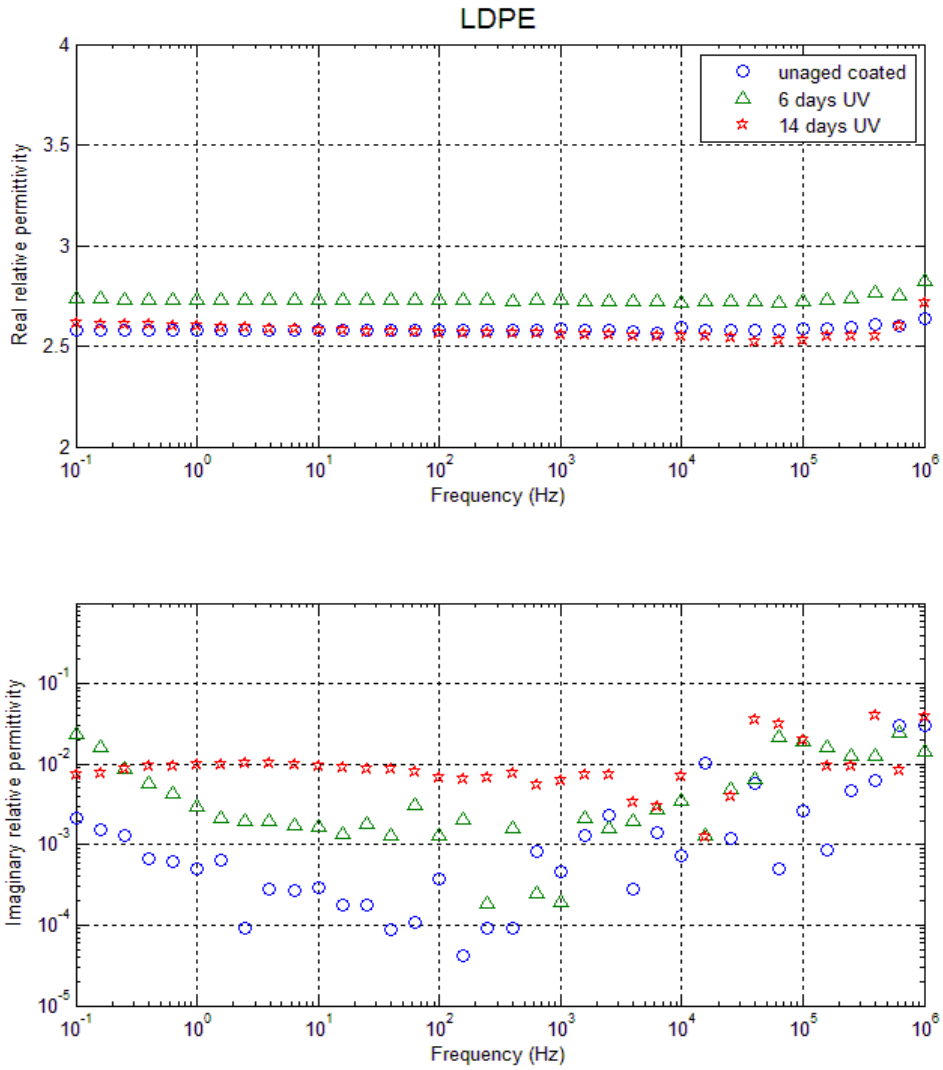

Figure 7.11: Relative permittivity of UV aged LDPE

The dielectric spectroscopy of XL3 and XL4 with UV ageing (Figure 7.12 and 7.13) are similar to that obtained for HDPE. However, samples were aged at a constant 40^{o}C temperature due to heat supplied from the UV bulb. The content of water inside XL4 and by-products in XL3 were expected to be reduced. This leads to a slight

reduction of conductivity after a short ageing time. XL4 seems more transparent to UV light therefore the time to get the same degree of ageing compared to other materials should be longer. The results from FTIR and dielectric spectroscopy of 6 days UV aged XL4 show almost no effect of oxidation.

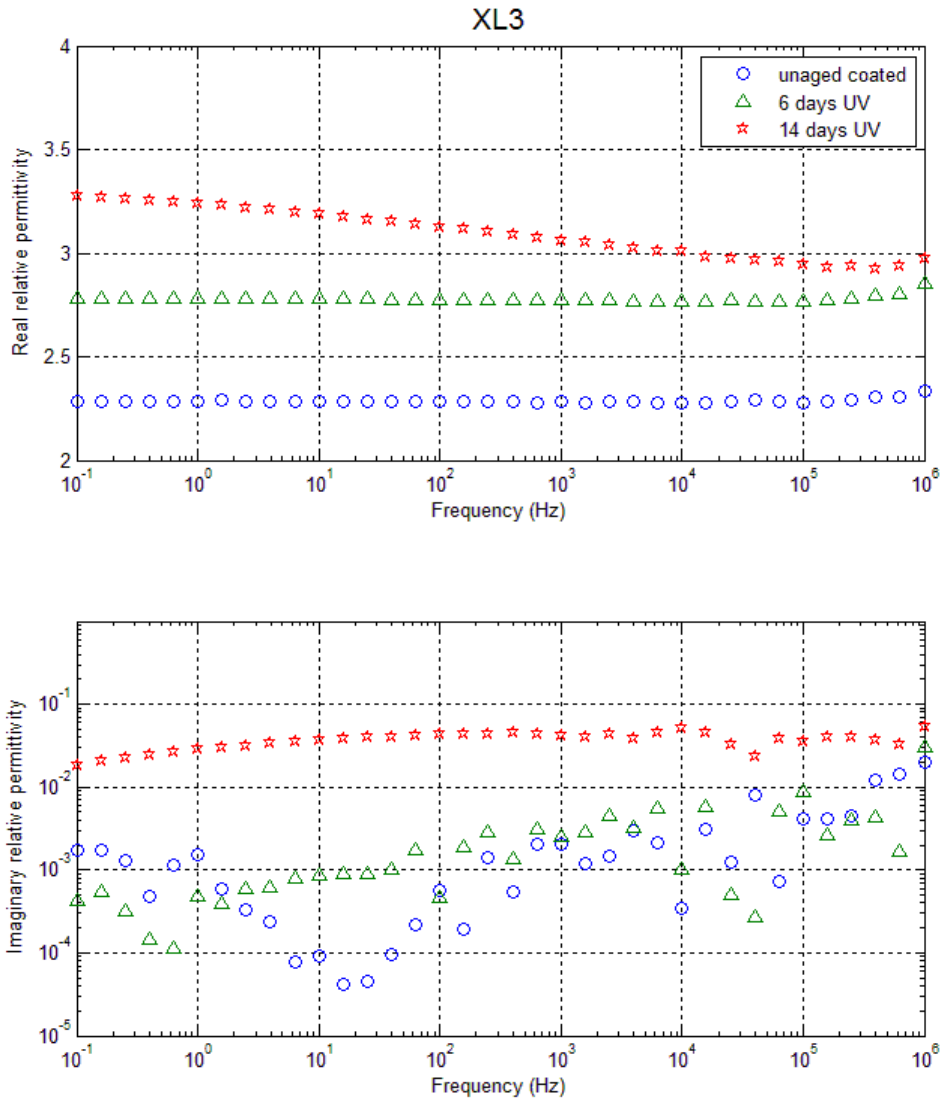

Figure 7.12: Relative permittivity of UV aged XL3

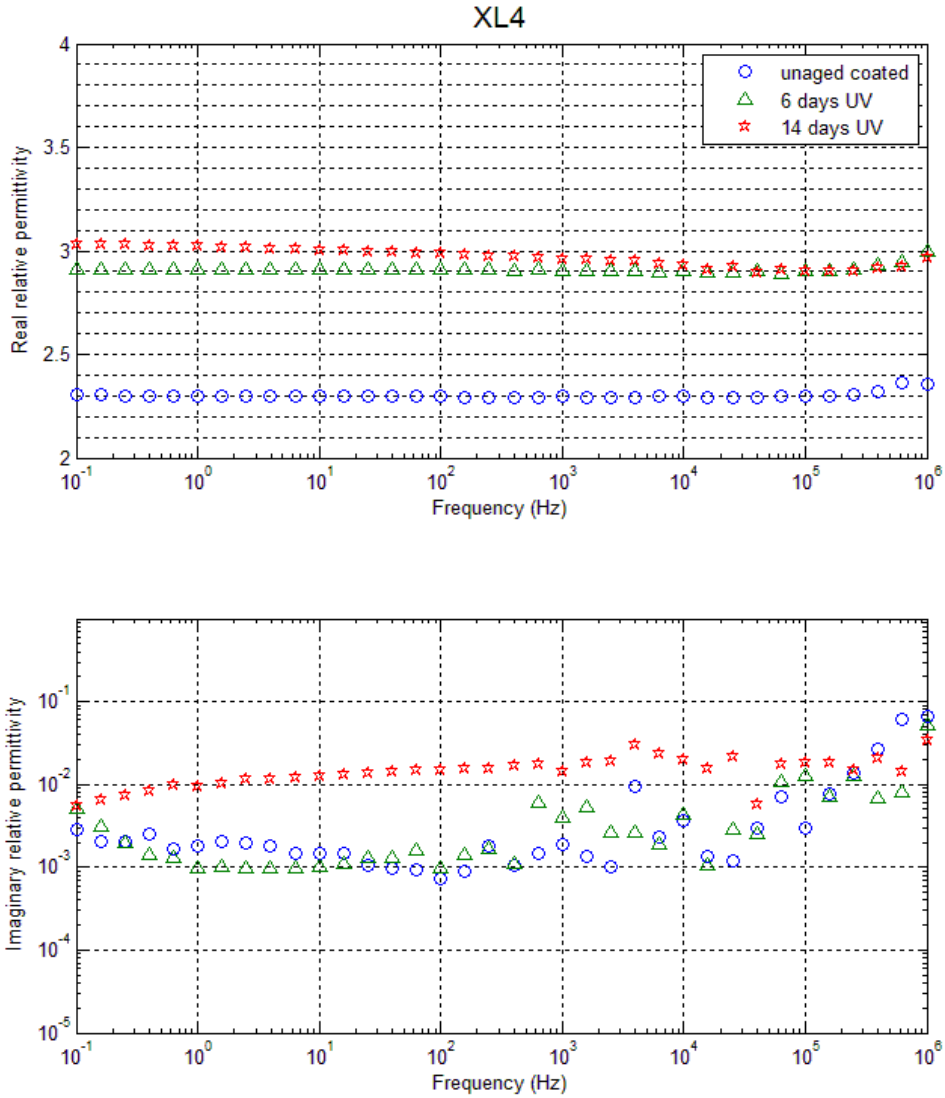

Figure 7.13: Relative permittivity of UV aged XL4

7.5. Discussion

Dielectric spectroscopy is known to be a very good method to obtain molecular dynamics for both low molecular weight materials and polymer systems [165-167]. In order to analyze dielectric spectra, models can be used to fit the data and relaxation peaks can be revealed. The empirical universal model [92, 94] has been used extensively by Scarpa, Das-Gupta, Lanca to study the behaviour of electrical and UV aged LDPE and XLPE [115-117, 119-122]. However, due to its universal origin, it is hard to correlate the relaxation peaks with molecular dynamics. The other

model that is also commonly used for dielectric spectroscopy analysis is the Havriliak/Negami (HN) model [98, 108, 168]. This is a derivation from Debye relaxation with two extra parameters, the broadening and asymmetric parameters. Normally a dielectric spectrum can be separated into a conduction component and several relaxation peaks. The dielectric loss factor (imaginary part of the relative permittivity) can be represented by the following equation [108]:

$$\varepsilon'' = \frac{a\sigma}{\varepsilon_0 \omega^s} - \sum_i \mathrm{im}\left[\frac{\Delta\varepsilon_i}{\left(1+(j\omega\tau_i)^{\alpha_i}\right)^{\gamma_i}}\right] \qquad (7.1)$$

Where σ is DC conductivity, a is a constant, s is the parameter related to the interfacial polarisation (0<s<1), i is the number of peaks, Δε is the dielectric strength of material, τ is relaxation time, α and γ are broadening and asymmetric parameters respectively (0<α,αγ<1). The measurement data can be fitted to equation (7.1) using a least mean square method [168]. The difficult part of the process is estimating how many peaks should be involved and how to relate these peaks with molecular dynamics. In fact, the combination of the dielectric spectroscopy and other spectroscopy methods, FTIR for example can provide a very concrete view of molecular structure. Figures 7.14 to 7.24 show the fit curves for normal and impulse aged dielectric response of four investigated materials. All fitting parameters are shown in Table 7.1. Dielectric spectroscopy of all samples can be fitted using one conduction function and two relaxation peaks. The conduction term is easy to understand as the combination of electric conductivity and interfacial polarisation, whereas the high frequency peak can be less important as it is out of measurement range. In fact most error from the fitting occurs over the frequency region higher than 10 kHz, where the high frequency measurement of this system is not reliable. This peak can be the relaxation of side chain motions or molecules which can easily move in amorphous regions [109, 169]. In normal polyethylene, only a very weak peak can obtained as material is non-polar and normally, material has to be lightly oxidized or chlorinated to obtain a clear relaxation peak [109]. The existence of a weak peak which appears in region of 1 kHz to 10kHz is controversial, either it is a real relaxation peak or just noise measurement. Several publications show a similar profile for dielectric spectroscopy of LDPE and also XLPE [104, 116, 118, 170]. Work from Das-Gupta and Scarpa suggests this is the consequence of cluster water [116]. However, this is quite ambiguous and not clearly supported. It is well known

that the relaxation frequency of free water is in the frequency range of GHz and the frequency of peak relaxation will move to a lower frequency region when the water motions are constrained [171, 172]. The effect of water with peaks at 4 MHz and 3 kHz in HDPE was obtained but at extremely low temperature [173]. Water absorbed by fillers of nano-composites usually exists in the interfacial region of fillers and this usually leads to an increase in conduction and relaxation over the low frequency region [98, 174, 175]. Water absorption can move the position of relaxation peak to a frequency higher than 1 kHz in the case of $CaCO_3$ filled HDPE left in 100% humidity for more than 10 days [176] and of course manufactured samples in this research would not have contained that much water. The idea of relating this peak to chain end motion, branch-point motion and chain rotation [109, 164, 177] is supported by data obtained in Table 7.1. LDPE and XL3 have the same base material; however, the dielectric strength of the first peak of LDPE is higher than XL3. The relaxation time of the first peak of XL3 is also longer than LDPE. This can be understood that the local segmental motions in XL3 are limited due to crosslinked chains compared to LDPE. All materials after impulse ageing have higher relaxation strength and shorter relaxation time. This is in agreement with the fact that impulse ageing can cause chain scissions and chain segments can fluctuate more easily. In Figure 7.17, the spectrum contains one peak in a region of 50 Hz if two relaxation functions are used. However, this peak does not significantly affect to the whole fitting process. When this peak is removed, the fitted curve consists of one conduction and one relaxation component (Figure 7.18). The obtained relaxation peak has the same strength and position as the second peak in Figure 7.17. In all other cases, the fitted curves need at least two relaxation components to return reasonable low errors and meaningful shape parameters. For all impulse ageing samples, the DC conductivity is significantly increased (Table 7.1).

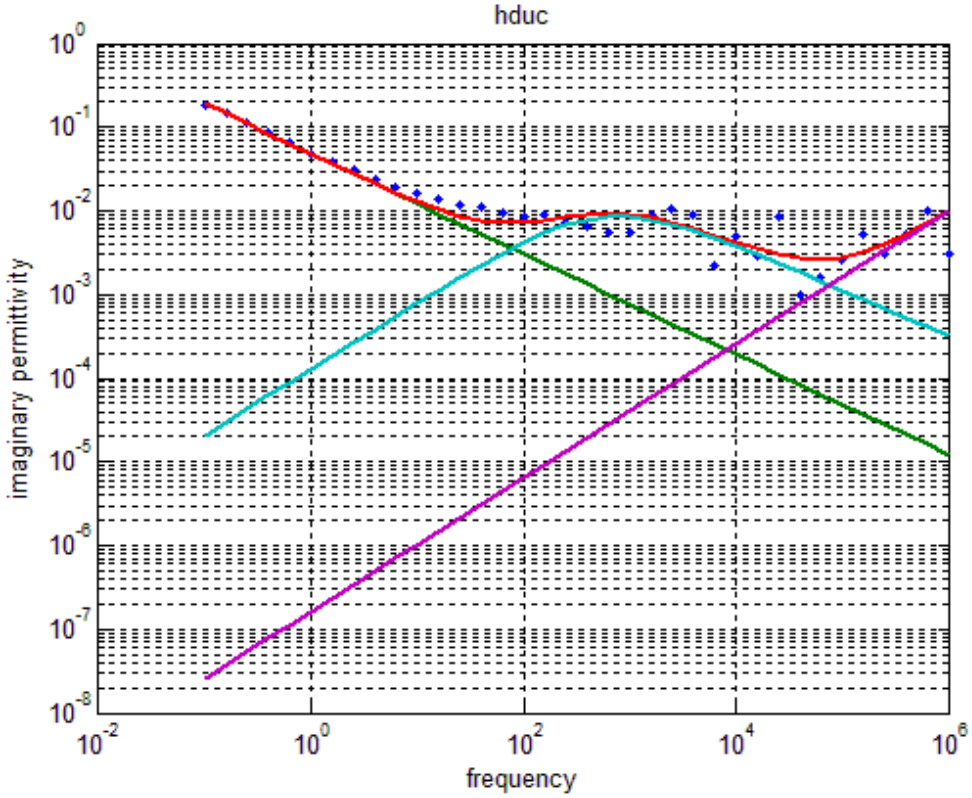

Figure 7.14: Imaginary relative permittivity of uncoated HDPE. Red: combined curve, Green: conduction, Blue: first relaxation, Purple: second relaxation

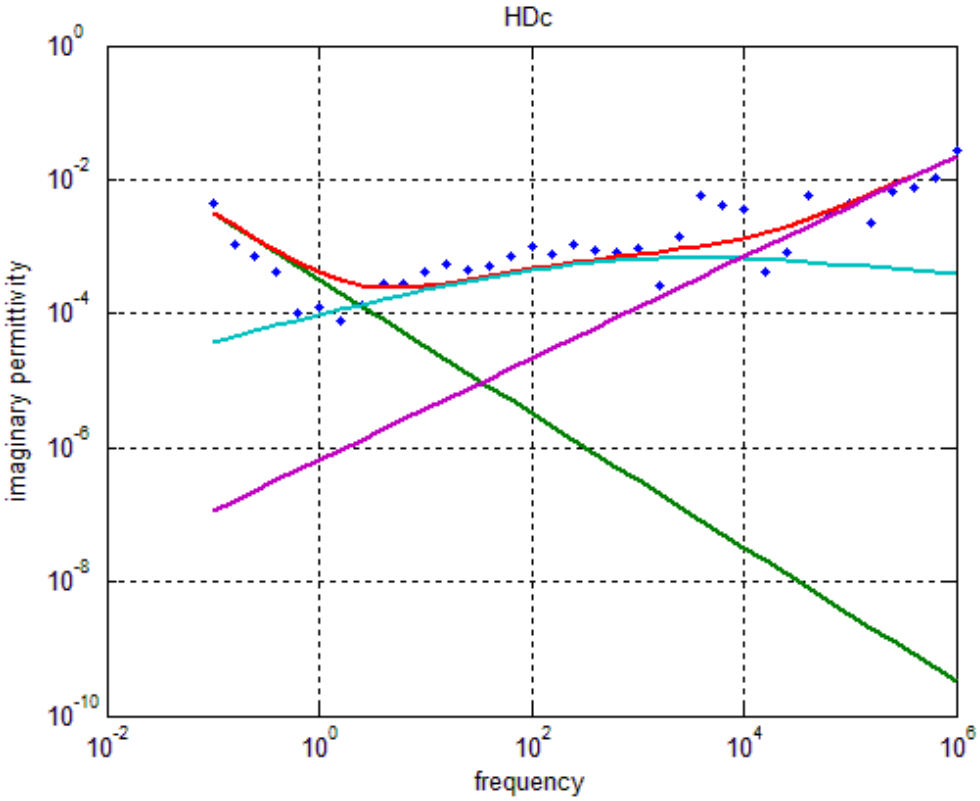

Figure 7.15: Imaginary relative permittivity of coated HDPE. Red: combined curve, Green: conduction, Blue: first relaxation, Purple: second relaxation

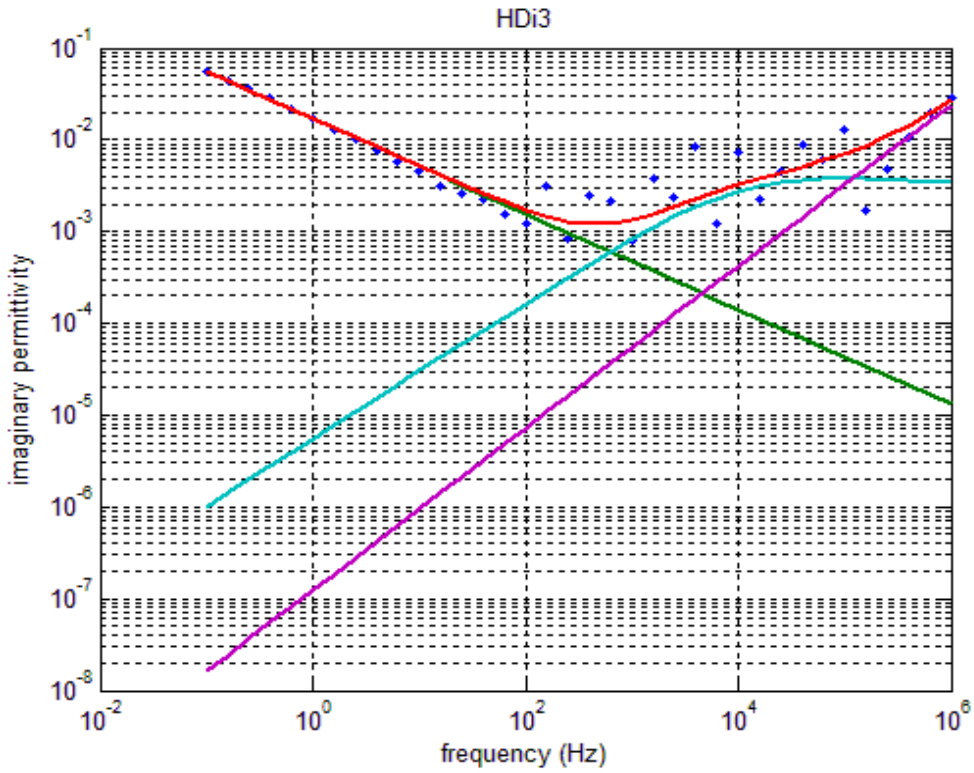

Figure 7.16: Imaginary relative permittivity of 3000 impulses aged HDPE. Red: combined curve, Green: conduction, Blue: first relaxation, Purple: second relaxation

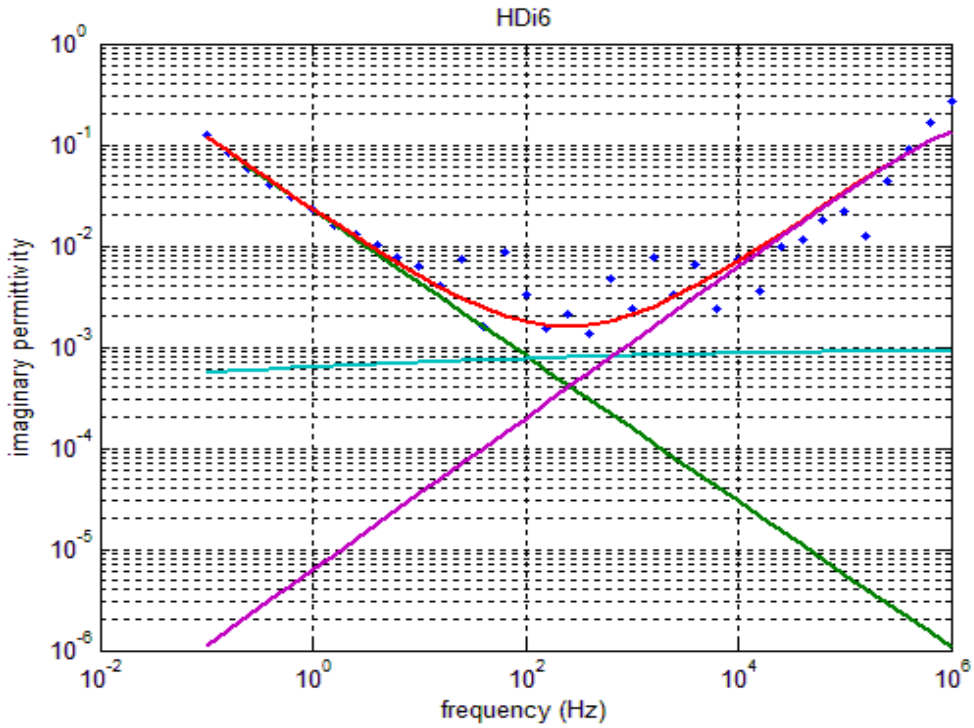

Figure 7.17: Imaginary relative permittivity of 6000 impulses aged HDPE. Red: combined curve, Green: conduction, Blue: first relaxation, Purple: second relaxation

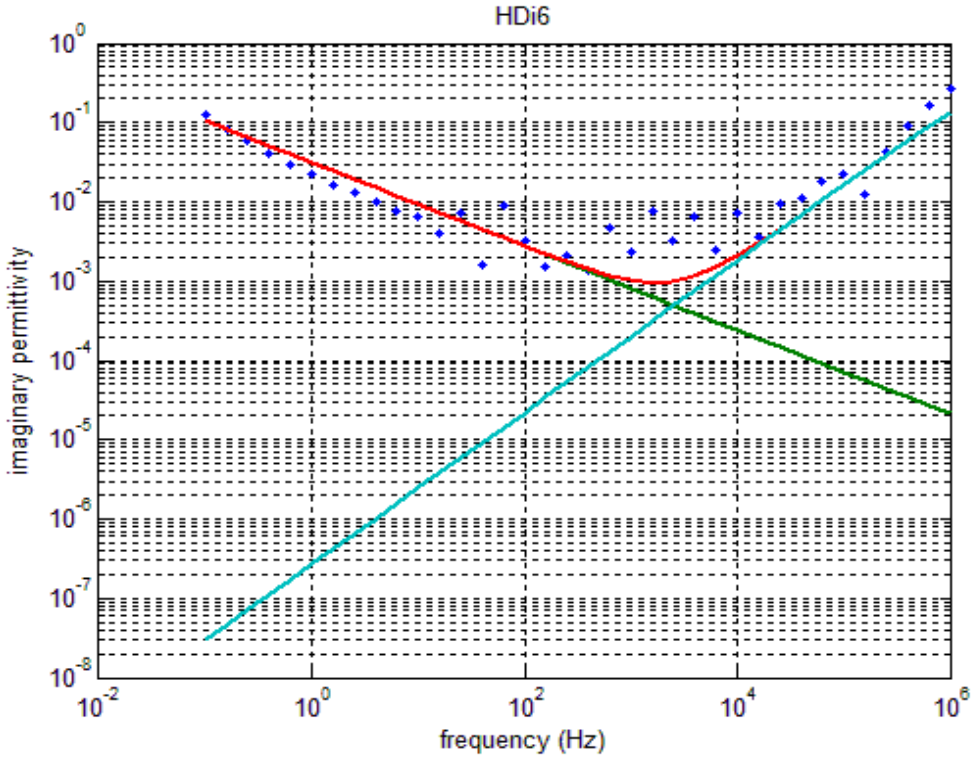

Figure 7.18: Imaginary relative permittivity of 6000 impulses aged HDPE with one relaxation component. Red: combined curve, Green: conduction, Blue: first relaxation

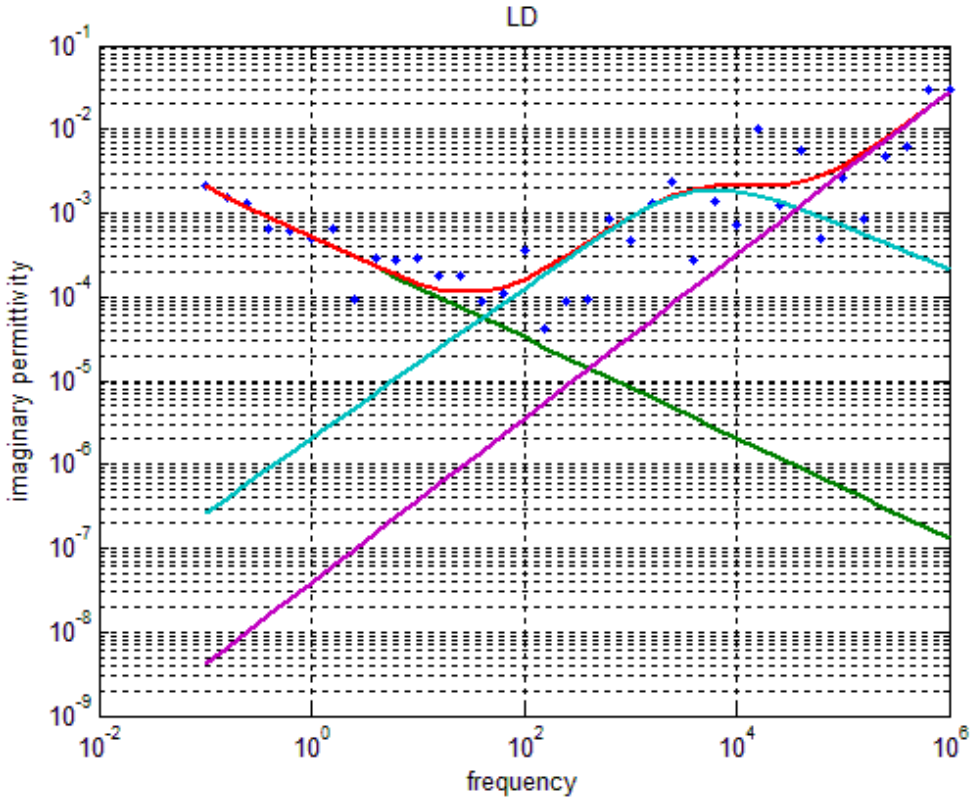

Figure 7.19: Imaginary relative permittivity of coated LDPE. Red: combined curve, Green: conduction, Blue: first relaxation, Purple: second relaxation

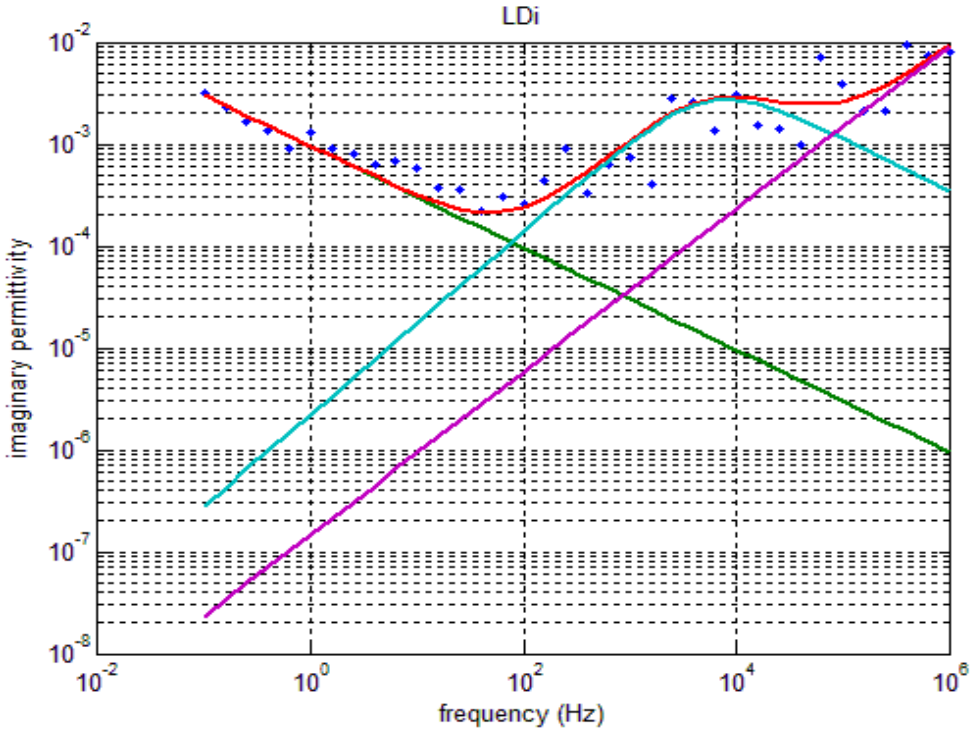

Figure 7.20: Imaginary relative permittivity of 3000 impulses aged LDPE. Red: combined curve, Green: conduction, Blue: first relaxation, Purple: second relaxation

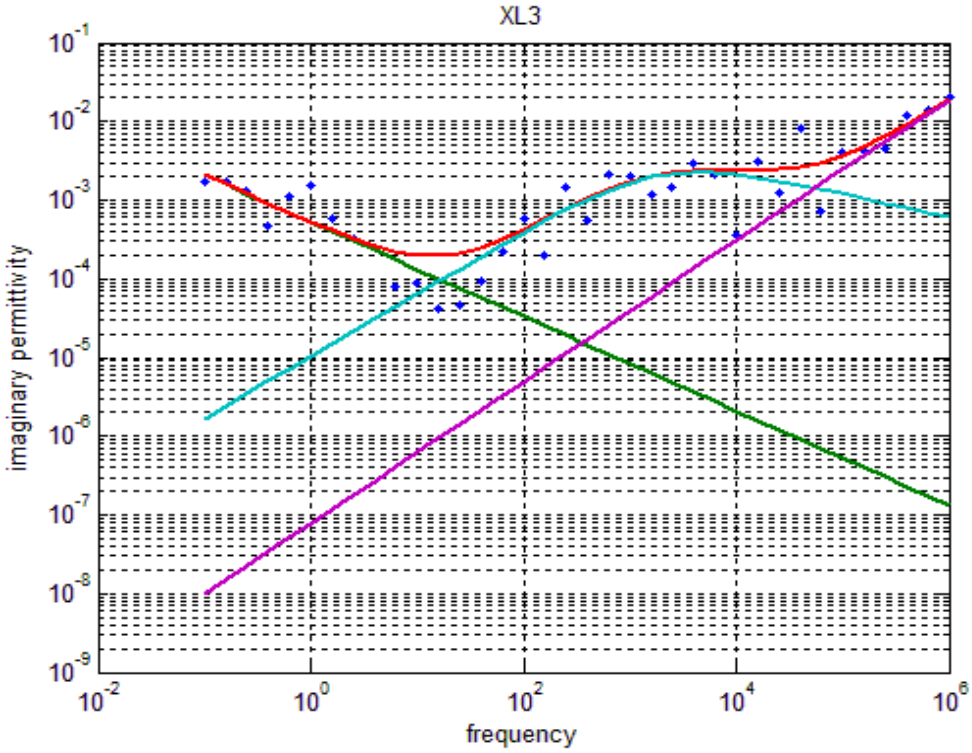

Figure 7.21: Imaginary relative permittivity of coated XL3. Red: combined curve, Green: conduction, Blue: first relaxation, Purple: second relaxation

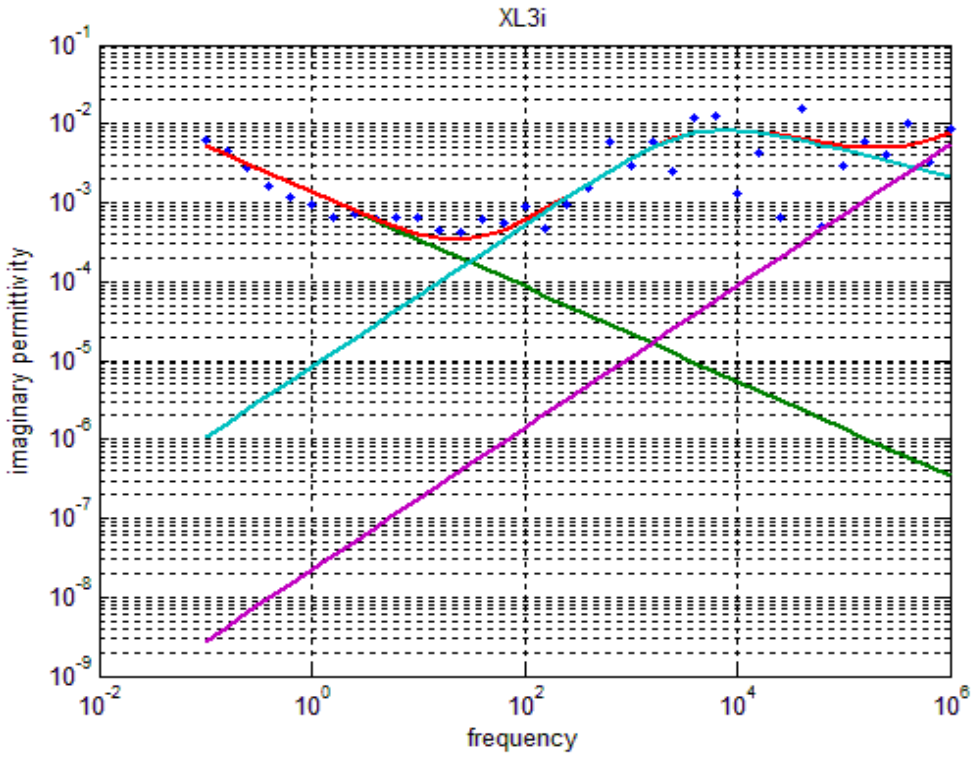

Figure 7.22: Imaginary relative permittivity of 3000 impulses aged XL3. Red: combined curve, Green: conduction, Blue: first relaxation, Purple: second relaxation

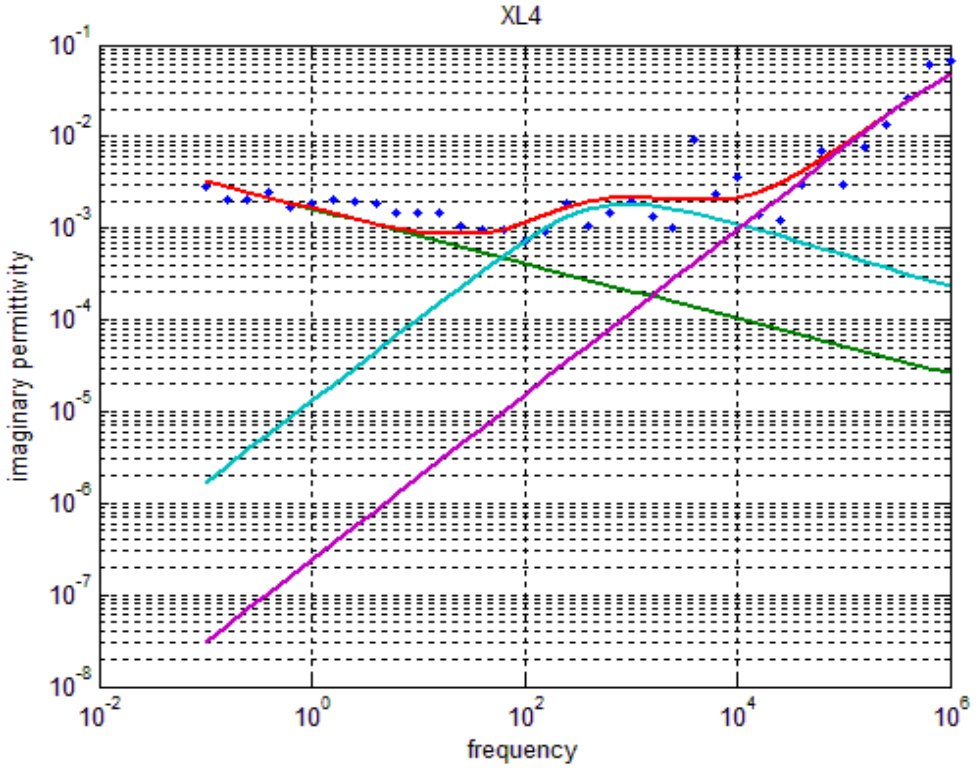

Figure 7.23: Imaginary relative permittivity of coated XL4. Red: combined curve, Green: conduction, Blue: first relaxation, Purple: second relaxation

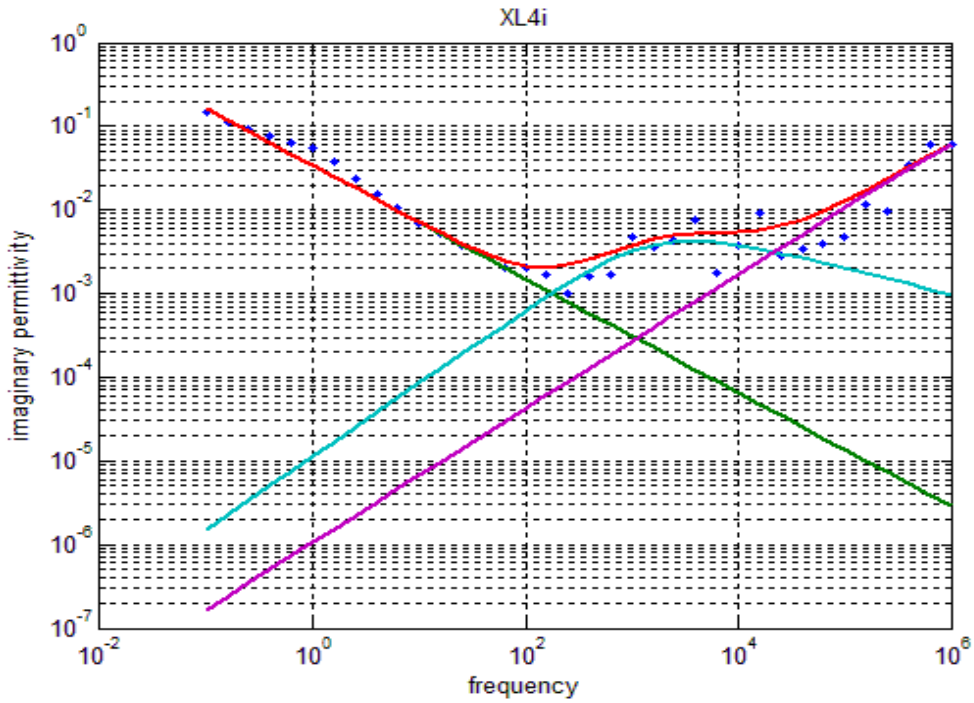

Figure 7.24: Imaginary relative permittivity of 3000 impulses aged XL4. Red: combined curve, Green: conduction, Blue: first relaxation, Purple: second relaxation

material	σ	a	s	Δε1	τ1	α1	γ1	Δε2	τ2	α2	γ2	error
HDPE uncoated	6.40E-13	2	0.6	0.27	3.00E-04	0.8	0.7	0.3	3.70E-09	0.8	0.7	2.70E-04
HDPE coated	8.90E-15	2	0.99	5.60E-03	3.40E-04	4.30E-01	4.00E-01	4.50E-01	7.80E-09	7.60E-01	5.40E-01	1.40E-04
HDPE 3000 imp	1.97E-13	2	0.55	3.80E-02	5.30E-05	7.00E-01	1.00E-01	5.90E-01	4.40E-10	5.40E-01	4.90E-01	1.00E-04
HDPE 6000 imp	3.77E-13	2	0.72	0.055	1.98E-02	0.11	0.2	0.72	6.60E-08	0.75	0.58	2.36E-02
HDPE 6000 imp	3.66E-13	2	0.53	0.66	6.60E-08	0.96	0.52					2.80E-02
LDPE coated	6.90E-15	2	0.6	6.00E-03	4.10E-05	9.00E-01	6.00E-01	5.00E-01	4.00E-08	9.80E-01	2.00E-01	2.88E-04
LDPE 3000 imp	1.05E-14	2	0.5	7.95E-03	3.18E-05	8.98E-01	5.99E-01	5.00E-01	1.33E-09	8.00E-01	9.00E-01	5.70E-05
X3 coated	7.00E-15	2	0.6	1.00E-03	1.00E-04	8.00E-01	4.00E-01	0.5	2.60E-08	0.9	0.2	5.89E-05
X3 3000 imp	1.82E-14	2	0.6	3.00E-02	4.80E-05	9.00E-01	4.00E-01	0.5	6.50E-09	0.9	0.2	3.20E-04
X4 coated	1.20E-14	2	0.3	7.00E-03	4.00E-04	8.90E-01	3.90E-01	0.5	9.00E-08	0.9	0.2	1.10E-03
X4 3000 imp	5.20E-13	2	0.68	1.70E-02	1.20E-04	8.70E-01	3.70E-01	6.00E-01	1.70E-08	0.8	0.7	2.00E-03

Table 7.1: Parameters from fitting proccesses

Figures 7.25 to 7.40 show the same fitting process for thermally and UV aged samples and all parameters of the fitting process are detailed in Table 7.2. Similar results have been obtained in previous work for oxidized HDPE and LDPE [96, 109]. The FTIR results from Chapter 5 show that the oxidation occurs in all crosslinked

samples and all UV aged samples. This is in agreement with the appearance of a relaxation peak over the region from 50 to 100 Hz at room temperature [109, 110, 178]. This peak contributes significantly to the overall loss of these materials. With thermally aged LDPE and HDPE (except for 6 days thermally aged HDPE), the oxidation relaxation peak was also obtained. Therefore, the effect of oxidation in HDPE and LDPE still exists but is hard to observe using FTIR. The change in DC conductivity is not very clear for the thermal and UV aged samples as the effect of relaxation due to oxidation dominates the material loss process.

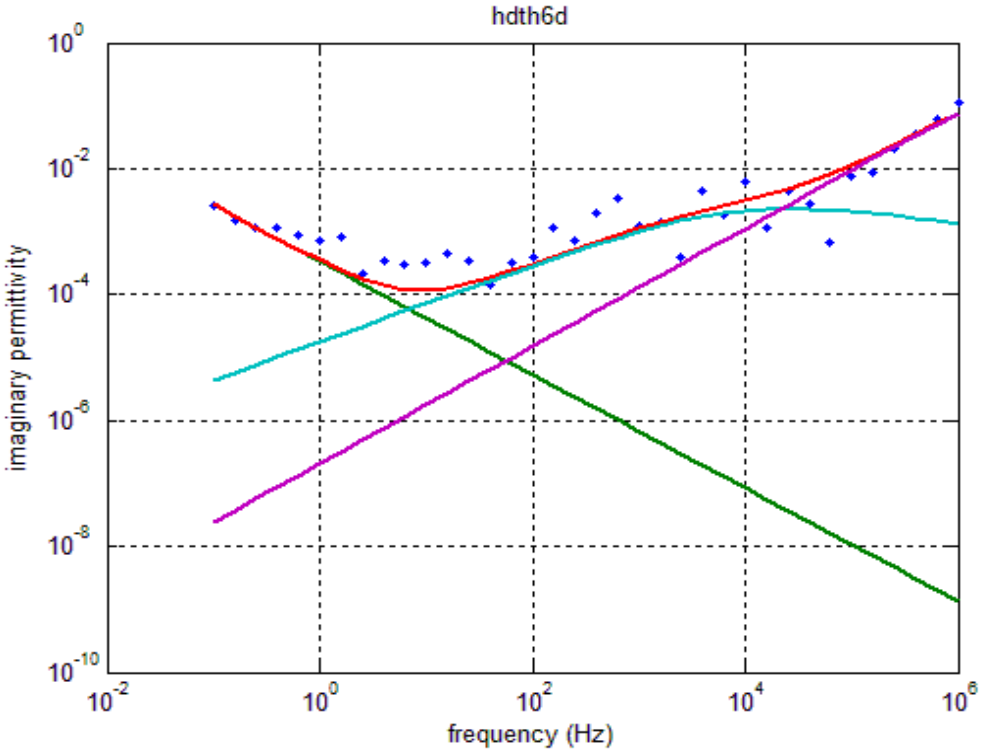

Figure 7.25: Imaginary relative permittivity of 6 days thermal aged HDPE. Red: combined curve, Green: conduction, Blue: first relaxation, Purple: second relaxation

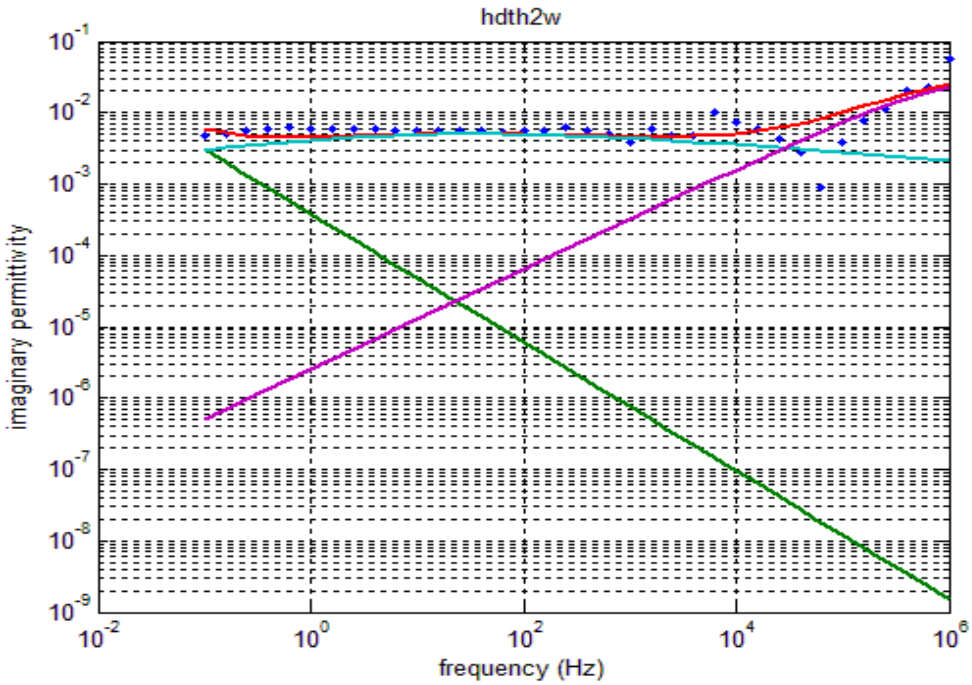

Figure 7.26: Imaginary relative permittivity of 2 weeks thermal aged HDPE. Red: combined curve, Green: conduction, Blue: first relaxation, Purple: second relaxation

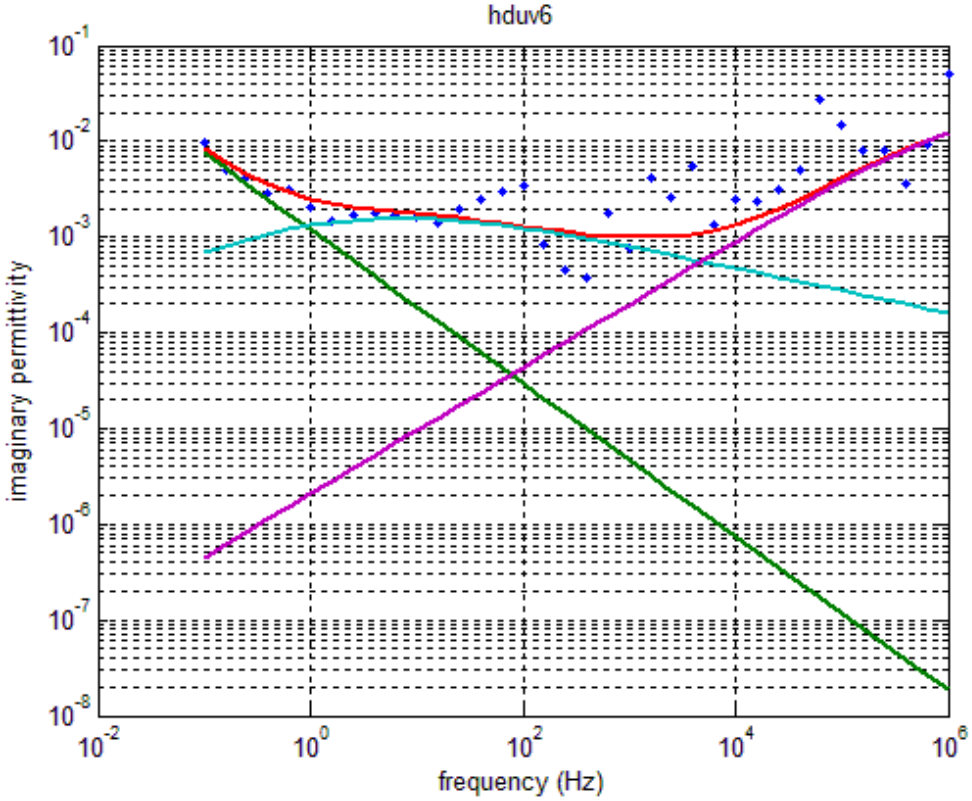

Figure 7.27: Imaginary relative permittivity of 6 days UV aged HDPE. Red: combined curve, Green: conduction, Blue: first relaxation, Purple: second relaxation

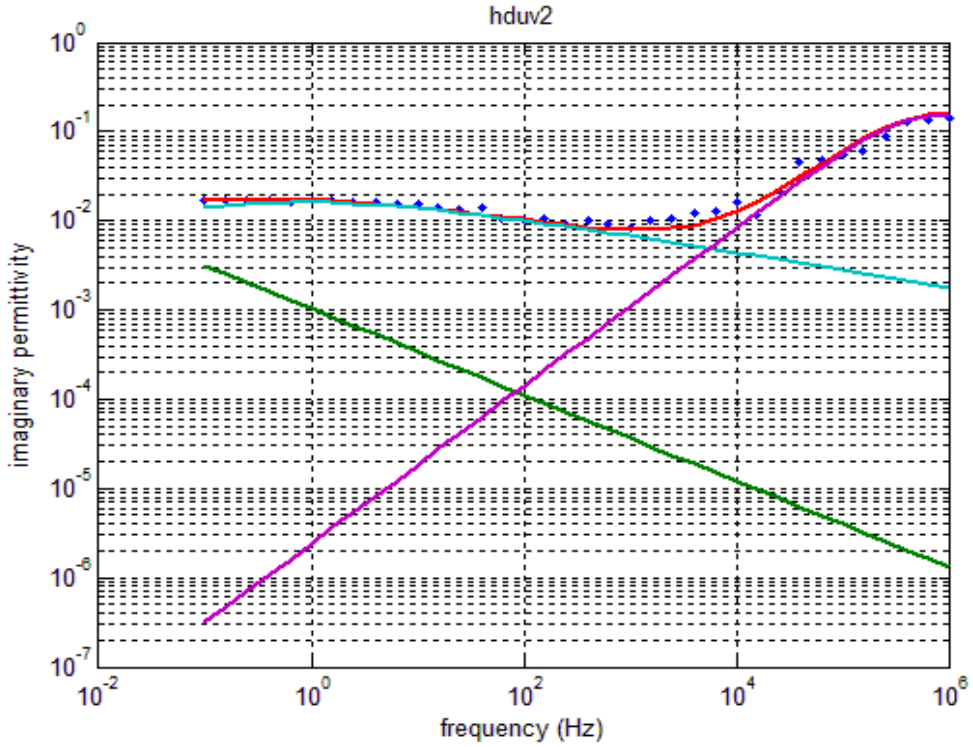

Figure 7.28: Imaginary relative permittivity of 2 weeks UV aged HDPE. Red: combined curve, Green: conduction, Blue: first relaxation, Purple: second relaxation

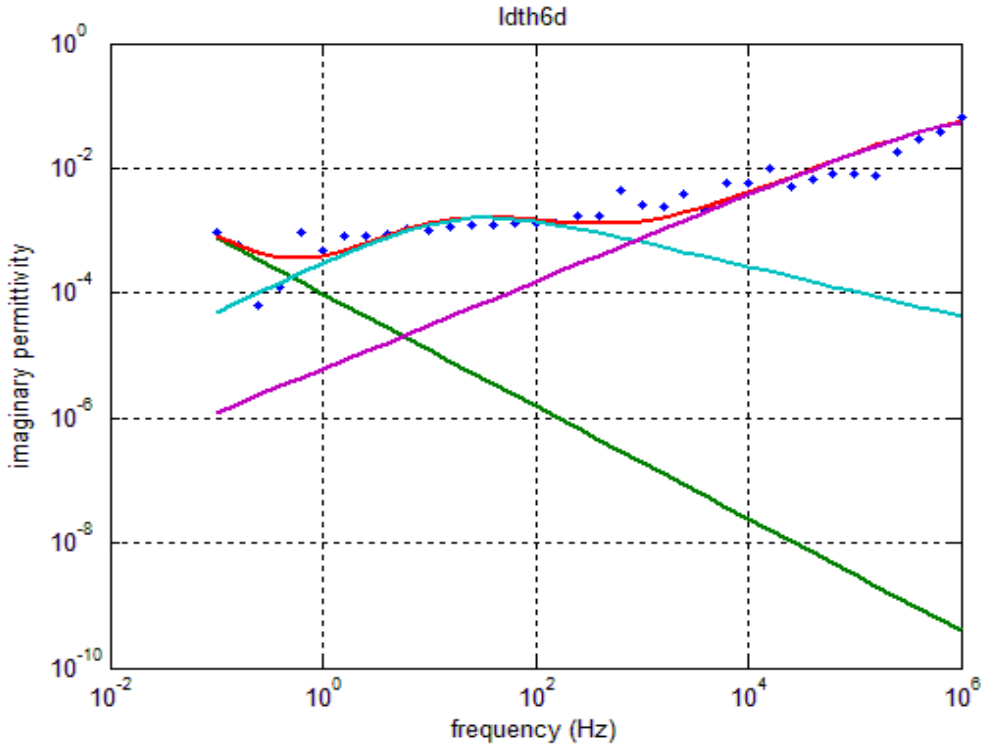

Figure 7.29: Imaginary relative permittivity of 6 days thermal aged LDPE. Red: combined curve, Green: conduction, Blue: first relaxation, Purple: second relaxation

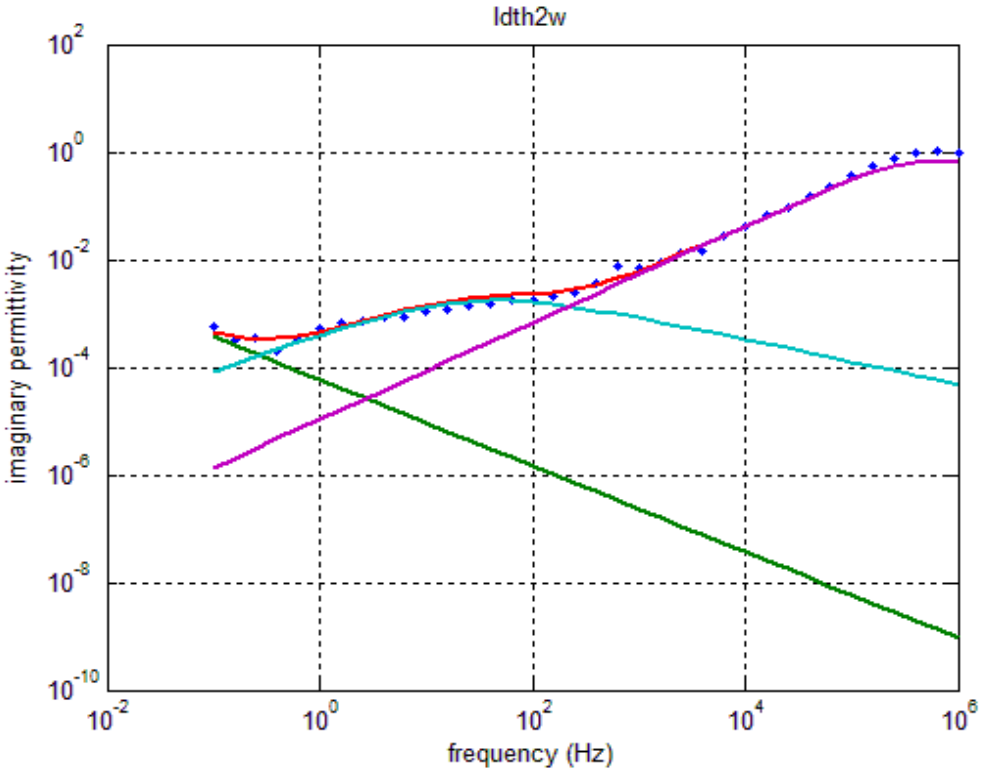

Figure 7.30: Imaginary relative permittivity of 2 weeks thermal aged LDPE. Red: combined curve, Green: conduction, Blue: first relaxation, Purple: second relaxation

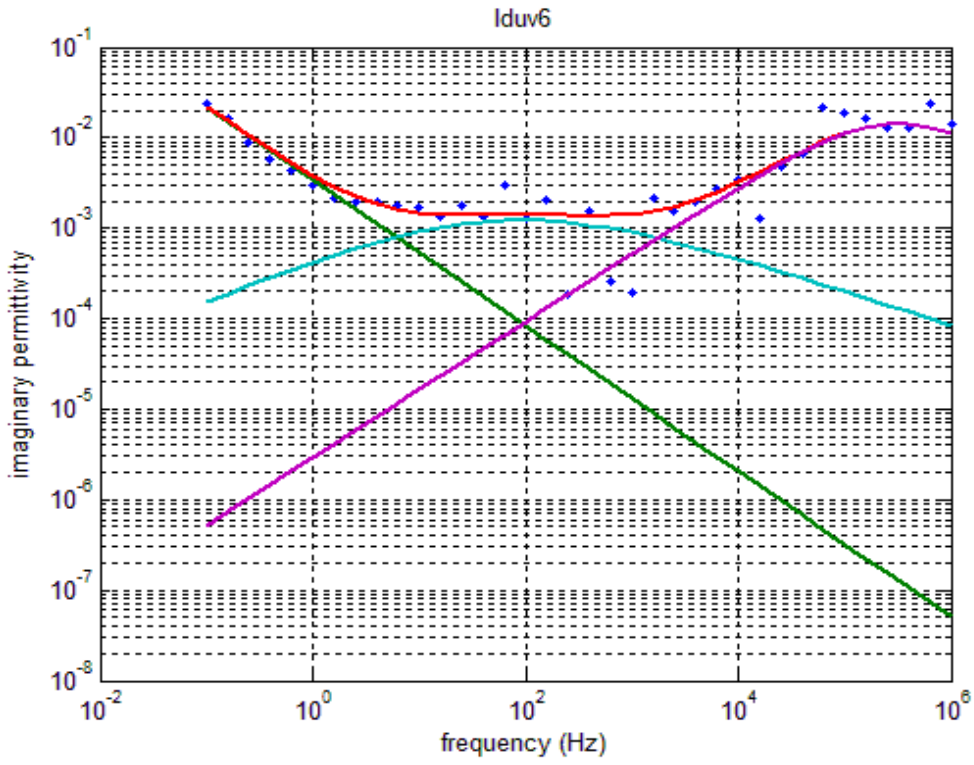

Figure 7.31: Imaginary relative permittivity of 6 days UV aged LDPE. Red: combined curve, Green: conduction, Blue: first relaxation, Purple: second relaxation

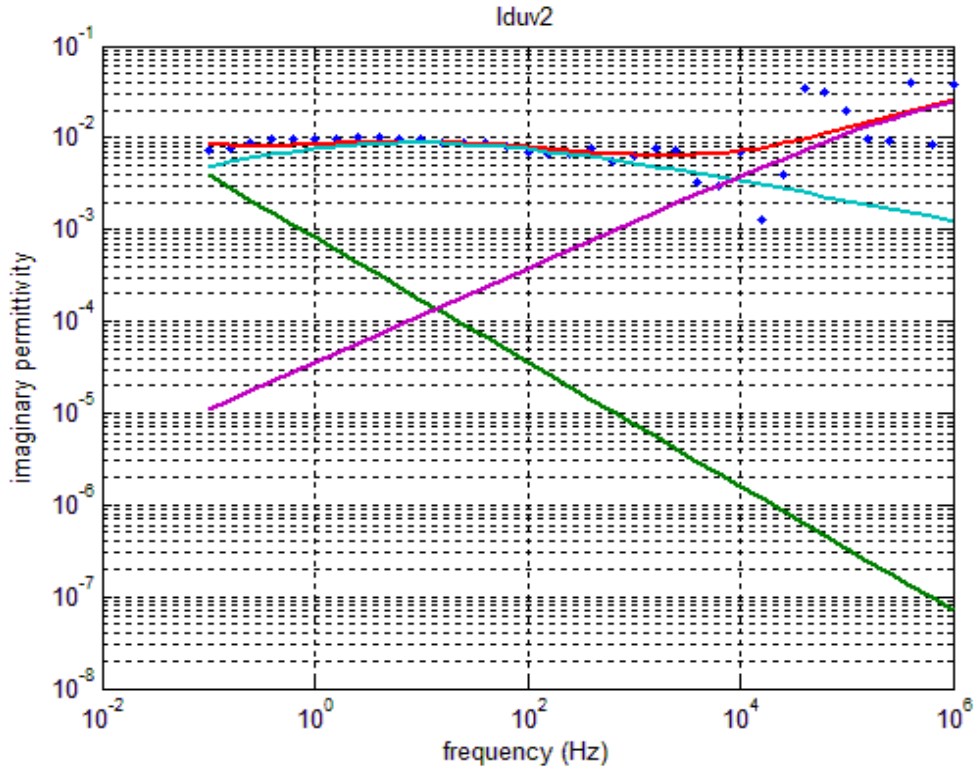

Figure 7.32: Imaginary relative permittivity of 2 weeks UV aged LDPE. Red: combined curve, Green: conduction, Blue: first relaxation, Purple: second relaxation

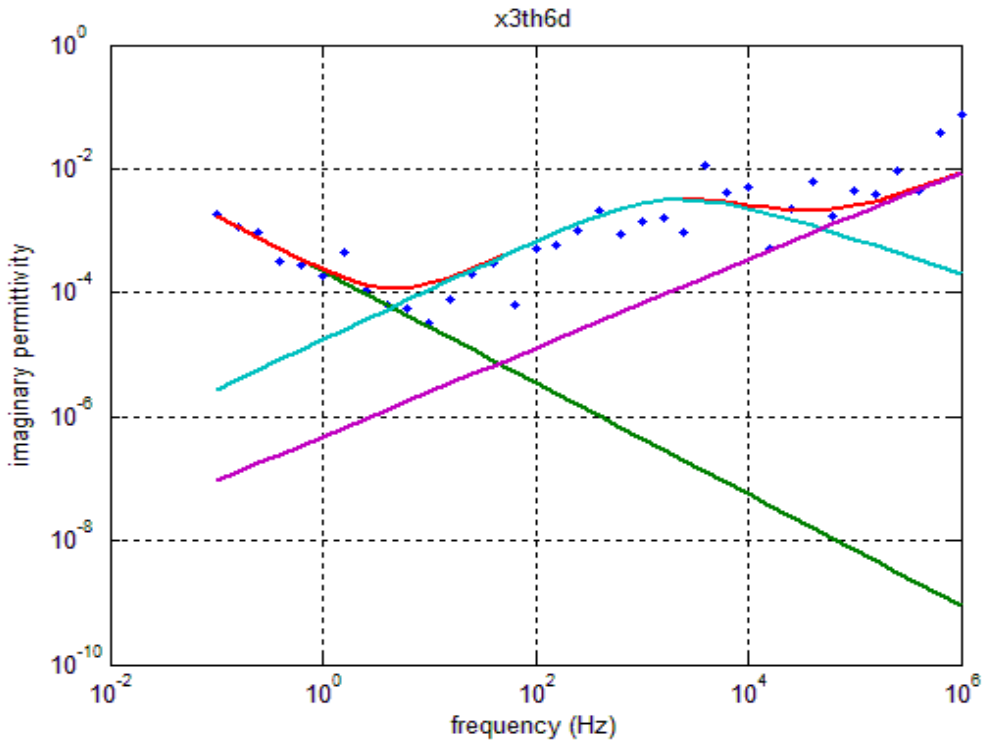

Figure 7.33: Imaginary relative permittivity of 6 days thermal aged XL3. Red: combined curve, Green: conduction, Blue: first relaxation, Purple: second relaxation

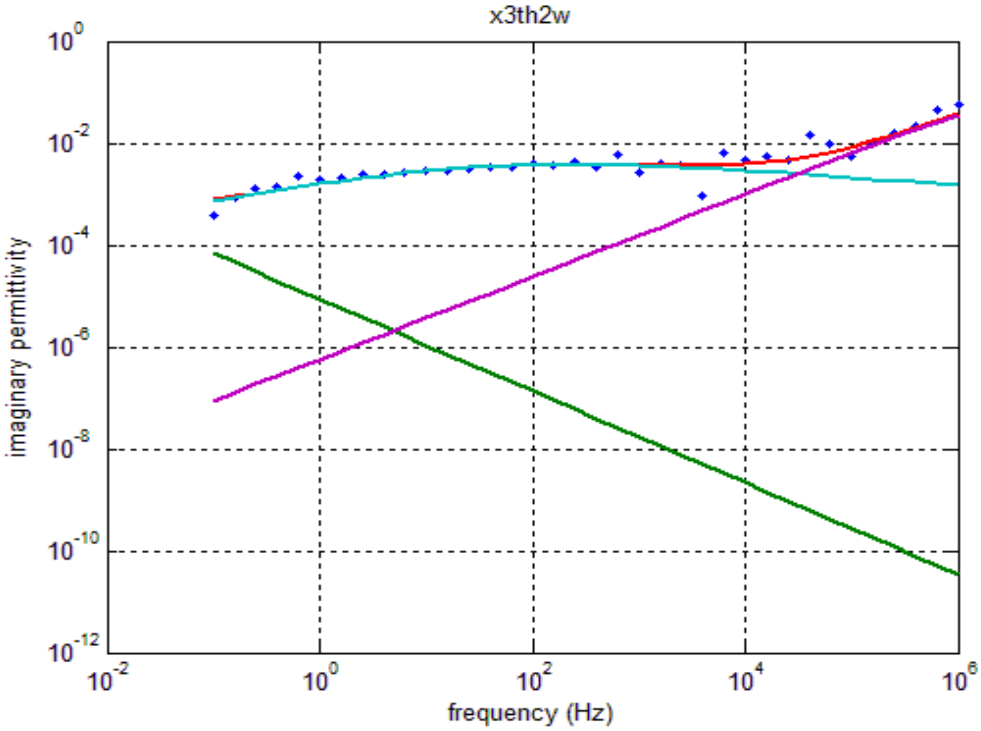

Figure 7.34: Imaginary relative permittivity of 2 weeks thermal aged XL3. Red: combined curve, Green: conduction, Blue: first relaxation, Purple: second relaxation

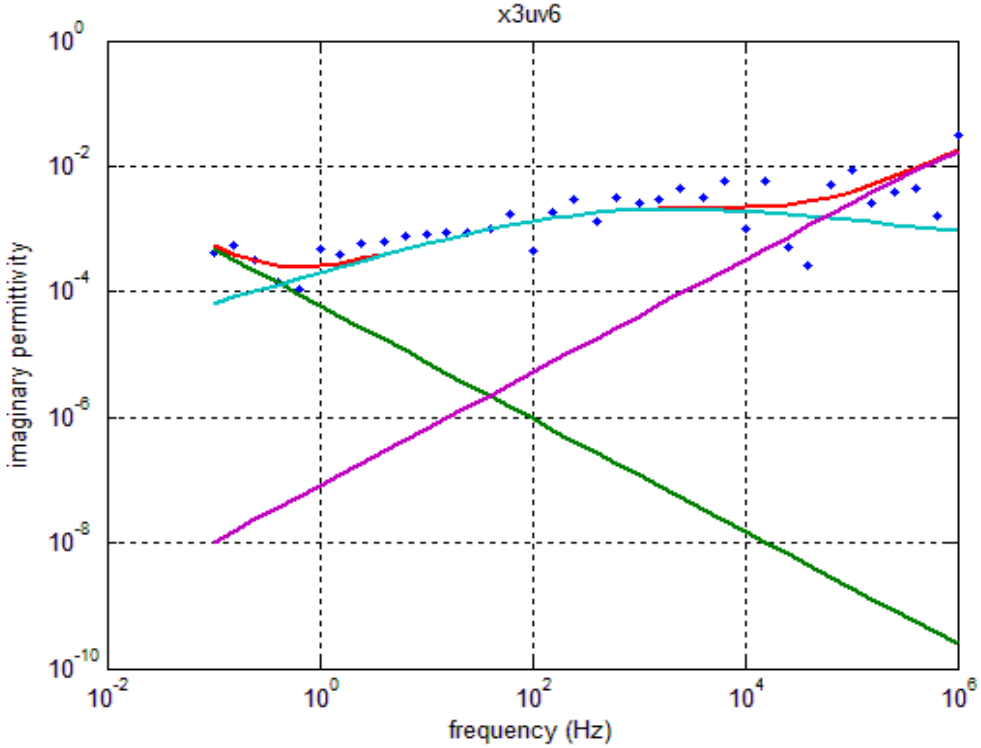

Figure 7.35: Imaginary relative permittivity of 6 days UV aged XL3. Red: combined curve, Green: conduction, Blue: first relaxation, Purple: second relaxation

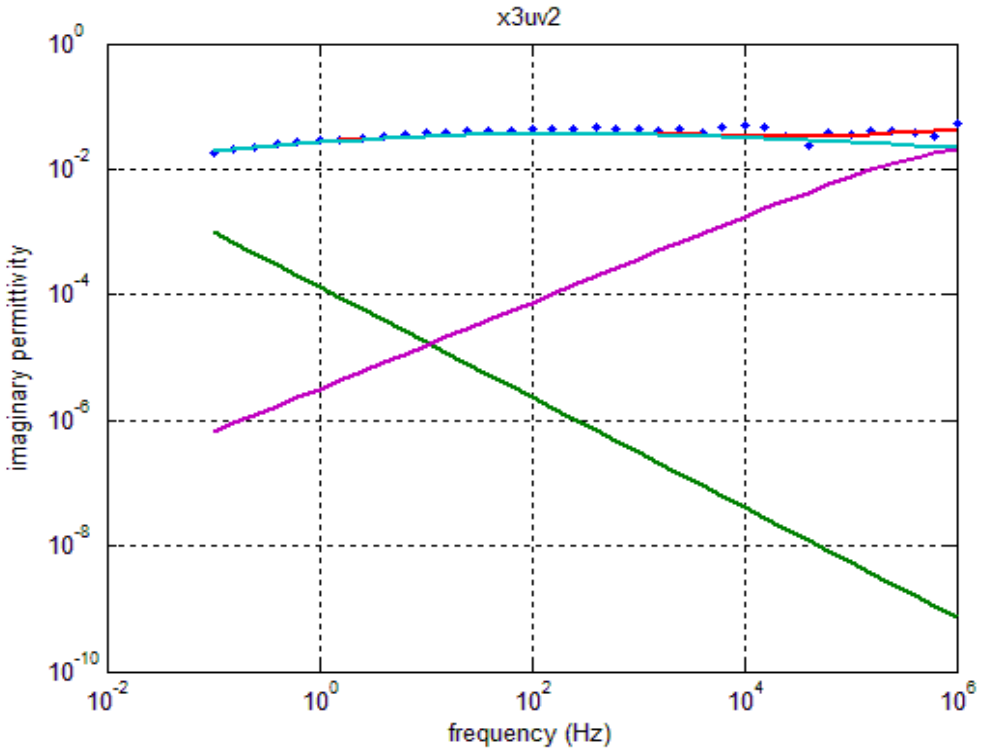

Figure 7.36: Imaginary relative permittivity of 2 weeks UV aged XL3. Red: combined curve, Green: conduction, Blue: first relaxation, Purple: second relaxation

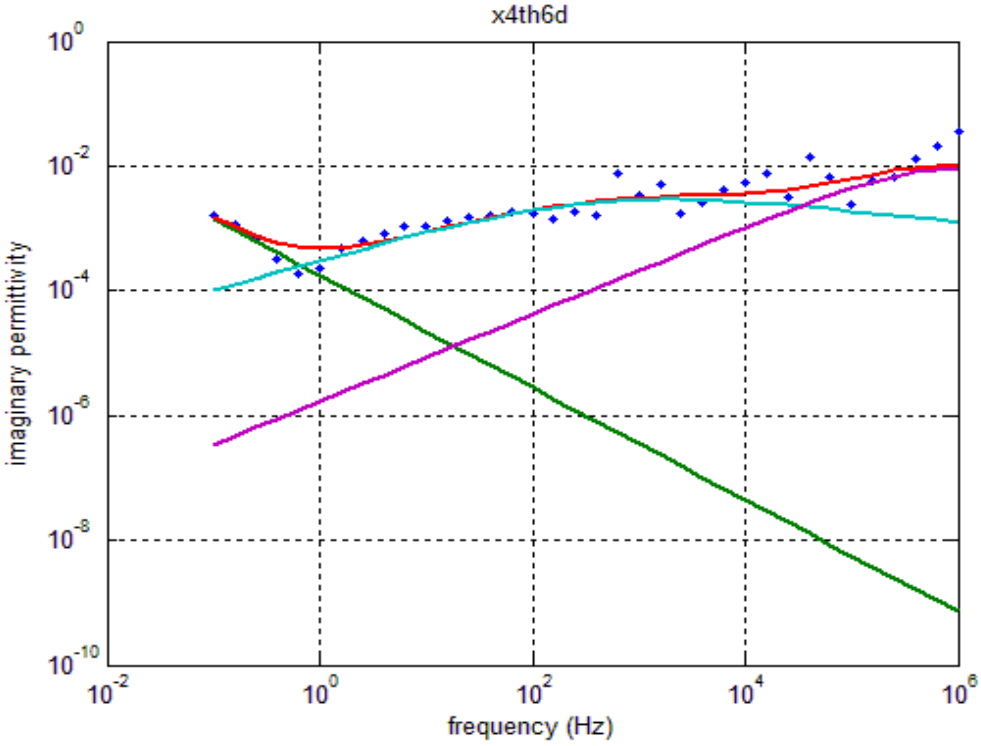

Figure 7.37: Imaginary relative permittivity of 6 days thermal aged XL4. Red: combined curve, Green: conduction, Blue: first relaxation, Purple: second relaxation

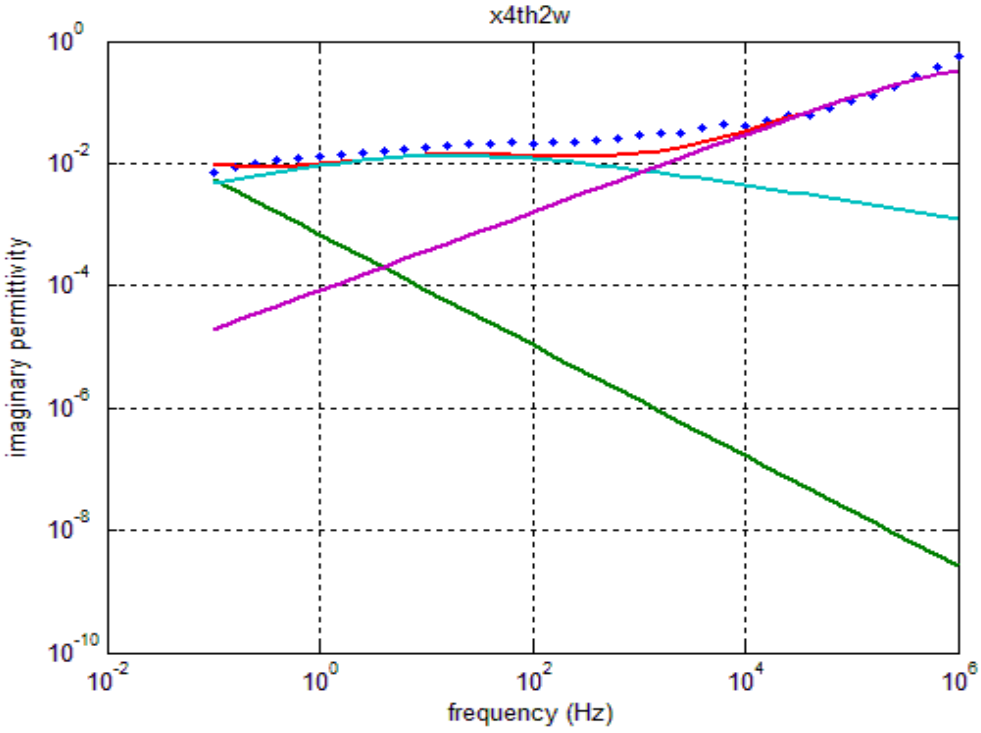

Figure 7.38: Imaginary relative permittivity of 2 weeks thermal aged XL4. Red: combined curve, Green: conduction, Blue: first relaxation, Purple: second relaxation

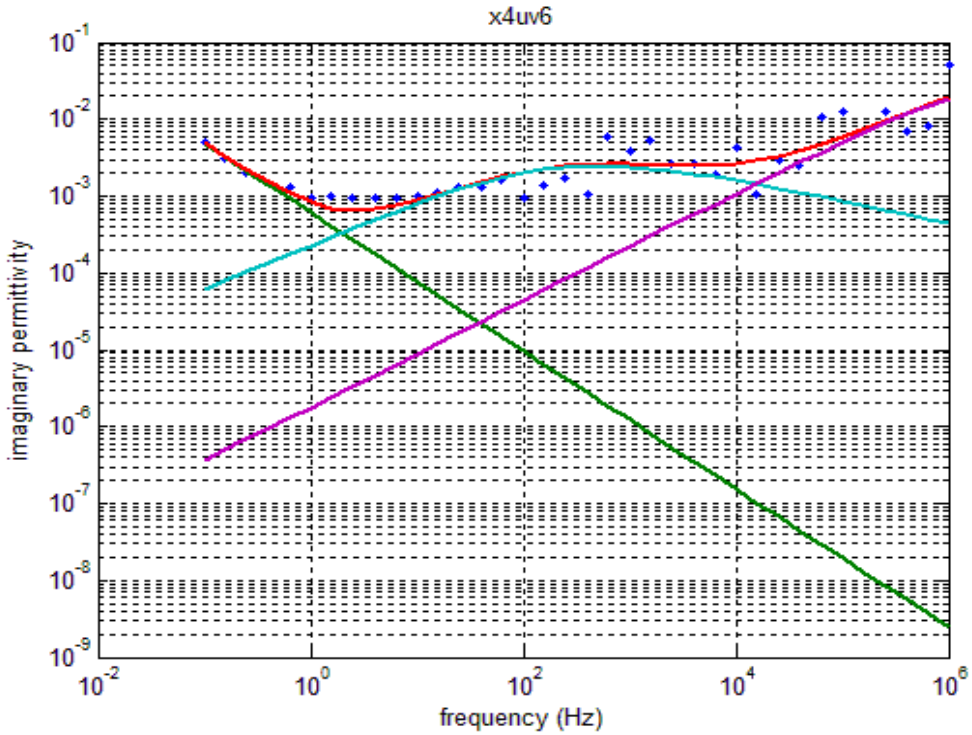

Figure 7.39: Imaginary relative permittivity of 6 days UV aged XL4. Red: combined curve, Green: conduction, Blue: first relaxation, Purple: second relaxation

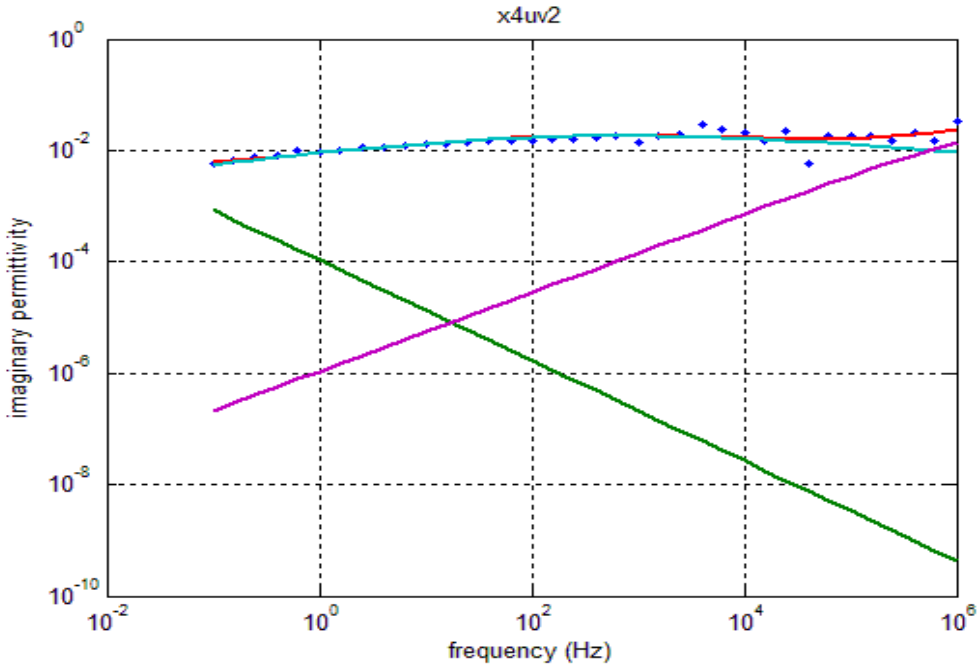

Figure 7.40: Imaginary relative permittivity of 2 weeks UV aged XL4. Red: combined curve, Green: conduction, Blue: first relaxation, Purple: second relaxation

material	σ	a	s	Δε1	τ1	α1	γ1	Δε2	τ2	α2	γ2	error
HDPE coated	8.90E-15	2	0.99	5.60E-03	3.40E-04	4.30E-01	4.00E-01	4.50E-01	7.80E-09	7.60E-01	5.40E-01	1.40E-04
HDPE 6dth	7.79E-15	2	0.900051	0.012727	2.2E-05	0.616538	0.407489	0.672871	3.68E-08	0.932803	0.47752	0.001372
HDPE 2wth	8.85E-15	2	0.899998	0.059469	0.100096	0.301733	0.400729	0.101917	8.36E-08	0.701417	0.700211	0.001229
HDPE 6duv	2.31E-14	2	0.801854	0.010446	0.091881	0.488087	0.490061	0.08072	6.39E-08	0.66049	0.50098	0.002184
HDPE 2wuv	1.11E-14	2	0.48307	0.130417	1.000316	0.396998	0.498835	0.464908	3.19E-07	0.886399	0.586301	0.001877
LDPE coated	6.90E-15	2	0.6	6.00E-03	4.10E-05	9.00E-01	6.00E-01	5.00E-01	4.00E-08	9.80E-01	2.00E-01	2.88E-04
LDPE 6dth	2.27E-15	2	0.9	0.006	0.01	0.8	0.5	0.3	1E-07	0.7	0.5	0.000838
LDPE 2wth	1.12E-15	2	0.8	0.007	0.007	0.7	0.6	1.7	3E-07	0.9	0.9	0.398459
LDPE 6duv	6.68E-14	2	0.805326	0.00656	0.002716	0.490031	0.795114	0.04358	5.66E-07	0.751019	0.89618	0.000397
LDPE 2wuv	1.26E-14	2	0.677552	0.069217	0.064249	0.373971	0.615524	0.149984	3.26E-08	0.512414	0.886476	0.002102
X3 coated	7.00E-15	2	0.6	1.00E-03	1.00E-04	8.00E-01	4.00E-01	0.5	2.60E-08	0.9	0.2	5.89E-05
X3 6dth	5.17E-15	2	0.900007	0.01001	9.75E-05	0.805395	0.703378	0.134985	8.99E-09	0.71585	0.602458	0.00564
X3 2wth	1.99E-16	2	0.899973	0.03293	0.005858	0.406994	0.403028	0.237282	2.98E-08	0.81191	0.720648	0.000769
X3 6duv	1.4E-15	2	0.9	0.014608	0.000412	0.500045	0.399968	0.070281	4.63E-08	0.900232	0.900018	0.000399
X3 2wuv	3.02E-15	2	0.880035	0.49182	0.017648	0.256768	0.452319	0.10142	1.47E-07	0.6879	0.499932	0.001532
X4 coated	1.20E-14	2	0.3	7.00E-03	4.00E-04	8.90E-01	3.90E-01	0.5	9.00E-08	0.9	0.2	1.10E-03
X4 6dth	4.1E-15	2	0.9	0.020569	0.000477	0.500275	0.400182	0.031391	1.73E-07	0.700234	0.900034	0.000936
X4 2wth	1.61E-14	2	0.904234	0.086431	0.022083	0.43564	0.660389	1.330466	5.07E-08	0.63937	1.065111	0.076579
X4 6duv	1.42E-14	2	0.899621	0.012917	0.000897	0.595967	0.498084	0.123403	5.66E-08	0.696271	0.502899	0.001237
X4 2wuv	2.49E-15	2	0.90012	0.189267	0.001345	0.288489	0.599425	0.113541	3.75E-08	0.705085	0.501929	0.000555

Table 7.2: Parameters from the fitting processes

7.6. Summary

The results from dielectric spectroscopy of all samples provide indication of some fundamental differences in the mechanisms that dominate the three ageing processes. Firstly, impulse ageing does not cause chemical changes or oxidation. The effect of impulse ageing only causes bond breaking and ionization. It may lead to an increase in ionic conduction and subsequent interfacial polarisation. The movement of molecules under an applied electric field may also become easier as the molecular lengths could be reduced. In contrast, UV ageing may provide all the effects from oxidation, bond breaking and crosslinking. The losses of UV aged samples increase as an effect of both conduction and relaxation processes. The efficiency of UV ageing is governed by the relative transparency of the material with respect to UV light. However, the results of dielectric spectroscopy of UV aged samples sometimes do not match with the dielectric strength of material. For example, the LDPE and HDPE after 14 days UV ageing present dielectric spectroscopy results similar to XL3 and XL4 but they have much more significant changes in breakdown strength. For thermal ageing, the oxidation process strongly depends on the additives in the material. The effects from change in morphology of material under an annealing condition should also be carefully considered.

Chapter Eight

Space Charge Measurement Profiles

8.1. Experiment; the Pulse Electro Acoustic method

There are several methods to measure space charge distribution including thermal step, laser intensity modulation (LIMM), laser induced pressure pulse (LIPP), as well as pulsed electro-acoustic stress (PEA) [100]. In this project only the pulsed electro-acoustic (PEA) method [179] was used. Figure 8.1 shows the schematic diagram of the PEA method [180]. The sample was stressed using a DC voltage. When an electrical pulse is applied parallel to the circuit, it produces acoustic waves at charge layers. These acoustic signals are measured by a piezoelectric transducer. This method provides the spatial charge profile within the sample.

PEA measurement can be used as a characterisation tool for material ageing. The space charge characteristics of aged and un-aged samples were measured and results compared. In order to prevent flashovers during PEA measurements, the samples

were not coated with gold electrodes. For impulse ageing, the normal Rogowski shaped samples were aged using 3000 lightning impulses, with 1.2 μs front-time, 40 μs tail time and peak electric field across the sample of approximately -85 $kVmm^{-1}$. The rim was removed after ageing. Similar samples were used for thermal and UV ageing.

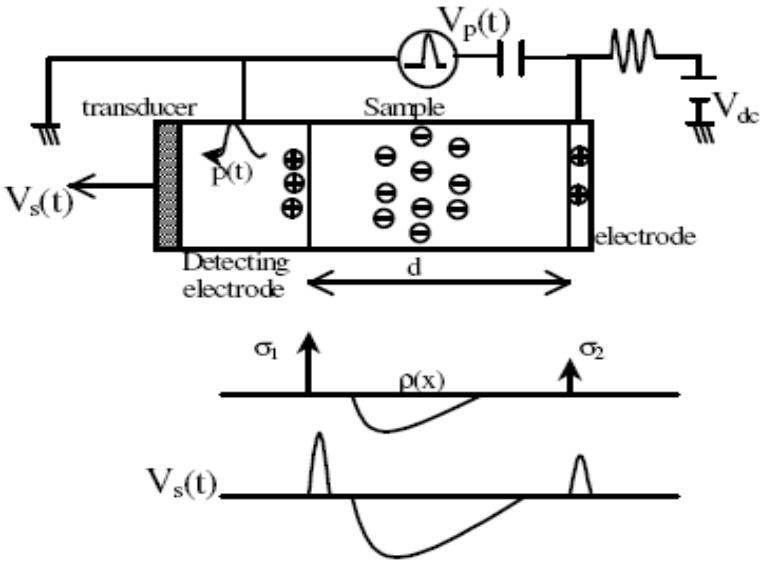

Figure 8.1: Schematic diagram of PEA method
(top) schematic diagram, (middle) charge density, (bottom) potential

Before any measurement was taken, the charge profile needs to be calibrated. This calibration step is very important if the charge profile is quantifiable. A fresh sample usually contains very small amounts of bulk charge. The application of a reasonable DC voltage at which no charge injection happens and provides signals high enough to overcome the noise will give a flat charge profile though the bulk. In order to obtain the value at which charge injection starts, a graph of applied voltage verses peak induced electrode charge can be obtained. The value of voltage at which the linear relationship starts to diverge is the value at which charges start to be injected. A fresh sample was calibrated in the normal way with an electrical field of less than 10 $kVmm^{-1}$ before the measurements were taken. However, as the aged samples may contain surface or trapped charge, a two step calibration method had to be used so that the charge profile of the aged samples can be estimated [180]. If the data for calibration is noisy, the zero voltage also needs to be subtracted from the measurement data. The samples were stressed with fairly low DC fields of 34 $kVmm^{-1}$. The sample was stressed between a semicon anode and an aluminium cathode. The observation of charge accumulation was taken over a period of 60

minutes. The charge decay measurement (i.e. DC voltage is switched off) was taken to clarify whether deep or shallow traps were created. The resolution is 150 µm, high enough to see the characteristics of the bulk and reduce noise. The peak pulse voltage for PEA equipment was set at 400 V.

8.2. Results obtained for impulse aged samples

Figure 8.2 shows that the charge profile is nearly unchanged after 60 minutes in case of virgin HDPE. There was almost no charge injection into the sample with the application of a constant electric field 34 kVmm^{-1}. The charge decay profile shows very small signals for charge density, this is most likely measurement noise.

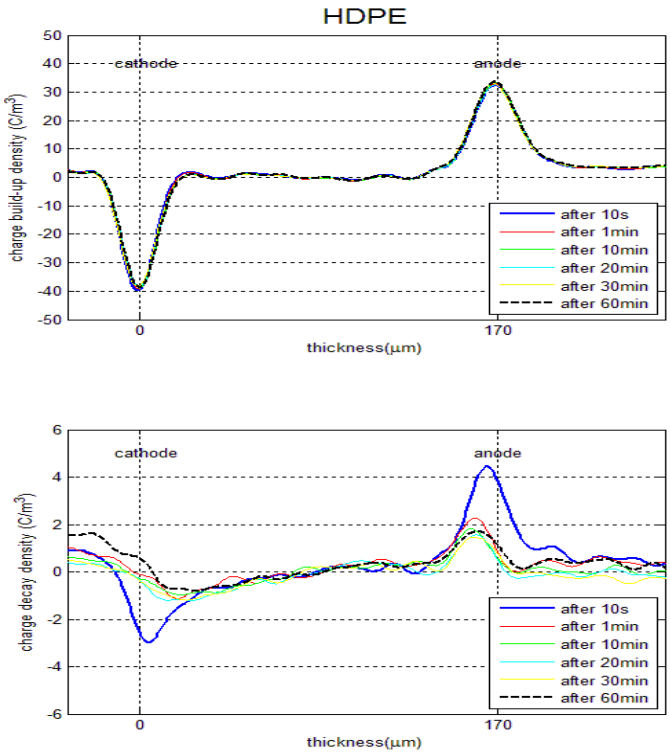

Figure 8.2: Space charge accumulation of normal HDPE (top) charging, (bottom) decaying

In contrast, homo-charges were injected more effectively at the cathode in cases of 3000 lightning impulse aged samples (Figure 8.3). The negative charges were injected into the bulk of sample and seem to saturate after 10 minutes in presence of an applied filed. The injected charges diffuse widely throughout the sample bulk. These homo-negative charges make the sample thickness appear thinner and

consequently there is a reduction in breakdown strength as the field inside the bulk increases. Closely monitoring the charge profile at the surface of the anode, there should be negative charge forming near the surface as the peak charge induced on anode increases after 60 minutes. The charge decay profile of impulse aged samples shows that the bulk charge reduces fairly slowly. In other words, charges may be trapped deeply in the material as a result of impulse ageing. This property is particularly worrying in terms of DC conduction and breakdown for HVDC cables.

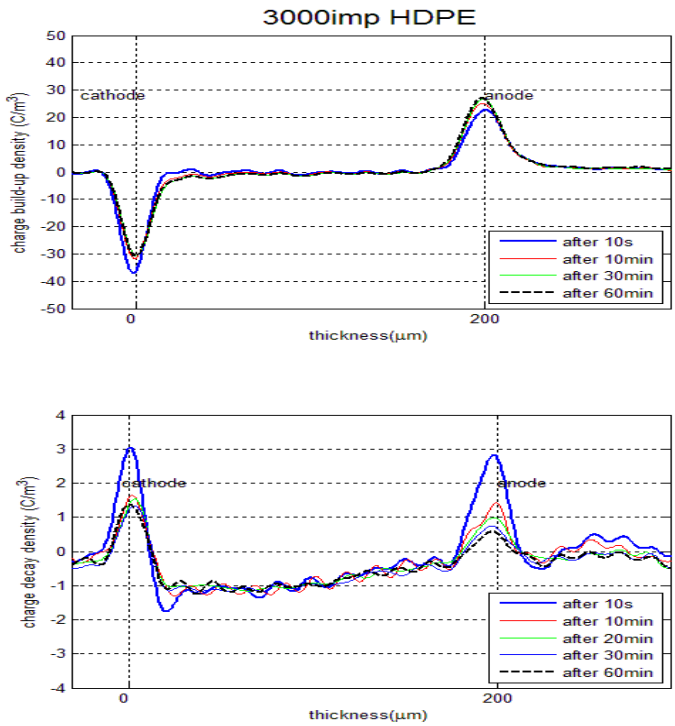

Figure 8.3: Space charge accumulation of impulse aged HDPE (top) charging, (bottom) decaying

Figures 8.4 and 8.5 show the charge profile for LDPE samples. In contrast to HDPE, there is no homo-charge injection in LDPE but huge amounts of hetero-charge were formed near the cathode. Previous work showed a similar formation of hetero-charges in LDPE if the material is quenched cooled [149, 150]. In the work of Tanaka, for slowly cooled LDPE the positive charges are first injected from the anode and then negative charges from the cathode, the positive charges dominate charge profile [150]. However, for quenched cooled LDPE, the positive charge quickly builds up at the cathode during the first 10 minutes then gradually migrates towards the anode. Also, it was found that the addition of antioxidant will take over

the effect of quenching. In conclusion, the quenching process changes the morphology of the material such as reducing crystallinity and spherulite size, or introduces structure defects into the bulk. Consequently, deep traps will be formed and anode injected positive charges will be trapped. However, work from Kwang S. Suh gives the reason for hetero-positive charges to the migration of charged low molecular weight polyethylene chains [149]. By considering the melting time, melting temperature and backing layer materials, Suh claims the carbonyl content increases during sample manufacturing will enhance trapping for homo-charge and reduce the formation of hetero-charge. The Xylene extraction removes the low molecular weight chains and leads to a reduction in the hetero-charge formation near cathode.

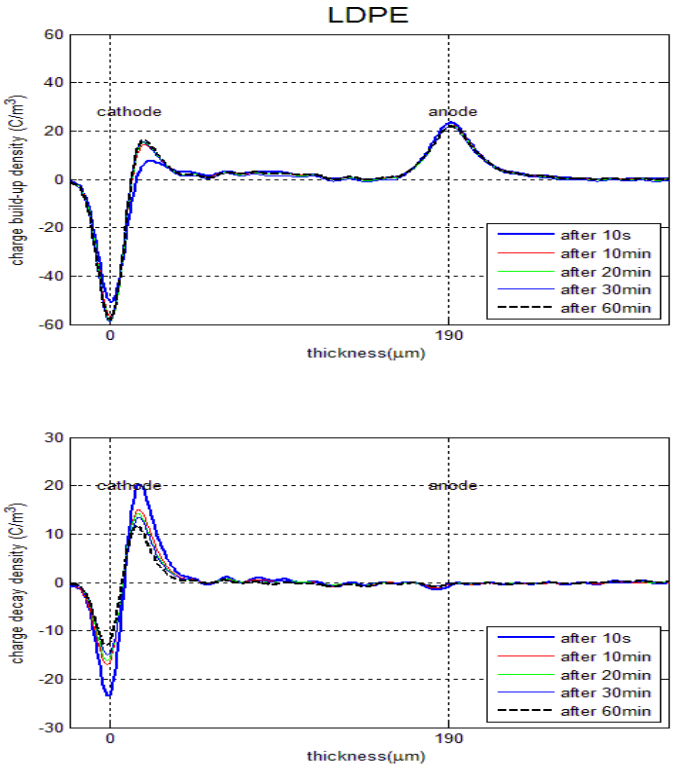

Figure 8.4: Space charge accumulation of normal LDPE (top) charging, (bottom) decaying

The results obtained from this research show that hetero-charge formation takes place for about 10 minutes. After that, the charge profile stays the same for the next 50 minutes. No “backward flow” was observed during the testing time. The charges

gradually decay away when the applied field was removed. After 60 minutes, quite a lot of charges still exist in the bulk.

The 3000 lightning impulse aged LDPE shows the same charge profile pattern as that of virgin LDPE. The differences in peak charges for the two samples can be ignored. This is in good agreement with the fact that the breakdown strength of samples was hardly changed after the ageing process. Also, from charge decay profiles, hetero-charge did not spread through the bulk of samples. About half of the space charge decayed after 60 minutes in both cases.

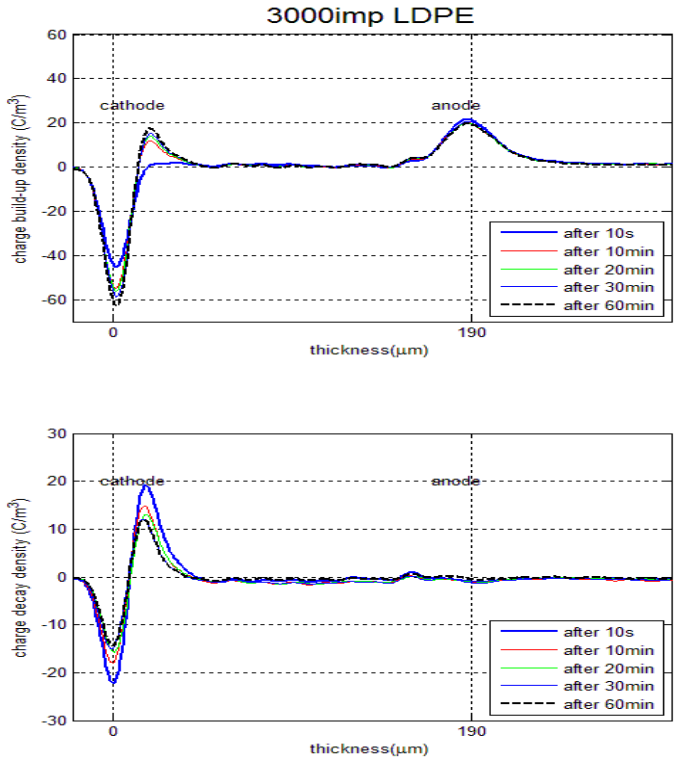

Figure 8.5: Space charge accumulation of impulse aged LDPE (top) charging, (bottom) decaying

Although having the base material of LDPE (LD100), the trigonox-crosslinked polyethylene (XL3 and XL1) shows a very different space charge profile (Figures 8.6 and 8.7). The XL1 sample was made from LD100 with 1% trigonox addition and crosslinked for 5 min at 200^{o}C. The result shows bipolar charge injection has taken place with the domination of positive charges. The positive charges seem attracted to the cathode but are limited by the negative charges from cathode. With the same electrical field stress of 34kV/mm, very little positive charges were formed near the

cathode in the bulk of XL3 sample. A small amount of negative charge was observed near the anode. The same space charge behaviour was obtained in the work of Martinotto [141] where the amount of space charge significantly decreases with the increase in the crosslinking degree.

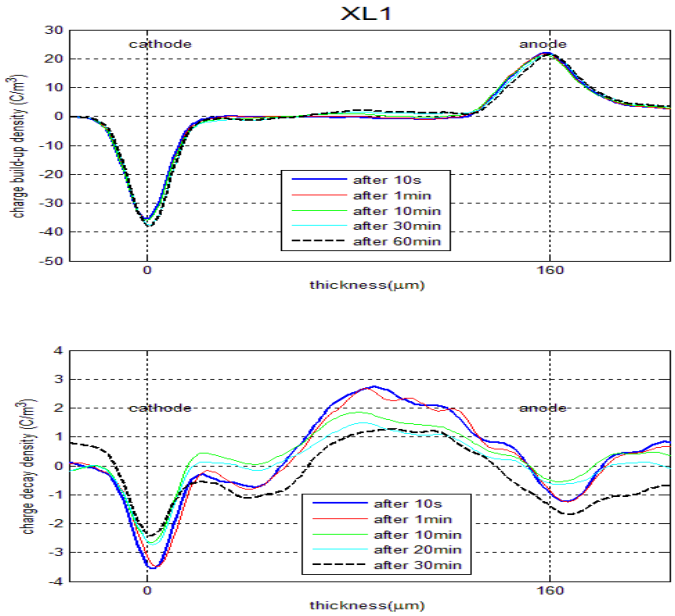

Figure 8.6: Space charge accumulation of XL1 (top) charging, (bottom) decaying

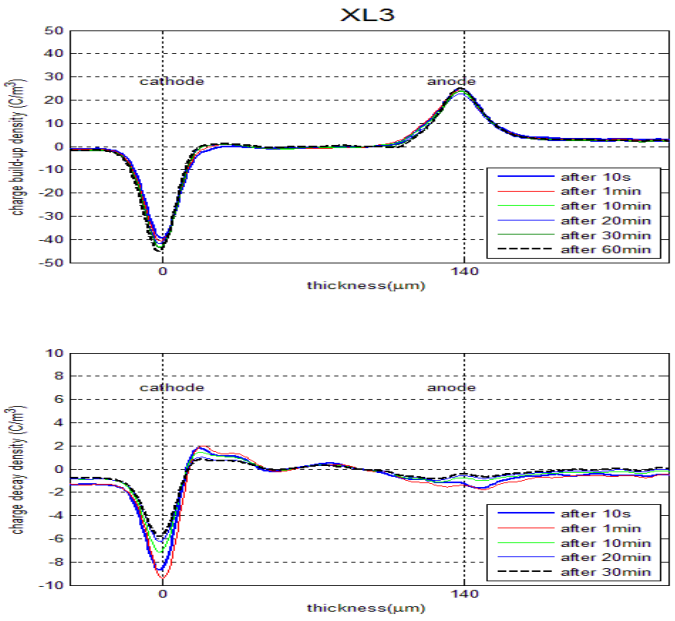

Figure 8.7: Space charge accumulation of XL3 (top) charging, (bottom) decaying

Positive charge formation is more consistent and deeper in the bulk of impulse aged sample (Figure 8.8). The shape of bulk charge is similar to that of the impulse aged HDPE but is positive as opposed to negative. The rate of charge decay in XL3 seems faster than in HDPE. However, the amounts of charges are quite small for both virgin and impulse aged XL3. Therefore, it is hard to draw any conclusion about the efficiency of charge injection.

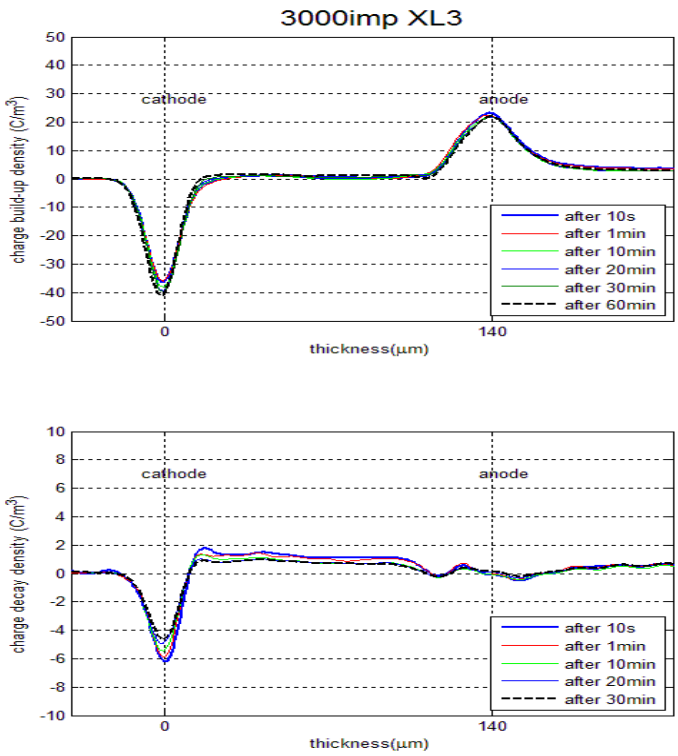

Figure 8.8: Space charge accumulation of impulse aged XL3 (top) charging, (bottom) decaying

For the crosslinked polyethylene 4421, three types of samples were considered, namely, an uncrosslinked sample (LDPE4), the crosslinked sample (XL4) and impulse aged crosslinked sample. All three types show positive charge injection domination (Figures 8.9 to 8.11). This is the effect of the silane group grafted on to the molecular chains. Results for LDPE4 shows that a lot of homo-charge is injected only from the anode. Meanwhile, both homo-charges from the anode and hetero-charges from the cathode were injected in bulk of XL4. An interesting point is the small negative charge region that formed in the middle of the bulk. This can be the effect of water diffusion into sample after the cure moisture crosslinking process. Charge decay rates are extremely slow for both LDPE4 and XL4. Previous

researches also show that normally positive homocharge is injected into silane XLPE [181, 182]. The charge injected into impulse aged XL4 is higher than for virgin XL4 and the peak charge is also higher.

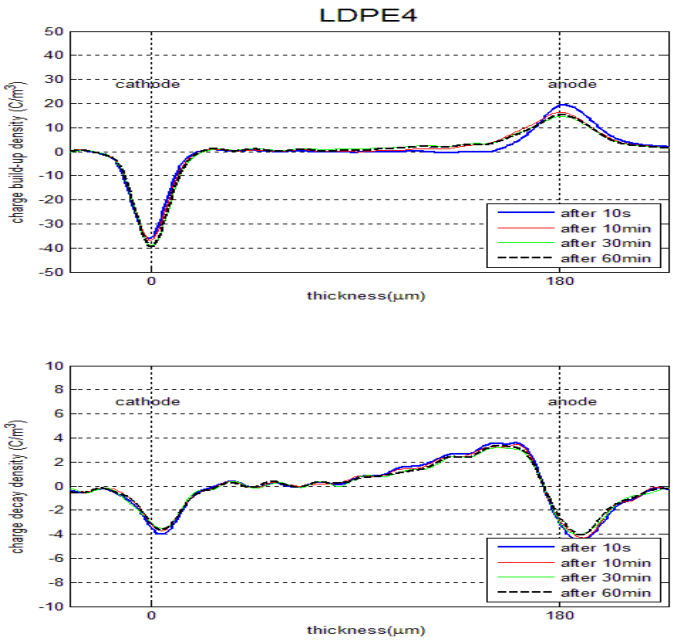

Figure 8.9: Space charge accumulation of LDPE4 (top) charging, (bottom) decaying

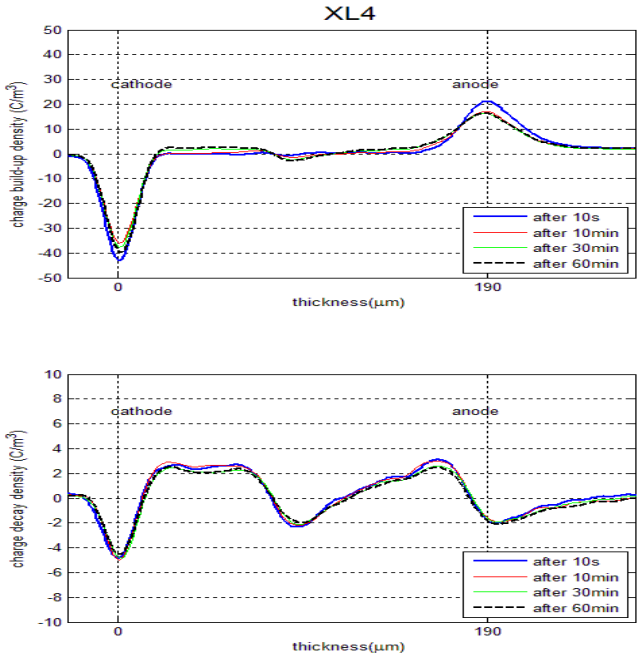

Figure 8.10: Space charge accumulation of XL4 (top) charging, (bottom) decaying

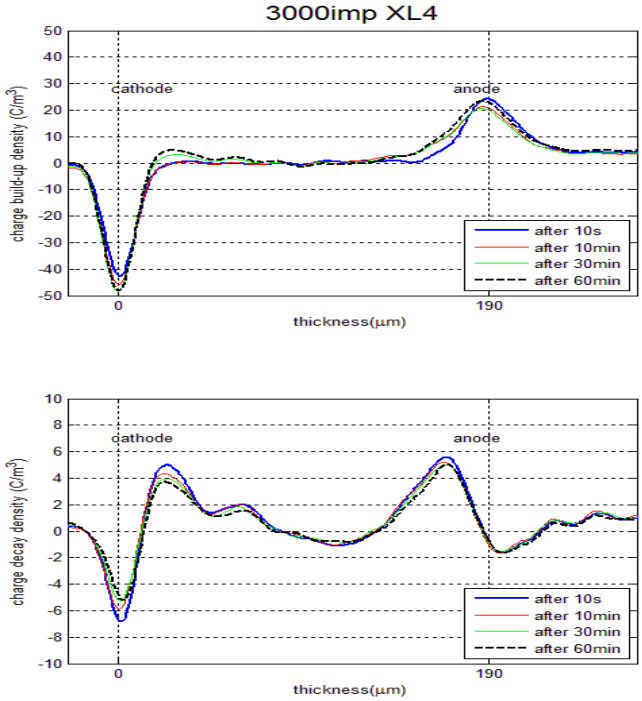

Figure 8.11: Space charge accumulation of impulse aged XL4 (top) charging, (bottom) decaying

8.3. Results obtained for thermal aged samples

Figures 8.12 to 8.19 show the space charge profile of all four materials after thermal ageing. After 14 days thermal ageing, the homo charge injection is enhanced for all materials. For HDPE (Figure 8.12 and 8.13) the bipolar charge injection from both anode and cathode are more effective and the amount of charge increases with ageing time. More positive charge was injected, but also decays at a faster rate. Charges were injected in the bulk but were not widespread as seen with impulse ageing.

For LDPE (Figure 8.14 and 8.15) the amount of positive hetero charge at the cathode gradually reduces with time and is finally replaced with negative homo-charge injection. Whereas, the homo positive charge from the anode keeps increasing with time. The positive homo charge in thermally aged LDPE is also higher than the negative but the rates of decay are more balanced than seen within HDPE.

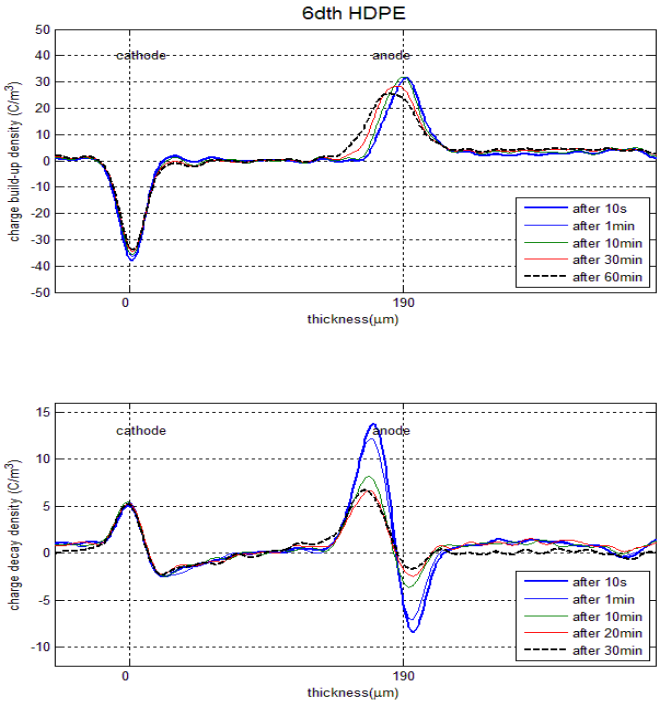

Figure 8.12: Space charge accumulation of 6 days thermal aged HDPE (top) charging, (bottom) decaying

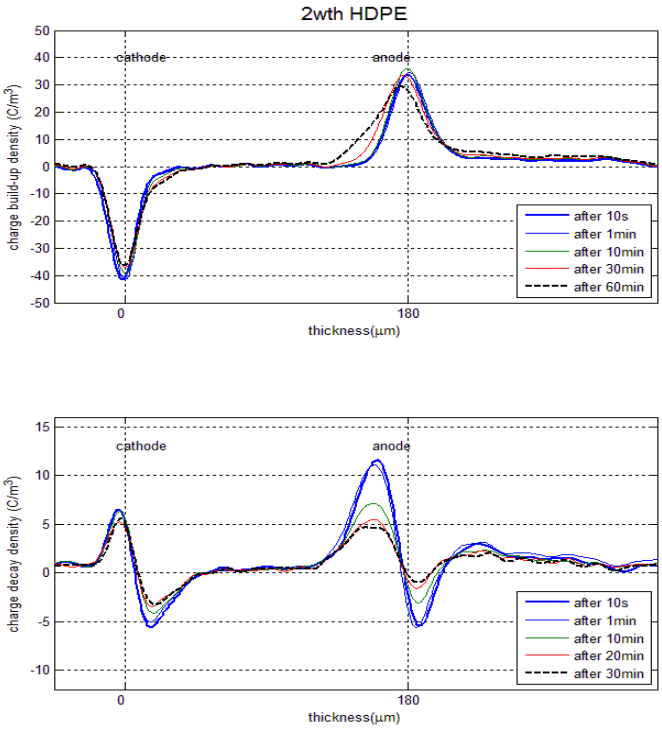

Figure 8.13: Space charge accumulation of 14 days thermal aged HDPE (top) charging, (bottom) decaying

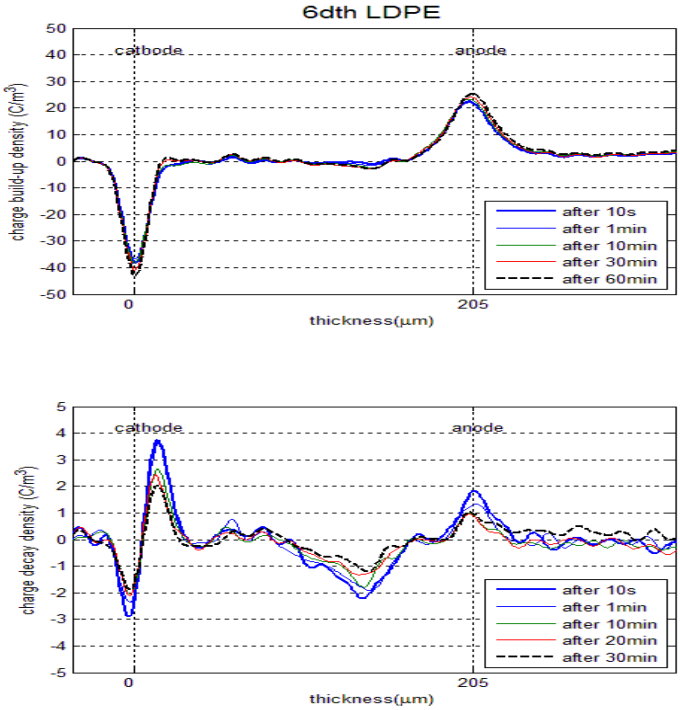

Figure 8.14: Space charge accumulation of 6 days thermal aged LDPE (top) charging, (bottom) decaying

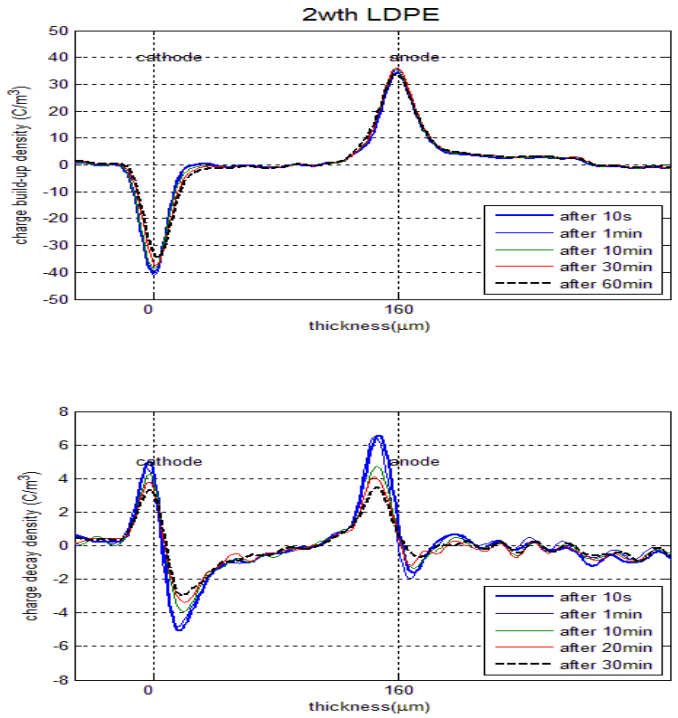

Figure 8.15: Space charge accumulation of 14 days thermal aged LDPE (top) charging, (bottom) decaying

For XL3 (Figure 8.16 and 8.17), positive charge injection from the anode dominates the bulk charge. A small negative charge was injected from the cathode after 6 days of ageing. After 14 days of ageing the amount of positive charge increases whereas the negative charge region is smaller. It is thought that charge recombination has occurred. The same thermal ageing effect was obtained in the work of Lanca [24].

Results for XL4 are shown in Figures 8.18 and 8.19. The negative charge region in the middle of the virgin sample has disappeared, suggesting an elimination of any water due to the thermal ageing process. Only positive charges were injected from the anode [181]. Charge decay is higher than that of the virgin sample. However, after 60 minutes of short circuit, a lot of charge still exists in the bulk of sample. It suggests both shallow and deep trapped charges were formed inside the material.

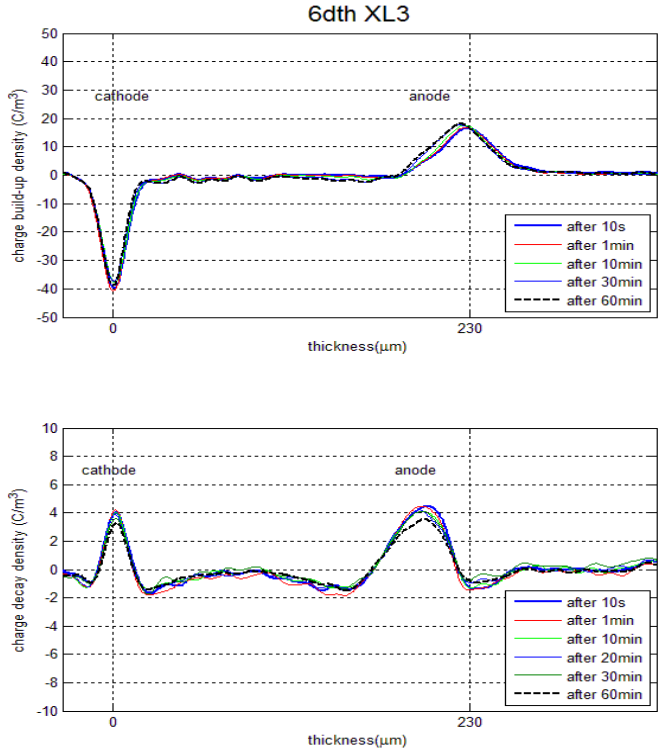

Figure 8.16: Space charge accumulation of 6 days thermal aged XL3 (top) charging, (bottom) decaying

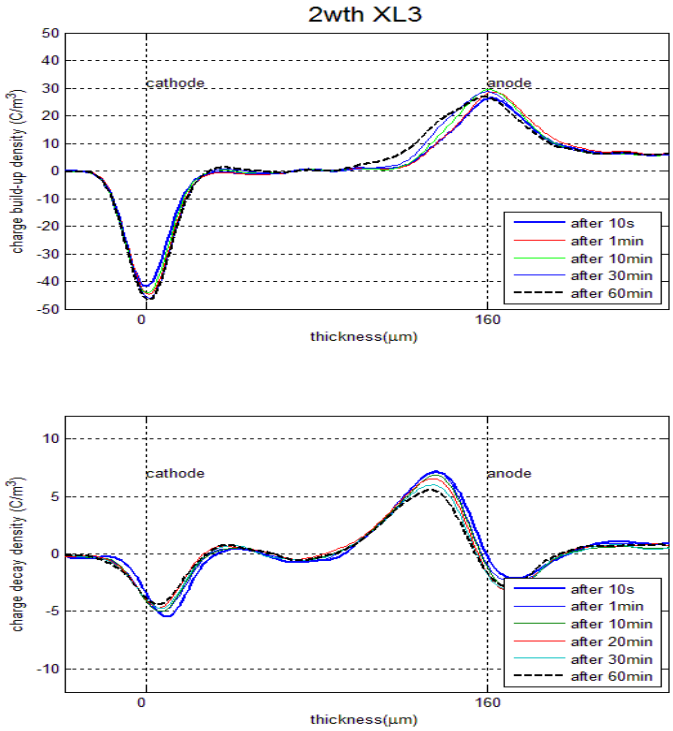

Figure 8.17: Space charge accumulation of 14 days thermal aged XL3 (top) charging, (bottom) decaying

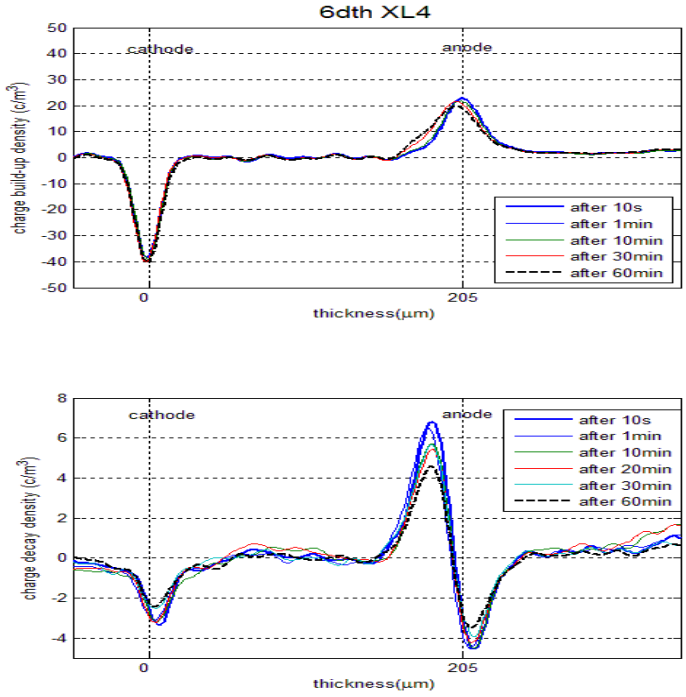

Figure 8.18: Space charge accumulation of 6 days thermal aged XL4 (top) charging, (bottom) decaying

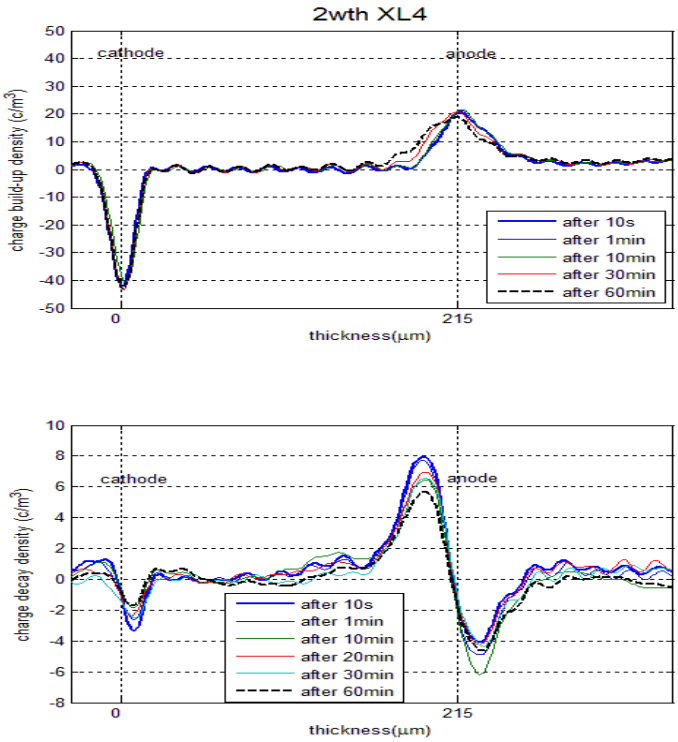

Figure 8.19: Space charge accumulation of 14 days thermal aged XL4 (top) charging, (bottom) decaying

8.4. Results obtained for UV aged samples

Figures 8.20 to 8.27 show the space charge measurement results for samples that have undergone the UV radiation ageing process. Bipolar charges were injected only near the sample surface. The magnitudes of charge peaks near the surfaces increase with ageing time [38]. This highlights that UV radiation has more effect on the surface of sample rather than the whole bulk. The effect of UV is clearer in the case of XL3 compared to the other three materials as XL3 absorbs more UV light. The space charge profile of LDPE changes after UV ageing. The hetero charge near the cathode gradually reduces as increasing ageing time and finally is replaced by homocharge. It is likely that the UV causes crosslinking in the LDPE changing the morphology of the material and consequently affecting the space charge profile [141]. The charges near the surfaces decay quite quickly over the first 30 minutes of the measurement.

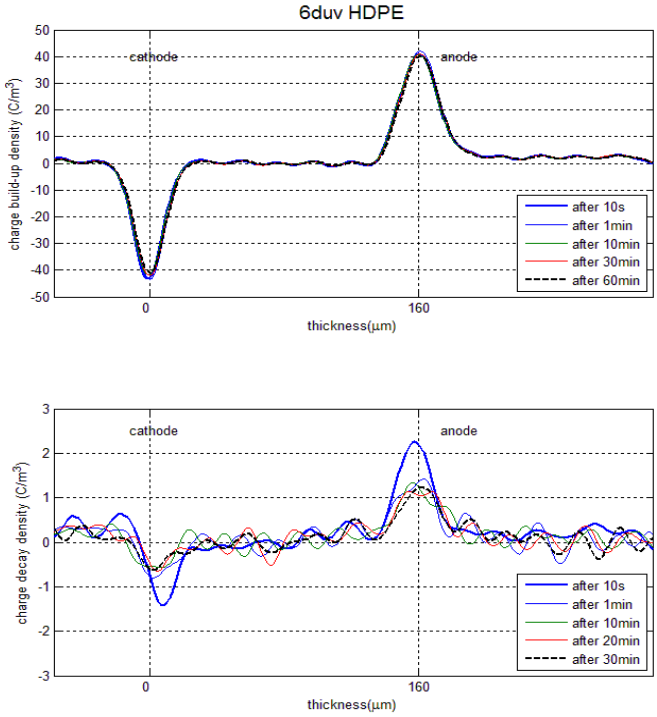

Figure 8.20: Space charge accumulation of 6 days UV aged HDPE (top) charging, (bottom) decaying

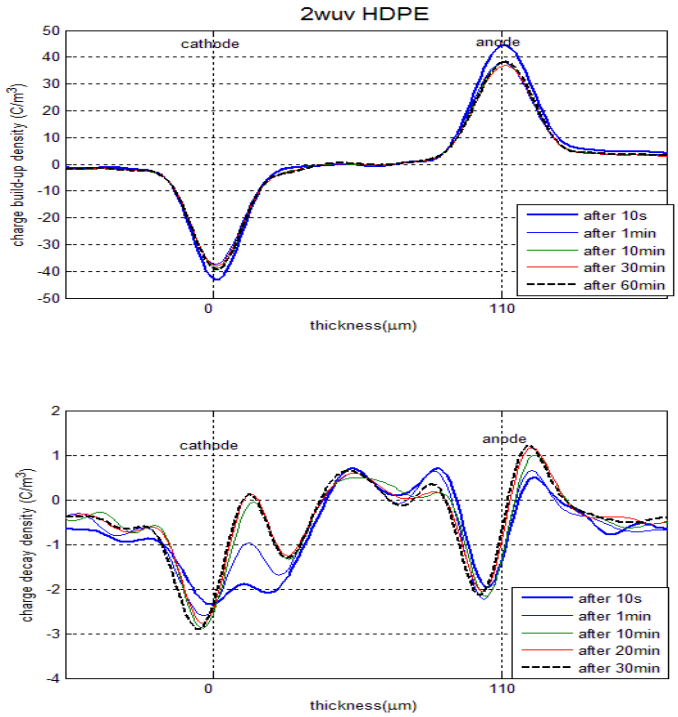

Figure 8.21: Space charge accumulation of 14 days UV aged HDPE (top) charging, (bottom) decaying

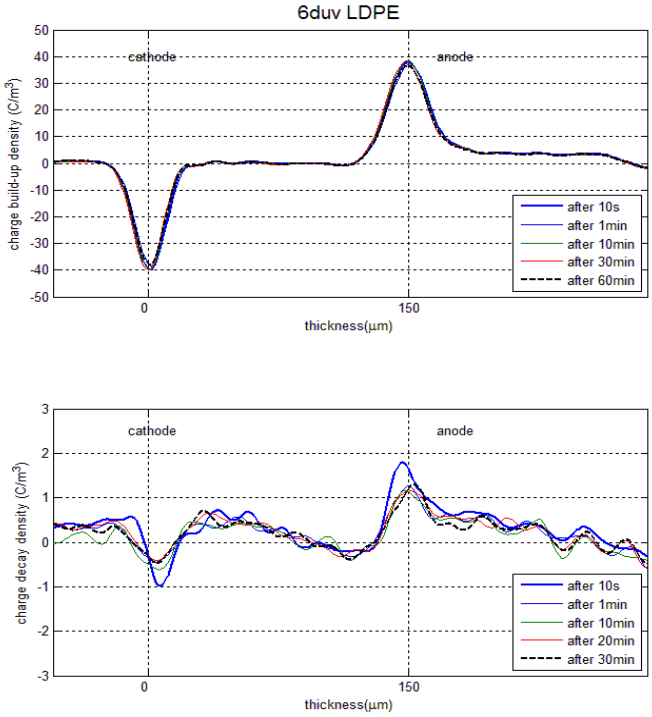

Figure 8.22: Space charge accumulation of 6 days UV aged LDPE (top) charging, (bottom) decaying

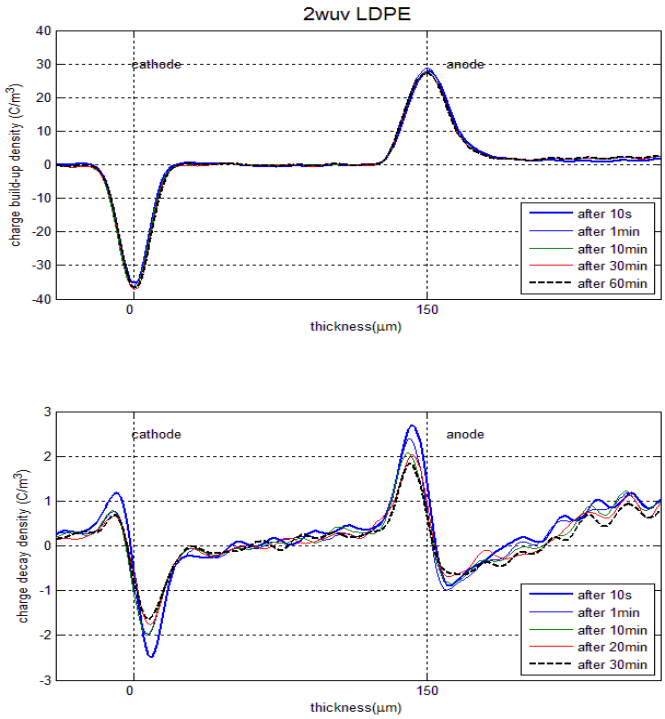

Figure 8.23: Space charge accumulation of 14 days UV aged LDPE (top) charging, (bottom) decaying

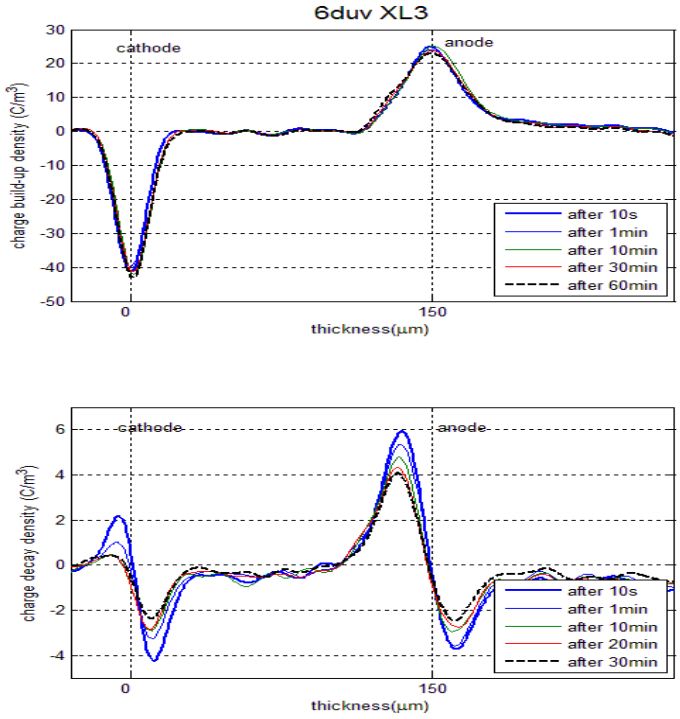

Figure 8.24: Space charge accumulation of 6 days UV aged XL3 (top) charging, (bottom) decaying

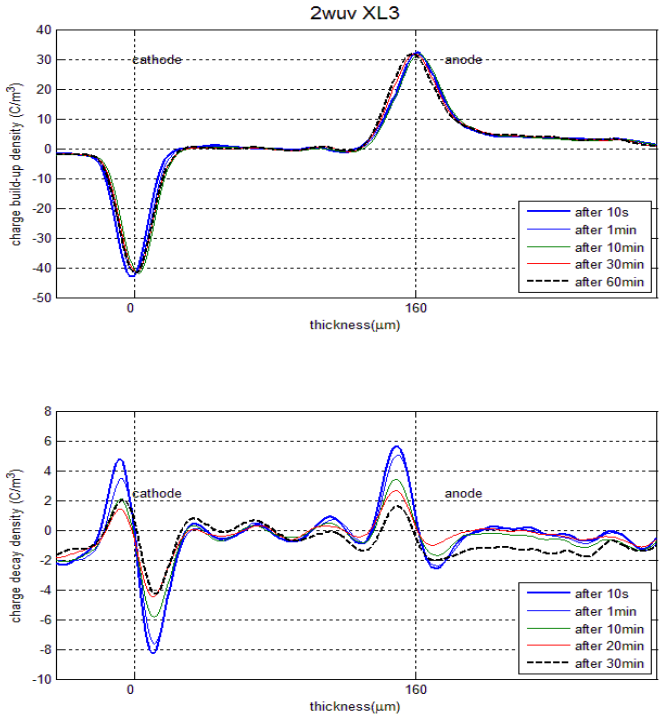

Figure 8.25: Space charge accumulation of 14 days UV aged XL3 (top) charging, (bottom) decaying

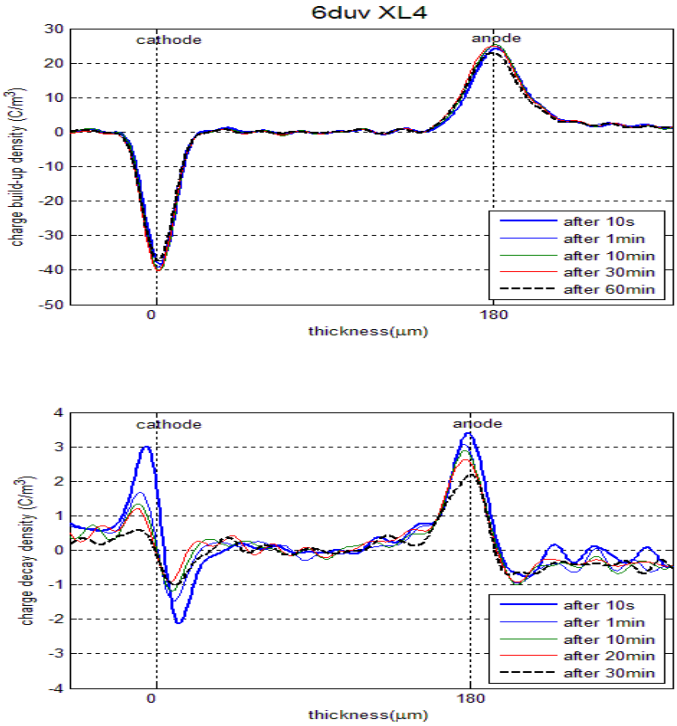

Figure 8.26: Space charge accumulation of 6 days UV aged XL4 (top) charging, (bottom) decaying

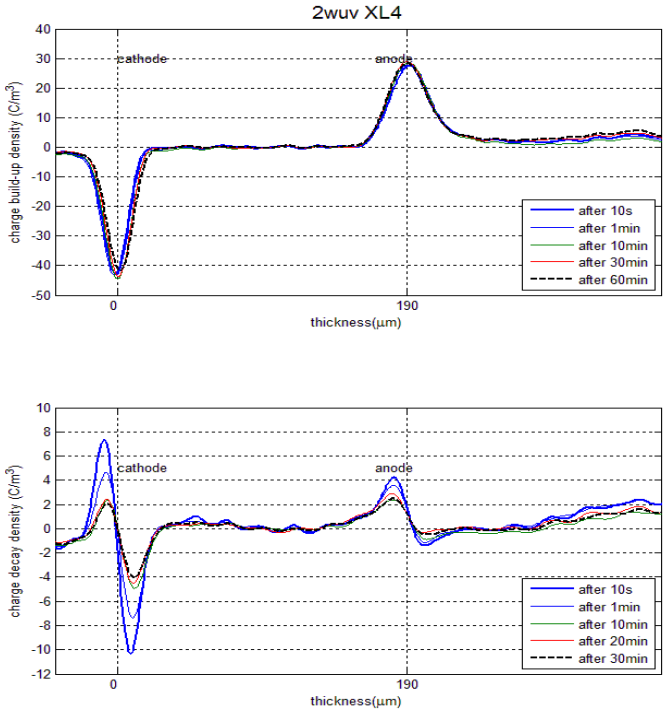

Figure 8.27: Space charge accumulation of 14 days UV aged XL4 (top) charging, (bottom) decaying

8.5. Discussion and Summary

The measurement of space charge in the presence of an applied voltage always includes the contribution of induced charges from the two electrodes (two high peaks). In order to account for this contribution, the volt-off measurement can be taken. It means that during the poling process, the voltage is quickly turned off before the space charge measurement and then back on again for poling. The charge decay measurement also provides the bulk charge profile without any charge from the poling electrodes. From the charge profile, the total charge $Q_{(t)}$ (only magnitude, without the sign of charge) can be evaluated by integrating the charge density across the sample thickness and multiplying by the electrode area. However, the measurements were usually taken with the same electrode size but various sample thicknesses. It is better to evaluate the average charge density using [131]:

$$q_{(t)} = \frac{1}{d}\int_{o}^{d} q_{(x,t)}dx \qquad \textbf{(8.1)}$$

Where $q_{(t)}$ is average charge density, $q_{(x,t)}$ is the charge density over the sample thickness axis x. The observation of average charge density profile with time can provide information about the mobility of trapped charges. The charge mobility can be calculated using [131]:

$$\mu_{(t)} = -\frac{3\varepsilon}{q_{(t)}^2}\frac{dq_{(t)}}{dt} \qquad \textbf{(8.2)}$$

The average charge density can be fitted using either an exponential function or a power function. However, in this work the power function in equation (8.3) was found to give a better fit compared to an exponential one.

$$q_{(t)} = at^{-b} \qquad \textbf{(8.3)}$$

Where a and b are two parameters. Parameter b represents how fast the charge decay occurs when the stress is removed and sample is short-circuited. Figure 8.28 shows the charge decay profiles of various materials and Figures 8.29 to 8.32 present the results of charge decay profile of four different materials with different ageing conditions. All samples were discharged after 60 minutes of poling with an applied field of 34 $kVmm^{-1}$. All data are fitted with the power function and Table 8.1 shows the parameters a and b for all investigated materials.

Materials	b	a
HDPE	0.061	1.283
HDPE 3000 impulse aged	0.059	1.264
HDPE 6 days thermal	0.078	1.222
HDPE 2 weeks thermal	0.095	1.320
HDPE 6 days UV	0.093	1.189
HDPE 2 weeks UV	0.088	1.232
LDPE	0.145	1.813
LDPE 3000 impulse aged	0.102	1.571
LDPE 6 days thermal	0.102	1.332
LDPE 2 weeks thermal	0.074	1.242
LDPE 6 days UV	0.093	1.189
LDPE 2 weeks UV	0.059	1.12
XL1	0.129	1.534
XL3	0.102	1.289
XL3 3000 impulse aged	0.092	1.296
XL3 6 days thermal	0.037	1.067
XL3 2 weeks thermal	0.037	1.101
XL3 6 days UV	0.067	1.167
XL3 2 weeks UV	0.122	1.378
LDPE4	0.019	1.058
XL4	0.018	1.033
XL4 3000 impulse aged	0.034	1.089
XL4 6 days thermal	0.049	1.173
XL4 2 weeks thermal	0.053	1.167
XL4 6 days UV	0.059	1.131
XL4 2 weeks UV	0.113	1.298

Table 8.1: Parameters of power function for different materials

Figure 8.28 shows that the quenched low density polyethylene accumulates a lot of charge after the same poling condition whereas the smallest amount of charge was observed in the HDPE sample. The charge decay rate of XL4 is very small compared to the other three materials. This means the charges are trapped very deeply in XL4. The increase in the amount of peroxide content for crosslinking from 0 to 3% reduces the charge accumulation in LDPE but the rate of charge decay also decreases. It suggests that the effect of the crosslinking process alters the morphology and produces by-products. The similar results were shown in the work of Montanari [131]. The XL4 and LDPE4 have the same charge decay rate but the XL4 has more charges in the bulk. Two points can be deduced here are that the slow

charge decay rate is related to silane groups and the amount of charge injection is related to water diffusion in the material after boiling the sample in a water bath.

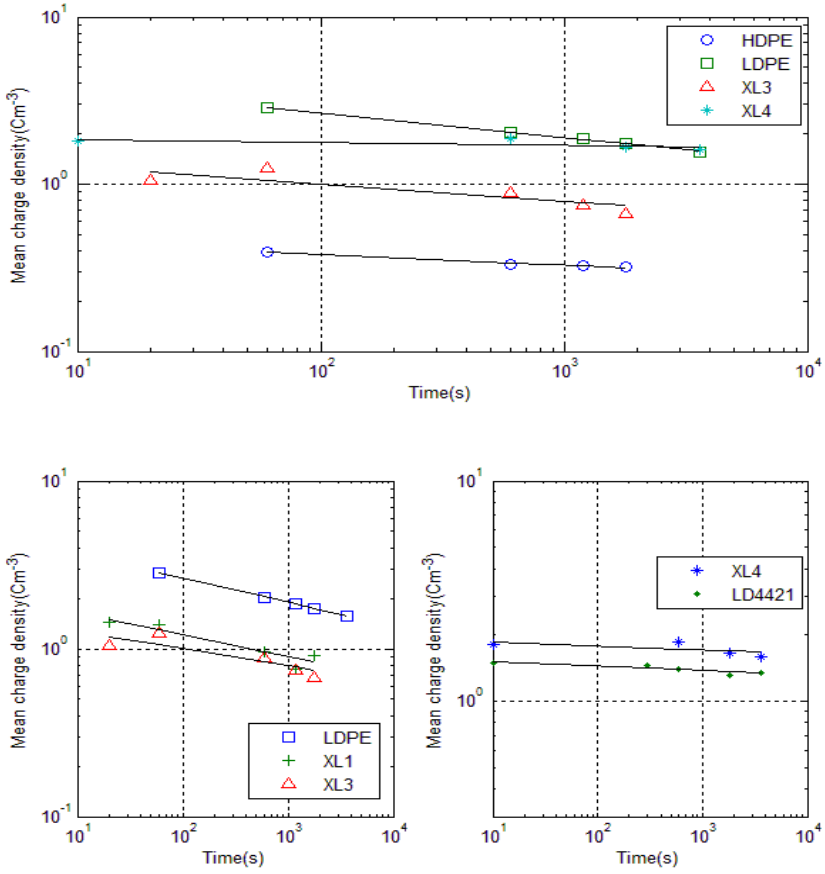

Figure 8.28: charge decay profiles of different materials

Figure 8.29 shows the results for HDPE under different ageing processes. All ageing processes seem to enhance charge formation in the material. The small reduction appears in the amount of charge after 6 days of UV ageing. The effect of UV crosslinking can contribute to this observation. Thermal ageing provides the largest charge injection. However, only impulse ageing makes the charges decay slower than normal HDPE sample.

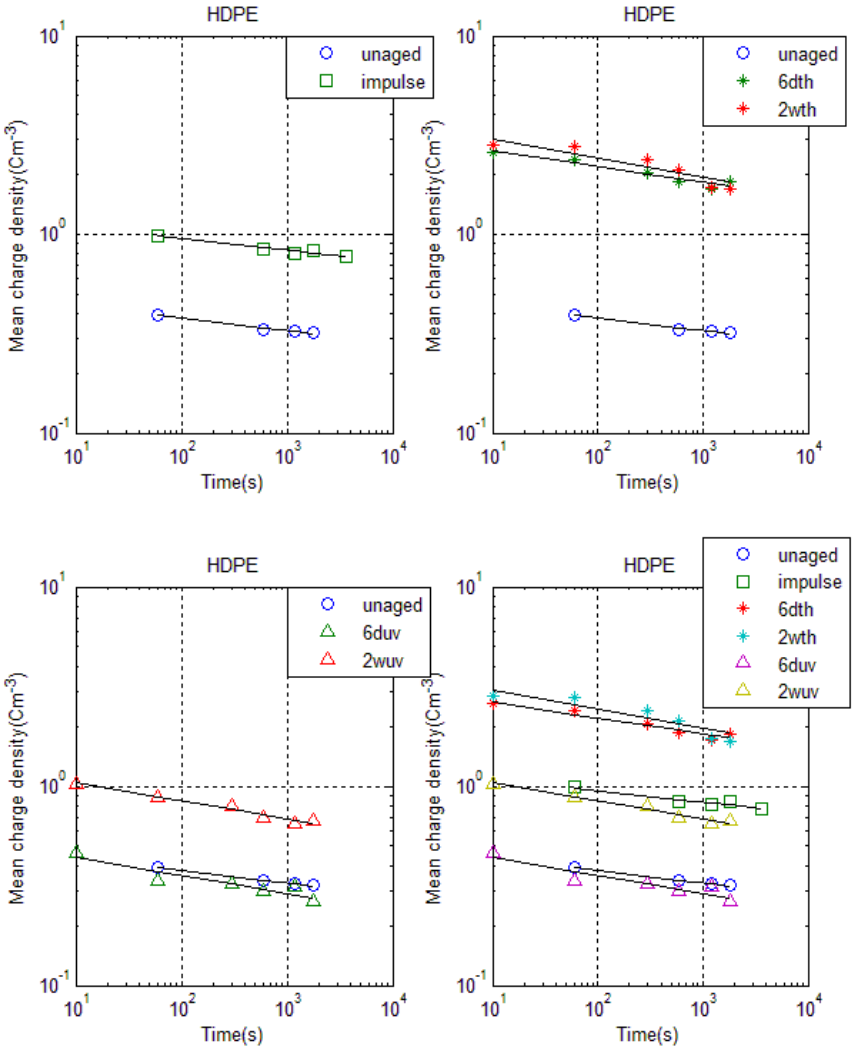

Figure 8.29: charge decay profiles of HDPE

A slightly different profile was obtained for LDPE (Figure 8.30) where most of ageing processes reduce the amount of charge in material. With thermal and UV ageing, the morphology change can be the key factor to change the space charge profile. The longer ageing time for UV and thermal ageing may lead to higher charge injection as oxidation and chains scission will become more significant. A same amount of charge was obtained in the case of the impulse aged sample but the charges decay with a slightly lower rate. Therefore, the effect of impulse ageing seems to be very small.

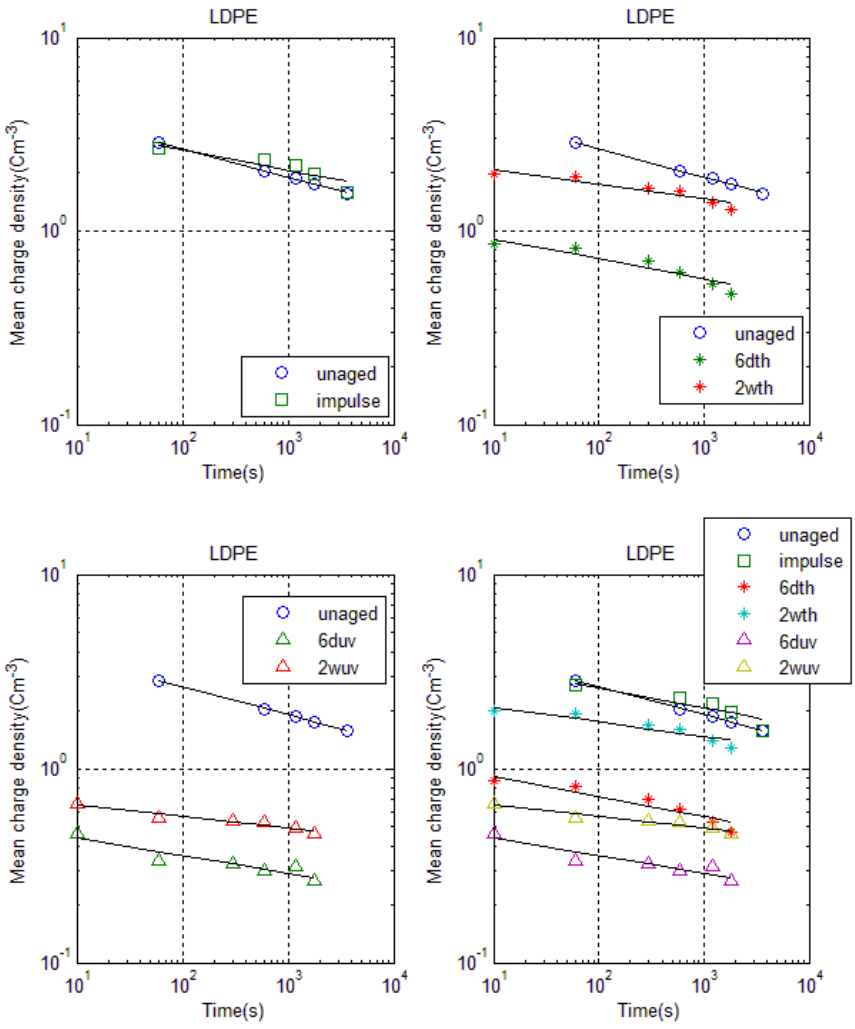

Figure 8.30: charge decay profiles of LDPE

XL3 behaves poorly with all three ageing processes (Figure 8.31) where the total charge after poling of aged samples is always higher than in the virgin case. The decay rates are also slower for aged samples. In this material, bond breaking and oxidation are the main reasons for changes in property. When chains are crosslinked together, it is hard to modify the molecular structure of the material if bonds are not subsequently broken.

The behavior of XL4 material (Figure 8.32) with UV and thermal ageing is similar to LDPE. In this case any change in morphology is thought less important than the effects of oxidation and removal of water. The charge deposited due to impulse ageing is higher than for virgin XL4. However, the charge decay rate is slightly faster.

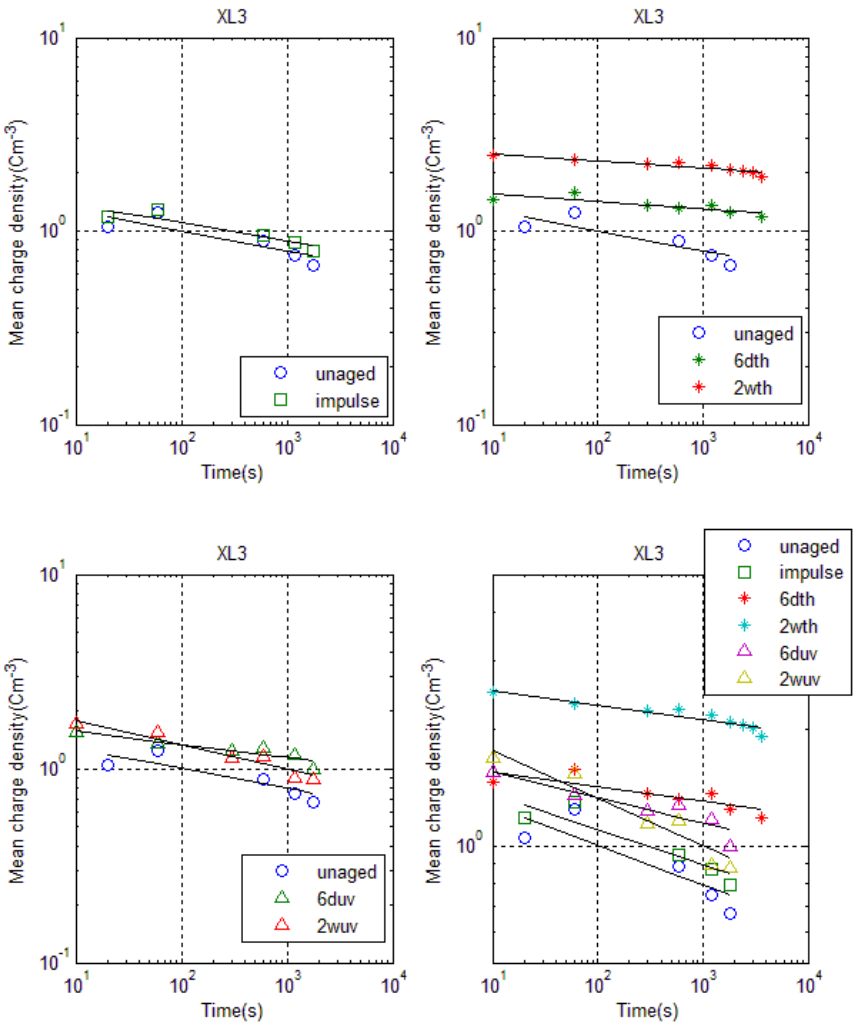

Figure 8.31: charge decay profiles of XL3

In summary, impulse ageing increases charge deposition in the material. Charges are usually spread through the sample bulk and decay slowly after removal of the applied field. UV ageing (up to 14 days) reduces the amount of charge injection and charges mainly stay near the interface between the sample and the electrodes. The effect of thermal ageing on space charge depends on the type of material and the condition of the sample. For UV and thermal ageing, it is possible for the space charge profiles to improve after a short ageing time but this is not true with impulse ageing. The reason for this is UV and thermal ageing can in the short term increase crosslinking, and crystalinity as well as removing by-products and water from the sample.

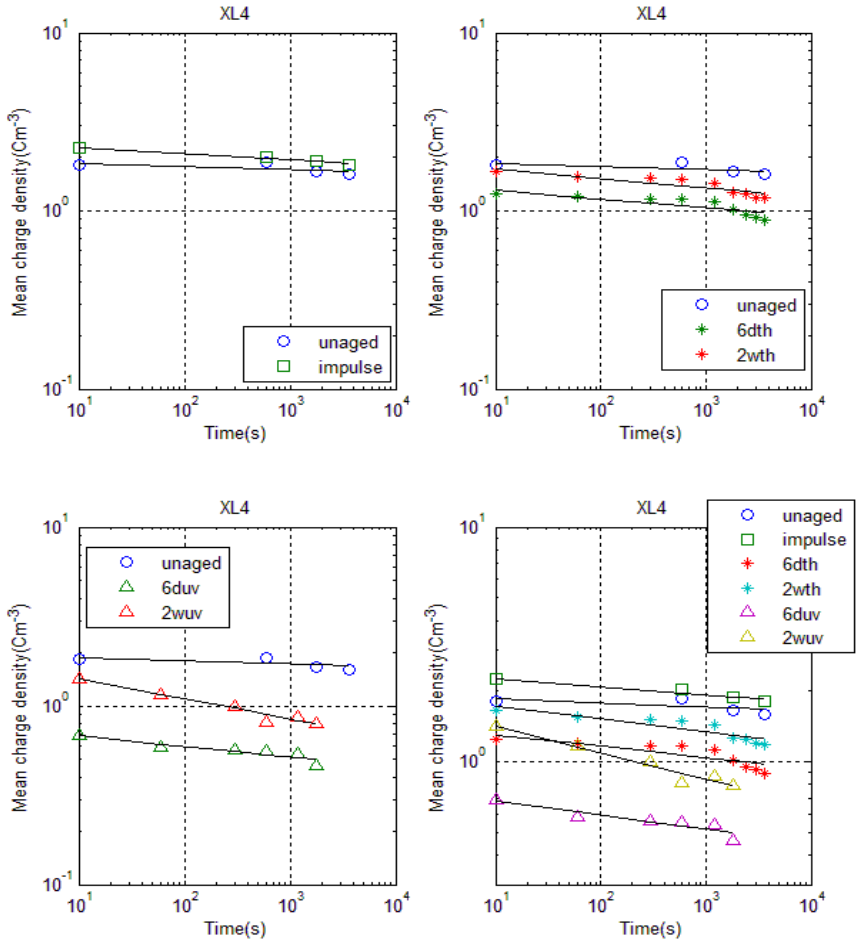

Figure 8.32: charge decay profiles of XL4

Chapter Nine

Conclusions and Future Work

9.1. Project achievements

This project developed an impulse ageing system for polymeric cable insulation materials. Furthermore, the mechanism for impulse ageing was highlighted and compared to other common ageing processes such as UV and thermal ageing. The project achievements can be listed as the following:

- The project developed methodologies for handling cable insulation materials and preparing moulded samples. The moulding process with polyethylene and related materials to achieve a desired shape is not straight forward. LDPE and HDPE have the advantage of not sticking to the mould after cooling and are released quite easily. However, the use of a vacuum to a closed mould cannot eliminate most of the air bubbles. While moulding crosslinked polyethylene from silane grafted low density polyethylene is similar to normal LDPE and HDPE the moulding thin films of

peroxides crosslinked polyethylene is a real challenge. With the presence of by-products during the crosslinking process, the mould release agent (normally silicone grease) can degrade and material can stick to the mould.

- A real time control system was successfully implemented to manage both risks of breakdown and measure fast events during the impulse ageing process. This system was based on the Labview programming language. Signals were recorded by a digital oscilloscope and a performance criterion applied to identify breakdown and prevent further damage from continuous breakdown events. Signals were also counted to achieve a desired ageing condition. The control system also includes noise suppression and ensures the lightning impulse parameters are determined accurately.

- The ageing experiments provided specific information about sample ageing. For impulse ageing, the impulse generator used was a single stage impulse generator for easy control of "low level" lightning impulses (a few tens kilo-Volts). The external controller of the optical trigger was built to control the trigger interval. Sample temperature was maintained at around 20^{o}C during the impulse ageing experiment. The air relative humidity has not been controlled. Therefore all the electrodes and sample were immersed in silicone oil. For thermal and UV ageing, samples were placed in an oven which provides a stable temperature during the ageing processes.

- The combination of three characterization tests including breakdown, dielectric spectroscopy and space charge measurement can show the effects of ageing. No single test can provide enough information about the mechanisms of ageing processes. Breakdown measurement is a common tool to decide the quality of an electrical insulation material. However, due to the stochastic nature of any breakdown event, it is quite hard to judge material condition if only a small variation exists in obtained data. Dielectric spectroscopy provides a good view of both the physical and electrical properties of a material. However, the small value of losses in polyethylene and measurement over an extensive frequency range is still a big problem. Space charge measurement gives insight into charge density under a DC applied field, but in a majority of applications the material will be under an AC stress.

9.2. Summary of results and conclusions

The four investigated materials have quite different behaviour under ageing. These differences are not only due to differences in chemistry but also from the production process required to create samples. The addition of crosslinking agents (peroxides, silane) may alter the electrical, mechanical or physical properties of the material. The moulding temperature, moulding time and backing layer material will affect the oxidation state of the material. Cooling rates will alter the morphology of the material and consequently other characteristics. Material which was crosslinked in boiling water can suffer from water diffusion whereas the peroxide crosslinking will create additional by-products.

The impulse ageing results showed that a significant number of lightning impulse events accelerate the ageing process of most polyethylene types. The effect of impulses on quench cooled LDPE may be too small to measure under the available experiments. Breakdown strength is reduced significantly for samples which experience a lot of lightning impulses. Dielectric loss measurements show that all four materials after ageing have a higher dielectric loss factor at low frequency and this loss due to ionic conduction and interfacial polarisation. For effectively aged materials (HDPE, XL3, XL4), smaller size molecules are generated and there are inhomogeneous regions in the bulk of sample. This may be the result of molecular damage created by lightning impulse voltage. In fact, despite the very short duration of the impulse, the high peak magnitude of the impulse voltage with a sharp rise time may be enough to cause damage. Also, more ions may be generated after impulse ageing as conduction at low frequencies is seen to increase. The results for PEA measurement show the injection of charge is more effective in the case of an impulse aged sample. More charges were injected and moved deeper into the bulk. The effect of lightning impulses on cable materials seems closely related to the order of the molecular structure. The addition of disorder to an already disordered quenched LDPE seems to be a minor effect.

Because UV and thermal ageing were undertaken in air, oxidation contributes significantly to the ageing mechanism [37]. Oxidation occurs in all polyethylene materials under UV but far faster in cases of materials containing additives (XL3, XL4). High energy UV radiation can break bonds more easily and act as a catalyst for oxidation. Lower thermal energy is required to activate the reaction of more

sensitive additives. The effect of oxidation is related to the physical rather than the electrical properties of the material, even though, reduction in electrical properties still occur. However, it seems there is no direct relation between oxidation degree and other electrical properties. UV ageing may cause both chain scission and additional crosslinking. The gel content should vary with ageing time. Thermal ageing causes changes in crystallinity, spherulite size and molecular structure [26]. The effect of water diffusion (XL4) and crosslinking by-products (XL3) is also revealed through the process of thermal ageing.

9.3. Suggestions for future work

From the above results, some work can be proposed to further improve our understanding about cable material ageing and lifetime of an insulation material:

- Impulse ageing needs to be related to a physical model. None of the proposed models in chapter 1 are shown to be applicable to impulse ageing. J. P. Crine's model does not apply to lightning impulses as the duration of lighting impulse is not long enough to break a bond [47]. The space charge model of Dissado [54] is designed for applied DC voltages, but for AC or lightning impulse voltages the space charge injection may be small or even insignificant. An electro-mechanical force model of J. Lewis [50] can be considered if the force due to a lightning impulse can actually alter the morphology of the material. The application of any model will require the verification from real data.

- Morphology may play an important role in lightning impulse ageing. The order of material is decided by the crystallinity. The effect of lightning impulses with materials which possess different crystallinity should be compared. Another approach is the consideration of lightning impulses on polymer blends. The small addition of LDPE in HDPE may improve the behavior of HDPE with lightning impulse and lead to the development of new materials that are not significantly affected by lightning impulses.

- The effect of space charge accumulation during the ageing process will be much more significant in the case of a switching impulse. The longer on-time of the switching impulse will increase chances of charge injection. The combination of molecular damage and space charge injection may cause different material

behaviour. The rate of applied impulse (trigger interval) should also be considered because it may vary space charge injection as well. A significant challenge would be to develop impulse ageing experiments with a high frequency of triggering. A high voltage impulse generator need a certain time for capacitor charging between each trigger event. This time may be longer than the required trigger interval.

- Finally, the synergy between more than one ageing processes should be investigated. Under real working conditions, cable insulation will suffer from multifactor ageing processes. The other ageing conditions such as thermal, electrical, mechanical, chemical ageing may be affected by the presence of additional repetitive impulse voltages.

Appendix A: Labview Program

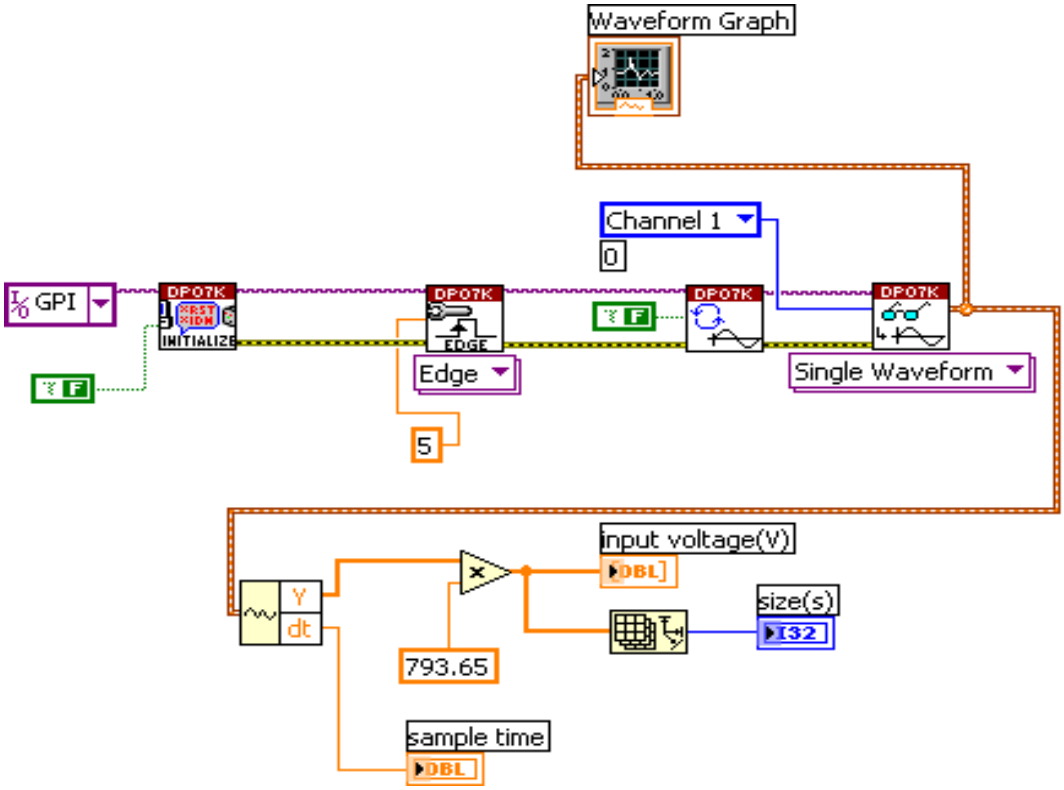

Figure A.1: Data acquisition program

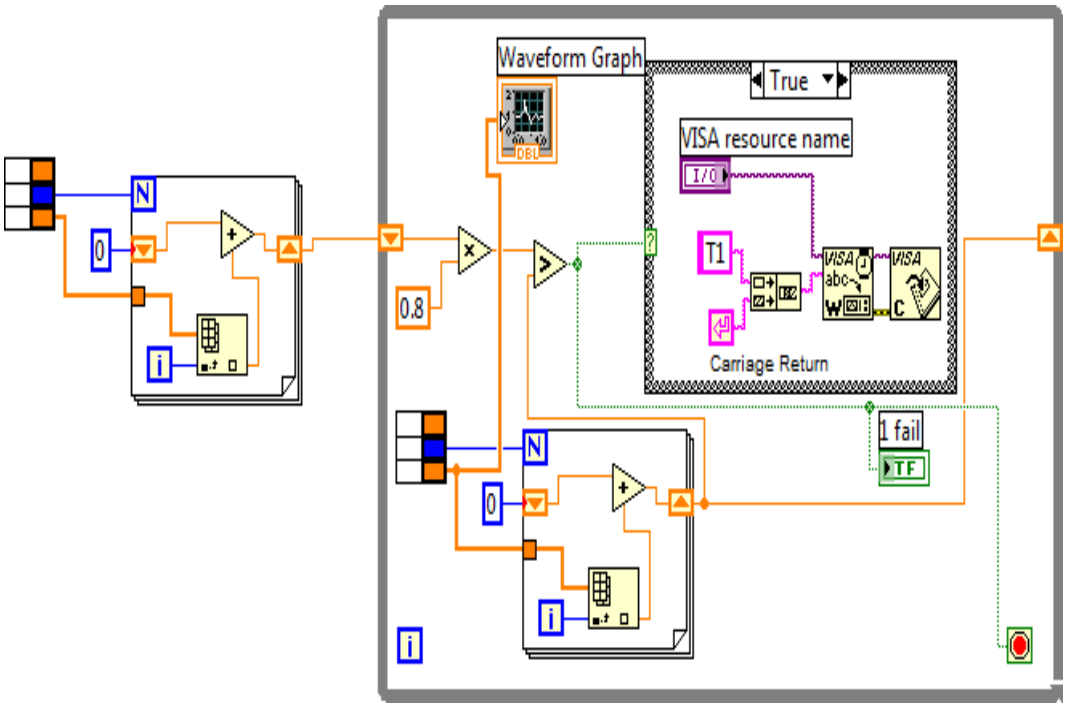

Figure A.2: Area check program

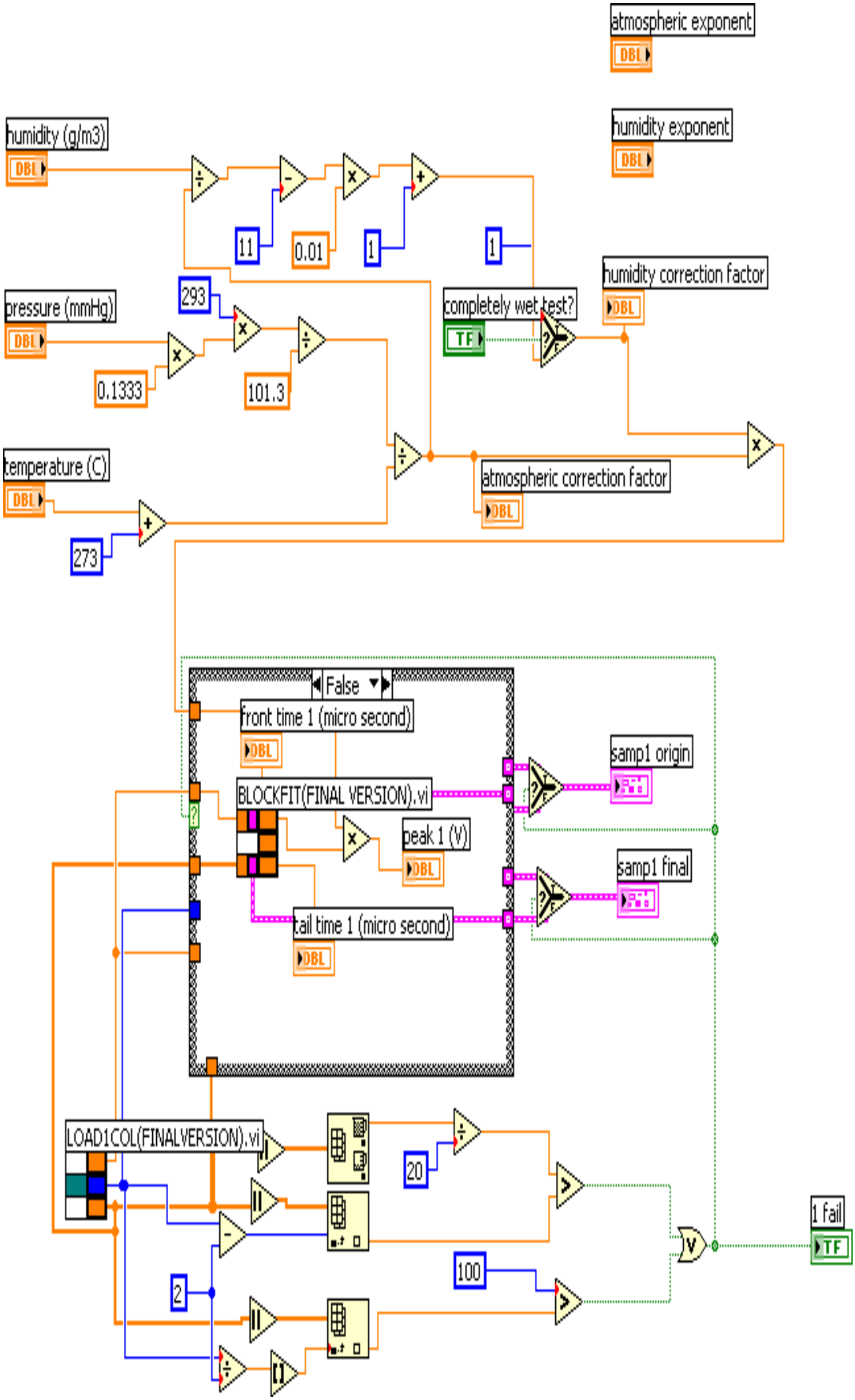

Figure A.3: Data processing program

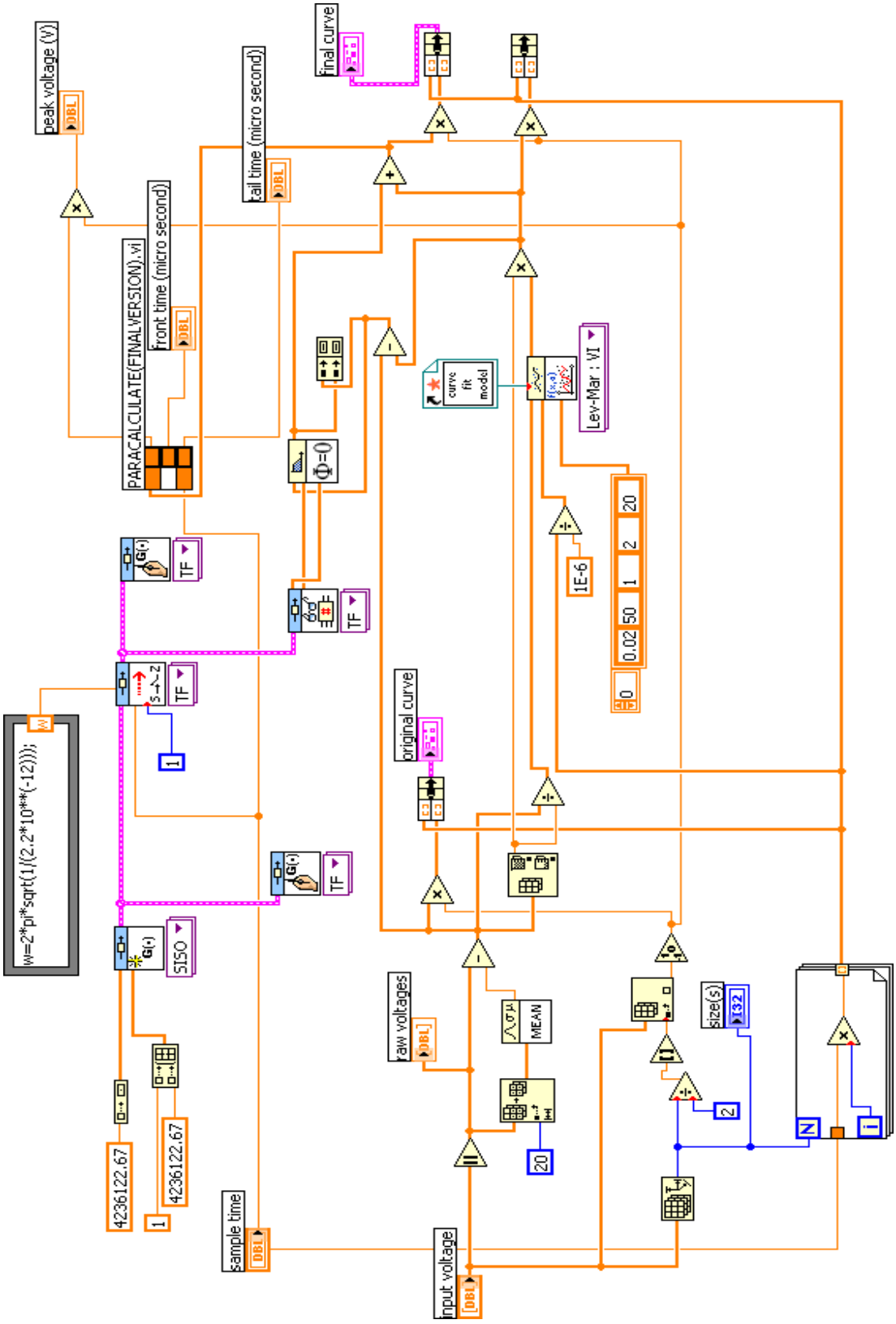

Figure A.4: Filtering and fitting program

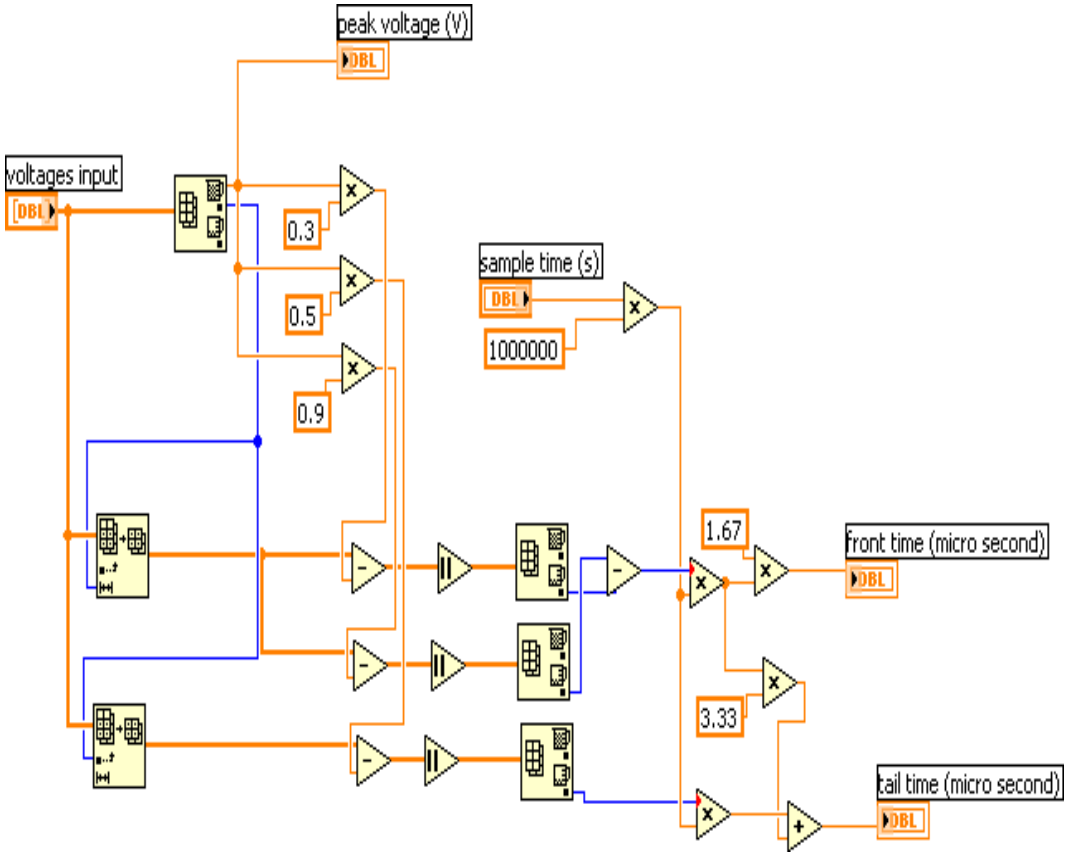

Figure A.5: Parameter calculation program

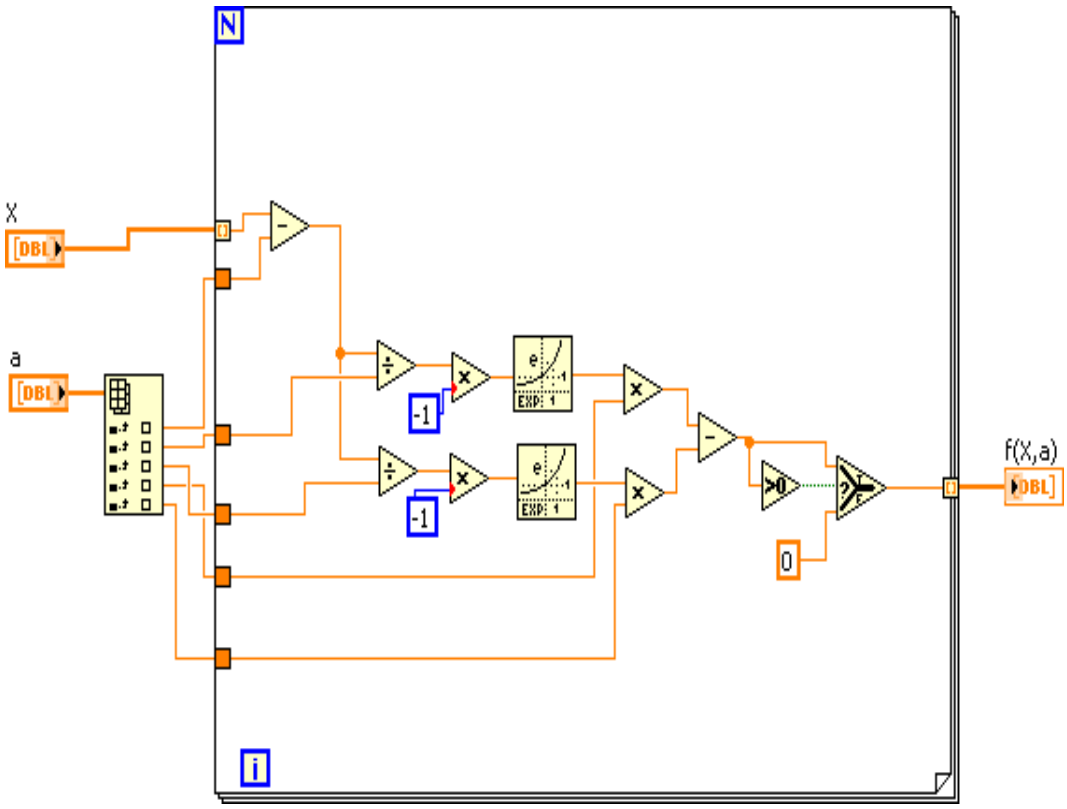

Figure A.6: Separated double exponential waveform program

Appendix B: Triggering Circuit to Control the Repetitive Rate of Lightning Impulses

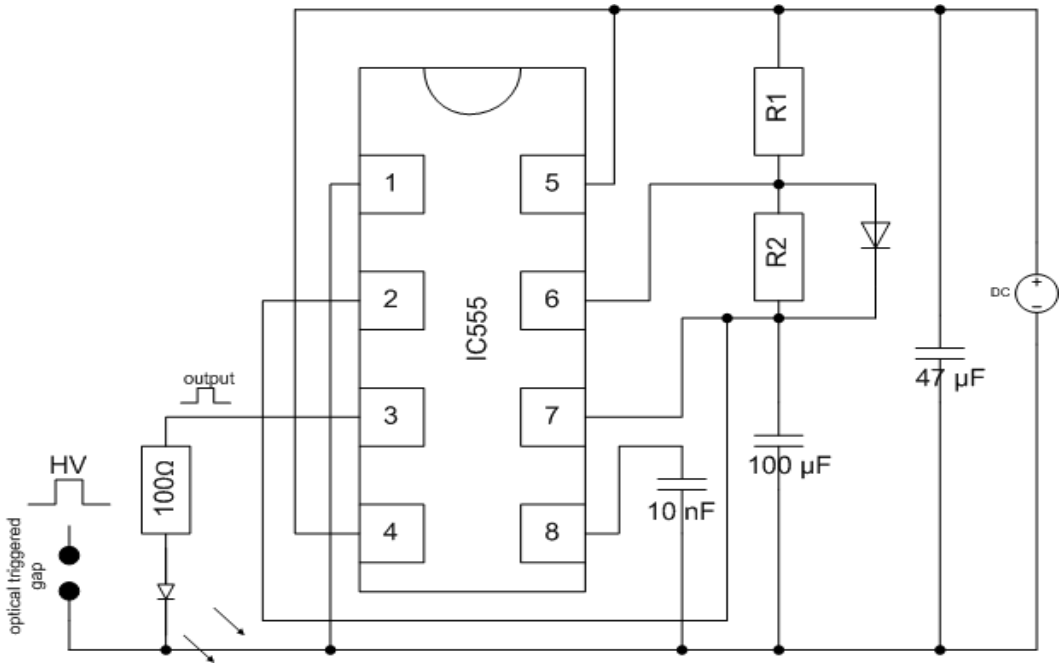

Figure B.1: Trigger circuit

An auto trigger of lightning impulse generator consists of an integrated trigger unit in the digital voltmeter. The digital voltmeter measures the voltage of a charging capacitor. If this voltage passes a certain chosen value, the trigger unit activates a spark generator to create an impulse. The trigger interval directly depends on the charging time of a capacitor and it is varied with different impulse voltage levels. Furthermore, the trigger interval is not consistent. Consequently, a constant repetitive rate of lightning impulse is really hard to achieve. An external trigger circuit was built, integrated with the impulse generator and software controlled kit to overcome this problem (Figure B.1). This circuit is used to generate short pulses with variable pulse width and duty cycle. R_1 controls the pulse width (from 15 Ω to 15 kΩ which corresponds to 1 ms to 1 s) and R_2 decides the pulse off state (145 kΩ to 1145 kΩ which corresponds to 1 s to 10 s). Only one trigger is needed at a time, therefore, the pulse width has to be kept small. Created pulses activate the photodiode (HFBR1402Z) to generate an optical signal with wavelength of 820 nm and trigger the spark.

Appendix C: Geometry Correction for the Dielectric Spectroscopy

A problem is raised when the abnormal high real relative permittivity for polyethylene is measured. A test was conducted with different circular samples of the same material, thickness but different diameter. Obtained results show that the real part of the relative permittivity directly depends on the sample diameter. The closer the sample diameter to the electrode diameter, the better the result would be. The smaller diameter sample results in the higher the real part of the relative permittivity. If the circular electrode has an effective area A and a circular sample has a thickness of t and a surface area A_1 (Figure C.1)

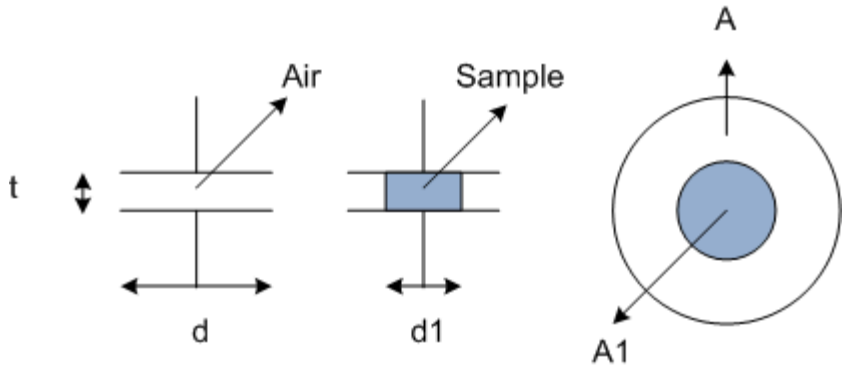

Figure C.1: Dielectric loss measurement

An empty electrode system possesses a capacitane:

$$C_0 = \varepsilon_a \varepsilon_0 \frac{A}{t} \quad \textbf{(C.1)}$$

The sample A_1 has a capacitance of:

$$C_s = \varepsilon_s \varepsilon_0 \frac{A_1}{t} \quad \textbf{(C.2)}$$

The measured capacitance consists of sample capacitance and a capacitance of an unoccupied air gap with area A_2=A-A_1:

$$C_m = \varepsilon_m \varepsilon_0 \frac{A_1}{t} = \varepsilon_s \varepsilon_0 \frac{A_1}{t} + \varepsilon_a \varepsilon_0 \frac{A_2}{t} \quad \textbf{(C.3)}$$

Solartron system returns value of ε_m whereas ε_s is needed:

$$\varepsilon_s = \varepsilon_m - \varepsilon_a \frac{A_2}{A_1} = \varepsilon_m - \varepsilon_a \frac{d^2 - d_1^2}{d_1^2} \quad \textbf{(C.4)}$$

The values for ε_m, d, d_1 are known, the value for ε_a need to be measured. Unfortunately, the measurement for ε_a using Solartron system also depends on the sample thickness t. Average values for ε_a against thickness t are shown in Table C.1.

Thickness (μm)	ε_a
160	0.84
170	0.85
180	0.86
190	0.87
200	0.88
210	0.88
220	0.89
230	0.89
240	0.90
250	0.90
260	0.91

Table C.1: The real part of the relative permittivity of air against sample thickness

References

1 B. K. Gupta, B. A. Lloyd, G. C. Stone, S. R. Campbell, D. K. Sharma, and N. E. Nilsson, "Turn Insulation Capability of Large AC Motors Part 1 - Surge Monitoring," *Energy Conversion, IEEE Transactions on,* vol. EC-2, pp. 658-665, 1987.

2 J. Amarnath, D. R. K. Paramahamsa, K. Narasimharao, B. P. Singh, and K. D. Shrivastava, "Very fast transient over-voltages and transient enclosure voltages in gas insulated substations," in *Electrical Insulation and Dielectric Phenomena, 2003. Annual Report. Conference on*, 2003, pp. 506-509.

3 J. Ramirez, E. Da Silva, J. Sanz, J. Bermudez, and J. Rodriguez, "Comparison of the accelerated aging under different thermal cycles and voltages impulses in XLPE cables," Nashville, TN, United states, 2005, pp. 229-232.

4 M. A. Abdallah, "Behavior of XLPE medium voltage cable under switching impulse," in *14th International Symposium on High Voltage Engineering*, Beijing, china, 2005.

5 M. Marzinotto, C. Mazzetti, M. Pompili, and P. Schiaffino, "Behaviour of EPR high voltage cable models under swithching impulse stress," presented at the 13 th International Symposium on High Voltage Engineering, Millpress, Rotterdam, Netherlands, 2003.

6 S. Boev, "Electric aging of polyethylene in pulsed electric field," in *IEEE International Pulsed Power Conference*, Monterey, CA, USA, 1999, pp. 1365-1368.

7 G. C. Stone, R. G. Van Heeswijk, and R. Bartnikas, "Electrical aging and electroluminescence in epoxy under repetitive voltage surges," *IEEE Transactions on Electrical Insulation,* vol. 27, pp. 233-244, 1992.

8 R. A. Hartlein, V. S. Harper, and N. Harry, "Effects of voltage surges on extruded dielectric cable life project update," *IEEE Transactions on Power Delivery,* vol. 9, pp. 611-619, 1994.

9 S. Grzybowski, P. Trnka, and J. C. Fulper, "Aging of high voltage cables by switching impulse," Arlington, VA, United states, 2007, pp. 165-168.

10 S. Grzybowski, P. Shrestha, and L. Cao, "Electrical aging phenomena of XLPE and EPR cable insulation energized by switching impulses," in *2008 International Conference on High Voltage Engineering and Application, ICHVE 2008, November 9, 2008 - November 13, 2008*, Chongqing, China, 2008, pp. 422-425.

11 S. Bahadoorsingh and S. M. Rowland, "The relationship between insulation ageing and power network performance," in *2007 International Conference*

on Solid Dielectrics, ICSD, July 8, 2007 - July 13, 2007, Winchester, United kingdom, 2007, pp. 180-183.

12 L. A. Dissado and J. C. Fothrgill, *Electrical degradation and breakdown in polymer*: *IEE materials and devices series 9, Peter Peregrinus Ltd. On behalf of the Institution of Electrical engineers*, *1992*.

13 C. A. Spellman, H. M. Young, A. Haddad, A. R. Rowlands, and R. T. Waters, "Survey of polymeric insulator ageing factors," London, UK, 1999, pp. 4.160.P1-4.163.P1.

14 J. C. Fothergill, "Ageing, space charge and nanodielectrics: Ten things we don't know about dielectrics," Winchester, United kingdom, 2007, pp. 1-10.

15 T. L. Hanley, R. P. Burford, R. J. Fleming, and K. W. Barber, "A general review of polymeric insulation for use in HVDC cables," *IEEE Electrical Insulation Magazine,* vol. 19, pp. 13-24, 2003.

16 A. S. Vaughan, G. Chen, P. L. Lewin, S. J. Dodd, and S. G. Swingler, "Dielectric ageing: Materials, measurements and modelling of nano- to meso-scale processes," London, United kingdom, 2006, pp. 27-32.

17 Z.-H. Fan, T. Takahashi, J. Suzuki, H. Miyata, S. Iemura, T. Itoh, T. Nakiri, and N. Shimizu, "Relation between electroluminescence and degradation in XLPE," *Dielectrics and Electrical Insulation, IEEE Transactions on,* vol. 8, pp. 91-96, 2001.

18 G. C. Montanari, G. Pattini, and L. Simoni, "Long Term Behavior of XLPE Insulated Cable Models," *Power Engineering Review, IEEE,* vol. PER-7, pp. 34-34, 1987.

19 G. Mazzanti and G. C. Montanari, "A comparison between XLPE and EPR as insulating materials for HV cables," *Power Delivery, IEEE Transactions on,* vol. 12, pp. 15-28, 1997.

20 A. Motori, F. Sandrolini, and G. C. Montanari, "Degradation and electrical behavior of aged XLPE cable models," in *Conduction and Breakdown in Solid Dielectrics, 1989., Proceedings of the 3rd International Conference on*, 1989, pp. 352-358.

21 A. Motori, F. Sandrolini, G. C. Montanari, and M. Loggini, "Electrical properties for detection of thermal aging in XLPE cable models," in *Properties and Applications of Dielectric Materials, 1991., Proceedings of the 3rd International Conference on*, 1991, pp. 761-764 vol.2.

22 M. Moudoud, M. Megherbi, M. Mekious, and O. Lamrous, "Thermal aging effect on charging and discharging currents in polymers under DC stress," in *Electrical Insulation, 2008. ISEI 2008. Conference Record of the 2008 IEEE International Symposium on*, 2008, pp. 506-509.

23 A. Tzimas, M. Fu, and L. A. Dissado, "Characterization of thermally aged XLPE cable peelings through space charge measurements," in *Electrical*

Insulation and Dielectric Phenomena, 2005. CEIDP '05. 2005 Annual Report Conference on, 2005, pp. 30-33.

24 M. C. Lança, M. Fu, E. Neagu, L. A. Dissado, J. Marat-Mendes, A. Tzimas, and S. Zadeh, "Space charge analysis of electrothermally aged XLPE cable insulation," *Journal of Non-Crystalline Solids,* vol. 353, pp. 4462-4466, 2007.

25 J. Jonsson, B. Ranby, C. Laurent, and C. Mayoux, "Influence of thermal and UV aging on electroluminescence of polypropylene films," *Dielectrics and Electrical Insulation, IEEE Transactions on,* vol. 3, pp. 148-152, 1996.

26 S. Grzybowski, P. Zubielik, and E. Kuffel, "Changes of Thermoplastic PE Cable Insulation Properties Caused by the Overload Current," *Power Engineering Review, IEEE,* vol. 9, pp. 34-35, 1989.

27 M. Reuter, E. Gockenbach, and H. Borsi, "Dielectric spectroscopy of multistress aged XLPE-cable insulation for examination of synergic effects," in *Electrical Insulating Materials, 2005. (ISEIM 2005). Proceedings of 2005 International Symposium on*, 2005, pp. 277-280 Vol. 1.

28 C. Kim, Z. Jin, P. Jiang, Z. Zhu, and G. Wang, "Investigation of dielectric behavior of thermally aged XLPE cable in the high-frequency range," *Polymer Testing,* vol. 25, pp. 553-561, 2006.

29 P. A. Roseen, T. Reitberger, S. M. Gubanski, and U. W. Gedde, "PD resistance of thermally aged polyethylene and carbonyl-containing model polymers," *Dielectrics and Electrical Insulation, IEEE Transactions on,* vol. 6, pp. 191-201, 1999.

30 J.-I. Weon, "Effects of thermal ageing on mechanical and thermal behaviors of linear low density polyethylene pipe," *Polymer Degradation and Stability,* vol. 95, pp. 14-20, 2010.

31 D. Srivastava, P. Kumar, and G. N. Mathur, "Aging characteristics of ternary blends of polyethylenes. I," *Materials and Manufacturing Processes,* vol. 16, pp. 419-425, 2001.

32 M. Celina and G. A. George, "Characterisation and degradation studies of peroxide and silane crosslinked polyethylene," *Polymer Degradation and Stability,* vol. 48, pp. 297-312, 1995.

33 T. Hashiguchi, M. Otsubo, S. Yamashita, N. Anami, C. Honda, O. Takenouchi, Y. Hashimoto, and M. Nakamura, "Multi aging test for polymer materials," in *Electrical Insulation and Dielectric Phenomena, 2001 Annual Report. Conference on*, 2001, pp. 601-604.

34 E. L. de Mattos Mehl, "Multiple stress aging of HV polymeric insulation," *Electrical Insulation, IEEE Transactions on,* vol. 25, pp. 521-526, 1990.

35 J. V. Gulmine and L. Akcelrud, "Correlations between structure and accelerated artificial ageing of XLPE," *European Polymer Journal,* vol. 42, pp. 553-562, 2006.

36 H. Sarma, C. Mahabir, and A. Shaikevitch, "Investigations on the aging of cross-linked ethylene vinyl silane copolymer," in *Electrical Insulation, 1996., Conference Record of the 1996 IEEE International Symposium on*, 1996, pp. 624-631 vol.2.

37 M. Fu, G. Chen, L. A. Dissado, J. C. Fothergill, and C. Zou, "The Effect of Gamma Irradiation on Space Charge Behaviour and Dielectric Spectroscopy of Low-density Polyethylene," in *Solid Dielectrics, 2007. ICSD '07. IEEE International Conference on*, 2007, pp. 442-445.

38 G. Chen and M. Fu, "The Influence of Gamma Irradiation on Space Charge in LDPE," in *Properties and applications of Dielectric Materials, 2006. 8th International Conference on*, 2006, pp. 131-134.

39 D. H. Mills, P. L. Lewin, and G. Chen, "Comparison between the electroluminescence and space charge of ultraviolet and thermally aged low density polyethylene," in *Electrical Insulation and Dielectric Phenomena (CEIDP), 2010 Annual Report Conference on*, 2010, pp. 1-4.

40 D. H. Mills, P. L. Lewin, G. Chen, and A. M. Ariffin, "Electroluminescence of ultraviolet and thermally aged low density polyethylene," in *Solid Dielectrics (ICSD), 2010 10th IEEE International Conference on*, 2010, pp. 1-4.

41 A. C. Gjaerde, "Multifactor ageing models - origin and similarities," *IEEE Electrical Insulation Magazine,* vol. 13, pp. 6-13, 1997.

42 T. W. Dakin, "Electrical Insulation Deterioration Treated as a Chemical Rate Phenomenon," *American Institute of Electrical Engineers, Transactions of the,* vol. 67, pp. 113-122, 1948.

43 L. Simoni, "A General Approach to the Endurance of Electrical Insulation under Temperature and Voltage," *Electrical Insulation, IEEE Transactions on,* vol. EI-16, pp. 277-289, 1981.

44 H. Endicott, B. Hatch, and R. Sohmer, "Application of the Eyring Model to Capacitor Aging Data," *Component Parts, IEEE Transactions on,* vol. 12, pp. 34-41, 1965.

45 G. C. Montanari and L. Simoni, "Aging phenomenology and modeling," *Electrical Insulation, IEEE Transactions on,* vol. 28, pp. 755-776, 1993.

46 C. Dang, J.-L. Parpal, and J.-P. Crine, "Electrical aging of extruded dielectric cables review of existing theories and data," *IEEE Transactions on Dielectrics and Electrical Insulation,* vol. 3, pp. 237-247, 1996.

47 J.-L. Parpal, J.-P. Crine, and C. Dang, "Electrical aging of extruded dielectric cables a physical model," *IEEE Transactions on Dielectrics and Electrical Insulation,* vol. 4, pp. 197-209, 1997.

48 J.-P. Crine, "Electrical aging and breakdown of crosslinked polyethylene cables," Cancun, Mexico, 2002, pp. 23-26.

49 J. P. Crine, "On the interpretation of some electrical aging and relaxation phenomena in solid dielectrics," *Dielectrics and Electrical Insulation, IEEE Transactions on,* vol. 12, pp. 1089-1107, 2005.

50 T. J. Lewis, J. P. Llewellyn, M. J. van der Sluijs, J. Freestone, and R. N. Hampton, "A new model for electrical ageing and breakdown in dielectrics," in *Dielectric Materials, Measurements and Applications, Seventh International Conference on (Conf. Publ. No. 430)*, 1996, pp. 220-224.

51 T. J. Lewis, "Ageing - A perspective," *IEEE Electrical Insulation Magazine,* vol. 17, pp. 6-16, 2001.

52 J. P. Jones, J. P. Llewellyn, and T. J. Lewis, "The contribution of field-induced morphological change to the electrical aging and breakdown of polyethylene," *Dielectrics and Electrical Insulation, IEEE Transactions on,* vol. 12, pp. 951-966, 2005.

53 J.-P. Crine, "Comparison between Lewis and Crine models for the electrical aging of dielectric polymers," Austin, TX, USA, 1999, pp. 508-511.

54 L. A. Dissado, G. Mazzanti, and G. C. Montanari, "The role of trapped space charges in the electrical aging of insulating materials," *Dielectrics and Electrical Insulation, IEEE Transactions on,* vol. 4, pp. 496-506, 1997.

55 G. Mazzanti and G. C. Montanari, "Electrical aging and life models: the role of space charge," *Dielectrics and Electrical Insulation, IEEE Transactions on,* vol. 12, pp. 876-890, 2005.

56 L. A. Dissado and A. Thabet, "Simulation of electrical ageing in insulating polymers using a quantitative physical model," *Journal of Physics D: Applied Physics,* vol. 41, p. 085412, 2008.

57 L. A. Dissado, A. Thabet, and S. J. Dodd, "Simulation of DC electrical ageing in insulating polymer films," *Dielectrics and Electrical Insulation, IEEE Transactions on,* vol. 17, pp. 890-897, 2010.

58 A. J. Peacock, *Handbook of polyethylene. Structures, properties and applications*: *Marcel Dekker Inc, New York, Basel*, *2000*.

59 T. Andrews, R. N. Hampton, A. Smedberg, D. Wald, V. Waschk, and W. Weissenberg, "The role of degassing in XLPE power cable manufacture," *IEEE Electrical Insulation Magazine,* vol. 22, pp. 5-16, 2006.

60 I. L. Hosier, "Morphology and electrical properties of polyethylene blends," PhD, Department of Physics, University of Reading, Reading, 1996.

61 G. R. Greenway, "The effect of processing conditions on the morphology and electric strength of polyethylene blends," PhD, Department of Physics, University of Reading, Reading, 2000.

62 B. S. IEC 60060-1, *High voltage test techniques- Part 1-General definition and test require ment*: *the International Electrotechnical Commission*, 1998.

63 B. S. IEC 60243-3, *Electrical strength of insulating materials- test methods - Part 3 -Additional requirements for 1.2/50 μs impulse tests*: *the International Electrotechnical Commission, 2001*.

64 K. F. Dieter Kind, *High Voltage Test Techniques*, 2 ed.: *Newnes 2005*.

65 E. Kuffel, W. S. Zaengl, and J. Kuffel, *High voltage engineering fundamental*, *second* ed.: *Newnes*, *July 17, 2000*.

66 M. S. Naidu and V. Kamaraju, *High voltage engineering*: *McGraw-Hill Education*, *31 Oct 1995*.

67 P. L. Lewin, T. N. Tran, D. J. Swaffield, and J. K. Hallstrom, "Zero-phase filtering for lightning impulse evaluation: A K-factor filter for the revision of IEC60060-1 and -2," *IEEE Transactions on Power Delivery,* vol. 23, pp. 3-12, 2008.

68 D. J. Swaffield, P. L. Lewin, N. L. Dao, and J. K. Hallstrom, "Lightning impulse waveshapes: Defining the true origin and its impact on parameter evaluation," in *15th International Symposium on High Voltage Engineering*, Ljubjana, Slovenia, 2007, pp. CD-Rom.

69 A. Knight, *Basic of Matlab and beyond*: *Chapman and Hall/CRC*.

70 J. Axelson, *Serial port complete, COM ports, USB virtual COM ports, and ports for embedded systems*, 2nd Revised ed.

71 J. K. Jeffrey Travis, *LabView for everyone, Graphical programming made easy and fun*, 3 ed.: *Prentice Hall*, *2006*.

72 Y. Murata, S. Katakai, and M. Kanaoka, "Impulse breakdown superposed on ac voltage in XLPE cable insulation," *IEEE Transactions on Dielectrics and Electrical Insulation,* vol. 3, pp. 361-365, 1996.

73 A. Rakowska and K. Hajdrowski, "Influence of high-voltage polarisation on impulse breakdown of polyethylene and crosslinked polyethylene," in *IEEE International Conference on Conduction Breakdown in Solid Dielectrics, ICSD 1995*, Leicester, Engl, 1995, pp. 636-640.

74 J. Artbauer and J. Griac, "Some Factors Preventing the Attainment of Intrinsic Electric Strength in Polymeric Insulations," *Electrical Insulation, IEEE Transactions on,* vol. EI-5, pp. 104-112, 1970.

75 J. J. O'Dwyer, "Theory of Dielectric Breakdown in Solids," *Journal of The Electrochemical Society,* vol. 116, pp. 239-242, 1969.

76 K. H. Stark and C. G. Garton, "Electric Strength of Irradiated Polythene," *Nature,* vol. 176, pp. 1225-1226, 1955.

77 G. C. Stone and J. F. Lawless, "Application of Weibull Statistics to Insulating Aging Tests," *IEEE transactions on electrical insulation,* vol. EI-14, pp. 233-239, 1979.

78 G. C. Stone, "Statistics of aging models and practical reality," *IEEE transactions on electrical insulation,* vol. 28, pp. 716-728, 1993.

79 T. T. Soong, *Fundamentals of probability and statistics for engineering*: *John Wiley & Sons, Ltd*, *2004*.

80 C. M. Douglas and C. R. George, *Applied statistics and probability for Engineers*, *Third* ed.: *John Wiley & Sons, Ltd*, *2003*.

81 J. C. Fothergill, "Estimating the cumulative probability of failure data points to be plotted on Weibull and other probability paper," *IEEE transactions on electrical insulation,* vol. 25, pp. 489-492, 1990.

82 F. B. Lalam and G. Hoang The, "Pressure effect on the electrical ageing of polyethylene," *Journal of Physics D: Applied Physics,* vol. 33, p. L133, 2000.

83 S. Ul-Haq and G. R. Govinda Raju, "Weibull statistical analysis of area effect on the breakdown strength in polymer films," in *2002 IEEE Conference on Electrical Insulation and Dielectric Phenomena, October 20, 2002 - October 24, 2002*, Cancun, Mexico, 2002, pp. 518-521.

84 Y. Sekii and T. Kazama, "A statistical investigation of dielectric breakdown of low-density polyethylene," in *Proceedings of the 2004 IEEE International Conference on Solid Dielectrics ICSD 2004, July 5, 2004 - July 9, 2004*, Toulouse, France, 2004, pp. 83-86.

85 J. Artbauer, "Electric strength of polymers," *Journal of Physics D: Applied Physics,* vol. 29, p. 446, 1996.

86 T. Okamoto, N. Hozumi, and M. Ishida, "Breakdown strength affected by the interface roughness at the semiconducting layer in XLPE power cables," in *Proceedings of the 3rd International Conference on Properties and Applications of Dielectric Materials, July 8, 1991 - July 12, 1991*, Tokyo, Jpn, 1992, pp. 127-130.

87 M. Okashita, M. Ymaguchi, M. Fujita, H. Shintate, S. Wang, and T. Shiono, "Relationship between impulse breakdown and morphology of polyethylene," in *Electrical Insulating Materials, 1998. Proceedings of 1998 International Symposium on*, 1998, pp. 549-552.

88 Y. Bok-Hee, C. Dae-Hee, and S. Sung-Ik, "Improvement of breakdown strength by additives and curing conditions on XLPE insulation for power cable," in *Electrical Insulation, 2004. Conference Record of the 2004 IEEE International Symposium on*, 2004, pp. 347-350.

89 S. G. Swingler, "On the short-term electric strength of polyethylene film," *IEE Conference Publication,* pp. 1-4, 1988.

90 V. Schweidler and E. Ritter, "Studien über die Anomalien im Verhalten der Dielektrika," *Annalen der Physik,* vol. 329, pp. 711-770, 1907.

91 R. R. Benedict, "Behavior of Dielectrics A Study of the Anomalous Charging Current and the Variation of Dielectric Energy Loss and Capacitance with Frequency in Solid Dielectrics," *American Institute of Electrical Engineers, Transactions of the,* vol. 49, pp. 739-750, 1930.

92 A. K. Johnscher, "The universal dielectric response and its physical significance," in *Properties and Applications of Dielectric Materials, 1991., Proceedings of the 3rd International Conference on*, 1991, pp. 1-11 vol.1.

93 A. K. Jonscher, *Dielectric Relaxation in Solids*: *Chelsea Dielectrics Press Ltd*, *1983*.

94 A. K. Jonscher, *Universal Relaxation Law*: *Chelsea Dielectrics Press Ltd 1995*.

95 L. A. Dissado and R. M. Hill, "A Cluster Approach to the Structure of Imperfect Materials and Their Relaxation Spectroscopy," *Proceedings of the Royal Society of London. Series A, Mathematical and Physical Sciences,* vol. 390, pp. 131-180, 1983.

96 N. G. McCrum, *Anelastic and Dielectric Effects in Polymeric Solids*: *John Wiley & Sons Ltd 1967*.

97 T. Blythe and D. Bloor, *Electrical properties of polymers*, *second* ed.: *Cambridge university press 2005*.

98 A. S. Friedrich Kremer, *Broadband Dielectric Spectroscopy*: *Springer*, *2002*.

99 A. Moliton, *Applied Electromagnetism and Materials*: *Springer*, *2006*.

100 G. G. Raju, *Dielectrics in Electric Fields (Power Engineering)*, 1st ed.: *CRC Press*, *2003*.

101 K. C. Kao, *Dielectric phenomena in solids*: *Elsevier academic press*, *2004*.

102 J. M. Fourmigue, J. L. Parpal, and J. N. Seguin, "Dielectric spectroscopy of XLPE cable insulation: comparison between time-domain and frequency-domain methods," in *Conduction and Breakdown in Solid Dielectrics, 1992., Proceedings of the 4th International Conference on*, 1992, pp. 235-240.

103 M. Ehsani, H. Borsi, E. Gockenbach, J. Morshedian, G. R. Bakhshandeh, and A. A. Shayegani, "Effect of aging on dielectric behavior of outdoor polymeric insulators," in *Solid Dielectrics, 2004. ICSD 2004. Proceedings of the 2004 IEEE International Conference on*, 2004, pp. 312-315 Vol.1.

104 J. C. Fothergill, K. B. A. See, M. N. Ajour, and L. A. Dissado, ""Sub-hertz" dielectric spectroscopy," in *Electrical Insulating Materials, 2005. (ISEIM 2005). Proceedings of 2005 International Symposium on*, 2005, pp. 821-824 Vol. 3.

105 L. Tong, J. Fothergill, S. Dodd, L. Dissado, U. H. Nilsson, F. Mingli, and F. Perrot, "Dielectric spectroscopy study of thermally-aged extruded model

power cables," in *Solid Dielectrics (ICSD), 2010 10th IEEE International Conference on*, 2010, pp. 1-4.

106 Fr, P. bing, D. Blischke, R. Gerhard-Multhaupt, and M. Salah Khalil, "Complete relaxation map of polyethylene: filler-induced chemical modifications as dielectric probes," *Journal of Physics D: Applied Physics,* vol. 34, pp. 3051-3057, 2001.

107 R. J. Sengwa, S. Choudhary, and S. Sankhla, "Dielectric spectroscopy of hydrophilic polymers-montmorillonite clay nanocomposite aqueous colloidal suspension," *Colloids and Surfaces A: Physicochemical and Engineering Aspects,* vol. 336, pp. 79-87, 2009.

108 J. P. Runt and J. J. Fitzgerald, *Dielectric Spectroscopy of Polymeric Materials: Fundamentals and Applications (ACS Professional Reference Book)*: American Chemical Society, 1999.

109 C. R. Ashcraft and R. H. Boyd, "A dielectric study of molecular relaxation in oxidized and chlorinated polyethylenes," *Journal of Polymer Science: Polymer Physics Edition,* vol. 14, pp. 2153-2193, 1976.

110 E. Suljovrujić, G. Stamboliev, and D. Kostoski, "Dielectric relaxation study of gamma irradiated oriented low-density polyethylene," *Radiation Physics and Chemistry,* vol. 66, pp. 149-154, 2003.

111 B. V. Hamon, "An approximate method for deducing dielectric loss factor from direct-current measurements," *Proceedings of the IEE - Part IV: Institution Monographs,* vol. 99, pp. 151-155, 1952.

112 B. Gross, "On the Theory of Dielectric Loss," *Physical Review,* vol. 59, p. 748, 1941.

113 V. Adamec, "Approximate method for deducing a.c. permittivity from d.c. measurements," *Electrical Engineers, Proceedings of the Institution of,* vol. 116, pp. 1119-1121, 1969.

114 L. A. Dissado and R. M. Hill, "Anomalous low-frequency dispersion. Near direct current conductivity in disordered low-dimensional materials," *Journal of the Chemical Society, Faraday Transactions 2: Molecular and Chemical Physics,* vol. 80, pp. 291-319, 1984.

115 P. C. N. Scarpa, A. T. Bulinski, S. Bamji, and D. K. Das-Gupta, "Dielectric spectroscopy of AC aged polyethylene in the frequency range of 10^{-5} Hz to 10^{6} Hz," in *Electrical Insulation and Dielectric Phenomena, 1995. Annual Report., Conference on*, 1995, pp. 81-84.

116 D. K. Das-Gupta and P. C. N. Scarpa, "Polarization and dielectric behavior of ac-aged polyethylene," *Dielectrics and Electrical Insulation, IEEE Transactions on,* vol. 3, pp. 366-374, 1996.

117 M. C. Lanca, M. T. Viciosa, C. J. Dias, J. N. M. Mendes, M. A. Bento, and D. K. D. Gupta, "Dielectric spectroscopy analysis of electrically aged low

density polyethylene," *Proceedings - International Symposium on Electrets,* pp. 505-508, 1999.

118 P. Sanzi, F. Monti, G. C. Montanari, and D. K. Das-Guptaz, "Polarization behaviour of cross-linked polyethylene (XLPE)," in *Electrets, 1999. ISE 10. Proceedings. 10th International Symposium on*, 1999, pp. 47-50.

119 P. C. N. Scarpa, E. L. Leguenza, and D. K. Das-Gupta, "Study of electrical ageing of cross-linked polyethylene by dielectric spectroscopy," *Proceedings - International Symposium on Electrets,* pp. 395-398, 1999.

120 P. C. N. Scarpa and D. K. Das-Gupta, "Dielectric spectroscopy of polyethylene with and without carbon black," in *Electrical Insulation, 1998. Conference Record of the 1998 IEEE International Symposium on*, 1998, pp. 149-152 vol.1.

121 E. L. Leguenza, P. C. N. Scarpa, and D. K. Das-Gupta, "Dielectric behavior of aged polyethylene under UV radiation," *Dielectrics and Electrical Insulation, IEEE Transactions on,* vol. 9, pp. 507-513, 2002.

122 D. K. Das-Gupta and P. C. N. Scarpa, "Modeling of dielectric relaxation spectra of polymers in the condensed phase," *Electrical Insulation Magazine, IEEE,* vol. 15, pp. 23-32, 1999.

123 E. Tuncer, Y. V. Serdyuk, and S. M. Gubanski, "Dielectric mixtures: electrical properties and modeling," *Dielectrics and Electrical Insulation, IEEE Transactions on,* vol. 9, pp. 809-828, 2002.

124 J. P. Crine, "On the interpretation of some electrical aging and relaxation phenomena in solid dielectrics," *IEEE Transactions on Dielectrics and Electrical Insulation,* vol. 12, pp. 1089-1107, 2005.

125 H. J. Wintle, "Charge motion and trapping in insulators surface and bulk effects," *IEEE Transactions on Dielectrics and Electrical Insulation,* vol. 6, pp. 1-10, 1999.

126 G. C. Montanari and P. H. F. Morshuis, "Space charge phenomenology in polymeric insulating materials," *Dielectrics and Electrical Insulation, IEEE Transactions on,* vol. 12, pp. 754-767, 2005.

127 A. Tzimas, S. M. Rowland, L. A. Dissado, M. Fu, and U. H. Nilsson, "The effect of dc poling duration on space charge relaxation in virgin XLPE cable peelings," *Journal of Physics D: Applied Physics,* vol. 43, p. 215401, 2010.

128 A. See, L. A. Dissado, and J. C. Fothergill, "Electric field requirements for charge packet generation and movement in XLPE," in *Solid Dielectrics, 2001. ICSD '01. Proceedings of the 2001 IEEE 7th International Conference on*, 2001, pp. 232-235.

129 J. M. Alison and R. M. Hill, "A model for bipolar charge transport, trapping and recombination in degassed crosslinked polyethene," *Journal of Physics D: Applied Physics,* vol. 27, p. 1291, 1994.

130 G. Chen and S. H. Loi, "Space Charge Modelling in Solid Dielectrics under High Electric Field Based on Double Charge Injection Model," presented at the MRS Fall Meeting, Boston USA, 2005.

131 G. C. Montanari, G. Mazzanti, F. Palmieri, A. Motori, G. Perego, and S. Serra, "Space-charge trapping and conduction in LDPE, HDPE and XLPE," *Journal of Physics D: Applied Physics,* vol. 34, p. 2902, 2001.

132 M. Abou-Dakka, A. Bulinski, and S. Bamji, "Space Charge Development and Breakdown in XLPE under DC Field," *IEEE Transactions on Dielectrics and Electrical Insulation,* vol. 11, pp. 41-49, 2004.

133 R. Hegerberg and B. Sanden, "Space charge and impulse breakdown strength in XLPE," in *Proceedings of the IEEE International Conference on Properties and Applications of Dielectric Materials*, Brisbane, Aust, 1994, pp. 154-157.

134 M. A. Brown, G. Chen, A. S. Vaughan, and P. A. Norman, "High voltage performance of bulk, and amalgamated, PE insulation systems. Part II. Breakdown, morphology and lifetime," *Journal of Physics D: Applied Physics,* vol. 36, p. 3197, 2003.

135 T. Takeda, H. Suzuki, and T. Okamoto, "Correlation between space charge distribution under DC voltage and dielectric breakdown properties in XLPE under impulse voltage superposed onto DC voltage," in *Electrical Insulating Materials, 2001. (ISEIM 2001). Proceedings of 2001 International Symposium on*, 2001, pp. 493-496.

136 M. Fu, G. Chen, and X. Liu, "Space charge behaviour in LDPE after AC electrical ageing," in *Proceedings of the 2004 IEEE International Conference on Solid Dielectrics ICSD 2004*, Toulouse, France, 2004, pp. 217-220.

137 G. Chen, M. Fu, X. Z. Liu, and L. S. Zhong, "Ac aging and space-charge characteristics in low-density polyethylene polymeric insulation," *Journal of Applied Physics,* vol. 97, pp. 1-7, 2005.

138 G. Chen, "Space Charge Measurement as a Diagnostic Tool to Monitor Ageing in Polymeric Materials," *Transactions on Electrical and Electronic Materials,* vol. 7, pp. 235-239, 2006.

139 G. C. Montanari, C. Laurent, G. Teyssedre, A. Campus, and U. H. Nilsson, "From LDPE to XLPE: investigating the change of electrical properties. Part I. space charge, conduction and lifetime," *Dielectrics and Electrical Insulation, IEEE Transactions on,* vol. 12, pp. 438-446, 2005.

140 P. Carstensen, J. Jonsson, A. A. Farkas, A. Campus, and U. H. Nilsson, "A study on the origin of space charge accumulation in polymeric HVDC cables," in *Solid Dielectrics, 2004. ICSD 2004. Proceedings of the 2004 IEEE International Conference on*, 2004, pp. 260-263 Vol.1.

141 L. Martinotto, F. Peruzzotti, F. Palmieri, G. C. Montanari, and S. Rai, "Space charge behavior of chemically cross-linked and radiation cross-linked

polyethylene," in *Electrical Insulation and Dielectric Phenomena, 2000 Annual Report Conference on*, 2000, pp. 109-112 vol.1.

142 Y. Maeno, N. Hirai, Y. Ohki, T. Tanaka, M. Okashita, and T. Maeno, "Effects of crosslinking byproducts on space charge formation in crosslinked polyethylene," *Dielectrics and Electrical Insulation, IEEE Transactions on,* vol. 12, pp. 90-97, 2005.

143 N. Hussin and G. Chen, "The Effect of Acetophenone and alpha-Methylstyrene on the Space Charge Properties of Low Density Polyethylene," in *Electrical Insulation and Dielectric Phenomena, 2008. CEIDP 2008. Annual Report Conference on*, 2008, pp. 702-705.

144 N. Hussin and G. Chen, "Space charge accumulation and conductivity of crosslinking byproducts soaked LDPE," in *Electrical Insulation and Dielectric Phenomena (CEIDP), 2010 Annual Report Conference on*, 2010, pp. 1-4.

145 M. Fu, G. Chen, L. A. Dissado, and J. C. Fothergill, "Influence of thermal treatment and residues on space charge accumulation in XLPE for DC power cable application," *Dielectrics and Electrical Insulation, IEEE Transactions on,* vol. 14, pp. 53-64, 2007.

146 W. Xinsheng, T. Demin, Y. Tanaka, T. Muronaka, T. Takada, C. Shinoda, and T. Hashizumi, "Space charge in XLPE power cable under dc electrical stress and heat treatment," *Dielectrics and Electrical Insulation, IEEE Transactions on,* vol. 2, pp. 467-474, 1995.

147 Y. L. Chong, G. Chen, I. L. Hosier, A. S. Vaughan, and Y. F. F. Ho, "Heat treatment of cross-linked polyethylene and its effect on morphology and space charge evolution," *Dielectrics and Electrical Insulation, IEEE Transactions on,* vol. 12, pp. 1209-1221, 2005.

148 K. Uchida, T. Kawashima, T. Uozumi, Y. Inoue, and S. Fukunaga, "Effects of morphology on space charge distribution in polyethylene," in *Electrical Insulating Materials, 1995. International Symposium on*, 1995, pp. 231-234.

149 K. S. Suh, J. H. Koo, L. Seung Hyung, P. Jung Ki, and T. Takada, "Origin of heterocharge in polyethylene," in *Properties and Applications of Dielectric Materials, 1994., Proceedings of the 4th International Conference on*, 1994, pp. 5-8 vol.1.

150 Y. Tanaka, G. Chen, A. Vaughan, and T. Takada, "Space charge formation in quenched low density polyethylene," in *Properties and Applications of Dielectric Materials, 2003. Proceedings of the 7th International Conference on*, 2003, pp. 970-973 vol.3.

151 Y. Tanaka, G. Chen, Y. Zhao, A. E. Davies, A. S. Vaughan, and T. Takada, "Effect of additives on morphology and space charge accumulation in low density polyethylene," *Dielectrics and Electrical Insulation, IEEE Transactions on,* vol. 10, pp. 148-154, 2003.

152 G. A. Cartwright, A. E. Davies, S. G. Swingler, and A. S. Vaughan, "Effect of an antioxidant additive on morphology and space-charge characteristics of low-density polyethylene," *Science, Measurement and Technology, IEE Proceedings -,* vol. 143, pp. 26-34, 1996.

153 T. Mizutani, "Effects of additives and morphology on space charge in LDPE," in *Electrical Insulating Materials, 2001. (ISEIM 2001). Proceedings of 2001 International Symposium on*, 2001, pp. 487-492.

154 Y. L. Chong, G. Chen, H. Miyake, K. Matsui, Y. Tanaka, and T. Takada, "Space charge and charge trapping characteristics of cross-linked polyethylene subjected to ac electric stresses," *Journal of Physics D: Applied Physics,* vol. 39, p. 1658, 2006.

155 C. Thomas, G. Teyssedre, and C. Laurent, "Space-charge dynamic in polyethylene: from dc to ac stress," *Journal of Physics D: Applied Physics,* vol. 44, p. 015401, 2011.

156 D. L. Pavia, G. M. Lampman, and G. S. Kriz, *Introduction to Spectroscopy: A Guide for Students of Organic Chemistry*, Third ed.: Thomson Learning, 2000.

157 R. M. Silverstein, F. X. Webster, and K. David, *The Spectrometric Identification of Organic Compounds*, 7th ed.: John Wiley & Sons, 2005.

158 V. G. Barkhudaryan, "Alterations of molecular characteristics of polyethylene under the influence of UV-radiation," *Polymer,* vol. 41, pp. 5787-5791, 2000.

159 L. K. Martin and C. Q. Yang, "Infrared spectroscopy studies of the photooxidation of a polyethylene nonwoven fabric," *Journal of Polymers and the Environment,* vol. 2, pp. 153-160, 1994.

160 K. Sirisinha and S. Chimdist, "Comparison of techniques for determining crosslinking in silane-water crosslinked materials," *Polymer Testing,* vol. 25, pp. 518-526, 2006.

161 K. Sirisinha, M. Boonkongkaew, and S. Kositchaiyong, "The effect of silane carriers on silane grafting of high-density polyethylene and properties of crosslinked products," *Polymer Testing,* vol. 29, pp. 958-965, 2010.

162 D. H. Mills, P. L. Lewin, and G. Chen, "Ageing of high voltage cable insulation," in *Electrical Insulation Conference (EIC), 2011*, 2011, pp. 439-443.

163 J. Ho and S. Boggs, "Effect of UV treatment on the dielectric strength of BOPP capacitor film," in *Electrical Insulation, 2006. Conference Record of the 2006 IEEE International Symposium on*, 2006, pp. 314-317.

164 G. Stamboliev and E. Suljovrujic, "A dielectric study of molecular relaxations in irradiated high density polyethylene," *Polymer Degradation and Stability,* vol. 95, pp. 593-599, 2010.

165 F. Kremer, "Dielectric spectroscopy – yesterday, today and tomorrow," *Journal of Non-Crystalline Solids,* vol. 305, pp. 1-9, 2002.

166 M. Arndt, R. Stannarius, H. Groothues, E. Hempel, and F. Kremer, "Length Scale of Cooperativity in the Dynamic Glass Transition," *Physical Review Letters,* vol. 79, p. 2077, 1997.

167 M. Müller, E. W. Fischer, F. Kremer, U. Seidel, and R. Stadler, "The molecular dynamics of thermoreversible networks as studied by broadband dielectric spectroscopy," *Colloid & Polymer Science,* vol. 273, pp. 38-46, 1995.

168 E. Schlosser and A. Schönhals, "Recent development in dielectric relaxation spectroscopy of polymers," *Colloid & Polymer Science,* vol. 267, pp. 963-969, 1989.

169 P. J. Purohit, J. s. E. Huacuja-Sánchez, D.-Y. Wang, F. Emmerling, A. Thünemann, G. Heinrich, and A. Schönhals, "Structure–Property Relationships of Nanocomposites Based on Polypropylene and Layered Double Hydroxides," *Macromolecules,* vol. 44, pp. 4342-4354, 2011/06/14 2011.

170 T. Liu and et al., "Dielectric spectroscopy measurements on very low loss cross-linked polyethylene power cables," *Journal of Physics: Conference Series,* vol. 183, p. 012002, 2009.

171 Z. Dendzik, M. Kośmider, and M. Sokół, "Dielectric relaxation of water clusters encapsulated in carbon nanotubes – Computer simulation study," *Journal of Non-Crystalline Solids,* vol. 354, pp. 4300-4303, 2008.

172 G. Bánhegyi and F. E. Karasz, "Dielectric properties of moist $CaCO_3$ filled polyethylene composites," *Colloid & Polymer Science,* vol. 265, pp. 394-405, 1987.

173 R. A. J. Carson, "Low-Temperature Dielectric Relaxation in Polyethylene," *Proceedings of the Royal Society of London. Series A, Mathematical and Physical Sciences,* vol. 332, pp. 255-268, 1973.

174 Z. Chao and G. C. Stevens, "The Dielectric Response of Polar and Non-Polar Nanodielectrics," *Dielectrics and Electrical Insulation, IEEE Transactions on,* vol. 15, pp. 606-617, 2008.

175 J. Mijović and H. Zhang, "Local Dynamics and Molecular Origin of Polymer Network−Water Interactions as Studied by Broadband Dielectric Relaxation Spectroscopy, FTIR, and Molecular Simulations," *Macromolecules,* vol. 36, pp. 1279-1288, 2003/02/01 2003.

176 P. A. M. Steeman, F. H. J. Maurer, and M. A. van Es, "Dielectric monitoring of water absorption in glass-bead-filled high-density polyethylene," *Polymer,* vol. 32, pp. 523-530, 1991.

177 A. Schönhals, H. Goering, F. R. Costa, U. Wagenknecht, and G. Heinrich, "Dielectric Properties of Nanocomposites Based on Polyethylene and Layered Double Hydroxide," *Macromolecules,* vol. 42, pp. 4165-4174, 2009/06/23 2009.

178 S. Edin, "Dielectric studies of molecular β-relaxation in low density polyethylene: the influence of drawing and ionizing radiation," *Polymer,* vol. 43, pp. 5969-5978, 2002.

179 Y. Li, M. Yasuda, and T. Takada, "Pulsed electroacoustic method for measurement of charge accumulation in solid dielectrics," *IEEE Transactions on Dielectrics and Electrical Insulation,* vol. 1, pp. 188-195, 1994.

180 G. Chen, Y. L. Chong, and M. Fu, "Calibration of the pulsed electroacoustic technique in the presence of trapped charge," *Measurement Science and Technology,* vol. 17, pp. 1974-1980, 2006.

181 K. R. Bambery and R. J. Fleming, "Space charge accumulation in two power cable grades of XLPE," *Dielectrics and Electrical Insulation, IEEE Transactions on,* vol. 5, pp. 103-109, 1998.

182 K. Jung Woo, N. Jin Ho, and K. S. Suh, "Interfacial charge behavior in SXLPE/XLPE laminate," in *Electrical Insulating Materials, 2001. (ISEIM 2001). Proceedings of 2001 International Symposium on*, 2001, pp. 509-512.

List of publications

1. D. J. Swaffield, P. L. Lewin, N. L. Dao, and J. K. Hallstrom, "Lightning impulse waveshapes: Defining the true origin and its impact on parameter evaluation," in *15th International Symposium on High Voltage Engineering*, Ljubjana, Slovenia, 2007, pp. CD-Rom.

2. N. L. Dao, P. L. Lewin, and S. G. Swingler, "Lightning impulse ageing of HDPE," in *2nd UHVnet Colloquium on High Voltage Measurement and Insulation Research*, Glasgow Caledonian University, Glasgow, UK, 2009, pp. 37-40.

3. N. L. Dao, P. L. Lewin, and S. G. Swingler, "Effects of lightning impulses on the dielectric properties of HDPE," in *International Electrical Insulation Conference*, Birmingham, UK, 2009, pp. 260-264.

4. N. L. Dao, P. L. Lewin, and S. G. Swingler, "Lightning impulse ageing of HV cable insulation," in *16th International Symposium on High Voltage Engineering*, Cape town, South Africa, 2009, pp. 562-565.

5. N. L. Dao, P. L. Lewin, I. L. Hosier, and S. G. Swingler, "A comparison between LDPE and HDPE cable insulation properties following lightning impulse ageing," in *2010 IEEE International Conference on Solid Dielectrics, ICSD 2010, July 4, 2010 - July 9, 2010*, Potsdam, Germany, 2010, pp. 72-75.

6. N. L. Dao, P. L. Lewin, I. L. Hosier, and S. G. Swingler, "The changes in electrical properties of XL4421 insulation under repetitive lightning impulse voltages," in *2010 IEEE International Symposium on Electrical Insulation, ISEI 2010, June 6, 2010 - June 9, 2010*, San Diego, CA, United states, 2010, pp. CD-ROM.

7. N. L. Dao, P. Lewin, I. L. Hosier, and S. G. Swingler, "A Comparison of Polymeric Cable Insulation Properties Following Lightning Impulse Ageing," presented at the UHVnet 2011, Winchester, UK, 2011.

8. N. L. Dao, P. L. Lewin, and S. G. Swingler, "Effect of Cross-linking on the Electrical Properties of LDPE and its Lightning Impulse Ageing Characteristics," in *17th International Symposium on High Voltage Engineering*, Hannover, Germany, 2011, CD-ROM.